

## INFORMATION TO USERS

This manuscript has been reproduced from the microfilm master. UMI films the text directly from the original or copy submitted. Thus, some thesis and dissertation copies are in typewriter face, while others may be from any type of computer printer.

**The quality of this reproduction is dependent upon the quality of the copy submitted.** Broken or indistinct print, colored or poor quality illustrations and photographs, print bleedthrough, substandard margins, and improper alignment can adversely affect reproduction.

In the unlikely event that the author did not send UMI a complete manuscript and there are missing pages, these will be noted. Also, if unauthorized copyright material had to be removed, a note will indicate the deletion.

Oversize materials (e.g., maps, drawings, charts) are reproduced by sectioning the original, beginning at the upper left-hand corner and continuing from left to right in equal sections with small overlaps. Each original is also photographed in one exposure and is included in reduced form at the back of the book.

Photographs included in the original manuscript have been reproduced xerographically in this copy. Higher quality 6" x 9" black and white photographic prints are available for any photographs or illustrations appearing in this copy for an additional charge. Contact UMI directly to order.

# U·M·I

University Microfilms International  
A Bell & Howell Information Company  
300 North Zeeb Road, Ann Arbor, MI 48106-1346 USA  
313/761-4700 800/521-0600



**Order Number 9232319**

**Microfabrication of thermally isolated structures for a silicon  
micromachined flow sensor**

**Whitney, Julie Ann Gordon, Ph.D.**

**University of Cincinnati, 1992**

**Copyright ©1992 by Whitney, Julie Ann Gordon. All rights reserved.**

**U·M·I**  
300 N. Zeeb Rd.  
Ann Arbor, MI 48106



**Microfabrication of Thermally Isolated Structures for a  
Silicon Micromachined Flow Sensor**

A Dissertation submitted to the

Division of Graduate Studies and Research  
of the University of Cincinnati

in partial fulfillment of the  
requirements for the degree of

**DOCTOR OF PHILOSOPHY**

in the Department of Mechanical, Industrial and Nuclear Engineering  
of the College of Engineering

1992

by

Julie Ann Gordon Whitney

B.S., Purdue University, 1982

M.S., Indiana State University, 1985

Committee Chair: Dr. Ivan E. Morse

# UNIVERSITY OF CINCINNATI

June 2, 19 92

*I hereby recommend that the thesis prepared under my supervision by* Julie Ann Gordon Whitney

*entitled* Microfabrication of Thermally Isolated Structures for a Silicon Micromachined Flown Sensor

*be accepted as fulfilling this part of the requirements for the degree of* Doctor of Philosophy

*Approved by:*

Ivan E Morse  
A. Thurman Henderson  
Richard Z. Hull  
Ernest L. Hall

## ABSTRACT

The research deals with the creation of a novel thermal isolation structure on a silicon micromachined flow sensor. The isolation structure uses a form of dopant-selective etching (DSE), which allows for silicon dioxide surface layers to be underetched. The heat transfer characteristics of the geometry of an existing micro flow sensor are modeled as well as a comparison of potential new flow sensor designs. A new flow sensor is made with the thermal isolation structure and improved geometry. The new flow sensor uses less power than a control sensor without thermal isolation, and has good flow sensitivity.

**Acknowledgements:**

I would like to thank my committee for their support and guidance:

Dr. Ivan E. Morse  
Dr. H. Thurman Henderson  
Dr. Richard Shell  
Dr. Ernest Hall

and special thanks to:

Chuck, John, Jeff, Chris, Amal, Don, Kieth, Bob, Husam, Mike, and Ian.

This work is dedicated to my wonderful husband, Jon, and to my parents. Without their support, encouragement and help this would have been an unfulfilled dream.



## TABLE OF CONTENTS

ABSTRACT	ii
ACKNOWLEDGEMENTS	iii
LIST OF TABLES	v
LIST OF FIGURES	vi
LIST OF SYMBOLS	ix
CHAPTER 1	
Introduction	1
CHAPTER 2	
Review of the Literature	19
CHAPTER 3	
Methodology	70
CHAPTER 4	
Tunnel Etching	78
CHAPTER 5	
Sensor Modeling and Redesign	130
CHAPTER 6	
The Redesigned Sensor	165
CHAPTER 7	
Conclusions and Recommendations	187
BIBLIOGRAPHY	195
APPENDIX A - Heat Transfer	201
APPENDIX B - Tunnel Etching Data	240
APPENDIX C	
Miscellaneous Calculations and Engineering Drawings	316

## LIST OF TABLES

TABLE #	TITLE	PAGE
1	Wafer Resistivity vs. Doping	92
2	Etch Rate vs. Doping	108
3	Wafer Etching Variation	114
4	Natural Gas Composition (Mole %)	146
5	Gas Property Table	148
6	Heat Transfer Coefficients	149
7	Output Voltage	150
8	Sensitivity vs. Power Requirements	173
9	Time Response of Redesigned Device	183
10	Summary of Results	228

## LIST OF FIGURES

FIGURE #	TITLE	PAGE
1	Solid Model of Flow Sensor Version 10.0	4
2	Dimensioned Drawing, Top and Bottom View, Flow Sensor Version 10.0	5
3	Dimensioned Drawing, Side View Flow Sensor Version 10.0	6
4	Solid Model of Flow Sensor Version 10.0 Showing Metal Leads	80
5	Top View of Original Flow Sensor	82
6	Engineering Drawing for Phosphorous Doping Mask, Tunnel Etching Tests	85
7	Engineering Drawing for Etching Initiation Holes Mask for Tunnel Etching Tests	86
8	Micro Photograph Showing Etch-Stop	94
9	Heavy Oxide vs. Light Oxide	96
10	Doped Direction Etching	99
11	Doped Direction Etching	100
12	Etch Depth vs. Wafer Type and Doping	101
13	Under Etch in Non-Doped Direction vs. Undoped Wafer Underetch	103
14	Undoped Direction Etching	105
15	Undoped Direction Etching	106

## LIST OF FIGURES, continued

FIGURE #	TITLE	PAGE
16	Tunnel Etching Test With Poor Surface Preparation	110
17	Profilometer Readings	112
18	Uneven Tunnel Etching	115
19	Tunnel Etching Test Wafer	117
20	Old vs. New Hydrazine	119
21	Close-up of Under Etching	121
22	Original Bridge Flow Sensor	125
23	Method for Tunnel Etching Cavity Creation	127
24	Tunnel Etching Progress with Time	129
25	Finite Element Model Solution	131
26	Resistance vs. Temperature	138
27	Log Resistance vs. Temperature	142
28	Temperature Difference, Parallel vs. Perpendicular Resistors	143
29	Thermal Isolation Structures on New Sensor Design	157
30	New Flow Sensor- Tunnel Etching Only Isolation Structure	159

## LIST OF FIGURES, continued

FIGURE #	TITLE	PAGE
31	New Flow Sensor - Tunnel Etching and Hole Isolation Structure	160
32	Thin Slice Flow Sensor	167
33	IV curve of Device J2 1	169
34	Test Stand Set-Up	170
35	Input Voltage vs. Time	172
36	Input Voltage vs. Time Current 1 mA	174
37	Input Voltage vs. Time Current 1.5 mA	175
38	Input Voltage vs. Time Current 2 mA	176
39	Input Voltage vs. Time Current 2 mA Repeatability	178
40	Input Voltage vs. Time Current 1.5 mA Repeatability	179
41	Ambient Temperature Effects On Device J2 1	182
42	Cross Sectional View of Bridge Resistor	201

## LIST OF SYMBOLS

Symbol	Meaning	Units
$A_s$	surface area	$m^2$
$A_{cs}$	cross sectional area	$m^2$
$\alpha$	thermal diffusivity	$m^2/sec$
$C_p$	heat capacity	$kJ/kg\ ^\circ C$
$\delta_t$	boundary layer thickness	- -
$h$	convection heat transfer coefficient	$W/m^\circ C$
$i$	current	amps
$k$	thermal conductivity	$W/m^2^\circ C$
$L$	length	$m$
$\mu$	viscosity	$kg/m\ sec$
$Nu$	Nusselt Number	unitless
$Pe_L$	Peclet number based on length	unitless
$Pr$	Prandlt Number	unitless
$q$	Heat Flux	$W$
$R$	Resistance	Ohms
$R_{TH}$	Thermal Resistance	$^\circ C/W$
$Re_L$	Reynolds number based on length	unitless

### LIST OF SYMBOLS, continued

Symbol	Meaning	Units
$\rho$	density	$\text{kg/m}^3$
S	sensitivity	$\text{mV/cm/sec}$
T	Temperature	$^{\circ}\text{C}$
$U_{\infty}$	free stream velocity	$\text{m/sec}$
V	voltage	volts
$\nu$	kinematic viscosity	$\text{m}^2/\text{sec}$
X	distance	m

## CHAPTER 1

### INTRODUCTION

A flow sensor, which is currently under development by the University of Cincinnati (UC) and the Institute for Advanced Manufacturing Sciences (IAMS), is a micro electro-mechanical device which uses conduction to determine the mass flow rate of gases. The device is extremely small, about 3/4 of a millimeter on a side, and is composed primarily of single crystal silicon. Many features make this device truly unique. Gold has been deeply doped into the device giving it very high sensitivity. The device is so small that its response time is smaller than any other flow sensor. In addition this sensor is possible only through micromachining, a relatively new manufacturing process by which very exact anisotropic chemical etching creates the microgeometries of the device. The many potential applications for such a devices include: medical devices to monitor breathing, natural gas sensors for homes and appliances, industrial sensors for pneumatically controlled equipment, and portable sensors for hand-held measurements. The combination of rapid response and tiny size make micro electro mechanical devices the obvious choice for demanding applications like aerospace and medicine.



## **Problem Statement**

The purpose of this research is to define an etching process by which silicon resistors can be thermally isolated from surrounding single crystal silicon. The process, hereafter referred to as tunnel etching, is a form of dopant selective etching. The process needs to be defined in terms of rates, dopant concentrations and manufacturing processes so it can be incorporated into an actual device for the purpose of thermal isolation. A revised flow sensor design will serve as that new device. The device will be designed using a heat transfer model developed for this purpose.

If tunnel etching can be controlled it will give micromachining a new tool with which to create geometries, one which utilizes the strength of the single crystal silicon and its oxide rather than thin films or polycrystalline layers deposited on top of an oxide. Creating a working device which utilizes tunnel etching will prove its usefulness as a manufacturing option. The current flow sensor must be redesigned to address its manufacturability problems. Combining the structural redesign with a redesign based on an understanding of the heat transfer and tunnel etching process will yield a sensor with novel structural characteristics which should in turn yield a device which can produce sensitivities comparable to the current design but with only a fraction of the power requirements.

## **Objectives**

The objectives of this research are:

1. To determine the nature of tunnel etching to an extent that it could be reliably reproduced and used to create structures.
2. To model flow sensor version 10.0 and other potential designs for the purpose of developing a new design which will utilize tunnel etching for a thermal isolation structure.
3. To design and then manufacture a flow sensor which uses tunnel etching, and then show that tunnel etching has actually increased the thermal isolation within the device.

## **Device Overview**

The current flow sensor (version 10.0) is an electromechanical device created by micromachining in single crystal silicon. The design of the current version of the flow sensor is presented in figures 1, 2, and 3 on the following pages. The device is designed to use a Wheatstone bridge, an electrical configuration of four resistors, to detect temperature changes. The resistors are each created by phosphorous doping two thin strips, side by side, on a thin silicon bridge. Current flows easily into the phosphorous doped strip and encounters a finite resistance as it crosses the silicon gap to enter the

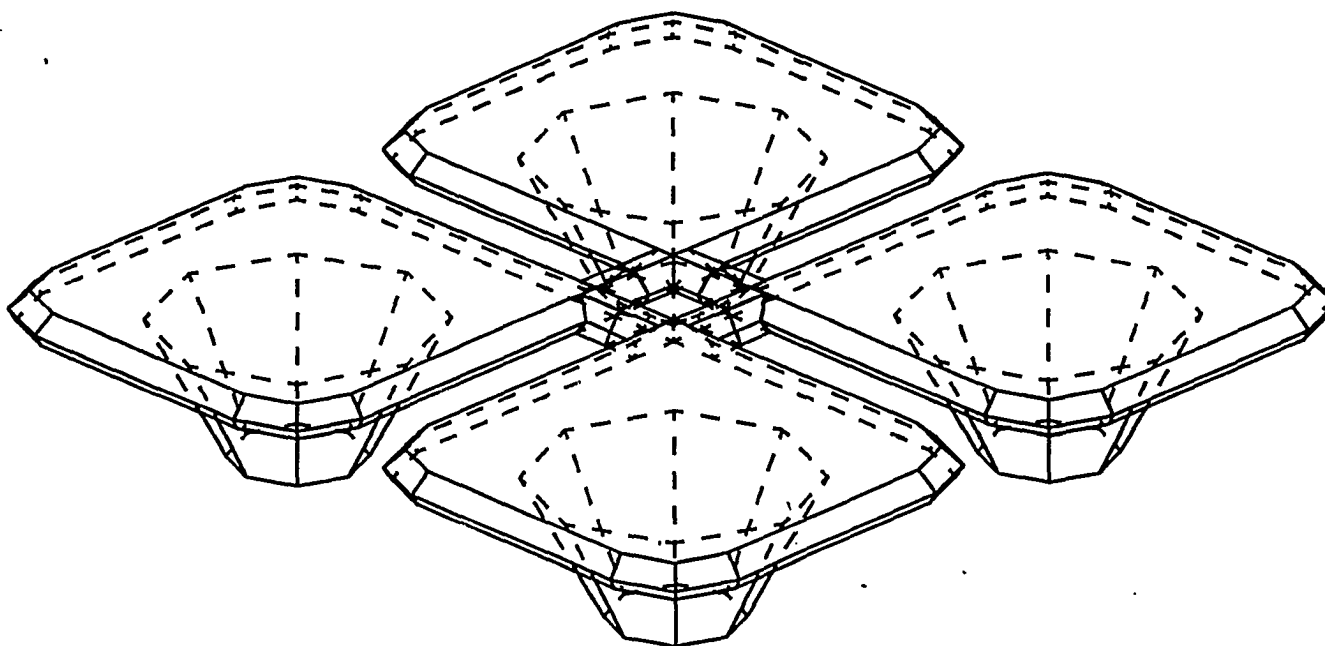
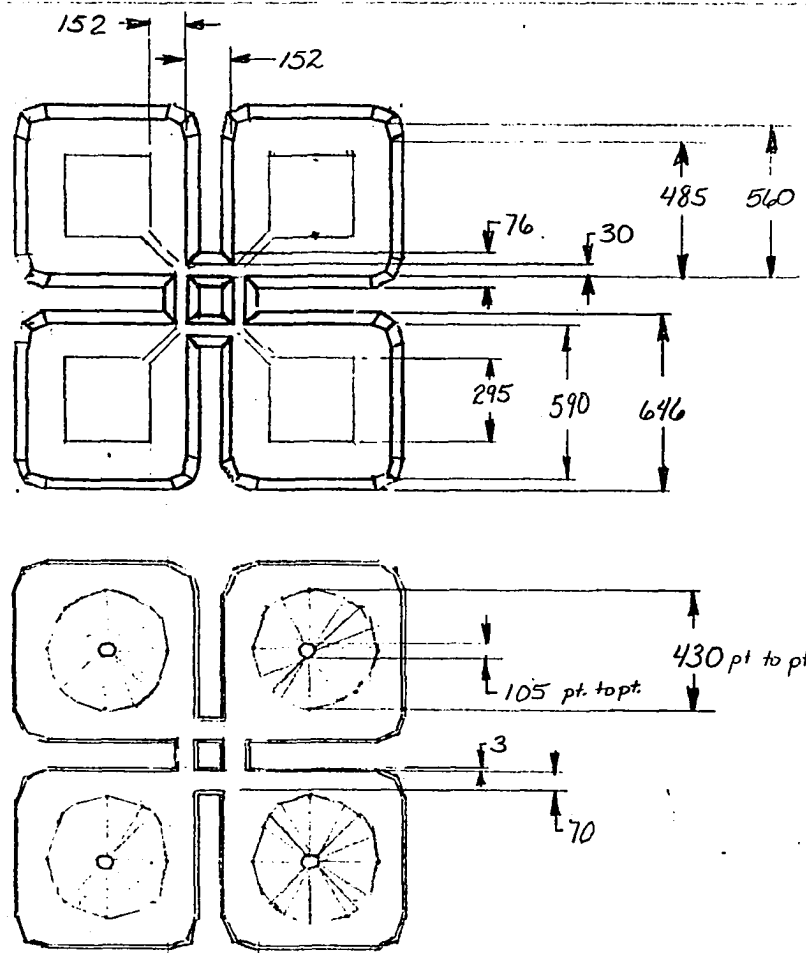


Figure 1 - Solid Model of Flow Sensor Version 10.0

This is a solid model of flow sensor version 10.0  
The model shows the actual shape of the feet after  
manufacturing, as well as the relative size of the feet  
and bridge sensing area.




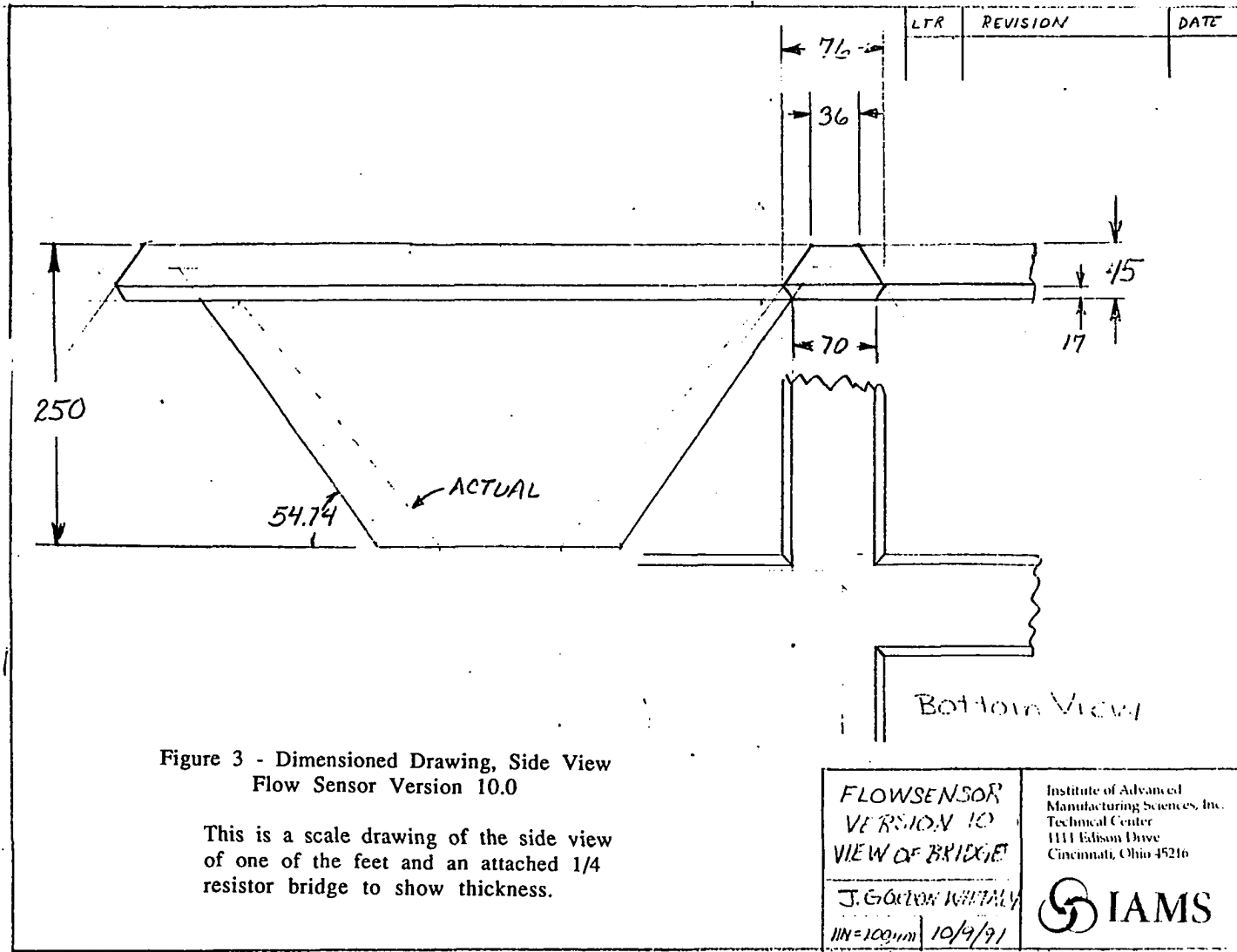


LTR	REVISION	DATE

This is a dimensioned drawing made from measurements of an actual flow sensor version 10.0

Figure 2 - Dimensioned Drawing, Top and Bottom View  
Flow Sensor Version 10.0

<p><b>FLOWSENSOR</b>  <b>VERSION 10</b>  <b>AS MANUFACTURED</b></p>	<p>Institute of Advanced  Manufacturing Sciences, Inc.  Technical Center  1111 Edison Drive  Cincinnati, Ohio 45216</p>
<p>J. Gordon Whitney</p>	
<p>1 IN = 500 μm   10/9/91</p>	



other phosphorous doped strip. Current passing through this resistive area gives up some of its energy as heat, raising the temperature of the silicon bridge above ambient conditions. Convective cooling caused by fluid flowing across the resistor removes some of the heat, differentially cooling the resistors. The resistive value of the bridge depends on the temperature of the silicon. As the resistors change their resistance the voltage output is changed by the Wheatstone bridge. The deep impurity gold doping serves to increase the sensitivity of resistance to temperature by as much as 1000 times.

Wheatstone bridges, named for the British physicist Sir Charles Wheatstone, are a very accurate way to measure resistance. Composed of four resistors arranged in a diamond shape, the output of the bridge is a galvanometer connected across two opposite points of the diamond. Traditionally, three of the four resistors are of a known value and the value of the fourth is determined from the unbalanced effect of the two half bridges. Piezo-resistive bridges have used this structure to increase sensitivity of devices, such as pressure sensors, to resistor strain. The enhanced sensitivity comes from placing the resistors in such a fashion that as the device is placed under stress, the value of two resistors opposite each other on the diamond will increase while the remaining two will decrease. This has the effect of doubling the output for any given stress input. The bridges configuration as applied to flow sensor version 10.0

operates differently. The bridge is powered by an applied constant current. The resistive value of each of the four resistors in the device is a function of its temperature. The unbalance in the bridge is created by different cooling rates for the four different resistors. Differentially cooling the resistors is achieved by placing two of the resistors perpendicular to the flow, and two parallel to the flow. Boundary layer theory suggests that the first perpendicular resistor will be cooled the most by convection because it sees the largest temperature gradient. The second perpendicular resistor will also see a large temperature gradient, although not quite as large as the first because the fluid will already be slightly heated from passing over the first resistor. The two parallel resistors will see the smallest temperature gradient because they are heating the air the entire length as it passes over them. The difference in temperature of the resistors between the parallel and the perpendicular can be related to ambient temperature of the gas. Wheatstone bridges have the advantage that ambient temperature can be removed from the flow signal by differential cooling. The disadvantage of the bridge configuration for this device is that the output signal is a function of the temperature difference of the differently oriented resistors. Since all four resistors increase or decrease in temperature depending on the flow conditions, sensitivity is lost by using a bridge structure.

The large feet of flow sensor version 10.0 serve both as a place for an electrical connection to the outside world and as a mechanical base on which the device stands. Original drawings showed that the feet were to be pyramidal in nature with a large flat pad on the bottom. Undercutting from exposed convex corners has left a significantly smaller and more conical base with a significantly decreased pad and a large mesa structure of silicon on top. These feet are composed of silicon and, like the bridge, have a layer of oxide on the top and deep impurity gold throughout the structure. The oxide top serves to electrically isolate the metal connection pad on the surface of the structure from the silicon feet. In some versions of the device the legs are bonded to a borosilicate glass for strength before final etching and in other versions the sensor is packaged as is.

Several of these devices have been constructed and tested. The devices are quite sensitive to the mass flow rate of a gas passing over it.

### **The Redesigned Flow sensor**

The redesigned flow sensor developed from the heat transfer model and the tunnel etching experiments ended up being a completely different configuration from the original design. The original design, known as version 10.0 was being manufactured both



with and without gold at the time the first redesigned sensor was made. The gold and non-gold devices were identical except the gold doping. As would be expected the sensitivity of the non-gold device dropped dramatically to generally less than 1 mV/cm/sec. One non-gold device did have a brief sensitivity of 15 mV/cm/sec at very high power, but it rapidly burned up. Later non-gold devices could achieve sensitivities around 30 mV/cm/sec, but only when power was around 500 mW. The gold device has excellent sensitivity but is difficult to manufacture and is unstable and unrepeatable in performance.

The redesigned device was modified to have a very predictable heat transfer of the top surface of a single resistor. The single resistor design utilized tunnel etching for a unique thermal isolation structure. Photographs of two sensor designs can be seen in Chapter 5, figures 27 and 28.

The discussion which follows describes how tunnel etching was defined, how different geometries were modeled, and finally a combination of the two in a new non-gold flow sensor design.

### **Problem Setting**

The gold doped flow sensor (version 10.0) has caught the attention of several organizations, including NASA and Senstar, who

wish to see this device become a manufactured reality. In moving from an experimental device to a manufactured product, several current problems will have to be addressed. These problems include: manufacturing losses, thermal isolation, device stability and repeatability. While these problems are specifically those of the flow sensor, solving these problems will provide new information which will increase our understanding of micromachining techniques and material behavior.

### **Manufacturing Losses**

The current device has been designed with four thin bridges arranged as the sides on a square, and at each corner of the square is a massive "foot" to which the electrical leads are connected and by which the device is mounted. See figure 1. This structure was designed to get a fast response time and to electrically and thermally isolate the individual branches of a Wheatstone bridge. Even under ideal conditions this device is extremely weak mechanically. To complicate the problem, single crystal silicon wafers, from which the device is manufactured, have a thickness tolerance greater than the thickness of the bridge. Coupling this with uneven etching rates, several failure modes frequently result.

Severe underetching of secondary planes exposed by the isolated feet causes the conical base sections to etch down to the

point where the flat pad of the device can be completely etched away. Under those conditions the base is reduced to a set of four pointed feet, which are very difficult, if not impossible, to mount. The solution to this problem has been to add an initial process step of thinning the wafer from a nominal 250 microns to 175 microns. This solution not only insures more of a base pad will be left but the starting wafer has a more exact thickness before regular processing. The disadvantage is that the thinned wafer is much more delicate and is much more likely to break while being processed. The method is not an adequate solution when full scale production of the devices needs to be done. In addition, thinning the wafers adds several steps to the manufacturing process, additional time constraints to the process and amplifies the problem of the delicacy of the device.

Other problems arise because the etching of the silicon, while critical to the structure, is difficult to control. The current configuration requires the final etching to actually separate the individual flow sensors. As the flow sensors are separated they fall down into a sieve which holds them as the rest of the wafer continues to etch. Since the etchant solution is currently not agitated, large temperature gradients exist and those sensors which fall downward in the bath are at a higher temperature and therefore a more chemically active part of the reaction vessel. This problem has led to devices whose silicon bridge structures are completely etched away, or at the least very thin and even more delicate than usual.

Partially etched wafers have been bonded to borosilicate glass part way through the etching process and have yielded much better results. The devices separate, but the glass holds them at the same level in the etchant. The glass also greatly enhances the strength of the very delicate device. The glass has the disadvantage of adding to the cost and total processing time for manufacture.

The design of the device itself requires some very difficult lithography alignment steps. Misalignment can lead to devices which are useless as flow sensors, or at the very least must be reworked.

These combined manufacturing/design problems have led to an extreme shortage of complete working devices available for characterization. Roughly 50% of all wafers break in process, although many of the broken pieces can still be processed in a laboratory environment. Since beginning this program roughly 33% of the wafers processed were unusable due to over-etching or alignment problems. Approximately another 20% were unusable due to uncontrolled gold doping. All other wafers are still in process and have not seen final etching, and as of this date have not been tested for appropriate gold doping. No flow sensors of this type were successfully produced between the early spring and late fall 1991. Since the addition of the borosilicate glass and a massive research effort in controlling gold doping, several lots of version 10.0 have been successfully produced in 1992. Initial characterization of these

devices has shown them to have stability and repeatability problems. The bridge resistors are unbalanced, and the device is being used with the input voltage as the flow signal, just as if the device were made of only one resistor.

### **Thermal Isolation**

As the resistors in the Wheatstone bridge begin to heat up the silicon, some of the heat is lost through convection to the passing gas (desirable) and some of the heat is lost as conduction out into the massive feet structures (undesirable). Flow readings obtained by the sensor are a function of differential voltages caused by uneven cooling of the Wheatstone bridge. Thermal shorting (heat conducted out to the feet structures) reduces the sensitivity of the device and reduces the controllability of the flow related output to actual mass flow input. It is possible that thermal shorting may be playing a large role in the flow readings of the existing device.

At the time this research project was initiated, the heat transfer characteristics of the device were completely unknown. No model existed which would indicate what percentage of the input energy was actually lost to convection. No measurement was available to suggest what the equilibrium temperature was for the resistor bridges in a no-flow situation.

It is not possible with currently available theory to predict a value for the average local heat transfer coefficient, a number which would be needed for accurate modeling of the convection. At the small dimensions of the micro flow sensor, a significant amount of the bridge heat loss may actually be diffusion heat loss which will be identical for all bridges resistors no matter which way they are facing. Diffusion heat transfer is similar to diffusion mass transfer where the heat will move from an area of high energy to an area of low energy, which in the case of the flow sensor, is out and away from the sensor in all directions. The Peclet number is a dimensionless parameter which compares heat lost due to convection to heat lost due to diffusion.

$$Pe_L = Re_L Pr = \frac{U_\infty L}{\alpha}$$

$\alpha$  = thermal diffusivity,  $\frac{m^2}{sec}$      $U_\infty$  = free stream velocity  $\frac{m}{sec}$      $L$  = length in meters

(1.1)

The numerator of the Peclet number represents the heat lost to convection, the denominator the heat lost to diffusion. The smaller The Peclet number, the more heat is lost to diffusion. For flow sensor version 10.0 this number is on the order of 10, depending on flow conditions, indicating that heat transfer coefficients calculated by conventional methods may be low by about 10%

## Long Term Stability

Deep doping with gold gives the flow sensor heightened sensitivity to temperature changes. Deep doping is a new idea pioneered at the University of Cincinnati. Gold diffuses very quickly and easily into silicon. Small amounts of gold strongly effect the resistance of the silicon, and therefore the electrical properties of the flow sensor. It was originally believed that once a set amount of gold was introduced into the silicon wafer, that gold would diffuse throughout and reach an equilibrium, giving stable electrical properties for the life of the device. Currently it is very difficult to control the amount of gold entering the device and how it acts in the silicon lattice once it is in. Doping the silicon with the desired amount of gold is difficult because the relationship between the resistivity of the silicon and the gold concentration, once the concentration of gold exceeds the concentration of other dopants, is a curve of extremely steep slope. In addition, drive-in experiments aimed at trying to force the gold into an equilibrium in the silicon, have shown resistivity values for wafers to be highly unpredictable after drive-in. A study is underway at IAMS to try to identify a method which will put a consistent and appropriate amount of gold into the wafers. The question still exists as to whether the gold can continue to migrate, or change the way it exists in the silicon lattice, after it has diffused into the silicon. Migration (movement of molecules within the lattice), or a change from interstitial to

substitutional lattice location will change the electrical properties of the device. If gold migration is possible, would it be possible to use isolation structures to limit where the gold could travel inside the device? The effect of too much gold could be counter balanced by defusing in phosphorous and the resistive properties of the device "tweaked" until they fall within acceptable limits. The feasibility and long term stability of these solutions are still unknown. Tests done on gold doped devices have found them to be unstable, subject to both drift and repeatability problems. The cause and cure for these problems is still under debate.

### **Process Variables**

The geometries possible for micro electro mechanical devices are limited by the manufacturing techniques used to produce them. The standard procedure for manufacturing involves: growing an oxide layer on a commercially produced single crystal silicon wafer, adding a photopolymer layer, exposing and developing the photopolymer, using the photopolymer as a mask to open holes in the silicon dioxide, stripping off the photopolymer and using the oxide as a mask to etch the silicon. Add to this process, adding metal for contacts and doping select areas with phosphorous and gold, and the number of process variables becomes a significant problem in successfully manufacturing the parts. In addition, many of these variables such as etching rates and doping amounts are difficult to



control. Currently there is no solution to this problem and loss rates as well as time to process are both very high. The redesigned flow sensor took into account both the number and complexity of the process steps required. The device was deliberately designed to be easier to manufacture.

### **Conclusion**

The micro-flow sensor is just one of a new breed of sensing devices which are rapidly being developed in this country and all over the world. The goal of micromachining is to produce three dimensional geometries which are more consistent, cheaper, and better than the devices which they are replacing.

Achieving that goal will require much more of an understanding of the devices themselves and the methods available to manufacture them than is currently available. Theory of operation needs to keep up with the actual devices which are now being produced in limited quantities in laboratories. Manufacturing methods need to provide more consistent control, and more manufacturing options are needed to increase the geometries available to the designer. People with a variety of backgrounds need to be brought to bear on the interdisciplinary nature of the problems at hand.

## CHAPTER 2

### REVIEW OF THE LITERATURE

"Some observers are saying that the ability to produce integrated circuits (ICs) that are functional in all three dimensions is comparable to the invention of the transistor in early electronics technology" (1)

#### **Why Microsensors?**

Classically a control system includes the following three items: sensor, controller and actuator. For many years the controller was the most expensive part of the loop. Improvements in the price/performance ratio for microprocessors led to distributed process control - introduced for the first time in the mid 1970's. In this system the computer was imbedded in a field mounted controller. Gradually a new generation of low cost controllers was developed. The 1980's saw the rapidly decreasing cost of digital signal processing yield a consecutive downward migration of microprocessors into transducers. Smart transducers and smart actuators came into the market offering an extended range of

1. Anon "Micromachining: A revolution in the making" Mechanical Engineering, Vol 111, N3, Mar. 1989, pp. 47-48

features including reprogrammability. Simultaneously the cost of a new generation of sensors, especially pressure transducers, started to move visibly downward as a result of the development of a new technology: the micromachining of silicon (1)(2). Micromachining was initially an expensive and exotic technology, but it was supported by the large solid-state technology research and development effort. It has been predicted that in the middle to late 1990's silicon microactuators will become an important commercial reality. (1)

Microsensors offer a unique host of attributes including potentially lower costs, higher accuracy and sensitivity and, of course, greatly reduced size. The monolithic nature of the sensor means that other electronic circuitry can be integrated on the same chip. A silicon sensor frequently can not isolate a single variable without compensating circuitry because it is so sensitive to external variables. (3) Smart sensors, which integrate signal processing on the same chip as the actual sensor, are only beginning to be explored.

1. Bryzek, Janusz; Mallon, Joseph R. Jr; Grace, Roger H. "Silicon's synthesis: Sensors to systems" InTech , Vol. 36, N1, Jan.1989, pp. 40-44
2. Buchy, Frank "Silicon Sensors Lead Pressure Transmitter Technology" Chilton's I&CS (Instrument and Control Systems), Vol. 60, N2, Feb 1987, pp.37-39
3. Anon "New on the Circuit: Solid State Pressure Sensors" Mechanical Engineering, Vol. 109, N 5, May 1987, pp.42-47

## **Mechanical properties**

Silicon makes up a quarter of all the natural resources of the earth's crust. It is harmless and is the only material on the earth that can be artificially mass-produced in the form of a very pure and nearly perfect crystal. It is well known for its electronic properties, but less well known and equally impressive are its mechanical properties (1). Silicon has the strength of steel and a great resistance to fatigue. It can be bent back and forth millions of times and will always return to its original shape without hysteresis. (2) The density of silicon is  $2.33 \text{ g/cm}^3$ , the modulus of direct elasticity is  $1.9 \times 10^{12} \text{ dyne/cm}^2$ , the bulk modulus of elasticity is  $7.7 \times 10^{11} \text{ dyne/cm}^2$ , the melting point is  $1,412 \text{ }^\circ\text{C}$ , the specific heat is  $.18 \text{ (18 } \sim 100 \text{ }^\circ\text{C) cal/g }^\circ\text{C}$ , the coefficient of thermal expansion is  $2.33 \times 10^{-6}$  (at room temperature) and the thermal conductivity is  $.3 \text{ cal/(s cm }^\circ\text{C)}$  (at  $20 \text{ }^\circ\text{C}$ ). The information above shows that silicon has excellent spring characteristics and therefore is a good material for diaphragms, beams and bridges. Many of these properties are dependent on direction. A large anisotropy appears in the piezoresistivity of the silicon crystal. An output which depends only on shearing stress can be obtained if the crystal orientation is such that

1. Igarashi, I "Semiconductor Dynamic Sensors" Sensors and Actuators, Vol. 13, N1, Jan. 1988, pp. 53-62

2. Anon "New on the Circuit: Solid-State Pressure Sensors" Mechanical Engineering, Vol. 109, N 5, May 1987, pp 42-47

if  $R_1$  is a resistor running parallel to the  $\langle 110 \rangle$  direction and  $R_2$  is a resistor running perpendicular on the same plane and the output signal is derived from a change in resistance. (1)

Making this high strength, highly versatile material into a sensor or actuator requires a whole new manufacturing science, and that science is called micromachining.

### Micromachining Technology

Micromachining has been defined as the technology of fabricating three dimensional structures on silicon wafers in a batch processing mode using in principle a technology developed for integrated circuits. (2) (3) (4) One article about etching defined micromachining as the removal of material from small dimensions that range from several microns to millimeters. (5) The latter

1. Igarashi, I "Semiconductor Dynamic Sensors" Sensors and Actuators, Vol. 13, N1, Jan. 1988, pp53-62
2. Bryzek, Janusz; Mallon, Joseph R. Jr.; Grace, Roger H. "Silicon's synthesis: Sensors to systems" InTech, Vol. 36, N1, Jan. 1989, pp. 40-44
3. Delapieere, Gilles "Micro-machining: A survey of the most commonly used processes" Sensors and Actuators, Vol.17 1-2 PT1, May3, 1989, pp.123-138
4. Linden, Y.; Tenerz, L.; Tiren, J.; Hok, B. "Fabrication of Three dimensional structures by means of Dopant-Selective Etching (DSE)" Sensors and Actuators, Vol. 16, 1989, pp. 67-82
5. Datta, Madhav; Romankiw, Lubomyr T. "Application of Chemical and Electrochemical Micromachining in the Electronics Industry" Journal of the Electrochemical Society, Vol. 136, N6, Jun.1989, pp. 285C-292C

definition emphasizes the etching mechanism and the scale which is one of the main features of this new technology. The first definition has several important parts. Integrated circuit (IC) fabrication technology is primarily a two dimensional process. Micromachining grew out of this technology when the etching and masking techniques were applied to the creation of three dimensional structures. Micromachining has progressed much because it has its origins in established IC technology, and by using accepted technology, micromachining has found more easy acceptance as a viable manufacturing technique. The total sensor R&D budget for all non-solid-state technologies may be on the order of \$500 million/year worldwide. A single integrated circuit technology, however, spends on the order of \$10 billion annually. This availability of funds has done much to drive micromachining research. (1) The batch processing portion of the definition is significant. The fabrication of thousands of sensors on the same silicon wafer would obviously lead to large economies of scale and therefore a lower price per sensor. (2) In addition to reduced manufacturing costs because of large lot sizes, the raw material itself

1. Bryzek, Janusz; Mallon, Joseph R. Jr.; Grace, Roger H. "Silicon's synthesis: Sensors to systems" InTech, Vol. 36, N1, Jan. 1989, pp. 40-44
2. Anon "New on the Circuit: Solid-State Pressure Sensors" Mechanical Engineering, Vol. 109, N 5, May 1987, pp 42-47

is prevalent and already available in the high quality single crystal form needed. "Small itself isn't the important feature; it's cheaper that is attractive in any application" (1)

What exactly are those processes which have been lumped under the general term of micromachining? The processes involved include etching, doping, oxidation, epitaxy, thin and thick film deposition, and lithography. (2) Structures are then fabricated by combinations of these steps. The heart of silicon microfabrication lies in the constraints and advantages of the etching of silicon.

### **Etching Silicon**

Material removed by chemical means dates back to 2,500 BC when the Egyptians etched copper jewelry with citric acid. The concept of masking for localized etching started in the 15th century AD when a vinegar based etchant was used in conjunction with linseed oil (mask) for decorating iron plate armor. In the 19th century hydrofluoric acid was discovered and used to etch glass. Photoresist and the concept of photoetching was developed and the basic principles of anodic removal of metal, by the passage of a DC

1. Rosen, Jerome "Machining in the Micro Domain" Mechanical Engineering, Vol. 111, N3, Mar 1989, pp. 40-46
2. Steckl, J. Microfabrication of Semiconductor Devices, Fall 1991, University of Cincinnati

current in a electrolytic cell, were discovered by Faraday. The 20th century applied these to industry. In the 1940's chemical machining was used to remove unwanted metal from printed circuit boards. Electrochemical machining was introduced in the late 1950's and early 1960's for finishing operations. (1) The micromachining technology was first developed at the IBM Research Laboratory in San Jose, California. (2) The main tools of micromachining are the etchants, both anisotropic and selective. Anisotropic etching means that different crystal planes are etched at significantly different speeds. This fact is used to create specific geometries including diaphragms, beams, and bridges. The processes for using etching fall into three groups: chemical anisotropic etching of single crystals, plasma etching, and sacrificial layer methods. (3)

The etching speed of a single crystal strongly depends on the crystalline orientation of the surface being etched, the cause of this anisotropy, however, is not clearly understood. The atomic density of the crystalline surface being etched seems to be a determining

1. Datta, Madhav; Romankiw, Lubomyr T. "Application of Chemical and Electrochemical Micromachining in the Electronics Industry" Journal of the Electrochemical Society, Vol. 136, N6, Jun.1989, pp. 285C-292C
2. Anon "Micromachining: A revolution in the making" Mechanical Engineering, Vol 111, N3, Mar. 1989, pp. 47-48
3. Delapieere, Gilles "Micro-machining: A survey of the most commonly used processes" Sensors and Actuators, Vol.17 1-2 PT1, May3, 1989, pp.123-138



factor, the slowest speed generally corresponding to the densest planes. In silicon the densest plane is the (111) plane, and nearly all profiles are etched following this plane. The principle anisotropic etching agents are mixtures of:

Ethylenediamine, Pyrocatechol, Water (EDP) (typically 750 ml - 120 g -240 ml at 115 °C) with an etching rate of 1.25 microns/min and a differential etching rate (100)/(111) of 35;

Hydrazine, Water (typically 50% / 50% at 118 °C) with an etching rate of 1.4 microns/min and a differential etching rate (100)/(111) of 16;

Potassium Hydroxide, Water (KOH) (typically 44 g - 100 ml at 85 °C) with an etching rate of 1.4 microns/min and a differential etching rate (100)/(111) of 400.

Of these three the most commonly used bath is aqueous KOH. KOH has most of the positive qualities (speed, dopant dependence, anisotropy) with the added advantage of safety. The biggest drawback of KOH is that it attacks SiO<sub>2</sub> masks at a significant rate. Many fabricators have overcome this drawback by using Si<sub>3</sub>N<sub>4</sub> as a mask, which can be purchased as part of the wafer. (1) Etching

1. Delapieere, Gilles "Micro-machining: A survey of the most commonly used processes" Sensors and Actuators, Vol.17 1-2 PT1, May3, 1989, pp.123-138

without applied current is termed chemical etching, photoetching, chemical milling, chemical blanking, or photochemical machining. Chemical micromachining (CMM) involves one or more chemical reactions by which a workpiece substrate is oxidized to produce a reaction product which is carried away from the surface of the medium. Although no external current is supplied, anodic and cathodic sights are present on the medium such that the rate of material removal (oxidation) is balanced by the rate of reduction of the etchant species. Stirring is an important part of controlling the reaction as agitation gets undepleted solution to the surface and thereby maintains a more uniform temperature which translates into a more constant etching rate. This same process can be used for metals as well as for silicon. Metal removal rates are on the order of 6 to 75 microns/minute. (1) When current is used to control the rate of the etching reaction, the process is called electrochemical etching. For electrochemical etching the workpiece is made the anode in an electrolytic cell. The cathode tool is separated from the anode by a narrow electrode spacing through which the electrolyte flows. When an electric current is passed through the cell the anode material dissolves locally. The electrolyte serves to remove the material and cool the workpiece. (1) (2) Electrochemical etching is

1. Datta, Madhav; Romankiw, Lubomyr T. "Application of Chemical and Electrochemical Micromachining in the Electronics Industry" Journal of the Electrochemical Society, Vol. 136, N6, Jun.1989, pp. 285C-292C

2. Faust, J.W.; Palik, E.D. "A study of the Orientation Dependent Etching and the Initial Anodization of Silicon in Aqueous KOH" Journal of the Electrochemical Society, Vol. 130, 1983, pp. 1413-1420

often preferred to standard chemical etching because of the improvement in control over the etch rate. Either method uses anode and cathode sights and is referred to as chemical etching. Because chemical etching is amenable to the mass-production methods of integrated circuits fabrication line and because it does not induce mechanical stress, chemical etching is the preferred method of sculpting silicon into the desired shape.(1)

Laser micromachining is one of the most promising of the different new micromachining techniques that are being investigated. Lasers can be used to generate maskless patterns using greatly enhanced rates of material removal on a local scale and can be focused down to make patterns with dimensions as small as several micron. (2)

Creating the desired geometry means not only controlling the etching rate but also the etching positions. A mask is used which allows etching only in the desired areas. The masking material depends on the etchant being used, silicon dioxide being the easiest to produce and the most versatile. The dimensions possible using this method are a function of the lithographic photochemical being used, and the expertise of the processor. Using X-ray lithography

1. Datta, Madhav; Romankiw, Lubomyr T. "Application of Chemical and Electrochemical Micromachining in the Electronics Industry" Journal of the Electrochemical Society, Vol. 136, N6, Jun.1989, pp. 285C-292C

2. Ibid.

processors can generate minimum dimensions in the .2 micron range, due to the reduced diffraction effects at shorter X-ray wavelengths. Device developers have not gone to such small dimensions because there is still a lot to learn at the level they are now working. (1)

While KOH, EDP and Hydrazine are by far the most common anisotropic etching agents, they are not the only ones possible. Wet chemical etching using ammonium hydroxide and water has been shown to be a good alternative to more traditional etchants. The etch rate of 9 wt. % at 75 °C is about 30 microns/hour, which is slightly lower than that for KOH, EDP or Hydrazine. The etchant showed excellent selectivity to SiO<sub>2</sub> and Si<sub>3</sub>N<sub>4</sub> and highly boron doped silicon. Aluminum was not attacked by silicon doped etchant when the silicon concentration in the etchant solution was higher than 0.1 gram/liter. This chemical is not as toxic as many other etchants and the etchant is anisotropic. The lowest etch rate was in the <111> direction. The pattern of an etch showing preferential crystal etching looks almost exactly as it did when the same pattern was etched with EDP. Stirring the etchant lead to a decrease in surface roughness although surfaces tend to be rougher than with the other etchants. Ammonium hydroxide is available from VLSI suppliers. (2)

1. Rosen, Jerome "Machining in the Micro Domain" Mechanical Engineering, Vol. 111, N3, Mar 1989, pp. 40-46
2. Schnakenberg, U.; Beneche, W.; Loechel, B. "NH<sub>4</sub>OH-based Etchants for Silicon Micromachining" Sensors and Actuators, A: Physical, Vol. 23, N 1-3, April 1990, pp.1036-1041

Any time wet anisotropic etching is done, convex corners are rapidly attacked. Corner compensation is a problem wherever it is desirable to leave a convex corner. Several studies on this subject have been done by Puers (1990) and by Ristic (1990). Puers examined the behavior of different etchants in terms of crystal orientation. The object was to come up with some ways to compensate corners. The square corner on top of the corner took up less material than other suggested compensation structures. Other structures such as the star corner took a lot of material and gave the same result. The secondary etching takes place in the (210) and (120) planes. The corner on corner was only tried for KOH. (1)

Ristic used a bridge structure to look at the effect of undercutting. The oxide bridge is required to be on the diagonal because of etch plane properties and the device would have to be laid down on top of the oxide. Because of what happens at the corners in etchants, it is recommended that structures not be laid any closer than 3 microns from an edge. (2)

Plasma etching uses a plasma instead of a liquid as the source for reagents. The main advantages of plasma etching are that the

1. Puers, B; Sansen, W. "Compensation Structures for Convex Corner Micromachining in Silicon" Sensors and Actuators, A: Physical, Vol. 23, N 1-3, April 1990, pp.1036-1041
2. Ristic, L.J.; Dhaded, A. C.; Chau, K.; Allegretto, W. "Edges and Corners of Multilayer Dynamic Microstructures" Sensors and Actuators, A: Physical, Vol. 23, N 1-3, April 1990, pp. 1042-1047

profiles obtainable are not dictated by the crystalline orientation and the plasma does not exert large forces on the microstructures. The disadvantages of plasma etching are the complexity of the set up and the number of parameters which must be monitored and controlled. The most feasible type of plasma etching is called reactive ion etching (RIE). In RIE the plasma is obtained by a glow discharge in a low-pressure gas, the substrates are placed on the electrode so that a large bias potential exists between the substrate and the plasma. This potential difference causes the positive ions to accelerate from the plasma to the substrate, and the ion bombardment causes the etching. Frequently polymer films act as a mask for this type of etching. The depth currently obtainable from this method is limited to a few tens of micrometers. (1) Reactive Ion Etching was used to make mini trenches which were refilled with polysilicon and planarized. (2)

Sacrificial layer methods involve freeing deposited or doped structures by means of under-etching another underlying thin layer. Although this is probably the oldest technique, the sacrificial layer method has not achieved the hoped industrial development, possibly due to the poor mechanical quality of polycrystalline materials.

1. Delapieere, Gilles "Micro-machining: A survey of the most commonly used processes" Sensors and Actuators, Vol.17 1-2 PT1, May3, 1989, pp.123-138

2. Pons, M.; Delpech, P.; Schiltz, A.; Inard, A. "Mini-trench Isolation: Trench Etching Oxidation and Refilling Planarization" Microcircuit Engineering 86, Proceedings of the International Conference of Microlithography, Interlaken Switzerland, Sept 23-25, 1986, pp 403-404

Advances have been made recently in controlling the internal stresses of polycrystalline silicon and interest in this technique is somewhat renewed. (1)

## Hydrazine

Mehregany and Senturia (1988) studied hydrazine as an etchant because "Hydrazine-water anisotropic etchant systems have been less thoroughly investigated than KOH or EDP"(2) Anisotropic etching using 50% / 50% hydrazine-water produces etching rates in (100) silicon at 115 °C of nearly 3 microns/minute which is higher than EDP solutions. The team reported the etching rate is reduced significantly in highly boron doped silicon ( $1.5 \times 10^{20}$  atoms/cm<sup>3</sup> stops the etch). No mention is made of the effect of high phosphorous doping on etching rates. When using EDP, etching has to be done in a specific temperature range to avoid formation of undesirable precipitates, and upon oxygen contamination the solution becomes darkly colored and it is hard to visually follow what is happening. EDP is carcinogenic. The differential etching rates of hydrazine are better than EDP but not as good as KOH.

1. Delapieere, Gilles "Micro-machining: A survey of the most commonly used processes" Sensors and Actuators, Vol.17 1-2 PT1, May3, 1989, pp.123-138
2. Mehregany, Mehran; Senturia, Stephen D. "Anisotropic etching of silicon in Hydrazine" Sensors and Actuators, Vol. 13, N 4, Apr. 1988, pp.375-390

Hydrazine is a suspected carcinogen and solutions containing hydrazine are explosive at high hydrazine concentrations, although a 50% / 50% dilution is considered stable. Safety precautions for using hydrazine should always be observed. (1)

### **Dopant Selective Etching (DSE)**

A modification to standard anisotropic etching is the use of dopants to selectively stop the etching of areas of the device. While it is known that the etch rate of highly boron-doped silicon substrates is slower in wet chemical anisotropic etchants, there is considerable disagreement as to the mechanism that actually produces this effect. Peterson (2) discusses two possibilities for this phenomenon. First at boron concentrations above  $5 \times 10^{19}$  atoms/cm<sup>3</sup> boron enters the lattice interstitially due to high tensile forces created in the lattice because of the substitutional boron atoms. The strong B-Si bond binds the lattice more rigidly, increasing the energy required to remove silicon atoms. An alternative explanation is that high enough surface concentrations of boron converted to boron oxides and hydroxides in an intermediate chemical reaction, passivate the surface and prevent further etching.

1. Mehregany, Mehran; Senturia, Stephen D. "Anisotropic etching of silicon in Hydrazine" Sensors and Actuators, Vol. 13, N 4, Apr. 1988, pp.375-390
2. Peterson, Kurt; Brown, Joseph "Standard manufacturing processes for advanced silicon sensor families" Technical Digest- IEEE Solid-State Sensor Conference Publ. by IEEE, NY, pp.31-33



The fact that KOH is not as effectively stopped by P+ regions together with the fact that KOH attacks oxide supports this explanation. (1)  
Etching takes the following steps:

- 1) Injection of holes into the semiconductor to raise it to a higher oxidation state
- 2) Attachment of OH- groups to the positively charged silicon
- 3) Reaction of the hydrated silicon with the complexing agent in the solution
- 4) The dissolution of the reacted products into the etching solution

If the dissolving rate is lowered, instead of the removal of material a passivating layer will grow on the surface which will slow down the etching. This is how a passivation layer could make DSE work. (2)  
Palik and colleagues also found evidence that the etch-stop

1. Mehregany, Mehran; Senturia, Stephen D. "Anisotropic etching of silicon in Hydrazine" Sensors and Actuators, Vol. 13, N 4, Apr. 1988, pp.375-390
2. Linden, Y.; Tenerz, L.; Tiren, J.; Hok, B. "Fabrication of Three dimensional structures by means of Dopant-Selective Etching (DSE)" Sensors and Actuators, Vol. 16, 1989, pp. 67-82

mechanism is a passivation layer formed during etching when they studied anisotropic etching of both KOH and EDP.(1) In further experiments a slush-layer was observed to build up on surfaces in directions that were selectively etch-stopped by doping. Their model suggests that the cathodic slush layer is formed when water attacks silicon back bonds but then OH- attack is inhibited. An insoluble hydrogenated silicate forms which sticks to the surface. The subsequent water attack continues and the slush layer thickens. This slush layer was observed to grow faster on the n-Si (111) plane (etch stopped) than on the p-Si (111) plane (still etching).(2) Riley, Sugiyama and Van Duzer (1984) posed the argument that the etch rate is only dependent on the hole concentration and not the atomic concentration of boron or stress. According to Raley, the etch rate ratio can be used to determine the hole concentration at heavily boron-doped silicon surfaces.(3) Raley's work also pointed to the need for a high enough density of the dopant material. As the amount of dopant decreased the etching rate rapidly dropped off. After an extensive study of highly boron doped silicon in EDP, the etch-ratio dependence of (100) silicon for high boron doping was

1. Palik, E.D.; Bermudez, V.M. ; Glembocki, O. J. "Ellipsometric Study of the Etch-Stop Mechanism in Heavily Doped Silicon" Journal of the Electrochemical Society, Vol 132, N 1, Jan. 1985, pp. 135-141
2. Raley, N. F.; Sugiyama, Y.; Van Duzer, T. "(100) Silicon Etch Rate Dependence in Boron Concentration in EDP water solutions" Journal of the Electrochemical Society, Vol. 131, 1984, pp. 161-171
3. Glembocki, O.J.; Stahlbush, R.E.; Tomkiewicz, M. "Bias-Dependent Etching of Silicon in Aqueous KOH" Journal of the Electrochemical Society, Vol. 132, 1985, pp. 145-151

found to decrease at a concentration of boron approximately on the order of  $10^{19}$  atoms/cm<sup>3</sup>. The decline followed a -4.3 power law dependence on average over three orders of magnitude of etching rate ratio.(1) For electrochemical etching using boron or phosphorous as an etch stop there is almost no effect on etching rate for concentrations up to  $N=10^{19}$  atoms/cm<sup>3</sup>. For concentrations greater than that there is a dramatic decrease in etching rate (etchstop) (2)

Bias-controlled, doping selective etching of silicon was reported early by Waggener (1970) and before that by Greenwood (1969) who discovered preferential etching of p-n junctions. "Despite its early discovery, doping selective etching has not received much attention from the research community involved in sensor and actuator development except just recently when we have seen reports on work where the DSE techniques have been used in sensor applications." (3) The advantages of DSE are that the finished pieces have no internal strain and can exploit the full strength of single crystal silicon. There are also several options for doping which will

1. Mehregany, Mehran; Senturia, Stephen D. "Anisotropic etching of silicon in Hydrazine" Sensors and Actuators, Vol. 13, N 4, Apr. 1988, pp.375-390
2. Lu, Shi-Ji; Zheng, Zheng; Tong, Qin-Yi "New Silicon Micromachining Methods using SOI/SDB Technology" Sensors and Actuators, A: Physical, Vol. 23, N 1-3, Apr. 1990, pp. 961-963
3. Linden, Y.; Tenerz, L.; Tiren, J.; Hok, B. "Fabrication of Three dimensional structures by means of Dopant-Selective Etching (DSE)" Sensors and Actuators, Vol. 16, 1989, pp. 67-82

give either high surface concentrations or peak concentrations buried under the surface increasing the possibilities for geometries.

(1) An etch stop dopant for one etch chemical or substrate does not always yield the same results for other etchants or substrates. When silicon dioxide is doped and etched in hydrofluoric acid, a high concentration of boron, which converts the oxide ( $\text{SiO}_2$ ) into borosilicate glass, results in a much lower etching rate. On the other hand a high concentration of phosphorous which converts the oxide into phosphosilicate glass results in a very high etch rate. (2)

Dopant Selective Etching (DSE) is used to overcome problems of thickness controllability and surface roughness. Problems occur using DSE because the differential etching rate is only about 10-100 times, moreover it is difficult to obtain the abrupt profile changes especially with deep profiles. (3) Many unique geometries have been produced using this dopant selective etching. Several of these will be described in the following section.

1. Linden, Y.; Tenerz, L.; Tiren, J.; Hok, B. "Fabrication of Three dimensional structures by means of Dopant-Selective Etching (DSE)" Sensors and Actuators, Vol. 16, 1989, pp. 67-82
2. Datta, Madhav; Romankiw, Lubomyr T. "Application of Chemical and Electrochemical Micromachining in the Electronics Industry" Journal of the Electrochemical Society, Vol. 136, N6, Jun.1989, pp. 285C-292C
3. Anon "Silicon Micromachining Technology: A Primer" Automotive Engineering, Vol. 94, N 4, Apr. 1986, pp. 61-66

## **Fabrication Techniques and Devices Created With Them**

Closed loop control has three components: controllers, sensors and actuators. While the declining cost of manufacturing integrated circuits has made digital computation as that used in controllers relatively inexpensive, sensors continue to comprise a large portion of the cost of a system. Micro-machining shows the promise of changing that. Current sensors will be replaced by devices much smaller, cheaper and more accurate. These sensors include current development being done to measure temperature, acceleration, gas and fluid flow, chemical composition, humidity, acoustics, tactile forces, and many other analog variables. (1) The first step in development is to produce a working sensor which can monitor the desired parameter.

The first generation devices of micromachining are many and varied, yet they are the products of a limited repertoire of simple geometric configurations that severely limit mechanical design capabilities for micromechanical devices. (2) There are several commonly used mechanical structures with which the device designer creates a sensor or actuator. These structures include diaphragms, beams, holes and bridges. Linden et al summarized the

1. Anon "New on the Circuit: Solid State Pressure Sensors" Mechanical Engineering, Vol. 109, N 5, May 1987, pp.42-47
2. Rosen, Jerome "Machining in the Micro Domain" Mechanical Engineering, Vol. 111, N3, Mar 1989, pp. 40-46

different 3-D structures which are now possible by using DSE. The highlight of this study was the description of the creation of thin membranes (diaphragms) and cantilever beams. (1)

### **Diaphragms and Pressure Sensors**

Pressure sensors account for 50% of total dollars spent in sensors. For the pressure sensor a diaphragm etched from silicon acts as the basic sensing element. (2) Despite the realization of many different micromachined structures for pressure sensing, only the diaphragm type is mass produced because of the strict requirements of industry including the sensors ability to withstand dust, vibration, high temperatures and contaminative environments. (3) Once the diaphragm is constructed there are several ways to detect pressure changes, however, only three methods are commonly employed: capacitance, piezoresistance and resonant or vibrating wire. Of these the capacitive method type is the most popular with piezoresistive

1. Linden, Y.; Tenerz, L.; Tiren, J.; Hok, B. "Fabrication of Three dimensional structures by means of Dopant-Selective Etching (DSE)" Sensors and Actuators, Vol. 16, 1989, pp. 67-82
2. Anon "New on the Circuit: Solid State Pressure Sensors" Mechanical Engineering, Vol. 109, N 5, May 1987, pp.42-47
3. Stoev, Ivan Georgiev; Yankov, Rossen Angelov; Jeynes, Chris "Formation of Etch-Stop Structures Utilizing Ion-beam Synthesized Buried Oxide and Nitride Layers in Silicon" Sensors and Actuators, Vol. 21, N 1-3, 2 PT2, 1990, Pp. 267-270

method second. (1) Structures with thin diaphragms are used not just as the basis of pressure sensors, but also for pressure switches, load cells, strain sensors, and displacement sensors. (2) A capacitive tactile sensor was manufactured using micromachining of KOH with SiO<sub>2</sub>/Si as the etch stop boundary. The tactile sensor used two oxidized wafers fused together and then etched out the structure. The diaphragm produced was nice and flat and the thickness was easy to control. (3) The diaphragm deformed as it moved over a surface and the capacitance of the structure changed. For piezoresistive devices thick-film or thin-film resistors may be deposited on the diaphragm in a Wheatstone bridge configuration. Stress on the diaphragm causes a current imbalance in the bridge. (4) Many devices use Wheatstone bridge configurations including the current design for the University of Cincinnati's flow sensor version 10.0.

A typical silicon diaphragm is formed by back-side etching which is combined with various schemes in controlling the diaphragm thickness profiles. An example might be a p<sup>+</sup> diffusion or

1. Buchy, Frank "Silicon Sensors Lead Pressure Transmitter Technology" Chilton's I&CS (Instrument and Control Systems), Vol. 60, N2, Feb 1987, pp.37-39
2. Rosen, Jerome "Machining in the Micro Domain" Mechanical Engineering, Vol. 111, N3, Mar 1989, pp. 40-46
3. Anon "Silicon Micromachining Technology: A Primer" Automotive Engineering, Vol. 94, N 4, Apr. 1986, pp. 61-66
4. Anon "New on the Circuit: Solid State Pressure Sensors" Mechanical Engineering, Vol. 109, N 5, May 1987, pp.42-47

a slight etch on the wafer's front side. P-stop techniques are used to form diaphragm thicknesses of 5 - 10 microns and V-grooved techniques are used for thicknesses greater than 20 microns. Typical square diaphragms range in size from a few hundred micrometers to a few millimeters. Thin film deposition is also used to form ultra thin diaphragms with typical thickness being about 2 microns. One of the problems in making dielectric diaphragms is the need to protect against a rupture caused by thermal stresses which accumulate during deposition of the dielectric layers. It is interesting to note that diaphragms are the most common automotive sensing structure.(1)

The simplest way of producing thin silicon diaphragms is known as the time-stop approach. The disadvantage of this method is that the final thickness varies greatly, resulting in a low manufacturing yield. Implantation of oxygen or nitrogen have made possible buried etch stop layers. Implantation does cause damage to the underlying crystal structure and post implantation annealing is often required especially for nitrogen etch-stop structures. Another, and probably the major drawback to this approach is that it takes a very high power ion implanter. Such machines are now available, but still expensive. (2)

1. Anon "Silicon Micromachining Technology: A Primer" Automotive Engineering, Vol. 94, N 4, Apr. 1986, pp. 61-66
2. Stoev, Ivan Georgiev; Yankov, Rossen Angelov; Jeynes, Chris "Formation of Etch-Stop Structures Utilizing Ion-beam Synthesized Buried Oxide and Nitride Layers in Silicon" Sensors and Actuators, Vol. 19, N 2, Aug. 1989, pp. 183-197



A novel approach to the manufacture of diaphragms was a sandwich structure of Si/Al<sub>2</sub>O<sub>3</sub>/Si. The structure was made as an epitaxial stack. This sandwich was used to produce very repeatable diaphragms because the etching could be stopped at the aluminum oxide boundary quite easily. This makes possible many structures and is very interesting. Unfortunately this structure would be very difficult to make on a lab scale. When and if industry produces this structure the geometries possible would be greatly increased. (1)

Other methods of sensing pressure are also novel but more complex. A novel pressure sensor consisting of a resonator enclosed in a cavity was recently produced. The enclosed cavity resonator had many advantages including isolation from potentially corrosive environments, however the method used to construct the device was a drawback. The process was extremely complex involving epitaxy grown on top of epitaxy and employing electrochemical etching and hydrogen evacuation of the chamber.(2) Diaphragms can be used to create structures to measure gases. Certain phthalocyanine

1. Ishida, Makoto; Ashiki, Mitsuaki; Sawada, Kazuaki; Yamaguchi, Shinsuke; Nakamura, Tetsuro "Epitaxially Stacked Structures of Si/Al<sub>2</sub>O<sub>3</sub>/Si for Sensor Materials" Sensors and Actuators, A: Physical, Vol. 21, N 1-3, 2 PT2, 1990, pp.267-270
2. Ikeda, Kyoichi; Kuwayama, Hideka; Kobayashi, Takashi; Watanabe, Teysuya; Nishikawa, Tadashil Yoshida, Takashi; Harada, Kinji "Three-dimensional Micromachining of Silicon Pressure Sensor Integrating Resonant Strain Gauge on Diaphragm" Sensors and Actuators, A: Physical, Vol. 23, N 1-3, Apr. 1990, pp. 1007-1010

compounds become conductive when fractionally oxidized (doped). The known capacity for some of these compounds to conduct has led to an interest in their use as microelectronic gas sensors. The gas concentration is measured by the conductance change. The film temperature effects on sensitivity and the rise and decay times have been studied experimentally. Different gases have different temperatures where their response peaks. The response and recovery times are on the order of a minute. (1)

### **Cantilever Beams and Accelerometers**

Suspended mass structures are used to make vibration sensors, accelerometers, and flow sensors. (2) The mass is created at the end of one or more cantilevered beams in order to increase the deflection of the beam with acceleration. The deflection sensing electronics, usually strain gauge types of structures, are placed on the beams. The sensitivity of the device to acceleration is determined largely by the size and number of beams supporting the same mass.

1. Wang, H. Y.; Ko, Wen H.; Batzel, D.A.; Kenny, M. E.; Lando, J. B. "Phthalocyanine Langmuir-Blodgett Film Microsensors for Halogen Gasses" Sensors and Actuators, B: Chemical, Vol. B1, N1-6, 1 PT1, 1990, pp.138-141
2. Rosen, Jerome "Machining in the Micro Domain" Mechanical Engineering, Vol. 111, N3, Mar 1989, pp. 40-46

Several accelerometers have been fabricated by different groups including the University of Cincinnati in conjunction with Sensotech of Columbus, OH. UC's design has two cantilever beams supporting the mass to reduce the amount of twisting that occurs when the device is working. The beam structure is placed in a cavity formed by fusing on another wafer with etched pits. Damping can be controlled by filling the cavity with various fluids. There are several ways to create a suspended mass or beam structure. The most critical part is producing the beam itself. An accelerometer made by etching from the back to get a membrane using an electrochemical etch stop, then etching from the front to get cantilever beams was described by Yamado, Higuchi, and Tanigawa (1990).(1) Linden, Tenerz, Tiren and Hok (1989) used DSE to create the cantilever beams and thin membrane structures for their components. The etch stop boron was diffused down to the desired thickness then the etching was done leaving a thin membrane. The cantilever beam took two etchants, one that was not dopant-selective to get through the doped layer and then one that was to cut the U shaped channel and then undercut the beam. (2)

1. Yamado, K; Higuchi, K.; Tanigawa, H. "Novel Silicon Accelerometer with a Surrounding Mass Structure" Sensors and Actuators, A: Physical, Vol. 21, N 1-3, 2 PT2, 1990, pp. 308-311
2. Linden, Y.; Tenerz, L.; Tiren, J.; Hok, B. "Fabrication of Three dimensional structures by means of Dopant-Selective Etching (DSE)" Sensors and Actuators, Vol. 16, 1989, pp. 67-82

Performance of an accelerometer is measured by sensitivity, durability, and accuracy. Two ways to increase sensitivity are to increase seismic mass or to increase beam flexibility. Thinning the beams leads to a degradation in the temperature characteristics caused by thermal expansion (1) Cantilever beam structures are used for a variety of sensors besides accelerometers. A batch-fabricated non-reversible valve with a cantilever beam was manufactured by Tiren, Tenerz and Hok (1989). The force, pressure, and deflection characteristics of the valve were all excellent. The structure was made of two wafers, each with its own structure which had been fused together. The top layer had anisotropically etched holes and the bottom layer had cantilever beams which covered the holes. Pressure from the hole side would move the cantilever beam and allow fluid to flow, pressure from the reverse side would force the beam to cover the hole and prevent flow.(2) Several pumps have been developed in which each valve was a cantilever beam structure. A peristaltic piezoelectric fluid pump was developed at Stanford University by Smits in 1980. Improving on that design a two valve and three valve pump have been designed both having a glass/silicon/glass underlying sandwich structure in 1988. (3)

1. Tiren, J.; Tenerz, L.; Hok, B. "Batch fabricated Non-reverse Valve with Cantilever Beam Manufactured by Micromachining of Silicon" Sensors and Actuators, Vol 18, n 3-4, Jul. 1989, pp.389-396

2. VanLintel, H. T. G.; Van De Pol, F. C. M.; Bouswstra, S. "Piezoelectric Micropump Based on Micromachining of Silicon" Sensors and Actuators ,Vol. 15, N2, Oct. 1988, pp. 153-167

3. Barth, Philip W. "Silicon Fusion Bonding for Fabrication of Sensors, Actuators and Microstructures" Sensors and Actuators, A: Physical, Vol. 23, N1-3, Apr. 1990, pp. 919-926

At Case Western Reserve University in Cleveland, Ohio, scientists have micromachined a constant flow-rate silicon microvalve actuator for patients with hydrocephalus (excessive fluid in the cranium). (1)

Many of the beam structures, including several just described, take advantage of a technology that allows silicon wafers to be bonded to other silicon wafers or to special glasses. Silicon fusion bonding (SFB) means the joining together of two silicon wafers without the use of adhesives. Much of the credit for the development of SFB goes to Kurt Peterson of Novasensor, a company founded in October of 1985. To create a fusion bond, two wafers are placed together and the temperature increased until the adjoining surfaces begin to form bonds between them. Time is needed at this elevated temperature for pockets of gasses to diffuse out through the lattice and for all of the bonding across the face to be complete. The bond strength of the final product approaches the yield strength of single crystal silicon, and is typically on the order of 1 GPa. A drawback is that extreme cleanliness is required. Barth (1990) comments that the economics of the technique are not favorable for very large scale integration as compared to competing techniques, but the economic considerations are favorable for both power

1. Anon "Micromachining: A revolution in the making" Mechanical Engineering, Vol 111, N3, Mar. 1989, pp. 47-48

devices and silicon microstructures. He also feels that the complexity of the process will limit the serious pursuit of SFB.(1) Similar to SFB, glass structures can be bonded to silicon devices. When an electric field is applied between borosilicate glass and the silicon wafer at an elevated temperature (about 450 °C) a seal is formed which can be used to protect fragile sensor elements. Corning 7740 glass is frequently used as it has the same expansion characteristics as silicon. (2) Sometimes the glass serves as part of the structure itself as many glasses can be effectively etched like silicon and are also good electrical insulators.

### **Holes, Grooves and Filters**

An etch pit forms when local etching is faster than that of the bulk crystal and a hillock will form when the local etching is slower than that of the base plane. (3) If a pit goes deep enough the structure created is a hole, if the pit is long but does not cut through the base silicon the result is a channel or groove.

A gas chromatograph composed entirely of finely etched

1. Jaccodine, R.J. "Use of Modified Free Energy Theorems to Predict Equilibrium Growing and Etching Shapes" Journal of Applied Physics, Vol. 33, 1962, pp. 2643-2647
2. Anon "Silicon Micromachining Technology: A Primer" Automotive Engineering, Vol. 94, N 4, Apr. 1986, pp. 61-66
3. Kittilsland, Gjermund; Stemme, Gorsn; Norden, Bengt "Submicron Particle Filter in Silicon" Sensors and Actuators, A: Physical, Vol. 24, N 1-3, Apr. 1990, pp. 904-907

grooves and channels on a single chip, was developed at Stanford University. This device has served as the core of commercial chromatograph instruments for several years. Manufactured and marketed by Microsensor Technology (Fremont, California) its major application has been in on-line monitoring of gas components inside natural gas lines.(1)

Filters made of micromachined silicon have been reported several times in the literature recently. Kittilsland, Stemme, and Norden (1990) created a novel filter based on a two-step self-aligning fabrication process using lateral boron doping for DSE, anisotropic silicon etching and silicon dioxide undercut etching. They used the same holes which were created to let the fluid through to align the boron doping etch stop. The etchant used was EDP. They achieved a run-on hemispherical pattern created by the boron doped areas. The result of their work was a multiple purpose screen filter structure that filters particles down to 50nm.(2) Other devices which use the groove or hole geometry include brain probes, microminiature molds, valves, nozzles, switches, and fluid amplifiers (3)

1. Anon "Micromachining: A revolution in the making" Mechanical Engineering, Vol 111, N3, Mar. 1989, pp. 47-48
2. Wolffenbuttel, M. R.; Retien, P.P.L "Design Considerations for a Silicon Capacitive Tactile Cell" Sensors and Actuators, A: Physical, Vol. 24, N 3, Sept. 1990, pp. 187-190
3. Rosen, Jerome "Machining in the Micro Domain" Mechanical Engineering, Vol. 111, N3, Mar 1989, pp. 40-46

### **Bridges and Their Uses**

Bridges are actually difficult to create. The undercutting of secondary planes by anisotropic etchants would, at first, make bridge structures appear easy. This process was not very applicable to a bridge because anisotropic etching does not expose any secondary planes and the bridge is not undercut. Creating SiO<sub>2</sub> bridges over silicon pits requires very careful alignment with the crystal planes. A diagonal bridge with etch pit sides parallel to the (100) plane will have the advantage of quick etch times but the cavity sides will also be undercut. If the pit sides are parallel to the (110) plane the bridge will not be completely under etched, so there is not true bridge structure. "Still, this is the only way to form bridges."<sup>(1)</sup> Diagonal bridges can be formed suspended over a cavity because two etch pits started on either side of this structure will eventually interconnect under the silicon bridge and secondary planes will remove the material leaving the oxide hanging. Drawbacks to this method include the rather large side area required for the pit, and the limitation on the geometry. In addition, bridges created by this method have saw-tooth sides which are not as strong as smooth side bridges because of stress risers.

1. Linden, Y.; Tenerz, L.; Tiren, J.; Hok, B. "Fabrication of Three dimensional structures by means of Dopant-Selective Etching (DSE)" Sensors and Actuators, Vol. 16, 1989, pp. 67-82



Device makers have tried several tactics to circumvent bridge fabrication problems and have met with limited success. The most common method to create a bridge is to deposit a polysilicon structure on top of silicon dioxide. The silicon dioxide can be preferentially etched away with a buffered hydrofluoric acid leaving the polycrystalline bridge. One of the drawbacks to this method is that polysilicon structures are a fraction of the strength of single crystal silicon structures. A tactile cell (capacitive force sensor) was fabricated as a polysilicon bridge on top of a silicon wafer by Wolffenbittel and Retien (1990). The structure was difficult to make and the researchers felt that more work was needed to reduce the structural problems.(1) The fabrication of microbridges, cantilever beams and gears etc. by putting polysilicon over silicon dioxide and then removing the oxide to free the geometry has only a few commercial sensors being made with this technology. The main reason, according to Parmameswaran, Ristic, Dhaded, Baltes, Allegretto and Robinson (1989), was the incompatibility between these techniques and traditional IC techniques. Their recommendation was to go with a diagonal microbridge structure because using a mask and etching silicon would go along with traditional IC methods. (2)

1. Wolffenbittel, M. R.; Retien, P.P.L "Design Considerations for a Silicon Capacitive Tactile Cell" Sensors and Actuators, A: Physical, Vol. 24, N 3, Sept. 1990, pp. 187-190
2. Parmameswaran, M.; Ristic, L. J. ; Dhaded, A.C.; Baltes, H.P.; Allegretto, W.; Robinson, A.M. "Fabrication of Microbridges in Standard Complementary Metal Oxide Semiconductor Technology" Canadian Journal of Physics, Vol 67, N 4, Apr. 1989, pp. 184-189

Another novel approach to creating a bridges structure was achieved by Bouwstra, Legtaenberg, Tilmans, and Elwenspoek (1990). A v-grove channel under a thin Si<sub>3</sub>N<sub>3</sub> bridge was fabricated for a flow sensor application. The geometry was achieved by using a (110) wafer rather than the standard (100) wafer. In this way secondary planes were exposed and thin silicon bridges could be created. (1) Unfortunately, (110) wafers are not the standard type used, and other geometries which would need to be on the device would be drastically effected by this change.

### **Future Applications**

A recent NSF report speculated on some possible future applications for micromachined structures. Microminiature scissors and a buzz saw for delicate microsurgical procedures, microminiature machines that can scrape fatty deposits from clogged arteries to lesson the chance of heart attacks and "smart" pills that can be implanted in humans and animals to dispense a precise amount of medication through microscopic valves were all considered possible. (2) At MIT's Artificial Intelligence Laboratory there is a plan to build a single-chip microrobot that contains sensing, guidance and

1. Bouwstra, Siebe; Legtenberg, Rob; Tilmans, Harrie A.C.; Elwenspoek, Miko "Resonating Microbridge Mass Flow Sensor" Sensors and Actuators, A: Physical, Vol. 21, N 1-3, 1 PT2, 1990, pp. 332-335
2. Anon "Micromachining: A revolution in the making" Mechanical Engineering, Vol 111, N3, Mar. 1989, pp. 47-48

control systems attached to a macroscopic airfoil. (1) (2)

## **Flow Sensors**

Many descriptions of mass flow sensors of different configurations can be found in the literature. Each sensor design has its own unique features. An overview of several of the most recent designs, as well as how they compare to the University of Cincinnati's flow sensor version 10.0 is given below.

A flow sensor was designed and produced by Johnson and Higashi (1987). It was constructed of a temperature sensitive metal resistance film laminated within a 0.1 micron thick film of dielectric material and suspended in the form of two bridges over an etched pit in silicon. The bridge structure was an oxide bridge with the metal deposited on top. The bridge was created by placing it diagonally on the crystal so that the etch pits are diamond shape and intersect under the bridge and then undercut it. The bridge itself has the dimensions of 0.4 x 0.5 mm and the pit depth is 0.13 mm. This design achieves excellent thermal isolation because the oxide is an insulator. Most of the heat in a no flow case was lost out the bottom to the air and then the base silicon, rather than being

1. Anon "Micromachining: A revolution in the making" Mechanical Engineering, Vol 111, N3, Mar. 1989, pp. 47-48
2. Bryzek, Janusz; Mallon, Joseph R. Jr; Grace, Roger H. "Silicon's synthesis: Sensors to systems" InTech , Vol. 36, N1, Jan. 1989, pp. 40-44

conducted out the bridges. The small mass of the bridge gives it a fast response time 0.003 sec and the bridge itself gets quite hot while the rest of the device is within 1 °C of ambient. The designers noted that different gas compositions affected the flow rate readings, which they attempted to nullify by placing a heat sink resistor on the main chip as a compensation point. The effect of temperature change was adequately handled this way, but gas composition is not totally taken care of. This fact is very interesting as it is unknown how the University of Cincinnati's flow sensor version 10.0 will respond to variations in gas composition in a natural gas pipeline. The thin film metal resistors are not linear in their response and this had to be compensated for in the circuitry. This design was not useable if the sensor is immersed in water or another media which thermally shorts the metal bridge to the silicon etched pit. The designers also placed a filter before the sensor in the air flow to keep dust from clogging the reading. With the filter in place the dust collection during extended durability tests was not significant. The bridge itself was hot enough that water vapor did not condense on it. (1)

Another flow meter was described by Tai and Muller (1988). The structure was a polysilicon bridge 0.2 mm long, 0.005 mm wide and 0.0015 mm thick with a lightly doped region 0.0019 mm long at

1. Johnson, R.G.; Higashi, R.E. "A Highly Sensitive Chip Microtransducer for Airflow and Differential Pressure Sensing Applications" Sensors and Actuators, Vol. 11, 1987, pp.63-72

the center. The device had a power requirement of 2 mW for "acceptable" sensitivity at moderate flow rates. This is a second generation device, the first had problems that the heat generated by the polysilicon was thermally shorted out by the underlying silicon substrate. Thermal shorting/isolation problems are a consistent theme for all of the flow sensors reported. The current device was made by creating an elevated glass platform for the polysilicon deposition and then etching out the glass leaving glass posts and the bridge itself suspended in air similar to the current University of Cincinnati's flow sensor version 10.0 configuration. Unlike flow sensor version 10.0 the silicon is used only as a base platform and the structure is made of the composite layers which were deposited on top. Again polysilicon forms the main structure which is not as strong as single crystal silicon. The edges of the bridges were heavily doped to provide thermal isolation and low resistance for electrical conduction. (1)

Honeywell's Micro Switch Division (Freeport, Ill) sells a low-air flow sensor that employs microbridge structures whose technology was developed at Honeywell's Physical Sciences Center (Bloomington, Minnesota) Called the AWM2000 Series Microbridge, it measures differential pressure from either 0.0 to 0.2 or 0.0 to 2.0 inches of

1. Tai, Y. C.; Muller, R. S. "Lightly Doped Polysilicon Bridge as a Flow Meter" Sensors and Actuators, Vol 15, 1988, pp. 63-75

water column full scale and air flow rates as low as 1 cm<sup>3</sup>/min. It is being used in medical respiratory-related functions and commercial building controls. Temperature sensitive resistance films are laminated within a thin film of thermally isolated dielectric material that is 1 micron thick. The films are suspended in the form of two adjacent bridges over an etched cavity in a silicon wafer. The bridges are 400 microns wide and 500 microns long. This is much larger than the 16 micron bridges for UC's flow sensor. The cavity depth is 130 microns. During operation the upstream resistor is cooled by air flow and the downstream resistor is also cooled but not as much. The differential developed is a measure of the flow rate.(1)

A high sensitivity two dimensional flow sensor with an etched thermal isolation structure measures flow by detecting temperature differences in two directions on a heated membrane. This allows flow direction to also be determined. The first experiments with this device show a typical 3 degree error in direction and 5% error in flow velocity. The device structure is a thin membrane suspended by four thin beams from a solid rim. The rim is used as a reference to ambient temperature. The membrane is heated and two thermocouples measure the temperature at two perpendicular places on the membrane. This configuration is very different from the

1. Anon "Micromachining: A revolution in the making" Mechanical Engineering, Vol 111, N3, Mar. 1989, pp. 47-48

three devices just described and the University of Cincinnati device in that those devices used the change in resistance of a Wheatstone bridge rather than thermocouples to give the output reading. Similar to the Wheatstone bridge the thermocouple voltages are proportional to the temperature difference. The sensor is 6 mm by 6 mm, considerably larger than the present University of Cincinnati design. The heat transfer analysis for this model included several experimental values for the heat transfer coefficient. The membrane had an average ambient overheat of 17 K. (1) Of the devices mentioned in the literature which had measured the overheat of a bridge all were in the 17 K - 24 K overheat range.

Another fundamentally different way to measure flow is to measure the change in resonant frequency of a microbridge. This frequency change depends on the temperature of the bridge. Two examples of this application have been recently constructed. Bouwstra, Legtenberg, Tilmans, and Elwenspoek (1990) developed a flow sensor which was made of very thin bridges of  $\text{Si}_3\text{N}_4$  suspended over a v-channel. The bridges have different natural frequencies when they are at different temperatures due to different geometries

1. Van Oudheusden, B. W.; Wan Herwarden, A. W. "High-Sensitivity 2-D Flow Sensor with an Etched Thermal Isolation Structure" Sensors and Actuators, A: Physical, Vol. 22, N 1-3, 3PT3, 1990, pp. 425-430

because of thermal expansion. (1) A surface acoustic wave (SAW) device has also been used to measure gas flow. The output of the device is the frequency of vibration of a membrane which changes with temperature. A previous SAW device did not work well because it was not thermally isolated and it was poorly packaged. SAW devices have several advantages including linearity, sensitivity, accuracy and ease of conversion from analog to digital. (2)

The University of Cincinnati's flow sensor version 10.0 is fundamentally a hot wire anemometer on a silicon chip. The legs are electrically, thermally and mechanically separated from each other by etching, the silicon/silicon dioxide bridge being the only connection. The entire sensor is bonded into glass for strength. There is some debate as to where in the process this is best done (or if it is needed) as strength while being processed becomes an issue. The active component of the sensor is a Wheatstone bridge which is heated above ambient temperature by the resistors supplied by a current. Gas flowing over the sensor will preferentially cool the front and back legs which are perpendicular to the flow, more than the

1. Bouwstra, Siebe; Legtenberg, Rob; Tilmans, Harrie A.C.; Elwenspoek, Miko "Resonating Microbridge Mass Flow Sensor" Sensors and Actuators, A: Physical, Vol. 21, N 1-3, 1 PT2, 1990, pp. 332-335
2. Joshi, Shrinivas G. "Uses of a Surface-Acoustic Wave (SAW) Device to Measure Gas Flow" IEEE Transactions on Instrumentation and Measurement, Vol. 38, N 3, Jun. 1989, pp. 824-826



two side bridges which are parallel to the flow. This differential cooling takes its origin from classic boundary layer theory. To increase heat transfer the bridges are made as long and thin as possible. The device is doped with gold to increase its sensitivity to very small changes in fluid flow rate. The original structure which did not have the legs separated had an estimated 90% of the current shorted out through the external crystal structure. When the legs were separated, only 10% of the original drive current was required. Dr. Henderson predicts that future devices could have a response time in the nanosecond range. (1) The Society of Automotive Engineers point out that mass flow sensors, with thin-film hot anemometers fabricated on thin dielectric diaphragms or bridge structures will exhibit a thermal response time of less than 5 - 10 ms. This fast response time means real-time data can be fed into a central processor for more efficient engine control. (2) Similarly other applications can use the response time already available from this device for real time measurement and control.

The core of many flow sensors is a Wheatstone bridge which is created on micromachined bridge structures. These bridges are not the classical oxide bridges suspended over silicon pits as described earlier, but rather thin polysilicon silicon beams with silicon

1. Henderson, H. Thurman; Hsieh, Walter " A Miniature Anemometer for Ultrafast Response" Sensors, Dec. 1989, pp. 22-26
2. Anon "Silicon Micromachining Technology: A Primer" Automotive Engineering, Vol. 94, N 4, Apr. 1986, pp. 61-66

underneath them, or as in UC's case, silicon beams with nothing under them. Van Putten recently conducted a study which looked at Wheatstone bridge configurations. Much of his time was spent on heat transfer and how it effects the output of the bridge. The device used as an example was 4 mm square with low level P-type doping by ion implantation. An equation was given for the magnitude of the resistors as a function of temperature, and one of the key parts of this equation, the temperature coefficient of the resistance material ( $1/K$ ) is a function of the dopant levels. (1)

### **Heat Transfer**

A description of the operation of a Wheatstone bridge as a sensing element requires a careful study of the heat transfer. That study has two parts: a theoretical investigation and an experimental investigation.

Van Putten (1988) created a Wheatstone bridge based flow sensor and looked at the theoretical heat transfer. The sensor was considered to be a flat plate with two heating elements incorporated on it. The sensor overheat temperature was caused by the stored energy on the chip which was simply the difference between the

1. Van Putten, A.F.P. "A Constant Voltage Constant Current Wheatstone Bridge Configuration" Sensors and Actuators, Vol. 13, 1988, pp. 103-115 58

heat being transferred in from the bridge resistors and the heat being conducted/convectioned out. Overheat temperature is the temperature difference between a heated object and ambient. Radiation heat loss was neglected for his argument. The heat transferred out was given as an equation, and an equation was also given for the time constant of the plate sensor. The principle of operation was based on the formation of a boundary layer, and the locally developed heat transfer was important for the generation of temperature gradients on the chip and hence the differential reading which was to be interpreted as flow. Van Putten gave a local heat transfer coefficient which was based on boundary layer theory. Measurements of readings for this device were done in a wind tunnel and results for flow and output as well as temperature and output were given. (1)

A similar theoretical study was conducted by Tai and Muller (1988) for their flow sensor structure. The object of the study was to look at ways to increase the sensitivity of their polysilicon flow sensor by taking a close look at the convection heat transfer. They calculated the boundary layer thickness when the flow was tripped from the start of the device and developed as it reached the heated bridge. The equation used the definition of boundary layer thickness as the distance from the surface of the wafer to the edges of the

1. Van Putten, A.F.P. "A Constant Voltage Constant Current Wheatstone Bridge Configuration" Sensors and Actuators, Vol. 13, 1988, pp. 103-115

boundary layer; where the edge of the boundary layer is defined to be the distance above the plate where the velocity is 99.5% of the free stream velocity. Their bridge was located 0.4 mm downstream of the start of the silicon chip and in air the boundary layer at that point should be 0.297 mm thick, using classical boundary layer theory. Considering the size of their bridge, they concluded that their problem was that the sensor was completely "immersed" in the boundary layer. Their solution was to move the bridge up higher into the flow-stream and away from the silicon substrate. One way they propose to do this is to etch channels under the bridge into the silicon substrate. They do not mention anything about the thermal boundary layer which begins as the air flows over the heated bridge.

(1) Tai's, Muller and Van Putten's calculations looked only at the heat transfer into a convective environment. Bouwstra, Legtenberg, Tilmans and Elwenspoek (1990) tried to compare the heat transfer both into the air and the conduction heat transfer out the bridge structure and into the base material. The bridge was constructed of  $\text{Si}_3\text{N}_3$  and was suspended over a v-groove. The bridge was made very thin so it would resonate at different frequencies when it was at different temperatures. Theoretical calculations predicted that only 10% of the total heat transfer would be to the air, and the rest would be conducted out to the base silicon. Actual measurements

1. Tai, Y. C.; Muller, R. S. "Lightly Doped Polysilicon Bridge as a Flow Meter" Sensors and Actuators, Vol 15, 1988, pp. 63-75

indicated that heat transfer by forced convection was only 7% of the total heat transfer. (1)

A local heat transfer coefficient for a flow sensor was found experimentally by Van Oudheusden and Wan Herwaarden (1990). Their device was a flow sensor which uses a membrane suspended by four thin bridges. The analysis used was called a "lumped sensor model". This model used a total thermal conductance  $H$  which was the sum of the heat transfer to the flow and the heat transfer through conduction to ambient. Neglecting the heat transfer of the beams to the air the heat conduction through the beams at steady state was calculated. All other heat transfer amounts were shown to be less than 2% of the measured energy input. The curve of heat transfer with flow as read by the sensor showed an average value of  $H$  of 1.45 mW/K. The response time was measured as 150 ms at zero flow. A two dimensional model was also done to take into account the direction of the flow and how it would read on the two thermocouples. (2) Again this device is considerably larger than flow sensor version 10.0.

Many structures are made of polycrystalline films because of

1. Anon "Micromachining: A revolution in the making" Mechanical Engineering, Vol 111, N3, Mar. 1989, pp. 47-48
2. Van Oudheusden, B. W.; Wan Herwaarden, A. W. "High-Sensitivity 2-D Flow Sensor with and Etched Thermal Isolation Structure" Sensors and Actuators, A: Physical, Vol. 22, N 1-3, 3PT3, 1990, pp. 425-430

the possibility of forming bridges and other more difficult structures this way. Tai and Muller (1988) used their polycrystalline flow sensor to look at the heat transfer through polycrystalline. The thermal conductivity of polycrystalline silicon was found experimentally to be 0.3 W/cm K, basically identical to single crystal silicon. This value agreed with their theoretical predictions. Two methods were used to find the heat transfer out of the bridge, one was to put the device in a vacuum chamber and the other was to place it in an oil bath.(1)

Van Oudheusden (1989) also looked at the difference in heat transfer between laminar and turbulent flow for his flow sensor. The presence of turbulence increased the overall heat transfer, while reducing the induced temperature difference across the sensor (the parameter being measured). When modeling the direction of flow-induced temperature difference, he determined that the distribution of the convective heat transfer and the influence of the thermal conduction in the sensor are both significant and hence must both be included in any theoretical calculations. The sensor modeled was 4 mm x 3 mm and a thickness of 0.3 mm, larger than the 1400 micron square device developed by the University of Cincinnati. Van Oudheusden's sensor was mounted on a ceramic substrate for

1. Tai, Y. C.; Muller, R. S. "Thermal Conductivity of Heavily Doped LPCVD Polycrystalline Silicon Films" Journal of Applied Physics, Vol. 63, 1988, pp. 1442-1447

strength. The thermal contact between the sensor and the solid substrate increased the heat transfer (conduction out through the substrate), reduced the sensitivity of the device, and slowed the response time from a theoretical 0.02 seconds to an actual 2 seconds. For the heat transfer analysis the sensor was regarded as quasi-isothermal surface, an assumption born out well by experimental evidence. Van Oudheusden did both a steady state and a dynamic analysis. In these experiments the flow remained laminar over the sensor up to a stream velocity of 15 m/s and turbulent flow over the sensor was fully developed by 20 m/sec. The sensor operated with a standard thermal overload of 24 K and the induced temperature gradient was observed to be less than 1% of the overload. (1)

Two years ago Scot Ma of the Mechanical Engineering Department at the University of Cincinnati began to look into trying to model the convective heat transfer of UC's flow sensor. As he searched the literature and examined the device to be modeled, he began to realize that the size of the sensor was smaller than the characteristic length needed to model the flow. The Peclet number for the sensor was also quite small. Both of these factors convinced him that classical boundary layer theory was no longer applicable for such small dimensions. He began to search the literature for a

1. Van Oudeuseden, B. W. "The Behavior of a Thermal-gradient Sensor in Laminar and Turbulent Shear Flow" Journal of Physics, E: Science and Instruments, Vol. 22, 1989, pp. 490-498

mathematical theory which would help him to accurately predict flow behavior. Mr. Ma has since been working on calculations involved in this very small scale heat transfer. His model takes into account both a laminar flow and its boundary layer and the thermal boundary layer that is formed as the flow reaches a heated element on a flat plane.(1)

### **Gold Doping**

In addition to the remarkably small size of the University of Cincinnati's mass flow sensor, its other outstanding feature is the use of deep impurity gold to increase the sensitivity of the device to temperature changes. The effects are dramatic as the gold doping makes sensitivity an exponential function which can increase its effect 1000 times. (2) The problem arises in controlling the amount of electrically active gold in the device. The gold can diffuse into either substitutional or interstitial spots and only the substitutional spots are electrically active.

An important item in the application of gold doped silicon devices is their stability to thermal and radiation effects capable

1. Ma, S. W.; Gerner, F. M.; Tseui, Y. G. "Composite Expansions on Forced Convection over a Flat Plate with an Unheated Starting Length" To be presented at the National Heat Transfer Conference, San Diego, California, August, 1992
2. Henderson, H. Thurman; Hsieh, Walter " A Miniature Anomometer for Ultrafast Response" Sensors, Dec. 1989, pp. 22-26



ofcausing impurity redistribution, decoration of boundaries by diffusing impurities etc. Studies were done by Bolotov, Emeksuzyan, Spiridonov, Schmalz and Trapp (1990); and Antonova, Vasilev, Panov and Shaimeev (1989) to look at the effect of the distribution of gold atoms in silicon near the Si/SiO<sub>2</sub> boundary and on the state of gold in the crystal bulk when it was hit by high-energy electron irradiation. Bolotov's study started with gold which was diffused into silicon wafers from the surface, and at the beginning of the experiment the concentration of gold increased toward the surface of the wafer. After gold diffusion into the wafer part of the gold in the silicon lattice is in the form of an electrically inactive component comprised of interstitial gold atoms (as small clusters). As gold was diffused in, the substitutional sites were filled and other processes began to dominate, that is the transition of the substitutional gold into the interstitial position, and runaway gold to some sinks particularly to the Si/SiO<sub>2</sub> interface. (1) Antonova et al. discovered the same cluster formation in silicon that had been doped with gold and well as phosphorous during the original growing of the crystal.(2) They also found that a high gold-impurity concentration in the inactive state, while only slightly influencing the initial electrical properties of the

1. Bolotov, V.V.; Emeksuzyan, V.M.; Spiridonov, V. N.; Schmalz, K; Trapp, M. "Radiation-induced Redistribution of Gold in SiO<sub>2</sub> Structures" Physica Status Solidi (A) Applied Research, Vol. 133, N 2, Jun. 1989, pp. 315-320

2. Antonova, I. V.; Vasilev, A. V.; Panov, V. I.; Shaimeev, S. S. "Formation of Clusters in Gold Doped Silicon" Physica Status Solidi (A) Applied Research, Vol. 116, N 1, Nov, 1989, pp. K33-K35

crystal, can appreciably effect the material parameters during various treatments and in ionizing radiation fields. Thermal treatment of the material up to 700 °C was shown by experiments not to lead to any noticeable change of the gold distribution in the volume. Fast (3.5 MeV) electron irradiation at a temperature of 300°C to 500°C both lower the concentration of electrically active gold and decay impurity clustering. Subsequent thermal treatments of the samples allow a recovery of the concentration of electrically active gold and the result was a silicon with a far more homogeneous distribution of impurity. (1) Botolov et al. found that during the irradiation the inactive interstitial component is dissolved in radiation introduced vacancies, also the radiation-induced decomposition of some complexes involving gold atoms could not be neglected. At the expense of the processes the substitutional gold concentration grew by 80%. (2)

### Microdynamics

Microdynamics is the name frequently used to describe the field of developing micromachines, understanding the

1. Wortman, J. J.; Evans, R. A. "Youngs Modulus, Shear Modulus, and poisson's Ratio in Silicon and Germanium" Journal of Applied Physics, Vol. 36, 1965, pp. 153-156
2. Bolotov, V.V.; Emeksuzyan, V.M.; Spiridonov, V. N.; Schmalz, K; Trapp, M. "Radiation-induced Redistribution of Gold in SiO<sub>2</sub> Structures" Physica Status Solidi (A) Applied Research, Vol. 133, N 2, Jun. 1989, pp. 315-320

micromechanical domain and the micromanufacturing process.(1) Modeling these microstructures for their dynamic, structural and thermodynamic properties means taking into account the problems incurred when dealing with such a small scale.

One school of thought says that with system size decreasing, microdynamics will eventually reach a demarcation point where a fundamentally different science and technology will become necessary. As components shrink many forces, such as centrifugal force, become less troublesome; others however become more vexing. The viscosity of air on the microscale becomes a major problem. Friction is one of the mechanical properties which requires a better understanding on the microlevel. It turns out that just getting friction when it's wanted can be a problem. Also on that scale Van de Waals forces, adhesion forces and electrostatic forces can be large. Testing and extracting useful information from devices this small is also a major problem. "What is showing now is only the tip of the iceberg" (2)

Structural modeling of a silicon flow sensor means taking into account the mechanical properties of single crystal silicon. The elastic behavior of single-crystal silicon is anisotropic: Young's modulus  $E$ , Poisson's ratio and the shear modulus depend on the

1. Rosen, Jerome "Machining in the Micro Domain" Mechanical Engineering, Vol. 111, N3, Mar 1989, pp. 40-46

2. Ibid.

direction of the applied force. (1) In their recent article Van Lintel and Van De Pol (1988) give an equation for flexural rigidity as a function of direction. Equations were also given for compressive stress to deflection of a beam taking these anisotropic properties into account. In 1964 Wortman and Evans published a paper which reduced to a few calculations and graphs finding Young's modulus, shear modulus and Poisson's ratio for silicon given an X-Y orientation of your choosing. (2) Now computer programs allow modeling parameters to be entered as a function of direction.

### Conclusion

Micromachining is a brand new technology which carries with it many unanswered questions and many exciting applications. The heart of micromachining are the techniques for etching and deposition which allow various structures to be made, while excluding other possibilities. Each new fabrication technique offers new potential because it adds another color to the designers palate, allowing entirely new structures which were not possible earlier.

1. VanLintel, H. T. G.; Van De Pol, F. C. M.; Bouswstra, S. "Piezoelectric Micropump Based on Micromachining of Silicon" Sensors and Actuators ,Vol. 15, N2, Oct. 1988, pp. 153-167
2. Wortman, J. J.; Evans, R. A. "Youngs Modulus, Shear Modulus, and poisson's Ratio in Silicon and Germanium" Journal of Applied Physics, Vol. 36, 1965, pp. 153-156

Mechanical analysis of these microstructures is still in its infancy. Heat transfer for small structures is just starting to be addressed, and the field of microdynamics is, for the most part, unexplored. "Micromachining shows signs of becoming the basis of a whole new industry." (1)

1. Buchy, Frank "Silicon Sensors Lead Pressure Transmitter Technology" Chilton's I&CS (Instrument and Control Systems), Vol. 60, N2, Feb 1987, pp.37-39

## **CHAPTER 3**

### **METHODOLOGY**

The University of Cincinnati has a patent on the smallest and fastest mass flow sensor currently known. The device takes advantage of deep impurity doping with gold to dramatically increase its sensitivity to temperature change, a concept pioneered at U.C. The device is understood electrically, however, its thermal and mechanical properties are completely unknown. The structure is delicate and complex enough that it is all but unmanufacturable.

#### **Action Overview**

The theory of operation on which flow sensor version 10.0 is based needs to be studied by creating a heat transfer model of an ideal sensor. This model can then be used to compare various configurations of resistors and their geometries. From this study and from the information gained from tunnel etching experiments a new design can be developed which will combine the best geometries with thermal isolation for a new and superior flow sensor design. The thermal isolation strategy will be novel, as it will allow the sensing element to be made in the single crystal silicon, rather than in a layer deposited on top of the silicon.

In studying the manufactureability of the modified version of the flow sensor, a new manufacturing technology, that of tunnel etching, will need to be explored. This technology was accidentally discovered by Mr. Burton, a master's degree student working for Dr. Henderson of the University of Cincinnati, in 1981. (1) While the effect of tunnel etching was noted, it has not been used as a manufacturing process to date. This process has potential application in the creation of silicon bridges without requiring that the bridge be created on the diagonal or out of polycrystalline silicon.

The thermal isolation problem of the existing flow sensor is addressed by the new suspended silicon island geometries which tunnel etching would make possible. If the gold doping can be controlled, tunnel etching would make it possible to isolate the resistors physically from the rest of the silicon structure, making gold migration into or out of those areas impossible. Even with the potential to isolate the silicon islands, migration could be used to move the gold to desired areas (into or out of the islands) before the tunnel etching. Similarly, isolating the silicon islands by air and silicon dioxide bridges reduces significantly the heat which can be conducted away from the resistors. This thermal isolation means that a far larger portion of heat lost will be to convection, which is

1. Burton, Gregory N. "Use of multiple internal reflection to enhance transient sensitivity in a gold-doped silicon IRFET" M.S. Thesis, December, 1981, University of Cincinnati

the heat transfer mechanism desired. If the gold cannot be controlled, this enhanced thermal isolation can enhance the sensitivity of a non-gold doped device to an amount comparable to gold doping.

The thermal masses of the island resistors will be several orders of magnitude smaller than the current structure, especially if a large percentage of the heat is being conducted out of the bridge into the feet. A redesign with reduced thermal mass can potentially speed up the response time of the device even further, or compensate for additional cooling taking place in the present device which is not part of the convective, boundary layer model.

The modified flow sensor should have no more process variables than the current configuration, and it should also be possible to redesign the flow sensor in such a way as to make it more forgiving of process variations. The combination of these two improvements will mean an improvement in flow sensor manufacturing yield. Successfully producing working sensors is the biggest issue currently faced by the microfabrication group at IAMS.

### **Mechanical Analysis**

The first step in improving and redesigning the mass flow sensor will be a careful analyses of the current structure. The



current version of the flow sensor will be modeled on a Finite Element Analysis (FEA) package, IDEAS by SDRC. The dimensions and shape of the structure are being generated from measurements of actual sensors made in the laboratory, using a measuring microscope at IAMS, as no drawings or dimensions existed from which to create an actual model. The devices selected for measurement were those which had been rejected because of too much gold and not due to geometry problems. Once the model is generated it will be tested with theoretical torque inputs on the corners to determine the maximum loading that this particular device can withstand before the yield strength of the material is reached.

### **Thermal Analysis**

Several different heat transfer models need to be made in order to determine where and how the heat transfer in the sensor is taking place. The first analysis, a comparison of characteristic times for different heat transfer paths, will be used to predict the percentage of heat actually being transferred into the passing gas from the top surface of the sensor.

From the information gained, a more complex heat transfer model can be developed to compare the sensitivity of various design types. These models will allow variations in surface area, orientation

to the flow, power and bridge construction to help identify the most promising configurations.

Tunnel etching will be used to produce thermal isolation structures. The effects of tunnel etching on thermal isolation can be calculated to determine the effectiveness of this approach and limiting factors on thermal isolation.

### **Tunnel Etching**

The modified design currently depends on tunnel etching for the unique isolation structures. Before the design can be completed, tunnel etching will be studied to determine its characteristics. It is unknown if the tunnel etching effect can be controlled to make it a viable manufacturing option. The etching rate, distances possible, flushing of etchants from the created tunnels, doping concentrations and other variables need to be understood before a robust design can be completed.

The first step in creating an improved design was to study the tunnel etching phenomena. A set of test masks were designed, made and used to reproduce the tunnel etching effect reported by Burton, and then check etching rates and distances in the tunnels as a function of many process variables. These masks enabled

variations in etching as a function of doped area and geometry to be checked. In addition other variables were checked using these masks: concentrations of phosphorous, freshness of the etchant solution, post-doping oxide thickness, and wafer type.

Once the process was controllable and predictable the next step was to design a flow sensor with the isolated island configuration.

The successful use of tunnel etching in the flow sensor opens a new group of possible geometries to all of micromachining.

### **The New Design**

Flow sensor version 10.0 needs some major revisions if it is to move from the laboratory scale to a small manufacturing scale. The new flow sensor design was developed from the heat transfer analysis, and represents a very different approach to the mass flow sensing problem. The characteristics of the sensor were predicted before it was made to determine that it was indeed superior to the standard version. Manufacturing problems which have occurred with the gold doping made it important to try to develop a sensor which will not require gold doping initially. Manufacturing problems which had been incurred with flow sensor version 10.0 were addressed in the redesign.

## **Processing**

Micromachining determines the geometries which can be created in silicon sensors. The modified flow sensor had to be produced in the most efficient and reproducible manner available. The number of process variables and the complexity of each individual step will both were studied and reduced. Because this sensor needs to move so quickly from laboratory prototype to manufactured reality, ease and consistency of manufacturing will be a major performance criteria.

## **Conclusion**

The method by which the isolation problem was attacked has three main parts, consistent with the objectives of the research project. The first step was to understand tunnel etching as a microfabrication process. This involves an experimental mask set and changing a number of different combinations of process variables to learn which factors most affected the etching process. The second step was the heat transfer model, which when combined with an understanding of previous manufacturing problems would yield information on which a redesigned flow sensor could be based. The redesign had to address all of these issues with a novel geometry based on tunnel etching. The third and final step was to actually create a device with the new configuration. The performance of the device is checked against the initial predictions, and discrepancies are discussed.

The proposed course of action looks at some of the manufacturing issues associated with the flow sensor and simultaneously produced new results which are applicable for micromachining as a whole. The structures created with tunnel etching can be used for a variety of thermal and electrical isolation problems. Tunnel etching allowed for a more robust mechanical design while at the same time enhancing the heat transfer characteristics. The manufacturing topics addressed in this redesign are applicable to all micromachined sensors.

## CHAPTER 4

### TUNNEL ETCHING

Mr. Burton reported in his Master's thesis in December 1981 (1) that he had discovered a novel method for creating oxide bridges. That method involved:

1. opening an oxide window on the surface of a single crystal, (100) silicon wafer,
2. diffusing in phosphorous from a  $\text{PClO}_3$  source (gaseous),
3. regrowing an oxide over the doped region,
4. opening etching windows to the phosphorous region
5. etching in a Hydrazine/water, 100 °C etching solution.

He reported that under these conditions the hydrazine, which would normally stop at the crystal boundaries, would rapidly etch along the phosphorous path under the silicon dioxide, creating an oxide bridge. Burton experimented with the ratio of hydrazine to water and concluded that a 50% Hydrazine, 50% water solution gave the fastest phosphorous etch rate. Burton also varied the duration of the diffusion and found the system to be fairly insensitive to diffusion duration.

1. Burton, Gregory N. "Use of multiple internal reflection to enhance gradient sensitivity in a gold-doped silicon IRFET" M.S. Thesis, University of Cincinnati, December, 1981

Currently oxide bridges can be made in very few ways owing to the properties of the silicon, its oxide and the etchants which are used to machine it. Using Burton's bridge technique to create air cavities attached to the base silicon only by oxide membranes is a novel solution to the problem of thermal isolation for the current flow sensor.

### Uses of Tunnel Etching

The current version (version 10.0) of the micro flow sensor consists of four single crystal silicon resistors suspended between four large silicon "feet", see figure 4. These resistors are arranged in a Wheatstone bridge configuration. The device is operated by placing a constant current across the bridge, which generates heat in each of the four resistors. Air passing over the resistors cools them. The device has a small quantity of gold diffused into it which strongly changes the resistivity as a function of temperature. Two of the resistors were arranged to be parallel to the flow and two are arranged to be perpendicular. As is shown in the next chapter the two resistors which are perpendicular to the flow should have a higher heat transfer coefficient than the two resistors parallel to it. The higher heat transfer means that the two perpendicular resistors cool faster and therefore have a higher resistance. The output of the device is measured as a voltage potential across the bridge. The Wheatstone bridge configuration was chosen as it should allow for corrections to be made within the device for changes in ambient temperature.

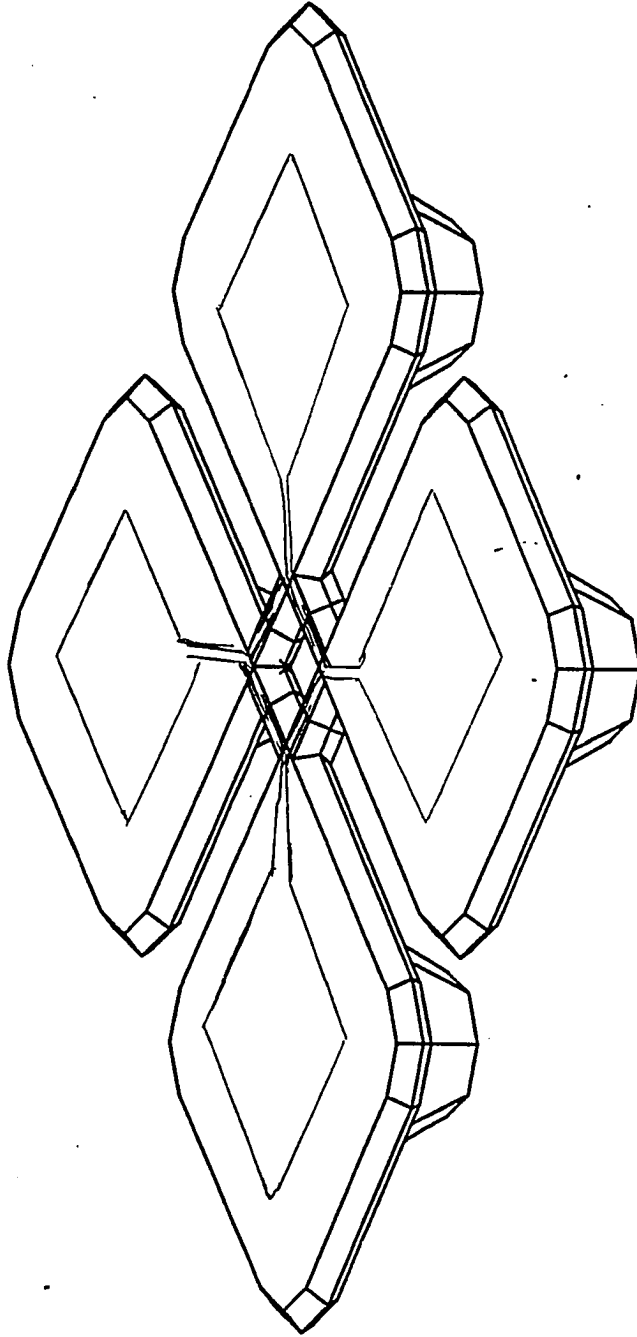


Figure 4 - Solid Model of Flow Sensor Version 10.0  
Showing Metal Leads



Ideally this device should lose most of its heat to convection from the resistors. The heat transfer model of the resistors showed that only 1/100th to 1/1000th of the heat generated was lost by convection at the resistors. Most of the heat was lost by conduction through the silicon to the "feet". The feet then dissipate the heat by convection to the air, owing to their large surface area, and by conduction into the external electrical package. The present device is known to make the entire package warm to the touch.

Thermal shorting is a serious problem for the present flow sensor. It requires that the device be operated at high voltages and currents (20-30 volts and 10 mA), to generate a high enough temperature on the bridge to yield the desired sensitivity. Thermal shorting also means that a gold doped sensor with its extreme sensitivity to small temperature changes is most desirable. Higher power requirements, while not insurmountable, create problems for the eventual application of the device. Gold, while enhancing the sensitivity remarkably, is currently a manufacturing problem as diffusion of a known quantity into the device and controlling the stability of the gold after it is in the device are both unresolved issues.

The original base which used to completely surround the sensing diaphragm, (see figure 5), was separated into the four individual "feet" to enhance thermal isolation . The feet were

Flowsensor before separation of feet

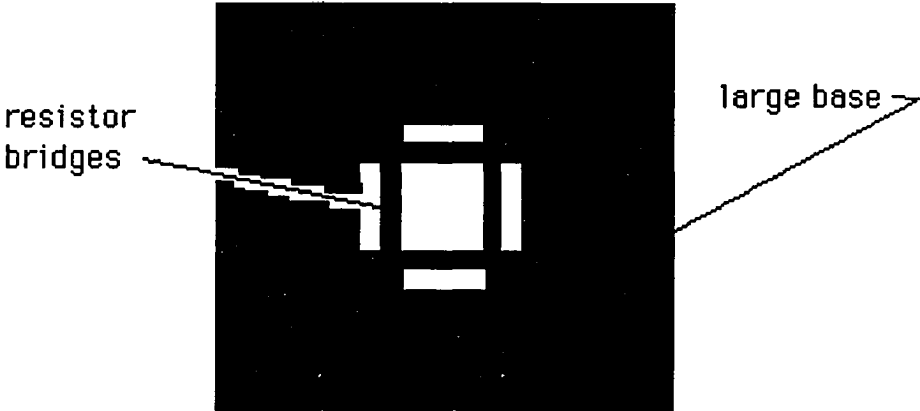


Figure 5 - Top View of Original Flow Sensor

originally separated with the idea of stopping thermal and electrical communication around the base. The separation the feet did enhance the sensitivity, but most likely for a reason which will be demonstrated in the next chapter. The change in the geometry of the device, while enhancing sensitivity, undermined the structural integrity of the device and breakage during manufacture became a major issue.

Silicon dioxide's thermal conductivity is only  $1.4 \text{ W/m}^\circ\text{C}$ , compared to  $125.6 \text{ W/m}^\circ\text{C}$  for single crystal silicon. Meanwhile the tensile strength of silicon dioxide is very comparable to single crystal silicon,  $8.4 \times 10^{10} \text{ dyne/cm}^2$  as compared to  $7 \times 10^{10} \text{ dyne/cm}^2$ . Thermal isolation can be approximated if the hot resistor can be separated from the rest of the silicon by air and thin oxide membranes. The oxide membranes provide a mechanical structure both to hold the resistor bridges and to allow metal to be laid down for electrical connections.

Once developed as a manufacturing process, tunnel etching can be used for many new micro sensor and actuator devices. Unlike current process which can create islands of polysilicon on top of oxide layers, the islands can now be made of single crystal silicon which is much stronger. Unlike other bridge techniques, the tunnel etching can be done in any direction along the surface of the wafer. The combination of strength and flexibility is valuable as

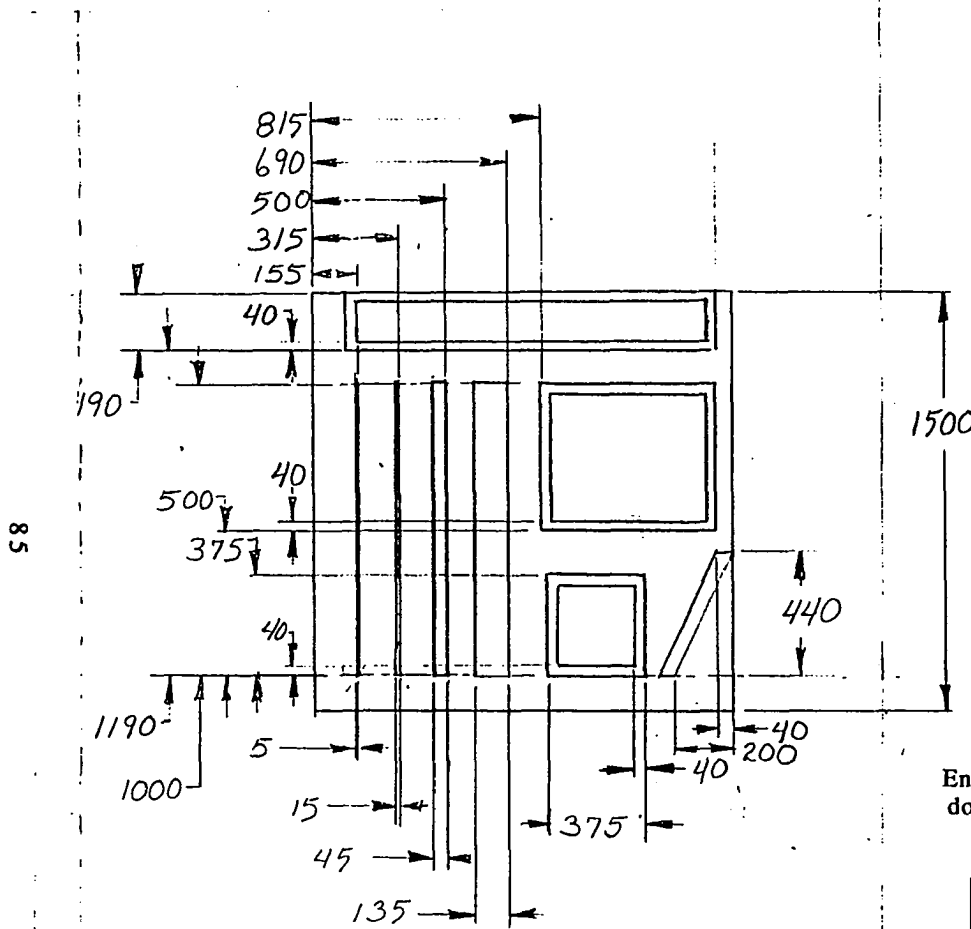
micromachining is confronted with the problems of having only a limited number of manufacturing techniques possible.

### **Overview of Findings**

Tunnel etching needed to be defined as a manufacturing process, rather than a one time lab-oddity, in order for it to be incorporated into an actual device. Burton's thesis described the tunnel etching process only briefly, showing some small bridges created with it. The doping concentration was given in terms of time with a  $\text{PClO}_3$  source. Since the time of Burton's work, the  $\text{PClO}_3$  gaseous phosphorous source is no longer used, and instead a solid source phosphorous wafer, made by The Carborundum Company is commonly used as the diffusion source.

#### **Tunnel Etch Experiments**


A special set of masks were developed to generate test wafers for tunnel etch experiments. The set of masks consisted of two masks, one for opening windows in oxide to allow for phosphorous diffusion and one for opening windows in a second oxide to allow for etching, see figures 6 & 7. The phosphorous doping areas consisted of lines of varying thicknesses, a diagonal line and three rectangles. The lines of varying thickness would be used to see if the width of the phosphorous path was important to etching rate. It is

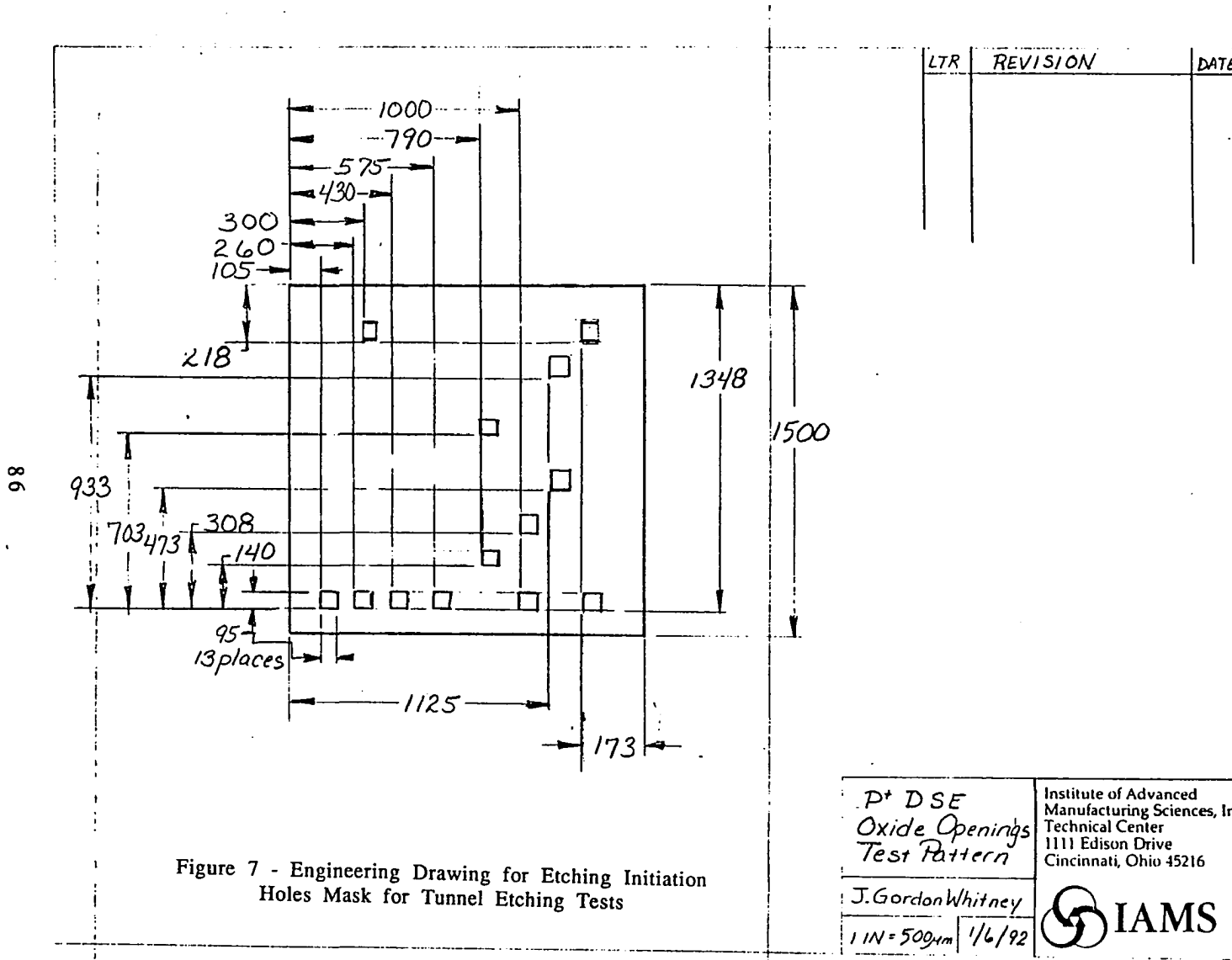


LTR	REVISION	DATE

Figure 6 - Engineering Drawing for Phosphorous Doping Mask

Engineering drawing for phosphorous doping mask for tunnel etching tests

<p>P<sup>+</sup> DSE Doping Test Pattern</p>	<p>Institute of Advanced Manufacturing Sciences, Inc. Technical Center 1111 Edison Drive Cincinnati, Ohio 45216</p>
<p>J. Gordon Whitney</p>	
<p>1 IN = 500 μm 1/6/92</p>	



reasonable to assume that in a long narrow tunnel the etchant might easily be depleted and fresh etchant would have a difficult time reaching the reaction surface. The diagonal lines and rectangular boxes were designed to check for the relationship between the phosphorous etching and the secondary etching of silicon beside it. It was originally believed that the phosphorous etching would take place much more rapidly than the secondary planes etching and that the relative speed of secondary planes etching to phosphorous etching would be important to device design.

The amount of phosphorous diffused into the silicon wafer from a solid source is a function of several things. The temperature of the diffusion, the length of time of the diffusion, and the type of source wafer. Since Burton recorded his doping concentrations in terms of time in diffusion for the  $\text{PClO}_3$  source, it was necessary to attempt to compare this doping to what was currently obtainable with a solid source.

The  $\text{PClO}_3$  source which Burton had used differs from the solid source phosphorous diffusion wafer in several important ways. The  $\text{PClO}_3$  source, starts as a  $\text{PCl}$  liquid through which oxygen is bubbled. The oxygen gas, now containing  $\text{PClO}_3$  molecules is then fed into a furnace tube where the phosphorous is deposited on the wafer surface and driven into the silicon by the heat. This method is much faster than a solid source, and this makes it of great importance to

industry. Unfortunately,  $\text{PClO}_3$  gas is highly toxic and great attention must be paid to proper ventilation. In addition a highly explosive phosphorous residue coats all duct work and must be periodically cleaned. Solid sources, in contrast, are slower to use but much safer. Wafers coated with a phosphorous rich compound are purchased commercially. Various compounds are available so the purchaser must know what resistivity is desired in the silicon wafer for given temperature and time constraints. The coated wafers, known as solid sources, can be handled like regular silicon wafers with gloves and tweezers. Each wafer is good for 1000 hours of diffusion at the specified temperature.

Tunnel etching trials were performed by preparing a wafer in the following manner:

1. Base clean: The wafer is boiled ( $70\text{ }^\circ\text{C}$ ) in a cleaning solution of 200 ml of deionized water, 50 ml of ammonium hydroxide, and 50 ml of hydrogen peroxide for 15 minutes. The wafer is then rinsed in deionized water and dipped for 10 seconds in a 2% hydrofluoric acid solution, and rinsed again. The wafer is then dried with nitrogen.
2. Oxidation: The wafer is loaded into an oxidation boat and placed in the mouth of the oxidation furnace and allowed five minutes to come to temperature. The oxidation boat is then pushed to the center of the oxidation furnace which is kept at  $1000\text{ }^\circ\text{C}$ . Oxygen is fed to the furnace at a constant rate of 50



liters/hr. The wafer is left in this dry oxidation for 30 minutes and then the path of the oxygen is changed so that it bubbles through hot deionized water (95°C) before entering the furnace. The wet oxidation is allowed to proceed for 60 minutes, and then the path of the oxygen is changed again and the wafer continues in a dry oxidation for another 30 minutes. At the end of the last dry oxidation the wafer boat is pulled to the front of the furnace and allowed to cool for 5 minutes before being unloaded.

3. Lithography: A thin coat of positive photoresist is spun onto the wafer. The wafer is then "soft baked" in a 90°C oven for 30 minutes. The wafer is then aligned to the phosphorous doping mask on an aligner and exposed with an ultraviolet light for 10 seconds. The pattern is then developed using a Shipley D-35 developer solution (5 parts deionized water, 1 part Shipley-35 developer) for 40-50 seconds. The pattern is inspected for proper alignment and development and then hard baked for 30 minutes at 114°C. After the resist is hard baked the wafers are set on an aluminum foil rack and the back sides of the wafer are painted with photoresist by hand, and then allowed to dry for another 30 minutes.

4. Buffered Oxide Etch: The wafer is wet in deionized water and then placed in a buffered hydrofluoric acid solution (3 parts ammonium fluoride (NH<sub>4</sub>F), 1 part hydrofluoric acid (HF))

for four minutes or until the oxide exposed by the open resist windows has been dissolved exposing bare silicon. The oxide etch is checked under a microscope and then the photoresist is removed using acetone and isopropyl alcohol.

5. Base Clean: This cleaning process is repeated exactly as described in step 1.

6. Phosphorous Diffusion: The solid source wafer should be activated by being placed in the phosphorous furnace for a minimum of 40 minutes prior to the diffusion. When the activation is over, the source wafer is ready for use and can be removed from the furnace. The tunnel etch test wafer is loaded onto a diffusion boat with the side to be diffused into placed next to the solid source wafer. The boat is placed in the mouth of the phosphorous furnace and allowed 5 minutes to come to temperature before being pushed into the furnace tube. During all diffusions a small flow of nitrogen gas (5 liters/ hr) was pumped into the furnace. The diffusion time and temperature varied from test to test. At the end of the diffusion time the boat with both the source and test wafer were brought to the front of the furnace and allowed 5 minutes to cool before being removed.

7. Base Clean: The test wafer was again cleaned using the procedure described in step one, with the exception that the hydrofluoric acid dip was omitted.

8. Oxidation: The wafer was loaded into the oxide furnace for

an oxidation as described in step 2. The duration of the wet and dry oxidation periods varied for different tests.

9. Lithography: Lithography was again done as in step 3, with the mask used for alignment being the oxide opening mask.

10. Buffered Oxide Etch: Oxide windows were opened on the surface of the test wafer using the procedure described in step 4.

11. Etching: Just before the wafer was etched it was dipped in a 10% hydrofluoric acid solution to clear all etching surfaces of oxide. Then the wafer was placed in a hot (90 °C) solution of 50% hydrazine and 50% water. The wafer was left in the etchant for varying lengths of time, removed, rinsed and measured for tunnel etching.

In addition to test wafers, several oxide free wafers were also doped to measure resistivity of the wafer after the various combinations of doping and oxides. Resistivity measurements were taken using a four point probe, and giving it the calculated depth for the phosphorous doping .

**Table 1 - Wafer Resistivity vs Doping  
10  $\Omega/\text{cm}^2$  Wafer**

<u>Wafer Doping</u>	<u>Average Resistivity</u>
1000°C, 1 hour	.21 $\Omega/\text{cm}^2$
975°C, 40 min	.40 $\Omega/\text{cm}^2$
950°C, 1 hour	1.24 $\Omega/\text{cm}^2$

Tunnel Etching as a Function of Phosphorous Doping

Wafers of two types were used for tunnel etching experiments. The 10  $\Omega/\text{cm}^2$  wafer is the wafer type currently used for the flow sensor. This wafer is doped with a small quantity of phosphorous as the crystal is grown to give the wafer that average sheet resistance. Additionally 20  $\Omega/\text{cm}^2$  wafers were purchased for development work on the new flow sensor design which emerged from this research project. The 20  $\Omega/\text{cm}^2$  wafer also has phosphorous doped into it during its manufacture, but it has less.

Initial experiments were all conducted on 10  $\Omega/\text{cm}^2$  wafers, to attempt of repeat Burtons initial findings. Doping these wafers at 950 °C for 30 minutes appeared to produce no tunneling. Any

doping at or above 975 °C for 1 hour appeared to create an overload of phosphorous, and a rapid tunneling would begin, but then stop after only 5 $\mu$ m of tunneling. This tunneling was progressing much faster than the secondary plane etching, as evidenced by its shape, see figure 8. This photograph shows the stopped etching where the 5 $\mu$ m and 15 $\mu$ m phosphorous strips entered the initial etch hole. Once this shape had been obtained, returning the wafer to the hydrazine etch had no effect. The stopped pattern could be briefly restarted if the wafer was dipped in a 10% hydrofluoric acid solution for 10 seconds, but again the etching would halt in less than an additional 5 microns. The restarted pattern also tended to be more uneven as the amount of surface contamination removed by the hydrofluoric acid varied from place to place on the wafer.

This etch stop mechanism was repeated 3 different times on 3 different wafers with varying doping concentrations: 975°C for 1 hr, 1000°C for 1/2 hr, and 1000 °C for 1 hr.

This finding of an etch stop contradicted what Burton reported in his thesis. After careful review of the thesis it was noted that Burton changed the hydrazine he was using frequently, while it had become the procedure of the current personnel not to change it.

The freshness of the hydrazine for normal silicon etching mostly effects the water content. As the hydrazine is reheated and

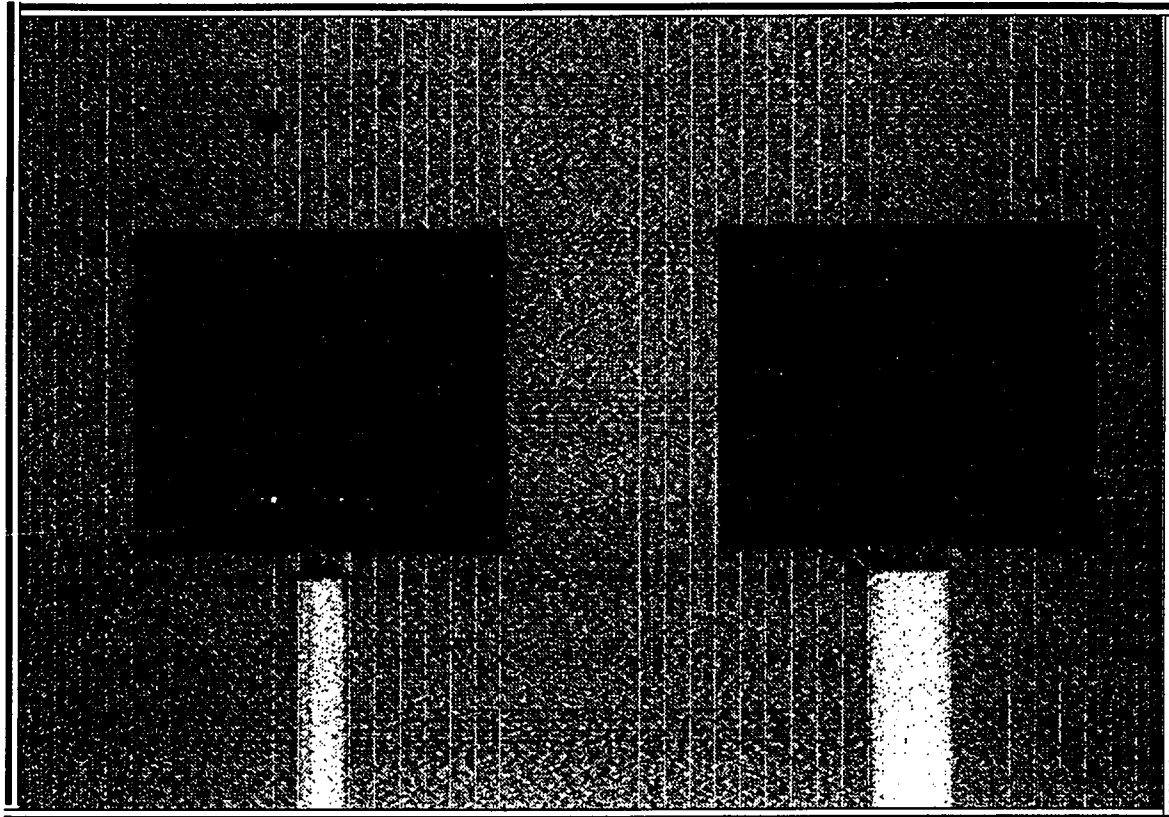


Figure 8 - Micro Photograph Showing Etch-Stop

Micro photograph of tunnel etching test wafer, doped at 100°C for 1 hour showing etch-stop after initial 5 micron lateral etching, Phosphorous doping paths are 5 and 15 microns wide. Total time etching: 2 hours.

reused water evaporates and the concentration of hydrazine increases. Burton reported that as water content is lost so is the solution's anisotropic etching properties. While no crystals form in the container, as is the case with EDP, the solution does slightly yellow with use. This color change is very difficult for the user to determine as the solution is in a beaker with condenser which is sitting in a warm oil solution, and the oil itself is much yellower than the hydrazine.

It became common practice of this researcher to change the hydrazine around every 10 hours of etching or if contamination was suspected. When the hydrazine was changed regularly the etch-stop problem disappeared, and wafers doped as heavily as 1000°C for 1 hour tunnel etched over 50µm without stopping.

When wafers were doped with small quantities of phosphorous, less than 950°C, 1 hour, the tunnel etching reduced drastically. The same loss of tunneling ability could be repeated if a reasonable quantity of phosphorous was diffused in, but then the oxidation done after the doping was large enough to absorb most of the phosphorous doped silicon into the oxide. Figure 9 shows the etching depth vs time for a 10 Ω/cm<sup>2</sup> wafer which was doped for 1 hr at 950°C, and then over the doped regions was grown a 30 minutes dry, 60 minutes wet, 30 minutes dry oxide, for an thickness of about .4 µm. The doped areas were taken up in the oxide growth, and the result

# Heavy Oxide vs. Light Oxide

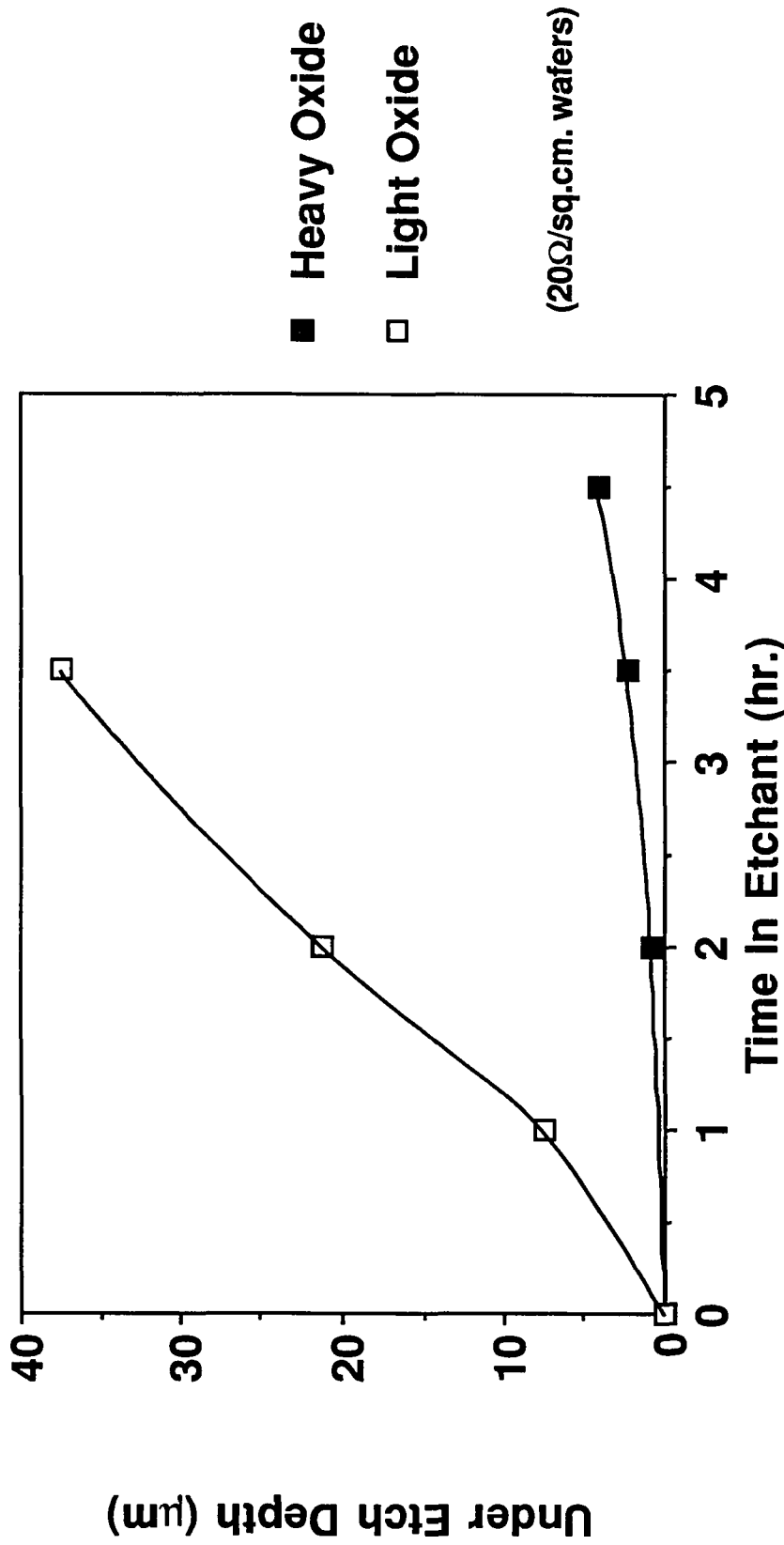


Figure 9 - Heavy Oxide vs. Light Oxide



was extremely poor tunneling. At the end of 3.5 hours total etching time the wafer with the lighter oxide had almost 30  $\mu\text{m}$  more of tunnel etching than the heavily oxidized wafer. Since the oxide is used as a structural element for the thermal isolation structures, this could place a limit on the lengths of the membranes feasible for holding up bulk silicon resistors. There are two ways to get around this problem. The first is to do the phosphorous doping with ion implantation rather than a surface deposition. Ion implantation will put the heaviest concentration of phosphorous under the surface of the silicon, leaving more silicon available for oxide growth. The second option is to use oxide grown on the backside of the device for more of the structural support. This method of using the backside for structural integrity was quite successful and was used on the sensor redesign.

The tunnel etch required the right amount of phosphorous in the available doped silicon. The etch rate was not only a function of the amount of silicon placed in the wafer, but the amount left over in unoxidized silicon after the second oxidation. Once this was discovered a standard 10 minutes dry, 30 minutes wet, and 10 minutes of dry oxidation cycle was used in tunnel etching experiments. This seemed to have a good combination of adequate oxide coverage and adequate doped silicon available to etch.

The etch rate was a function of the amount of doping and the depth into the tunnel that the etch had already progressed. As mentioned before, the most likely reason for decreasing rates as the tunnel progresses is the difficulty in getting fresh etchant to the active area. Figures 10, 11 and 12 shows the etch depth average verses time for various combinations of doping concentrations, oxide thicknesses and wafer types. There is a slight "S" shape to several of the etching curves. When the wafer is first placed in the etchant, initial etching is downward. As the etch pit from the tunnel starting hole increases, a larger cross section of phosphorous is exposed on the sidewall and tunneling begins. The tunneling progresses rapidly while the etch pit is close enough to the active tunneling surface that an exchange of new and used etchant is easy. As the tunnel gets deep the rate slows down again.

### Etching Rates

Measurements of tunnel depth were taken from the tunnels on the straight line phosphorous paths. Each wafer was divided into 5 areas. When the wafer is oriented with the flat down, the top of the wafer is area 1, the left hand side is area 2, the right hand side is area 3, the bottom above the flat is area 4, and the center of the wafer is area 5. For most wafers 5 measurements were taken through the microscope for each of the four different path thickness in each area of the wafer, for a total of 100 measurements per wafer

# Doped Direction Etching

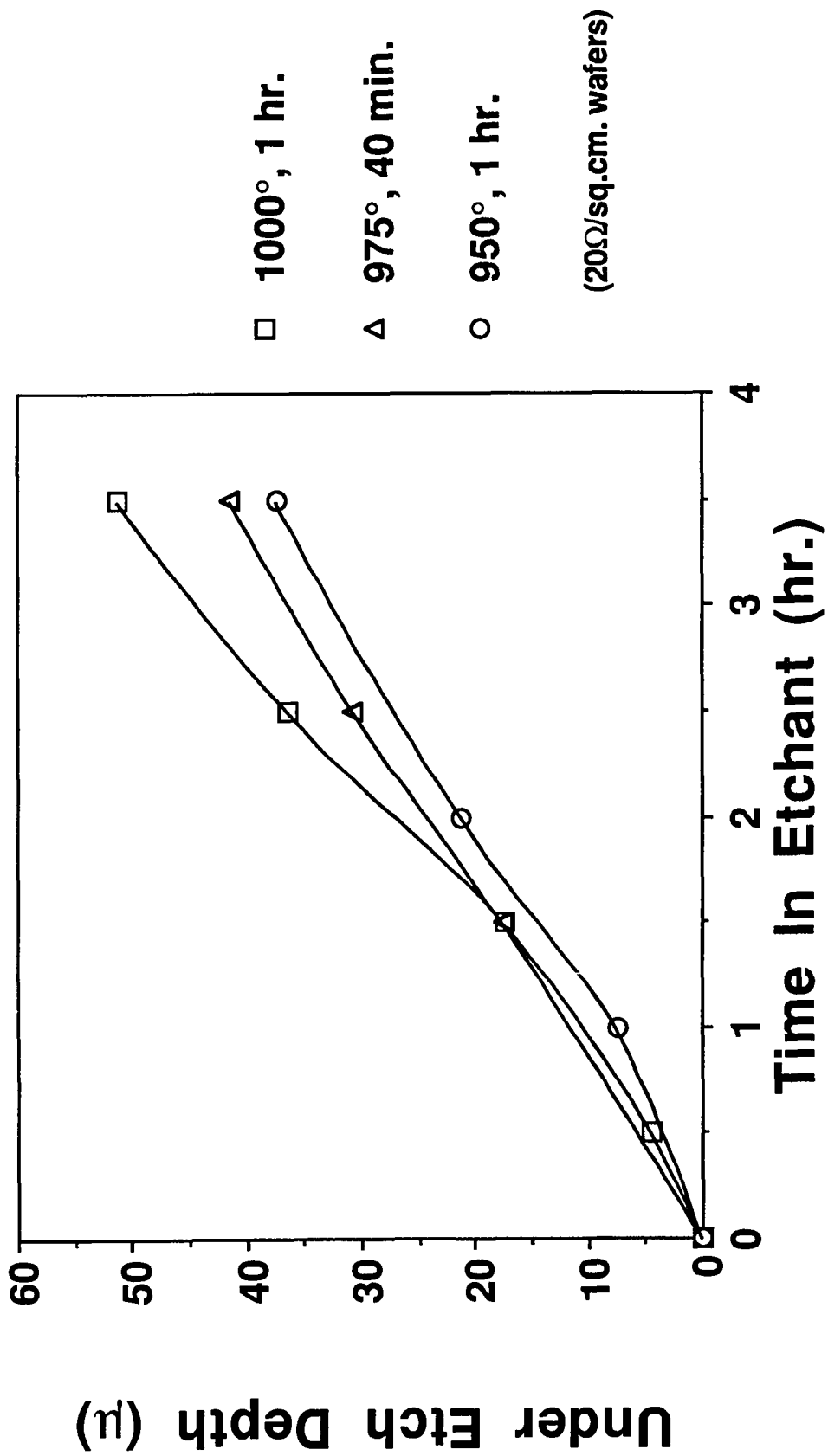


Figure 10 - Doped Direction Etching

# Doped Direction Etching

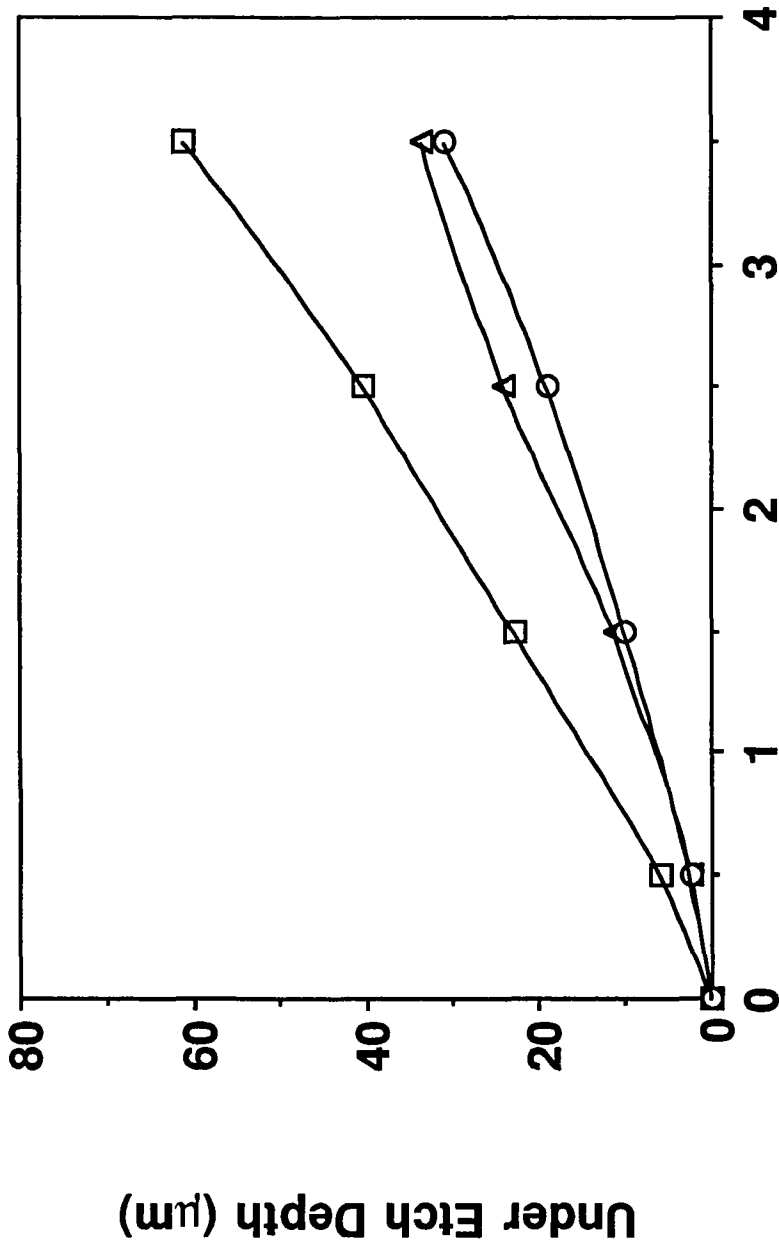


Figure 11 - Doped Direction Etching

- 1000° 1hr
  - △ 975° 40 min
  - 950° 1 hr
- (10Ω/sq.cm. wafers)

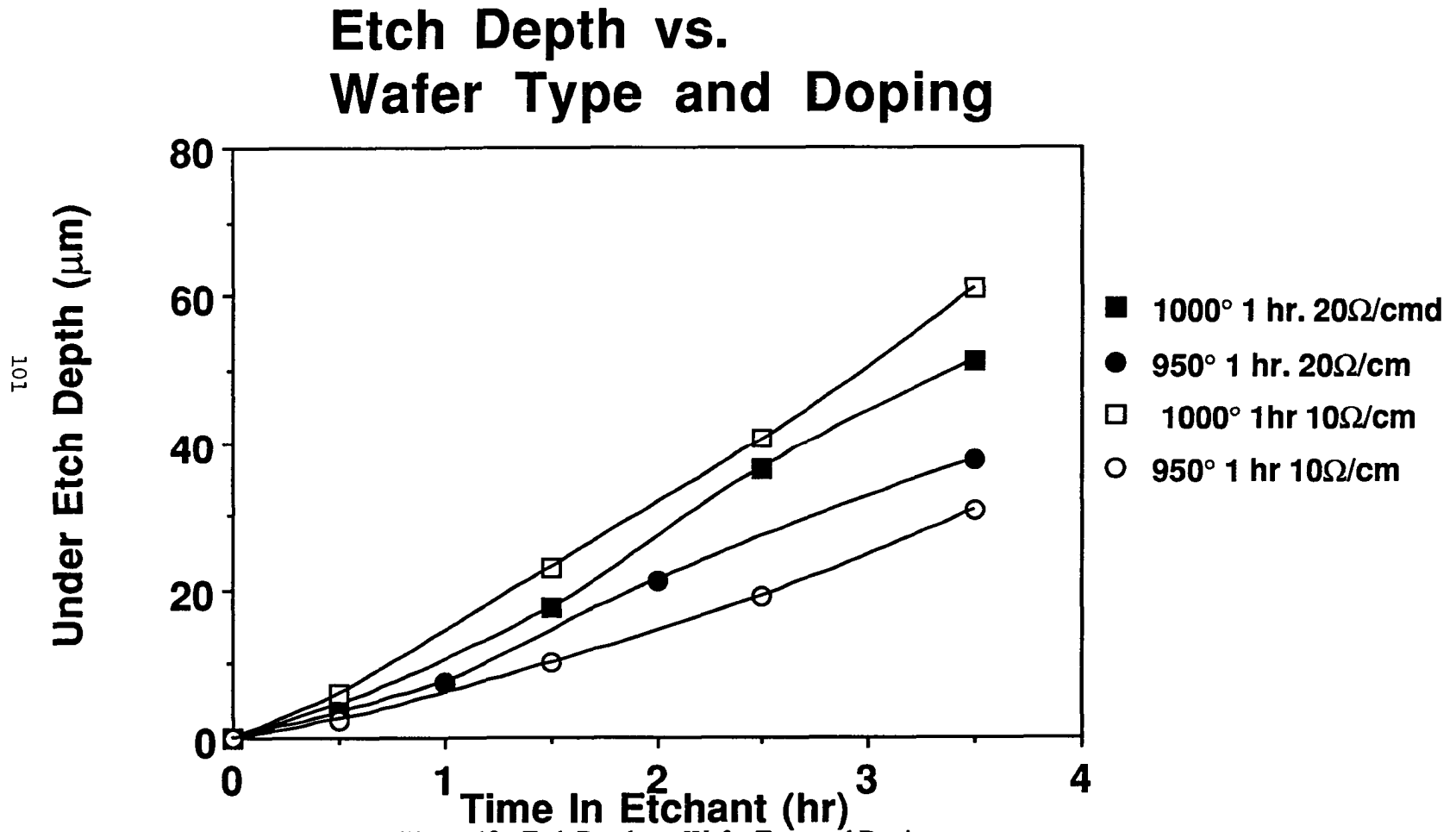


Figure 12 - Etch Depth vs. Wafer Type and Doping

101

per etch. In addition for each tunnel measurement taken the measurement of underetch in the non-phosphorous direction was also taken, for a total of 100 non-phosphorous direction measurements per wafer per etch. Three wafers of very different make-up were measured more thoroughly with 10 measurements of tunnel or under etch being taken in each of the 5 areas. These measurement were used to determine standard deviation for the etches.

Underetching in the non-phosphorous direction during the tunnel etching experiments was significant. The underetching in the non-phosphorous direction was frequently one third of the underetch in the phosphorous tunnel direction. This was quite unexpected as hydrazine is very anisotropic and would not normally significantly underetch the oxide. To prove this, one wafer was processed with the same masks but no phosphorous was diffused into it. The underetching on that wafer as compared to several phosphorous doped wafers is shown in figure 13. It is unlikely that any phosphorous got under the oxide in the non-path direction. Reviewing the steps in producing the test wafers shows that the main mask oxide is never stripped, and the holes which are opened to allow the etching to begin all extend significantly into non-doped regions.

## Under Etch of Doped vs. Undoped Directions

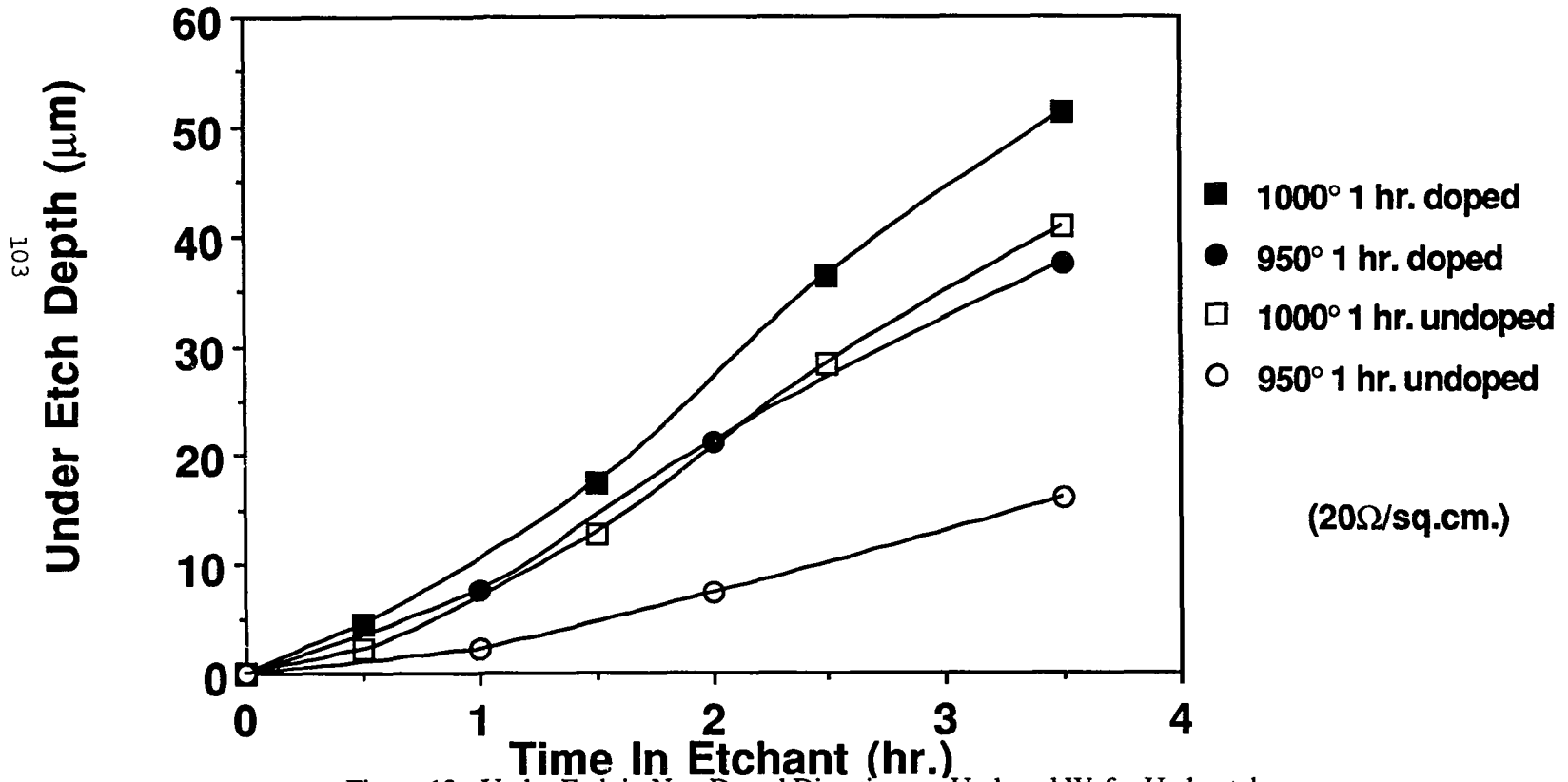


Figure 13 - Under Etch in Non-Doped Direction vs. Undoped Wafer Underetch

The most likely explanation for the severe underetching in the non-phosphorous direction is that as the doped areas are etched, the products of the reaction, including the phosphorous, settle on other close etching surfaces. These products then have the same effect as the phosphorous which was diffused into the silicon and allow etching to take place in an enhanced way through the crystal planes. Two other things observed in these experiments tend to support that argument. First, the amount of underetch is a function of the amount of phosphorous in the wafer. Wafers which are heavily doped with phosphorous experience more non-phosphorous direction underetching than wafers with less doping. Secondly when a non-doped  $20 \Omega/\text{cm}^2$  test wafer was etched in hydrazine which had been used for 11 hours to etch phosphorous doped experimental wafers the underetch was greater than when a second undoped  $20 \Omega/\text{cm}^2$  test wafer was etched in fresh hydrazine. This suggests that phosphorous freed during the tunnel etching experiments had built up slightly in the etching solution and was attacking the etching surface of the undoped wafer. Graphs of the under etching or tunnel etching which occurred in the non-phosphorous direction can be seen in figures 14 and 15. The first of these is the measurements for the  $20 \Omega/\text{cm}^2$  wafer, and the second for the  $10 \Omega/\text{cm}^2$  wafer. The figures show a strong correlation between the amount of phosphorous deposited into the wafer and the tunnel etching rate in the non-phosphorous direction. Another notable feature is the remarkable non-phosphorous tunneling which occurred in the



# Undoped Direction Etching

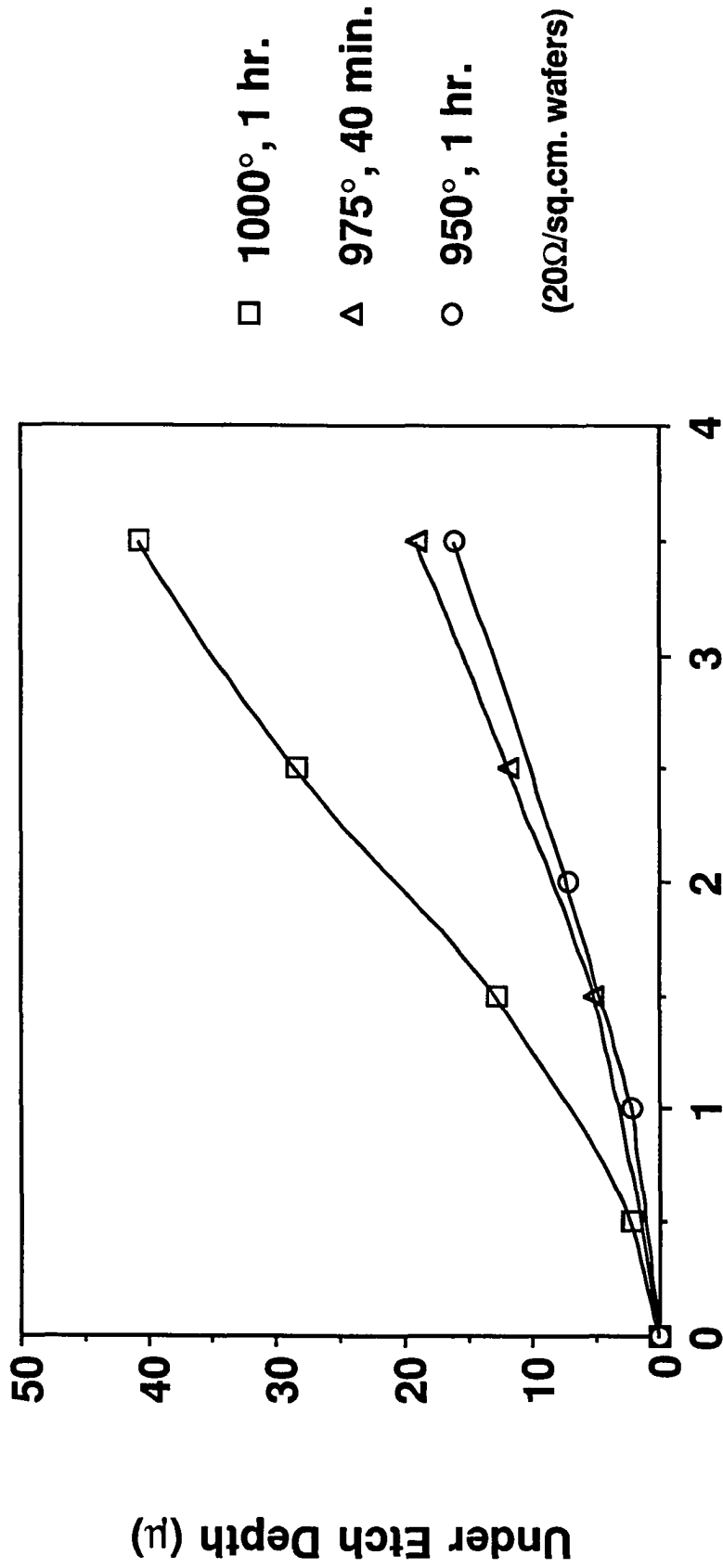


Figure 14 - Undoped Direction Etching

# Undoped Direction Etching

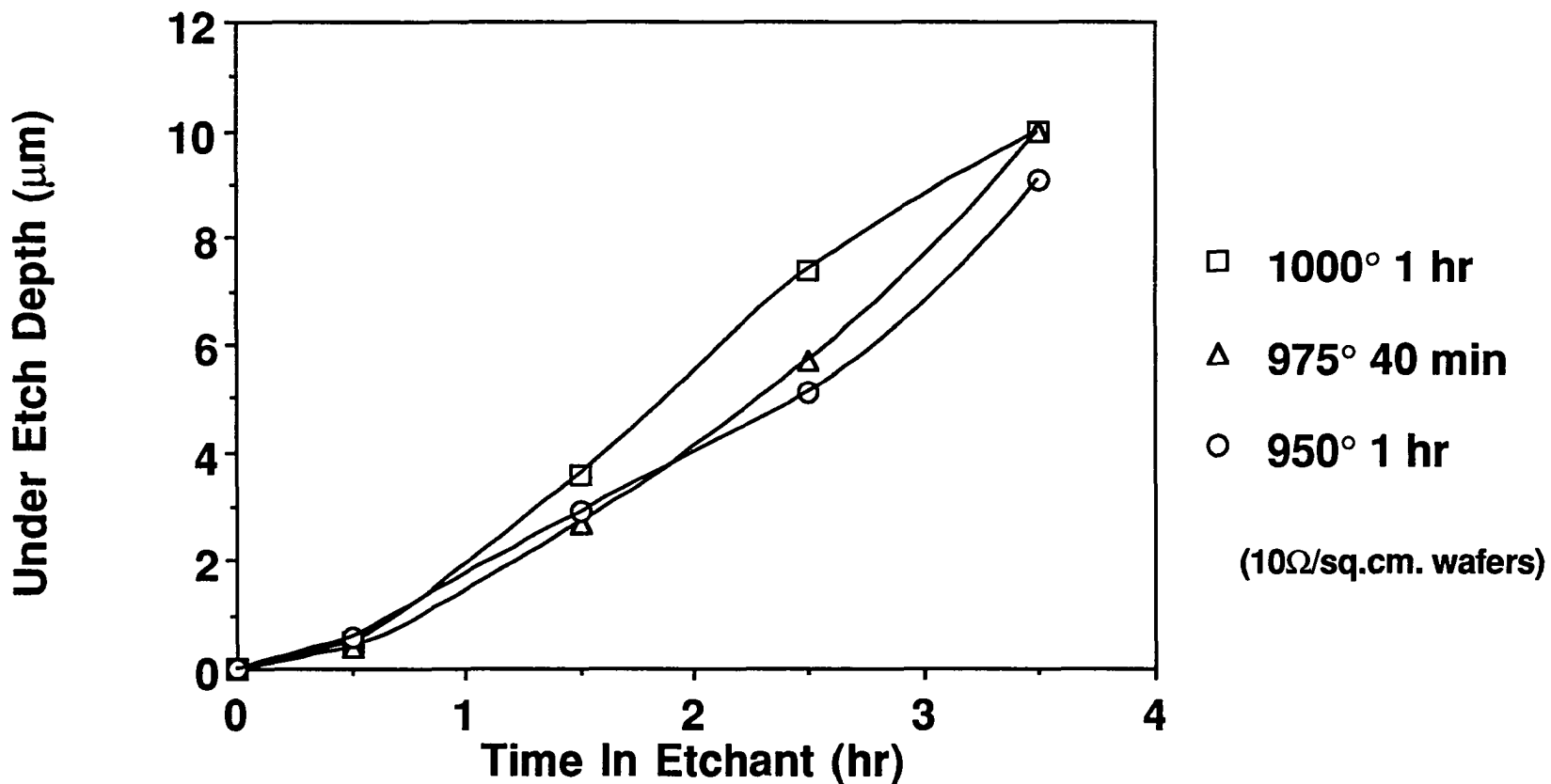


Figure 15 - Undoped Direction Etching

20  $\Omega/\text{cm}^2$  wafer which had been doped at 1000 °C for 1 hour. The most likely explanation for this large etching rate is that in addition to the heavy doping which the wafer received, it was the last wafer etched before the hydrazine was changed, and this added tunneling may be a result of a combination of heavy etchant enhancer released by the etching wafer and residual etchant enhancer already in the hydrazine.

The average etching rates for the tunnel etch experimental wafers are given in Table 2. The etching rates represent the net etching rate for the entire etch. Two rates are given, one for the tunnel which had only a thin strip of phosphorous to start the tunneling and the other from the largest strip of phosphorous, the strip actually being larger than the etch pit which started it. Since secondary plane etching was able to keep up with the tunneling, the two etching rates are very similar. The etching rate for the larger phosphorous path is consistently larger than for the thin phosphorous path probably for a combination of reasons. The tunnel etching starts with the phosphorous path and with a larger area starting the etching can progress slightly faster. In addition the larger path will release more etchant enhancer to the etching solution, if that is indeed happening, which will also enhance the etching rate.

## Table 2 - Etch Rates vs. Doping

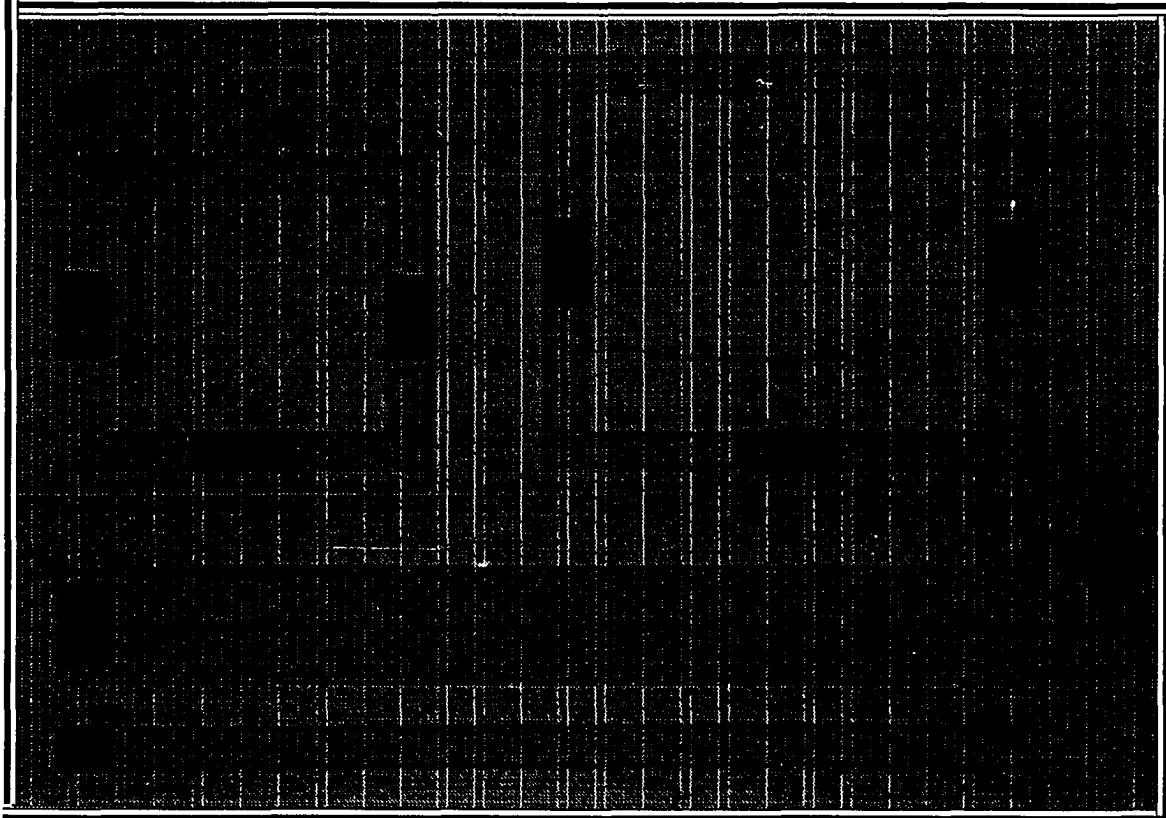
<u>Wafer Type</u> ( $\Omega/\text{sq.cm.}$ )	<u>Doping</u> ( $^{\circ}\text{C}$ )	<u>Total Time</u> (hr.)	<u>Total Mean</u>		<u>Total Etch</u>		<u>Total Etch</u>	
			<u>Etch Depth, 5<math>\mu\text{m}</math></u> ( $\mu\text{m}$ )	<u>Etch Depth, 150<math>\mu\text{m}</math></u> ( $\mu\text{m}$ )	<u>Rate, 5<math>\mu\text{m}</math></u> ( $\mu\text{m/hr}$ )	<u>Rate, 150<math>\mu\text{m}</math></u> ( $\mu\text{m/hr}$ )		
10	950	0.5	2	2	4	4	2	4
10	950	1.5	7	7	5	5	10	7
10	950	2.5	15	15	6	6	19	8
10	950	3.5	25	25	7	7	31	9
10	975	0.5	2	2	4	4	2	4
10	975	1.5	8	8	5	5	11	7
10	975	2.5	20	20	8	8	24	10
10	975	3.5	30	30	9	9	34	10
10	1000	0.5	5	5	10	10	6	12
10	1000	1.5	20	20	13	13	23	15
10	1000	2.5	38	38	15	15	40	16
10	1000	3.5	58	58	17	17	61	17
20	950	1.0	7	7	7	7	7	7
20	950	2.0	19	19	9	9	21	10
20	950	3.5	35	35	10	10	37	11
20	975	1.5	16	16	11	11	18	12
20	975	2.5	27	27	11	11	31	12
20	975	3.5	38	38	11	11	41	12
20	1000	0.5	4	4	8	8	4	8
20	1000	1.5	17	17	11	11	17	11
20	1000	2.5	35	35	14	14	36	14
20	1000	3.5	49	49	14	14	51	15

## Oxide Etch

On several occasions during the tunneling experiments it appeared that the phosphorous doped oxide was etching faster than the non-doped oxide. The phosphorous doped oxide was created when doped silicon regions were oxidized. This oxide etching was first noticed when the surface of one of the first test wafers was not prepared properly, and a thin oxide had formed from the wafer's extended time in the room air. When the wafer was placed in the hydrazine and later removed, the only areas which had etched at all were the thin oxide coatings over the doped regions, the thin oxides over the non-doped regions did not etch, see fig. 16.

Oxide etching was indicated again when a test wafer was doped with the correct amount of phosphorous to achieve tunnel etching, but then a thicker (30 minutes dry, 60 minutes wet, 30 minutes dry) oxide was grown on it which used up almost all of the phosphorous-doped silicon. When this wafer had been etching for a total of 5 hours the doped oxide began to etch back noticeably from the original opening, and it did this consistently all over the wafer.

Oxide etching at any measurable rate is not predicted by what is currently known about the etching properties of hydrazine. A wafer was prepared to check whether any oxide etching was indeed taking place. A wafer was patterned and doped with phosphorous



**Figure 16 - Tunnel Etching Test With Poor Surface Preparation**

This micro photograph shows a tunnel etching test wafer which had poor surface preparation prior to etching, resulting in the formation of a thin oxide in the etching initiation openings. The surface was etched for one hour then stripped of the oxide mask. Only areas over phosphorous doped regions etched.

950 °C for 1 hour. Then all of the oxide was stripped off in a buffered oxide etch, and a new thick oxide was grown simultaneously all over the wafer with a 30 minute dry, 60 minute wet and 30 minute dry oxidation. The wafer was then measured on the profilometer to get a preliminary reading on the surface profile. The profilometer showed that the oxide had not grown evenly all over the wafer, but had instead grown faster on the doped areas, see figure 17. The hills created on the doped areas consistently measured 85 Å. The faster growth rate is an indication of a looser lattice which would lend itself to the theory of a later faster etch rate.

The wafer was then placed in a hydrazine etch for two hours. When the wafer was taken back to the profilometer the peaks now measured 50 Å above the surrounding oxide. The profilometer reading is shown in figure 17. The profilometer measurement was taken from the sample which gave the most repeatable results, as there seems to be a problem in the first reading taken after the sensitivity has been changed.

The wafers which showed patterns that looked like fast phosphorous doped oxide etching were all in hydrazine for 5 hours total etch or longer. The same wafer was returned to the hydrazine for additional 4 hours etching. The doped oxide profile was again taken and the profilometer showed a height less than 50 Å above the

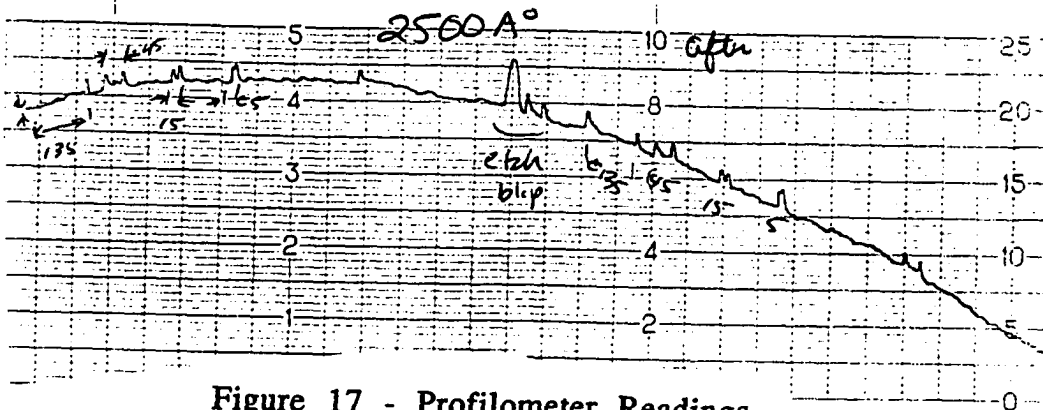
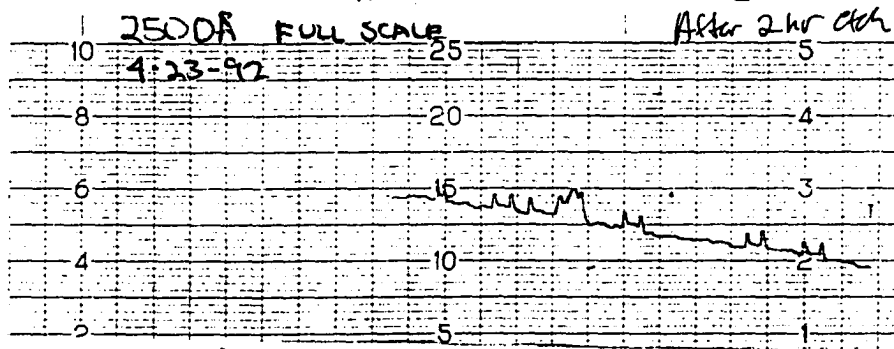
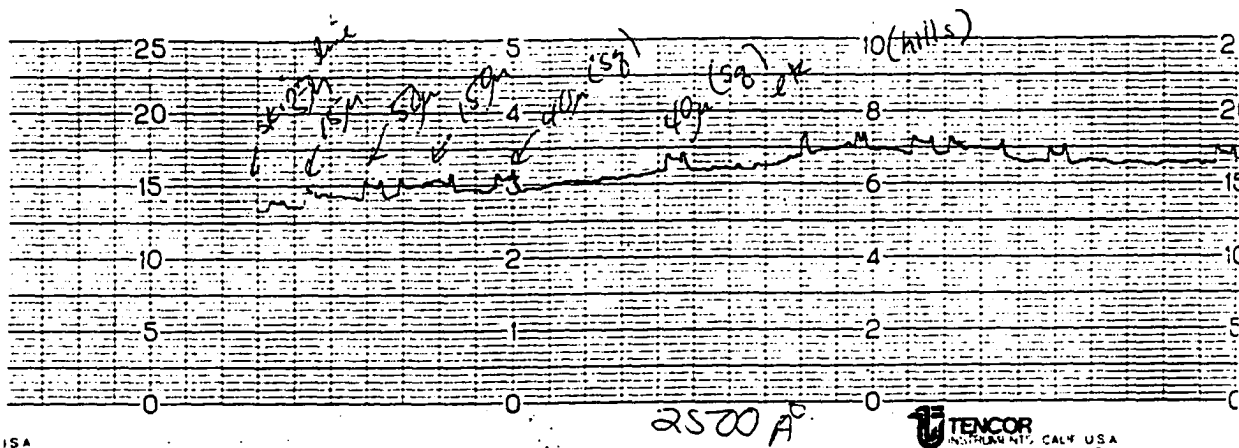


Figure 17 - Profilometer Readings

- (a) Initial profilometer reading across doped geometry. Doped geometry is labeled and shows up as peaks.
- (b) The profile measurement after 2 hours of hydrazine etching. Note the reduced peaks over doped areas
- (c) The profile measurement after an additional 5 hours in the etchant. Peaks exist at the edges of the geometries, but height readings are almost indistinguishable from base oxide



surrounding oxide. There is a notable overshoot which occurs as the mechanical profiling needle contacts the edge of the geometries, but then the reading settles out to a level almost indistinguishable from the level of the surrounding oxide.

### Tunnel Etch Uniformity

Good preparation of the wafer surface gives good tunnel uniformity on all areas of the wafer. The average and standard deviation of tunnel measurements are given in Table 3.

Non-uniform etches are usually caused by an uneven doping of phosphorous, or oxide forming on the etch windows all though the first results in more variation. Figure 18 shows two tunnels areas right next to each other on the wafer surface. One of those windows has started to etch because the phosphorous concentration in the silicon is higher, the other window has not. Uneven phosphorous doping was the result of the doping windows being not completely free of oxide before the doping process.

### Other Interesting Features of Tunnel Etching

Tunnel depth was easily viewed through the microscope without removing the oxide layer. The oxide layer was thin enough, usually .2 microns, that the light of the microscope was transmitted

**Table 3 - Wafer Etching Variation  
975°C 40min, 20 Ω/cm, 1.5 hours total etch**

Wafer Area (Ω/sq.cm.)	Phosphorous Path Width (μm)	Total Etch Depth		Standard Deviation (μm)		Total Etch Depth		Standard Deviation (μm)	
		In Doped Direction (mean)	Direction	In Doped Direction	Direction	Non-Doped Direction	Direction	Non-Doped Direction	Direction
1	5	13.7		2.13		3.6		0.80	
1	15	13.5		2.70		4.0		0.81	
1	45	14.9		1.53		4.2		0.63	
1	135	17.3		1.89		4.8		0.00	
2	5	16.8		0.80		5.4		1.02	
2	15	16.9		1.32		4.8		0.00	
2	45	17.3		1.29		5.2		0.81	
2	135	18.4		1.27		5.4		1.17	
3	5	15.8		1.47		5.0		0.76	
3	15	15.4		1.58		4.9		0.38	
3	45	15.4		1.24		4.8		0.00	
3	135	16.8		1.50		4.8		0.57	
4	5	16.0		0.81		4.3		1.16	
4	15	16.1		1.96		4.3		0.62	
4	45	16.3		1.89		4.8		1.79	
4	135	17.3		1.16		4.7		0.38	
5	5	16.7		1.19		5.2		0.81	
5	15	16.1		1.98		5.6		0.80	
5	45	17.6		1.50		5.8		1.24	
5	135	18.5		1.01		6.0		1.13	

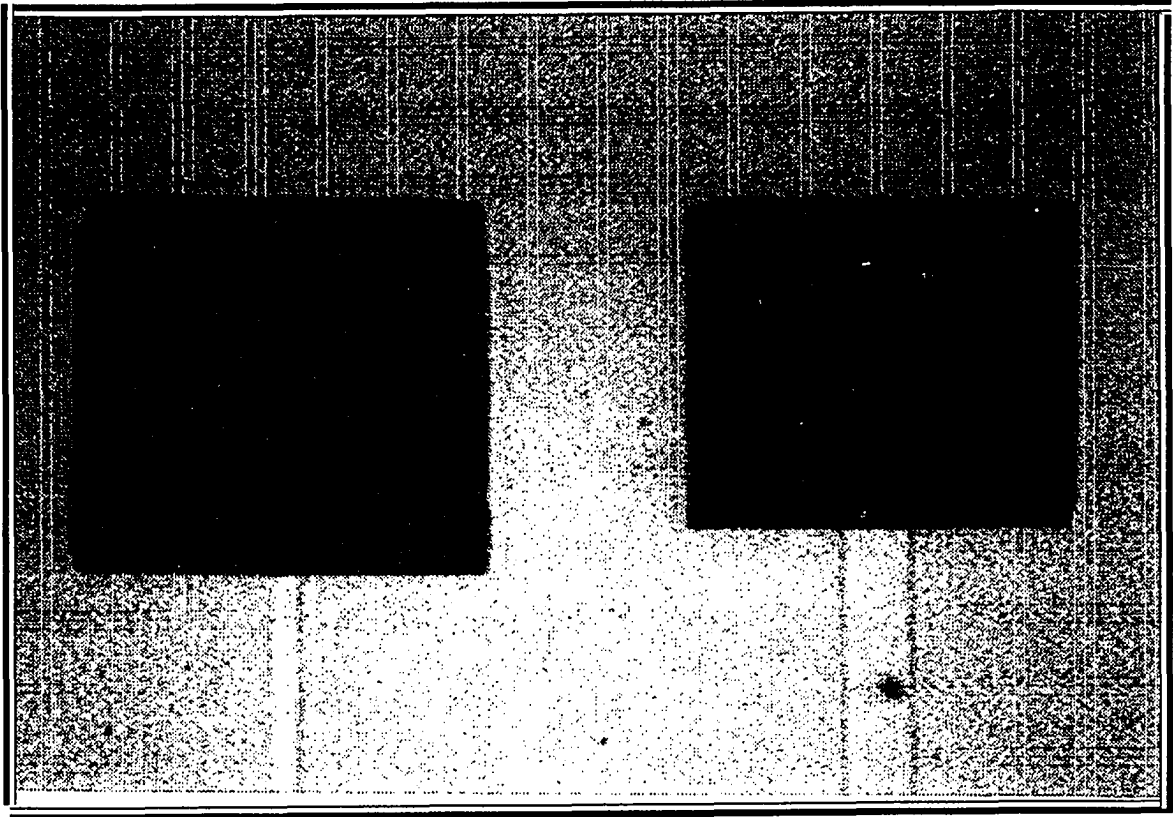


Figure 18 - Uneven Tunnel Etching

Micro photograph showing uneven tunnel etching due to uneven phosphorous deposition.

through it and it was possible to adjust the focus and follow the sides of the etch pit as it went down. The undermined phosphorous oxide appeared to have a scalloped surface, possibly due to an attack on the oxide from the etchant, or possibly due to stress induced puckering. This scalloped appearance was also noted by Burton when he did the initial etch experiments in 1981. One  $20 \Omega/\text{cm}^2$  wafer which was doped at  $975^\circ\text{C}$  for 40 minutes showed an undermined unscalloped oxide giving way to a standard scalloped area, see figure 19. While this would tend to support the idea that the oxides were behaving differently in the etchant, it should also be noted that the standard oxide is about 50% thicker than the phosphorous oxide.

Phosphorous doping was done at a variety of temperatures and times with the same solid source wafer. While the wafer was rated for  $950^\circ\text{C}$  operation, the engineers at Carborundum, the manufacturer, stated that higher temperature operation would still give uniform predictable results, but it would shorten the life of the solid source.

The freshness of the etchant used changes the etching rate, with the highest rates occurring with the freshest etchant. The change in rate with use is not rapid, as it is with etchants like EDP. The first batch of hydrazine changed by the author had not been changed in over six months and consequently was quite depleted. In

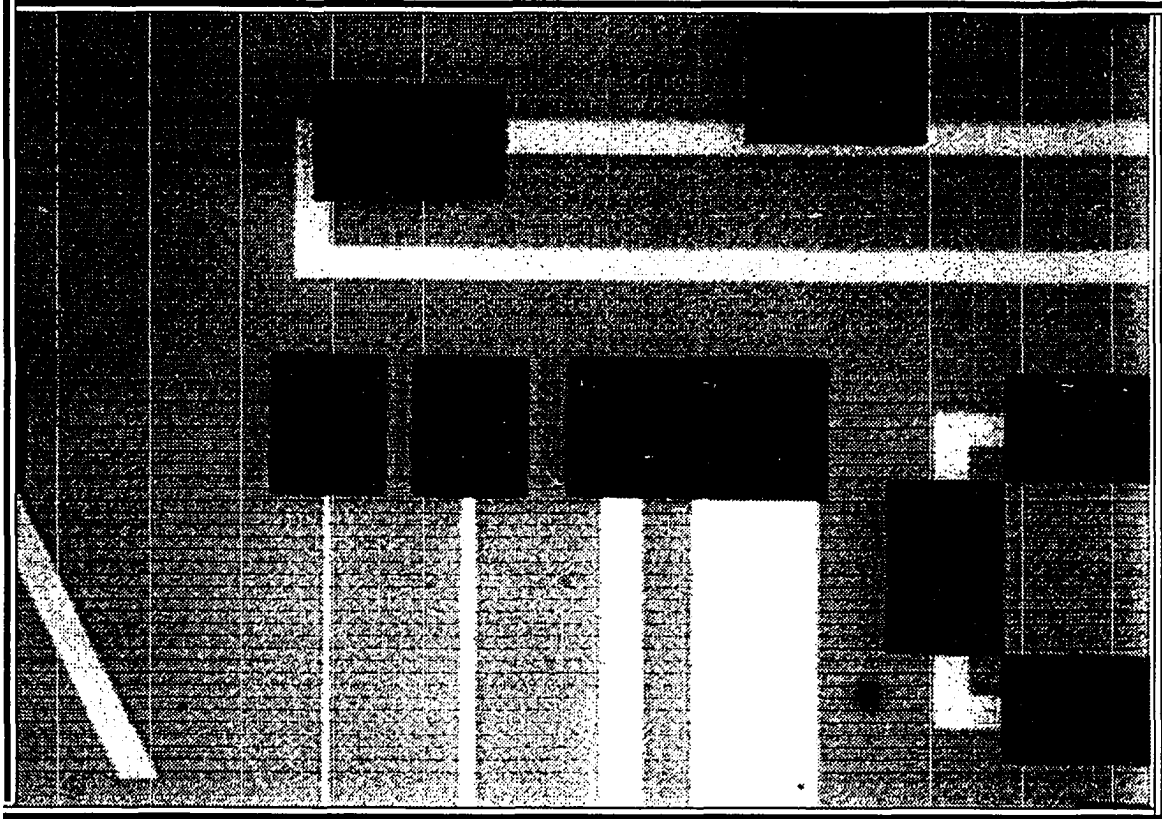


Figure 19 - Tunnel Etching Test Wafer

Micro photograph of tunnel etching test wafer. Note the scalloped appearance of the underetched oxide.

this instance changing the hydrazine almost doubled the etch rate. The standard etch rate for fresh hydrazine is 130 to 120  $\mu\text{m}$  of etch depth per hour. In addition to the slowing etching rate, the amount of tunnel etching which had already been done in the solution made a difference to any current tunnel etching. Figure 20 shows the tunnel etching which occurred on two undoped 20  $\Omega/\text{cm}^2$  wafers. The hole pattern was opened with the same oxide mask as was used for the doped test wafers, each wafer was etched in hydrazine, and tunnel etching was measured after 0.5, 1.5, 2.5, and 3.5 total hours in the etchant. After one half hour no tunneling was evident on either wafer. After all other etching times tunneling was measurable and the old hydrazine wafer tunnel etched significantly more than the new hydrazine wafer. After 3.5 total hours of etching, the tunneling difference was about 6 $\mu\text{m}$ . This is a significant difference when the mean underetch depth for the new hydrazine wafer was only 8  $\mu\text{m}$ .

### **Incorporating Tunnel Etching Into a Thermal Isolation Structure**

Tunnel etching by itself is a very interesting aspect of dopant selective etching, distinguished by its ability to enhance non-crystal dependent etching. Tunnel etching becomes most significant when it is successfully incorporated into a sensor or other silicon device for the purpose of thermal or electrical isolation.

# Old vs. New Hydrazine

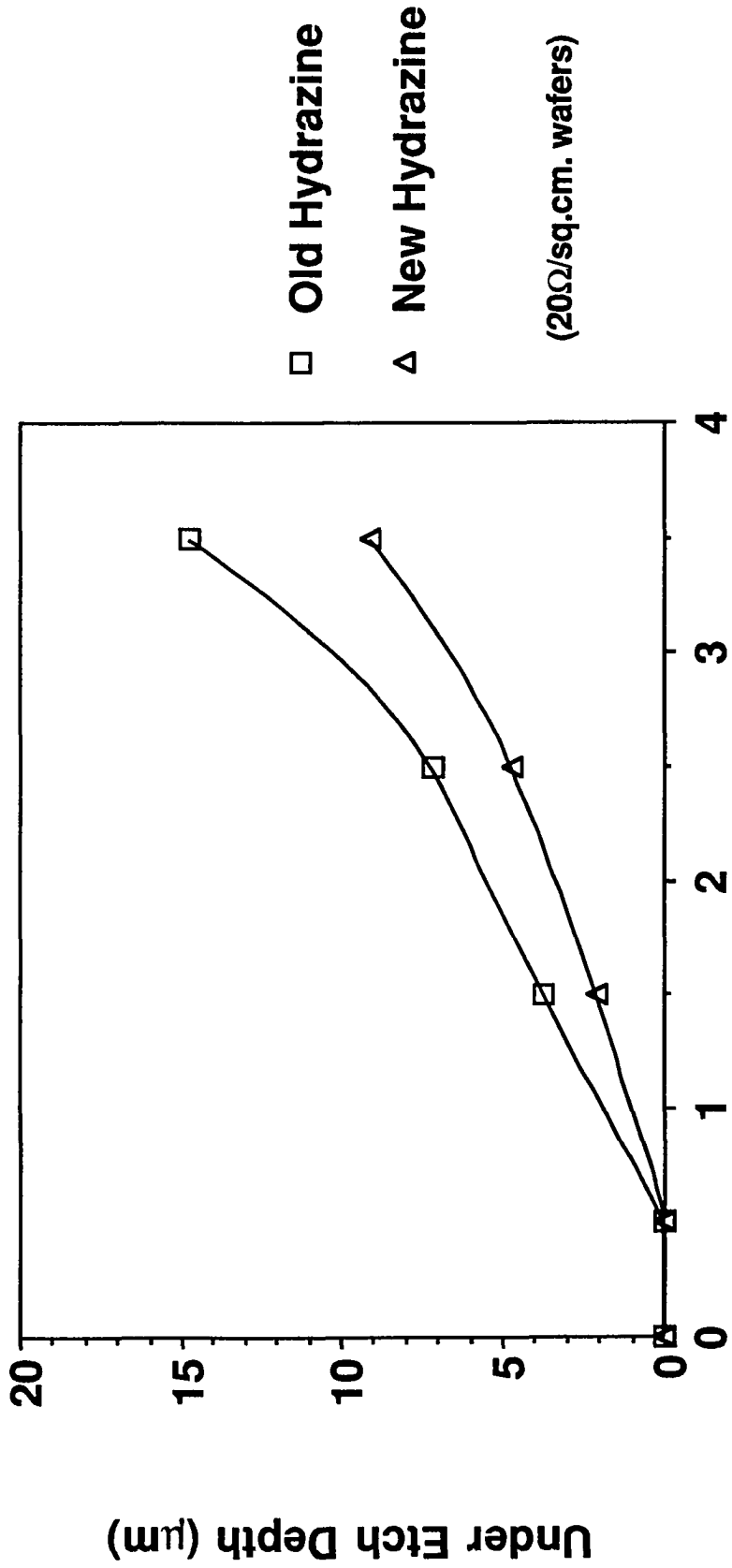


Figure 20 - Old vs. New Hydrazine

(20Ω/sq.cm. wafers)

### Structures Which Can Be Created

The original structures created by Mr. Burton with tunnel etching were all simple bridges. These structures separated the oxide on the top of the wafer from the bottom of a silicon etch pit. The tunnel etching was initiated by holes on either side of the bridge which exposed the phosphorous doped area under the silicon dioxide.

The lateral etching rate of the hydrazine in phosphorous doped silicon is approximately one order of magnitude less than the downward etching rate, depending on the freshness of the hydrazine and the concentration of phosphorous. This means that any secondary planes exposed by a tunnel etch will be etched much more rapidly than the phosphorous doped path. In addition, large structures which are to be freed by tunnel etching would take a long time in an etchant to complete, which increases the damage to the wafer.

The structures created by this researcher using tunnel etching have been different types of hollowed cavities created under the surface oxide by removing the silicon. Hollowed cavities are not initiated from one or two large holes, but instead are initiated from a series of smaller oxide openings located over the cavity area, see figure 21. The length of time needed to complete the cavity structure is then a function of the distance between the small hole openings. A compromise of 40 $\mu$ m between holes allows the



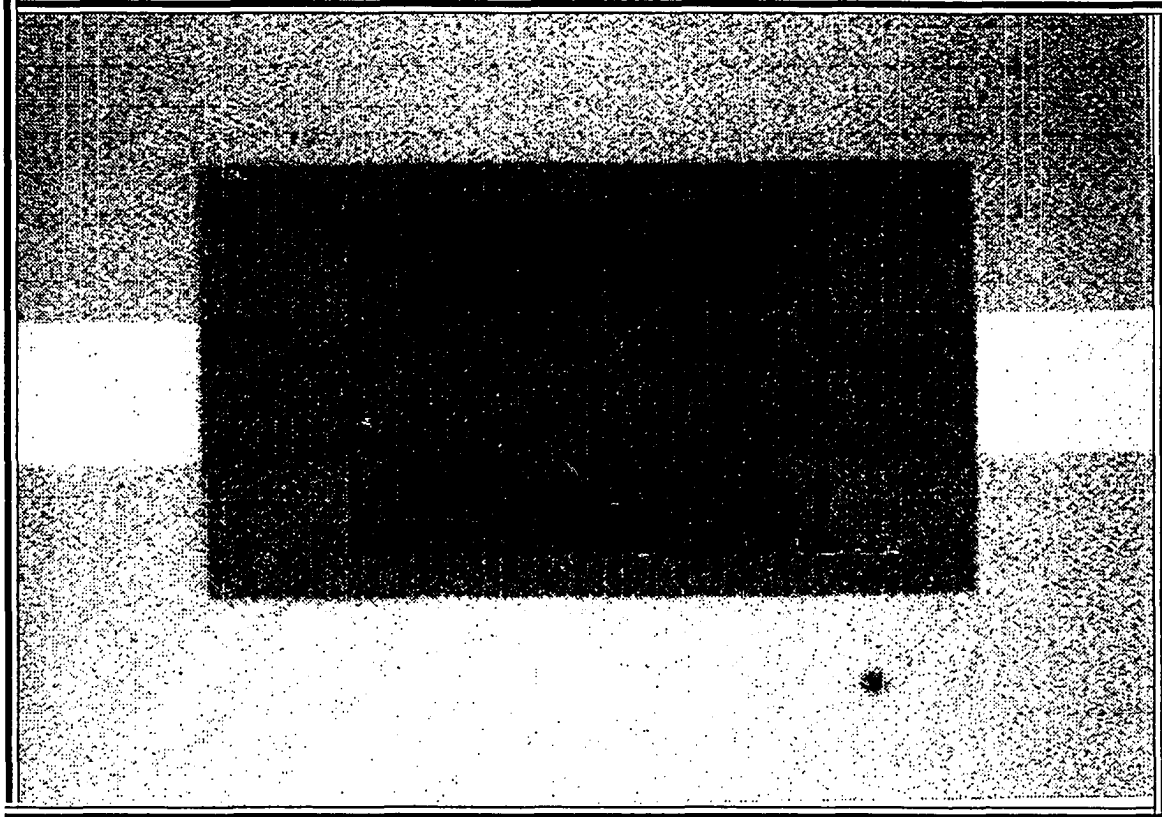


Figure 21 - Close-up of Under Etching

Micro photograph of a tunnel etching test wafer. The picture is a close up on a single underetched hole. Lines in the under etched oxide are where the wafer was taken out during etching for measurements and then returned to the etchant.

tunneling to finish in about 1.5 hours in the hydrazine etchant, which reduces inadvertent damage to the wafer.

### Strategies for Locating Oxide Hole Openings

Since the lateral etching rate of phosphorous doped silicon in hydrazine can be approximated as 12 to 15 microns/hour and the downward etching rate as 120 to 130 microns/hour, several important factors must be taken into consideration when incorporating this process into a device for manufacture.

1) Distance between oxide openings: The tunneling will progress in a rectangular pattern from the opening. The speed of secondary plane etching will quickly remove silicon between openings once initial contact has been made. This researcher suggests a horizontal and vertical distance of 40 microns between holes. When the geometry to be tunneled is such that 40 microns will not adequately cover the area, a closer placement of oxide holes is more desirable.

2) Avoiding surface geometries: Oxide holes should be arranged so that outside corners should connect with tunnel etching last where unwanted secondary plane etching will occur. Corner compensation is highly

recommended if additional time in the etchant is needed to extend the cavity downward in the silicon, and for manufacturing robustness. Another geometry problem is leaving an area of oxide without openings for a metal lead or other surface add-ons. Hole pattern design should begin around these geometric constraints with a reasonable margin allowed for misalignment of the next surface geometry. A tolerance of +/- 10 microns is usually sufficient for lithography.

3) Etch Pit Completion: The lateral etch rate is slow enough that the etch pit under the tunneling can be considered to be completed at all times. The exception to this rule is when several tunneling areas first join, it takes a finite amount of time for the new etch pit to reach its full depth.

4) Tunneling in non-doped direction: Non-doped direction tunneling is significant. To avoid having unwanted areas tunneled, oxide openings should be located over the phosphorous doped area, rather than on the edge of the doped area. This not only reduces unwanted etching, but it also reduces the number of openings needed.

5) Opening Size: Tunnel etching can be initiated from fairly small oxide openings. Rectangular openings which were only 5 microns by 10 microns had no difficulty in initiating tunneling with 100% effectiveness over an entire wafer. As the hole size decreases the main problem was the resolution of the lithography.

### **A Design Example for Tunnel Etching**

The current flow sensor version 10.0 was created by separating the base of an earlier version of the flow sensor into four feet. Separating these feet increased the sensitivity of the device, but weakened it structurally.

The earlier version of the flow sensor can be internally thermally isolated using tunnel etching. A structure could be created which would thermally isolate the silicon resistors from each other and from the base silicon. The following discussion describes how that isolation could be done, and how the design consideration developed above would be applied to a specific structure.

#### An Overview of Where Tunnel Etching is Needed

The structure to be isolated is shown in figure 22. There are four corner areas which need to have cavities placed under them

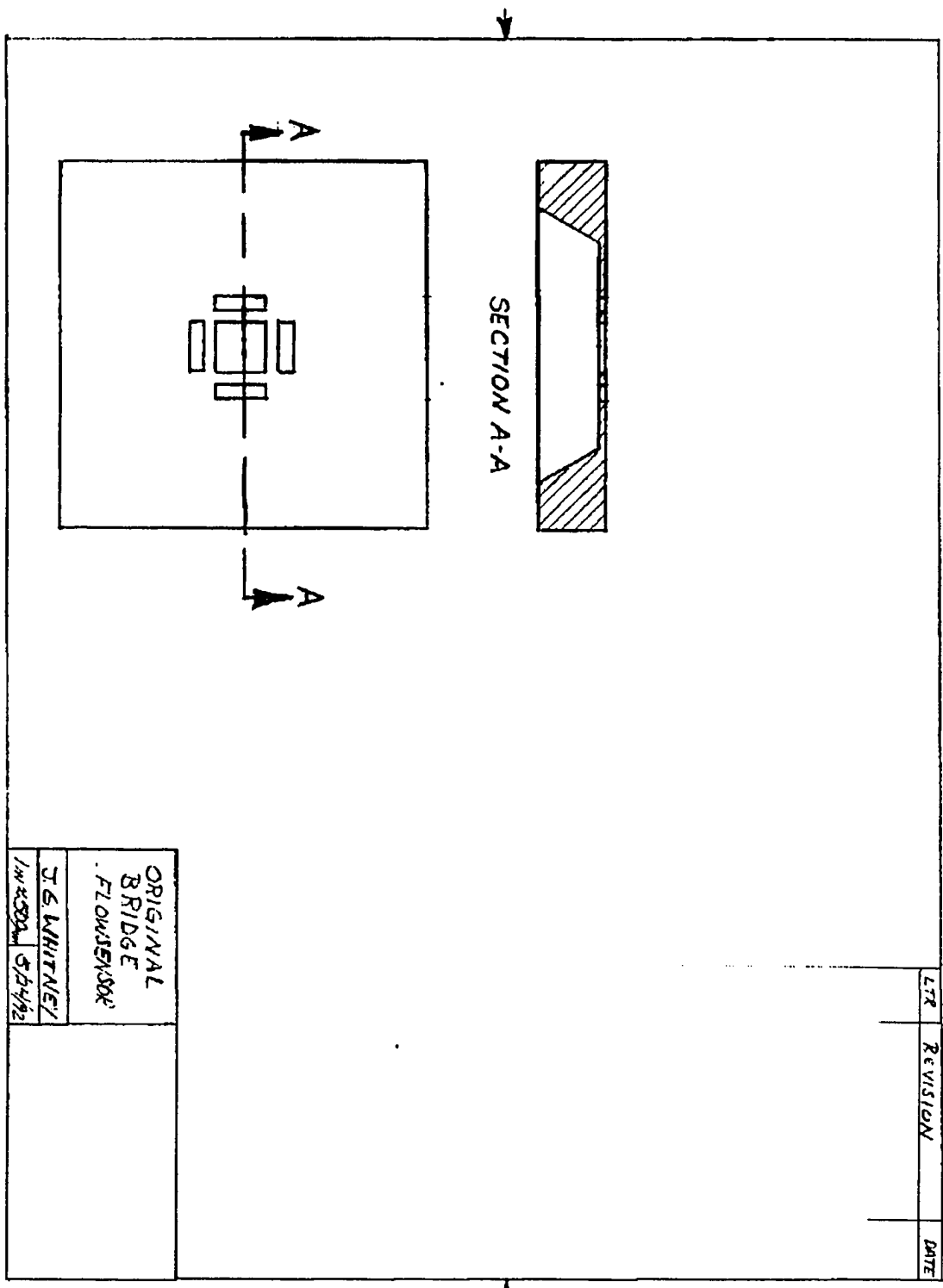


Figure 22 - Original Bridge Flow Sensor

with tunnel etching. The quality of the isolation which can be achieved will be a function of the cross sectional area of the oxide and the length of the oxide membrane. The most important area to isolate is the corners where the resistors come together.

Secondary plane etching is likely to occur at the corners of the resistor, and this is undesirable. Phosphorous doping should be done in a way that leaves the corners of these areas undoped. Leaving the corners of these areas compensates the ends of the bridge resistors against over etching. The suggested doping pattern for one corner of the device is shown in figure 23 a.

Since metal leads will extend over the oxide, a central strip of oxide will be left without any tunnel etching initiating holes. This leaves a large area where tunneling must clear the silicon, therefore the edges of this strip will have a higher number of initiating holes. In addition, since the central strip is on an angle, secondary plane etching will help to clear the silicon under the metal lead area. In addition tunneling will begin from the large holes which separate the resistors from the base silicon. The first placement of initiating holes is done on either side of the metal band and 40 microns in from the large holes and 20 microns from the phosphorous edge. This is shown for one corner of the device in figure 23 b.

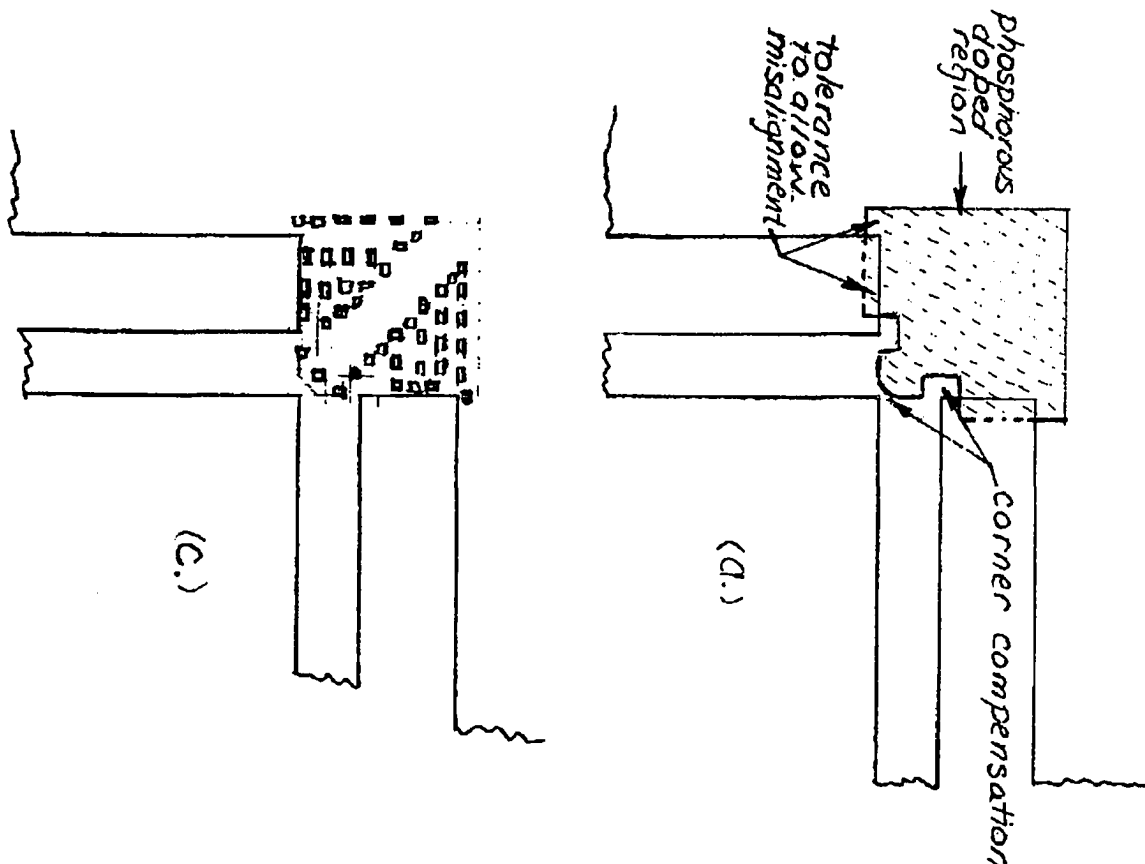
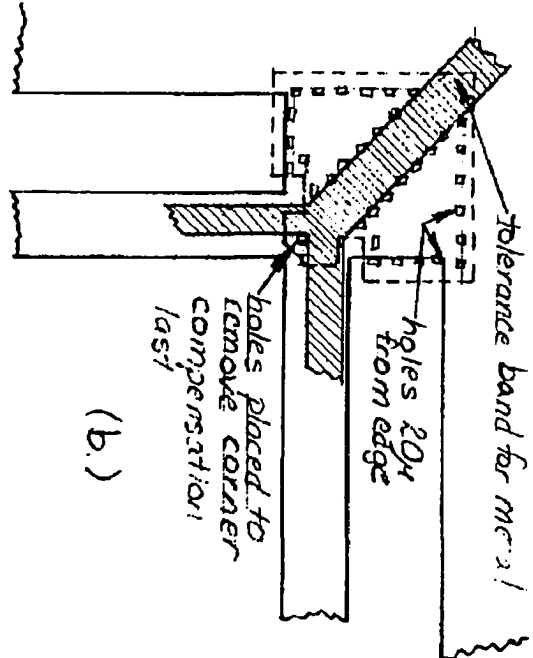


Figure 23 - Method for Tunnel Etching Cavity Creation

Method for tunnel etching cavity creation for original sensor corner isolation. Drawing shows 1 corner.

(a) Area for phosphorous doping  
 (b) Initial hole placement for geometric compensation  
 (c) Hole placement complete



The remaining large areas are filled in with oxide holes, being careful to allow for secondary plane etching at the corners of the resistors. The final initiating hole pattern for one corner is shown in figure 23 c. Figures 24 a, b, c and d show the progress of the etching over time. The tunnel etching is complete in (c), and over etched but still functional in (d). This difference in time between (c) and (d), allows for larger variation in manufacture with acceptable results.



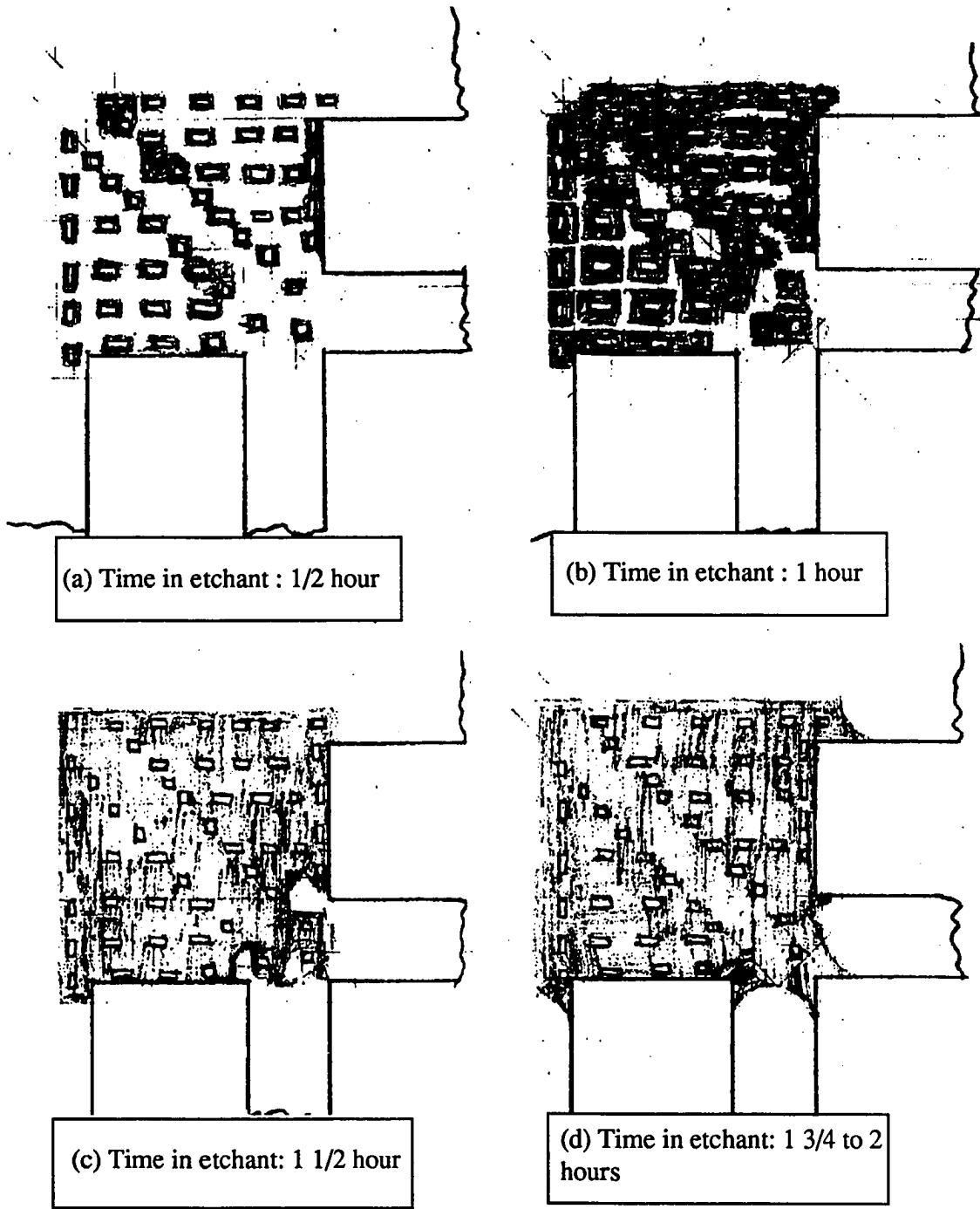


Figure 24 - Tunnel Etching Progress With Time

## CHAPTER 5

### SENSOR MODELING AND REDESIGN

Version 10.0 of the micro flow sensor had several major manufacturing difficulties. The gold which was diffused into the silicon to improve sensitivity was unstable, and caused the output signal to drift over time and measurements to be unrepeatable. The delicate structure of thin resistor bridges and large base feet was difficult to manufacture without breakage. The combination of these two problem areas led to the conclusion that a redesign would be necessary to render the part manufacturable.

#### Structural Analysis

The first step in the analysis was to create a computer model of the flow sensor to attempt to improve on the structural design. No drawings existed which specified the dimensions on the actual device from which a model could be taken. Measurements were taken through the microscope of an existing sensor which was rejected because the gold concentration was too high. These measurements were then translated into an engineering drawing, see figures 1 and 2. A model was created of the sensor in the IDEAS finite element software package and an analysis run. The analysis revealed that the high stress areas were where the resistors attached to the feet, which was as expected, see figure 25.

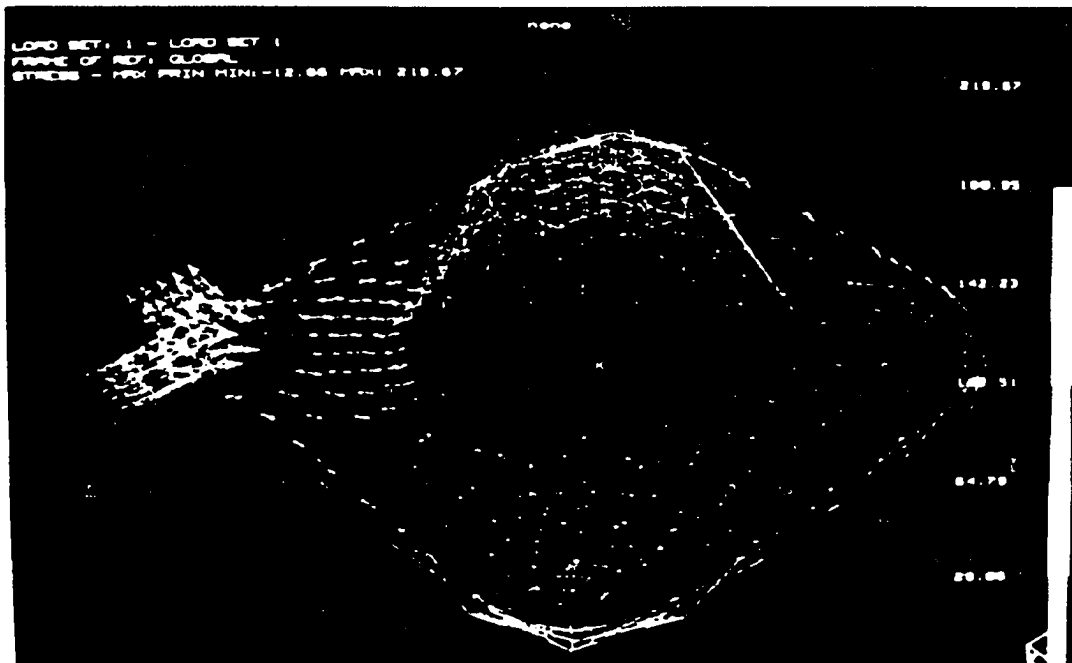
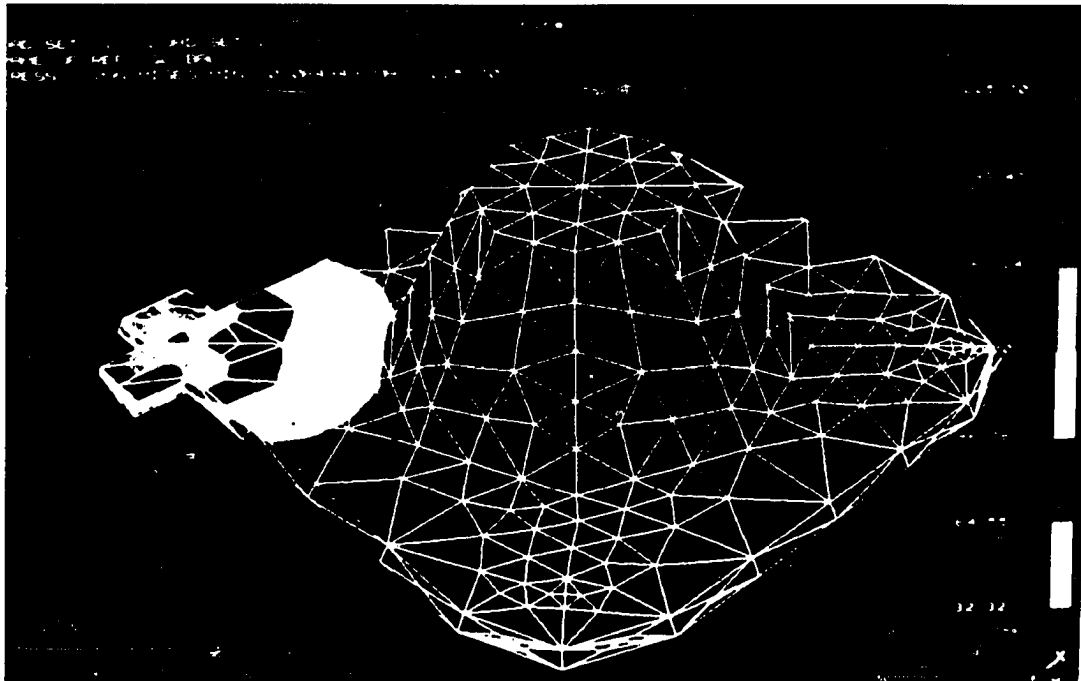


Figure 25 - Finite Element Model Solution

Several design changes were considered to enhance the current structure. It was suggested that the bridge be moved or that the feet be connected at the outer diameter by another set of bridges for structural integrity. Concern was raised as to the actual mode of heat transfer and how these changes might affect it. Separating the feet had increased the flow sensitivity over 10 times.

### **The Heat Transfer Model**

The flow sensor is a heat transfer device. No structural changes could be made without an understanding of how these changes would affect the heat transfer. The next step in the modeling process was to model the heat transfer in the current device.

#### Heat Transfer in the Current Device

The current version of the micro flow sensor, version 10.0, runs current through its four resistors, arranged as a Wheatstone bridge, to heat up the silicon bridges. The bridges are cooled by convection. Two of these resistors are parallel to the flow and two are perpendicular. The perpendicular resistors experience more cooling than the parallel resistors, and should be at a lower temperature. Since the silicon is doped with gold its

resistivity/temperature characteristics are an exponential relationship. Changes in resistance can be read by holding input current constant and monitoring voltage potential across the bridge.

The first step in modeling the sensor was to compare the heat energy transferred out of the bridge by convection, to the heat energy transferred out of each bridge by conduction to the feet. Thermal resistances were calculated for both cases. The air flow was modeled to be what the flow sensor would experience in its application as a natural gas flow meter. The sensor in that application would be placed in the center of a one inch diameter pipe with the high and low volumetric flow rates being 200 ft<sup>3</sup>/hr and 20 ft<sup>3</sup>/hr respectively. A static mixer has been suggested to be placed up stream of the flow sensor to give a flat velocity profile at  $U_{avg}$  over a large portion of the pipe diameter. This gives the velocity seen by the sensor as 3.1 m/sec (36697 ft/hr) on the high end and .31 m/sec (3667 ft/hr) on the low end, see Appendix A. The local Reynolds number for this flow is 157.1 maximum and the Nusselt number is 3.69 high end, and 1.16 on the low end. The heat transfer coefficient is therefore calculated by :

$$Nu_x = \frac{h L}{k_{air}} \quad (5.1)$$

This number is based on the assumption that the resistor is longer than the characteristic length of the flow. While for most applications this assumption is quite valid, in the case of the micro

flow sensor the bridge diameter is only about 35 microns top surface and 75 microns maximum width. The actual heat transfer coefficient will be slightly higher than that predicted by the calculations. The Peclet number suggests that losses to diffusion will be on the order of 10% of the losses to convection. As of this time there is no proven heat transfer coefficient which covers these microdimensions, so a standard heat transfer coefficient which neglects diffusion losses was used. The resistance to heat transfer by convection out of the bridge is  $2.77 \times 10^5$  °C/W for low flow and  $8.7 \times 10^4$  °C/W for high flow, see Appendix A.

Heat is transferred out of the bridges to the feet by conduction. The thermal resistance to heat loss in this way is a function of the thermal conductivity of the silicon and the cross sectional area of the bridge. The length the heat must travel is assumed to be half of the bridge total length. This value is conservatively large because heat is generated down the entire length of the bridge, and only the heat generated in the center of the bridge must travel half of the bridge length to get into the feet. The resistance to heat transfer by conduction to the feet is calculated as 210 °C/W, approximately 1000 times less than the resistance to heat loss from convection in the low flow condition.

The question was then raised, if almost all of the heat is lost to conduction to the feet, why is there any output signal at all? The

device is now operating such that each resistor is thermally shorted to two feet. The front perpendicular resistor is connected to the two front feet, the back perpendicular resistor is connected to the two back feet, and each of the parallel resistors are connected to a front and back foot. As the air passes across the flow sensor it also passes around the feet cooling them. The surface area of the feet is approximately 50 times greater than the total surface area of a single bridge resistor. The flow is directional and the front two feet will experience the greatest cooling. This means that the front two feet will have the greatest ability to cool attached bridge resistors, and only one resistor, the front perpendicular one, connects to both of these feet. The feet therefore act like cooling fins and create the change in temperature which shows up as an output signal. It is interesting to note that more recently produced flow sensor version 10.0 devices have not been operated as Wheatstone bridges because the sensitivity is so low. They have instead been operated as a single resistor, with the input voltage serving as the flow signal for a set current value. This low sensitivity when operated as a bridge is an indication of the extent of the thermal shorting.

Temperature measurements were taken of an operating flow sensor 10.0 under an infrared microscope. The device was powered with 10 mA and held in a no-flow situation. The large feet of the device showed a temperature of around 280°C, while the centers of the resistors were reading a little bit over 320°C. This value

correlates with John Doty's earlier observation that positive photoresist chars when placed on a device in operation, and the photoresist will burn at temperatures in excess of 300 °C. This was again confirmation that much of the heat energy was escaping into the massive silicon feet rather than from the resistors into the air. Flow sensor version 10.0 has a large thermal shorting problem.

### Thermal Isolation

The complex geometry of the feet and unknown air flow characteristics around the feet and bridge make an accurate thermal model of version 10.0 of the flow sensor impractical. The unmanufacturability of this flow sensor made a redesign mandatory. The first step in that redesign was to design a sensor whose heat transfer characteristics could be modeled and therefore designed to give appropriate sensitivity, with considerations of geometry size, response time and power requirements.

Tunnel etching offered a means to thermally isolate a hot resistor element. Thermal isolation would mean maximum difference in temperature for parallel and perpendicular resistors due to the surface cooling of convection. Thermal isolation would also produce the minimum power requirements, as a much smaller mass would need less energy to be heated to the same increment above ambient temperature, because it would lose less energy in



cooling. The calculations were therefore made assuming thermal isolation. Under the assumption of perfect thermal isolation all of the power input to the device would have to be lost to convection to the air. Previously most of the heat had been lost to convection to the feet, so with the assumption of thermal isolation came a dramatic drop in the power required to operate the device.

### Resistance Verses Temperature Profiles

To accurately model the devices' response to power, geometry and flow conditions, the first step was to acquire accurate information about the resistance verses temperature characteristics of the device. John Doty had made such measurements a few months earlier for one of the gold doped version 10.0 devices. The relationship is almost purely exponential, and so a slight simplification was made and a purely exponential relationship was assumed, see figure 26. This relationship shows at a glance why adding gold to the device had such an impact on the device sensitivity. Resistance is a strong function of temperature, the lower the temperature the higher the resistance.

The resistance of the bridges is a function of several factors. First is the base resistivity of the material, in this case silicon doped with gold. Next is the geometry of the resistor, in the case of the flow sensor there were two long parallel strips of phosphorous doped

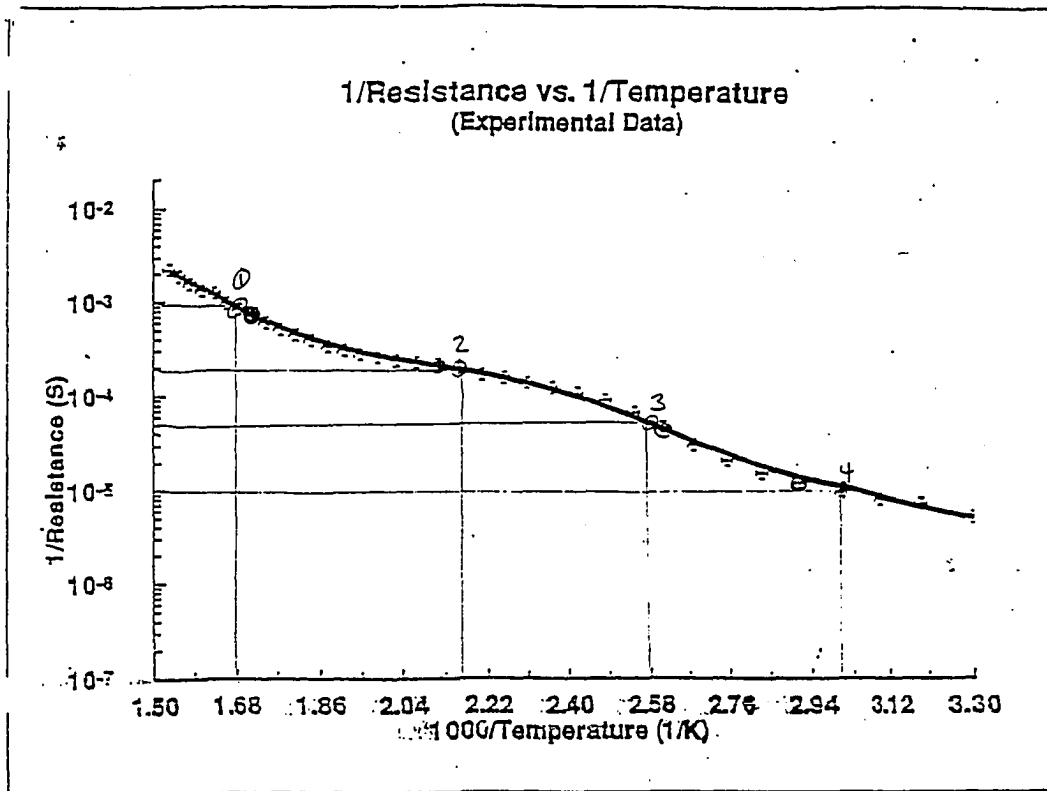


Figure 26 - Resistance vs. Temperature

Experimental plot confirming gold as the dominant deep impurity  
Measurements and graph by John Doty

Point 1. log R = 3 T = 322 °C

Point 2. log R = 3.7 T = 190 °C

Point 3. log R = 4.3 T = 115 °C

Point 4. log R = 5 T = 60 °C

silicon, each of these can be considered as good conductors. The resistor was created by forcing the current to move across a silicon band between these doped strips. The geometry of that band played an important role in resistive values.

Another resistivity versus temperature plot of interest is that of the base silicon, doped lightly throughout as is the common practice in manufacture. An example of such a curve is given in figure 27. For room temperature operation, resistivity of silicon is approximately a linear, rather than an exponential, function of temperature. One possible solution to the unstable gold problem would be to design the sensor with a large enough surface area that it would have acceptable changes in temperature, and therefore resistivity, with the flow rates expected. The other option is to operate the sensor at a high enough temperature that the resistance/temperature characteristics could be moved onto the intrinsic part of the curve, where the relationship became an exponential relationship like that of the gold doped silicon at room temperature.

### Temperature Difference Profiles

The flow sensor version 10.0 contains four resistors in a Wheatstone bridge. The output signal is generated when the resistor values change and the bridge becomes unbalanced, see Appendix C.

**PLEASE NOTE:**

**Page(s) missing in number only; text follows.  
Filmed as received.**

**U·M·I**

For the purposes of the model, the resistive values for  $R_1$  and  $R_3$  were considered to be the same, and likewise  $R_2$  and  $R_4$ . The reason for this assumption is theoretically their geometries should be identical and each pair is exposed to the same flow conditions.

The first step in modeling such a device was to find out the temperature relationship between the two resistors. The top surface area for both parallel and perpendicular resistors was the same, as was the current passing through them. Since the value of the paired resistors was considered to be the same, the current down each half bridge was considered to be one half of the total input current. Using the principle of energy conservation and the assumption of thermal isolation, each resistor had to dissipate the heat energy generated in it by convection once it had reached its steady state temperature. The energy generated in half bridge is calculated as:

$$i^2R(T) \quad (5.2)$$

Energy dissipated by convection from each half bridge is calculated as:

$$h A_s (T_1 + T_2/2 - 1.5 T_\infty) \quad (5.3)$$

# Log Resistance vs. Temperature

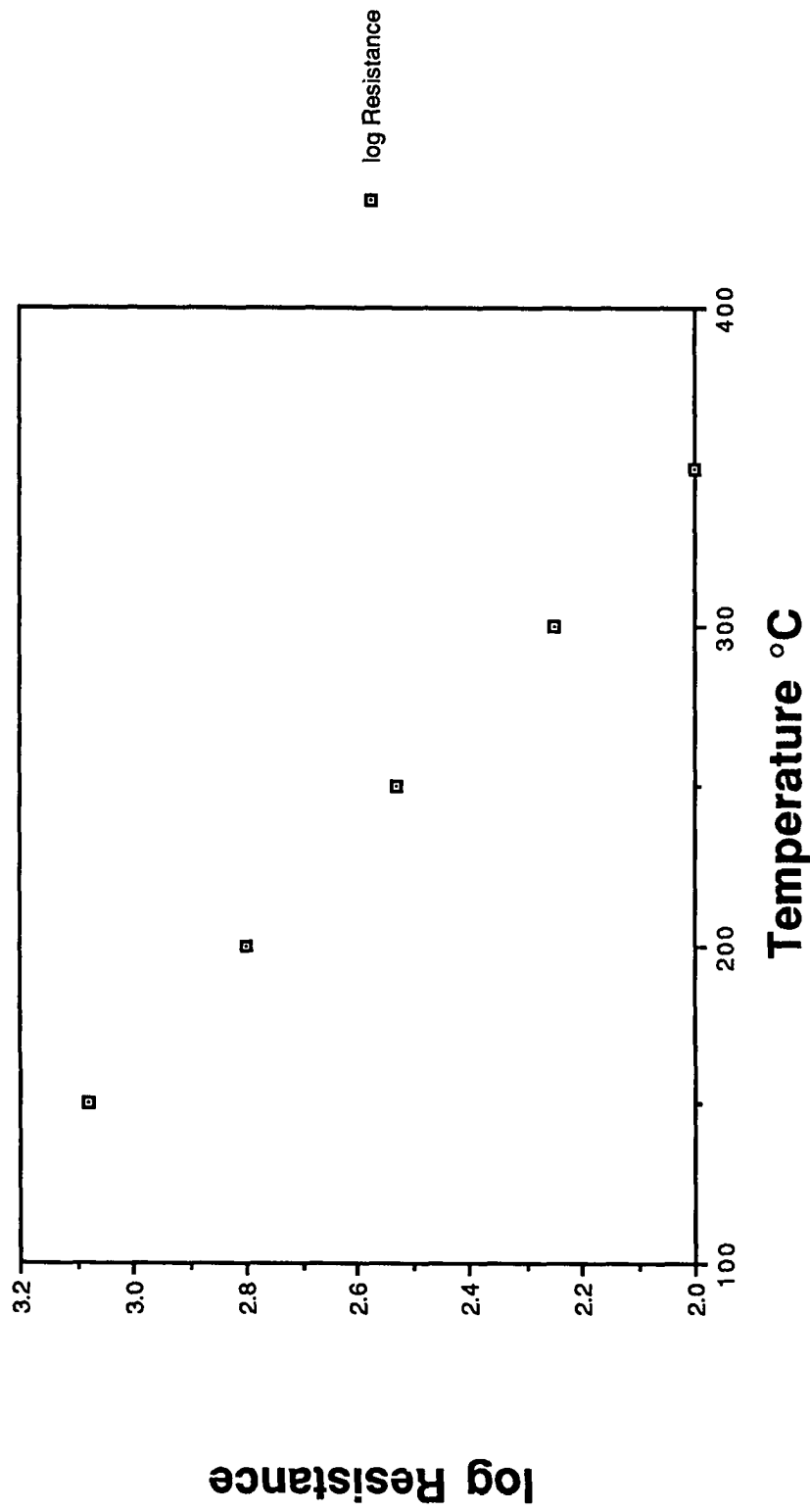


Figure 27 - Log Resistance vs. Temperature

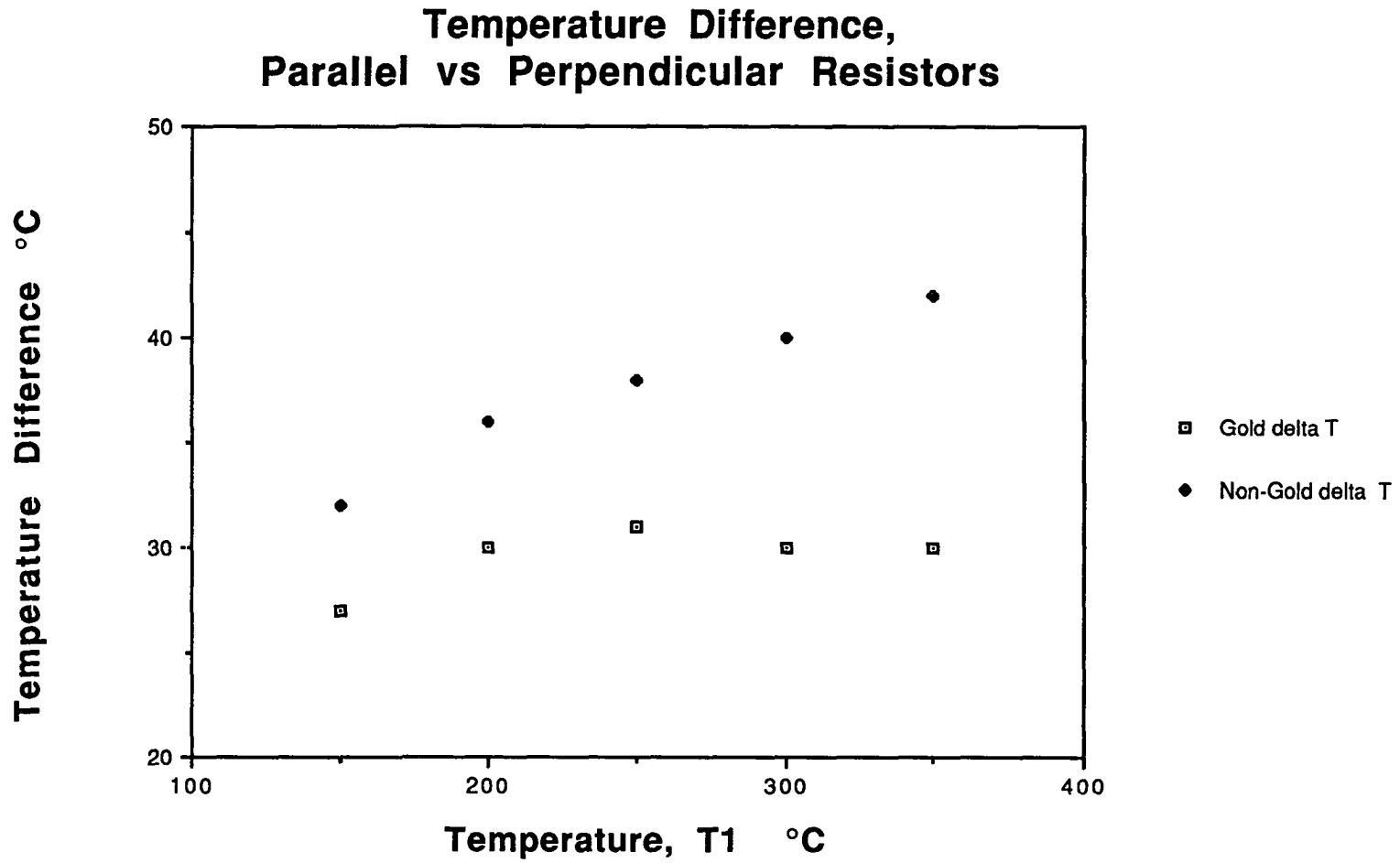


Figure 28 - Temperature Difference, Parallel vs. Perpendicular Resistors

These quantities will be equal at steady state temperature. If the resistance versus temperature relationship is substituted into the equation the relationship becomes:

$$\left[\frac{i}{2}\right]^2 \left[ 10^{(-.0077T_1+5.25)} + 10^{(-.0077T_2+5.25)} \right] = h A_s \left[ T_1 + \frac{T_2}{2} - 1.5 T_\infty \right] \quad (5.4)$$

Ambient temperature is assumed to be a constant 30°C. The equations can then be iteratively solved for T<sub>1</sub> and T<sub>2</sub>. Different values of T<sub>1</sub> will yield corresponding values of T<sub>2</sub>. The calculations are given in Appendix A.

The gold doped Wheatstone bridge device had the temperature difference profile given in figure 28. Above an operating temperature of 150 °C the difference in temperature can be assumed to be a constant 30 °C.

The same type of analysis can be done for a Wheatstone bridge which has not been doped with gold. Assuming the same resistor geometry a resistance verses temperature curve for the non-doped silicon operating in the intrinsic region was generated, and is shown in figure 27. Again this relationship is approximated as a pure exponential. Substituting this relationship into the energy balance equation and iterating for temperature differences gives a slowly increasing temperature difference with increased temperature, as shown in figure 28.



## Sensitivity to Gas Composition

One of the initial applications for the gold doped flow sensor is in the natural gas industry. The sensor should eventually become the main part of home gas meters, replacing a very large mechanical volumetric flow sensor. Knowing that the molar ratio of the different components of natural gas vary from well to well and from one time to another, one of the goals of the heat transfer model was to predict the effect of changing natural gas compositions on the current device. All calculations were made using the high and low flow velocity values of 3 m/sec and 0.3m/sec respectively.

The heat transfer model which was developed considered the device to have four bridge resistors all thermally isolated from each other. While this is not the current configuration of version 10.0, it is anticipated that the structures developed in the redesigned device will lead to a thermally isolated full bridge sensor.

Natural gas is composed of a variety of organic gases, with the highest quantities of simpler structured molecules and lower quantities of more complex molecules. The three main components of natural gas are methane, ethane and propane. In addition some pipeline mixtures have high amounts of either carbon dioxide or nitrogen. The following table is a summary of the major components of natural gas as it exists in pipelines after refining. The three mixtures selected represent the widest variation in molar composition of methane.

**Table 4 - Natural Gas Compositions (Mole %)**  
**Natural Gas from Pipelines**

	1 2 1 4	1 2 2 5	1 2 4 9
Methane CH <sub>4</sub>	94.3	72.3	88.9
Ethane C <sub>2</sub> H <sub>6</sub>	2.1	5.9	6.3
Propane C <sub>3</sub> H <sub>8</sub>	0.4	2.7	1.8
Nitrogen N <sub>2</sub> 0.0	17.8	2.2	
<u>Carbon dioxide CO<sub>2</sub></u>	<u>2.8</u>	<u>0.1</u>	<u>0.1</u>

(1)

The heat transfer model developed for the analysis of various sensor designs was used to predict the sensitivity of flow sensor version 10.0 to these changes in gas composition. Gas composition affects the model by changing the convection heat transfer coefficient. The gases which compose natural gas are similar to air, so that the original Reynolds number and Nusselt number calculations were still very similar. The flow was still very laminar and the equation chosen for the heat transfer coefficient remained the same.

$$h = .323 k \text{ Pr}^{\frac{1}{3}} \left[ \frac{U_o}{V X} \right]^{\frac{1}{2}} \quad (5.5)$$

The thermal conductivity "k", the Prandtl Number "Pr", and the kinematic viscosity "v" are all functions of the gas properties. While the thermal conductivity could be found for the various gases, the Prandtl number and kinematic viscosity had to be calculated for the individual gases as well as for the natural gas mixtures.

The Prandtl number is a function of the heat capacity, viscosity and thermal conductivity.

$$\text{Pr} = \frac{c_p \mu}{k} \quad (5.6)$$

The kinematic viscosity is the viscosity of the gas divided by the density.

$$v = \frac{\mu}{\rho} \quad (5.7)$$

The density of a gas is a function of its molecular weight, temperature and pressure. Densities for these calculations were done assuming room temperature and 1 atmosphere pressure.

A resulting property table is given in Table 5. The properties for the natural gas mixtures are based on the mole percentages as given in Table 4.

**Table 5 - Gas Property Table**

---

Gas	k (W/m °C)	Pr unitless	ρ (kg/m <sup>3</sup> )	μ (kg/m sec) x10 <sup>-6</sup>	ν (m <sup>2</sup> /sec) x 10 <sup>-6</sup>
Methane	.0302	.790	0.66	10.9	16.5
Ethane	.0173	.915	1.25	9.0	7.2
Propane	.0150	.890	1.83	8.0	4.3
Nitrogen	.0250	.740	1.16	17.8	15.3
CO <sub>2</sub>	.0233	.553	1.82	14.8	8.1
#1214	.0295	.785	.712	11.3	15.8
#1225	.0280	.713	.817	11.9	14.5
#1249	.0289	.794	.735	10.9	14.8

---

These properties were used to calculate new heat transfer coefficients for the high and low flow case for both the parallel and perpendicular bridge resistors. As was the case with air calculations, the heat transfer coefficient for the perpendicular resistor was almost exactly double the heat transfer coefficient for the parallel resistor, regardless of the gas or gas mixture. The results are given in Table 6.

**Table 6 - Heat Transfer Coefficients (W/m<sup>2</sup>°C)  
For Various Gases Over Flow Sensor Version 10.0**

---

Configuration: Flow:	Perpendicular Resistor		Parallel Resistor	
	Low	High	Low	High
Methane	192.2	607.9	99.7	313.8
Ethane	175.1	553.2	90.3	285.6
Propane	194.6	616.7	100.7	318.5
Nitrogen	161.7	511.1	83.5	263.9
CO <sub>2</sub>	187.9	593.7	96.9	306.5
#1214	191.5	606.3	99.0	313.1
#1225	183.8	582.5	95.1	300.8
#1249	194.5	612.2	99.9	316.1

---

Once the heat transfer coefficients were calculated the next question which needed to be answered was: "how much would variations in gas composition effect the output of the device?" The first step in answering this question was to iteratively find the operating temperature for given power inputs. This was done using the heat transfer model, noticing that the assumption that  $h_{perp}=2h_{parallel}$  was still approximately valid for all of these configurations. The model was checked for the device in each pure gas and then in the various gas mixtures. Assuming the present

geometry and perfect thermal isolation the output voltage variation is relatively small. The results of the calculations are shown in Table 7. The device should be able to be used in a variety of natural gas mixtures with only minimal effect of changing gas composition, although it would probably need recalibration for very large changes in gas application, for example from natural gas to air.

**Table 7 - Output Voltage from Thermally Isolated  
Flow Sensor Version 10.0 as a Function of Gas Composition**

<u>Gas</u>	<u>Output Voltage</u>			
	Low Flow (.3 m/sec)		High Flow (3 m/sec)	
<u>Input Current:</u>	<u>7 mA</u>	<u>0.6mA</u>	<u>7mA</u>	<u>0.6mA</u>
Methane	0.221	1.163	0.588	2.673
Ethane	0.192	1.026	0.547	2.489
Propane	0.217	1.161	0.609	2.673
#1214	0.221	1.161	0.588	2.673
#1225	0.202	1.063	0.567	2.579
#1249	0.217	1.161	0.609	2.673

### Power Requirements, Surface Area, Operating Temperature

The goal of the flow sensor is to have a device which will respond to flow changes with a sensitivity on the order of 10 mv/cm/sec. Thirteen different versions of flow sensors were modeled. The calculations can be found in the Appendix A . Table 9 in Appendix A is a summary of the results of those calculations.

The gold doped flow sensor when thermally isolated and not using the large feet as cooling fins did not have enough sensitivity. Similarly the same geometry non-doped flow sensor did not have enough sensitivity. When the resistance value of the non-gold doped device was increased for all temperatures the sensitivity of the device improved.

The same calculations showed that increasing the length of the two resistors, while not increasing their width increased the sensitivity of the device. Placing two fixed resistors into the Wheatstone bridge in place of the two parallel flow resistors also increased the sensitivity.

Another design used a single resistor instead of the Wheatstone bridge configuration. The single resistor was designed at first to have the same total surface area as the original gold doped device, and then that surface area was doubled. An original design constraint

had been to keep the size of the device constant, since its small size had been one of the features which made the device unique. There are two ways to consider the device size as the same. The first was that the sensing area not increase in size, hence the design which had a single resistor with a surface area equal to the total surface area of the four individual resistors. The second is to keep the overall dimensions of the device the same, as it is the overall dimensions which are important for classifying the device size. The larger surface area resistor could still be fit into a device of equal size to the old device because only two large contact pads were needed instead of the four large contact pads needed for a Wheatstone bridge.

Single resistor sensors turned out to have the highest sensitivity to flow rate. The disadvantage of a single resistor is that it is not possible to use the other resistors to compensate for ambient temperature effects. Since the operating temperature of an intrinsic device is significantly above ambient temperature, small changes in ambient temperature should have little effect on output measurements. Ambient temperature will have a greater effect on devices which operate at cooler temperatures.

All non-gold doped devices were designed to operate above 150 °C as that is the minimum temperature to achieve the strong resistance/temperature relationship. This was not considered to be a



major drawback for two reasons: first, the original device was operating with bridge temperatures in excess of 300 °C and second, that less of the total device would actually be at that elevated temperature due to thermal isolation.

### Summary of Results

A single resistor, larger surface area, non-gold doped device with tunnel etching to enhance thermal isolation was the best design. This device should give almost 9 mV/cm/sec sensitivity, given the approximations made in the mathematical model. Assuming thermal isolation, the total current input for this operation would be .5 mA and would give a voltage range of 1.66 to 4.25 volts. This is considerably less than the 20-30 volts and 10mA required for the current flow sensor.

The outside dimensions of the device will remain the same. In addition the heat transfer was calculated from the surface only so that the entire area surrounding the silicon can remain in one piece, and enhance the strength of the device. The device is designed to operate between 220 °C and 288 °C, the higher temperature under low flow conditions and the lower temperature under high flow conditions.

This device may not be suitable for medical applications because of the high bridge temperature, although the mass at this temperature is small enough that burns from the device may not turn out to be a problem. For applications requiring low temperature operation the device could be run with less power, but this is also likely to yield a loss in sensitivity.

### **The Redesign**

One of the key assumptions in the analysis of the designs is that tunnel etching could be used to enhance thermal isolation. While tunnel etching removes the silicon from between two layers of silicon dioxide, the oxide is needed to hold the device together and some heat is lost from the hot resistor through the oxide. The amount of heat lost in this manner is a function of the cross sectional area of the oxide and the length the heat has to travel before it reaches the base silicon. The thermal conductivity of the silicon dioxide is much less than that of the silicon,  $1.4 \text{ W/m}^\circ\text{C}$  compared to  $125.6 \text{ W/m}^\circ\text{C}$ , but it is not negligible. Another source of heat loss to conduction is through the metal leads and out to the main device.

The metal leads turned out to be the limiting structure for thermal isolation. In parallel with the metal leads is the thermal resistance of the oxide membranes. Two strategies were used for thermal isolation, one used a tunnel etch structure which went all the

way around the resistor, and one used a combination of a tunnel etch structure at each end of the resistor, and holes beside the resistor all along its length, see figure 29. The best thermal isolation could be achieved with the hole structure. The net thermal resistance to conduction for the two designs were  $.994 \times 10^5$  °C/W for the tunnel etch structure and  $1.2 \times 10^5$  °C/W for the combination of tunnel etching and etched holes. This is a sizeable improvement over the current design which has a thermal resistance to conduction of 210°C/W. The enhanced isolation puts heat lost to conduction about equal to heat lost to convection, an improvement over 100 to 1000 times more. The calculations for several isolation configurations are given in Appendix A .

Three different versions of resistor size and shape were developed to check for differences in performance not predicted by the heat transfer model. These differences could result from inaccuracy in calculating a heat transfer coefficient for micro scale air flow, inability to thermally isolate the device as designed or inaccuracies in judging the geometry needed to achieve the desired resistor values.

The final masks contained the six design versions, three variations on resistor configurations and two variations on thermal isolation. There were five masks needed for processing, or a total of

thirty drawings. Some of those drawings, for example the backside mask used to create the diaphragm, was used on more than one version and reduced the number of drawings actually needed, see engineering drawings of new flow sensor in Appendix C.

The first lot of devices was finished on April 20, 1992. Seven wafers started the process, four 20 ohm/cm and three 10 ohm/cm wafers. During processing it was discovered that placing the front etching early in the process created lithography problems for the rest of the manufacture. Additionally the diaphragm designed was too thin to be easily manufactured. When the devices were finished it was discovered that a missing opening between the resistor and the metal pad prevented good ohmic contact. A second lot of three 20 ohm/cm wafers was started on April 21, 1992 and completed April 27. The process was changed and the number of masks reduced from five to four. This process change involved moving the front side etch concurrent to the tunnel etch, which is the last step in the process. The metalization was a problem because of the thin aluminum lead size ( $5\mu\text{m}$ ) which was less than was possible for the standard photoresist used for metal lift-off. It was found that using 33 resist, and increasing the exposure time gave excellent results. The front etch mask and tunnel etch holes mask was combined by doing a double exposure rather than two separate lithographies. The results for the lithography were excellent. In the future, front etch holes will be significantly larger allowing for thicker diaphragms and

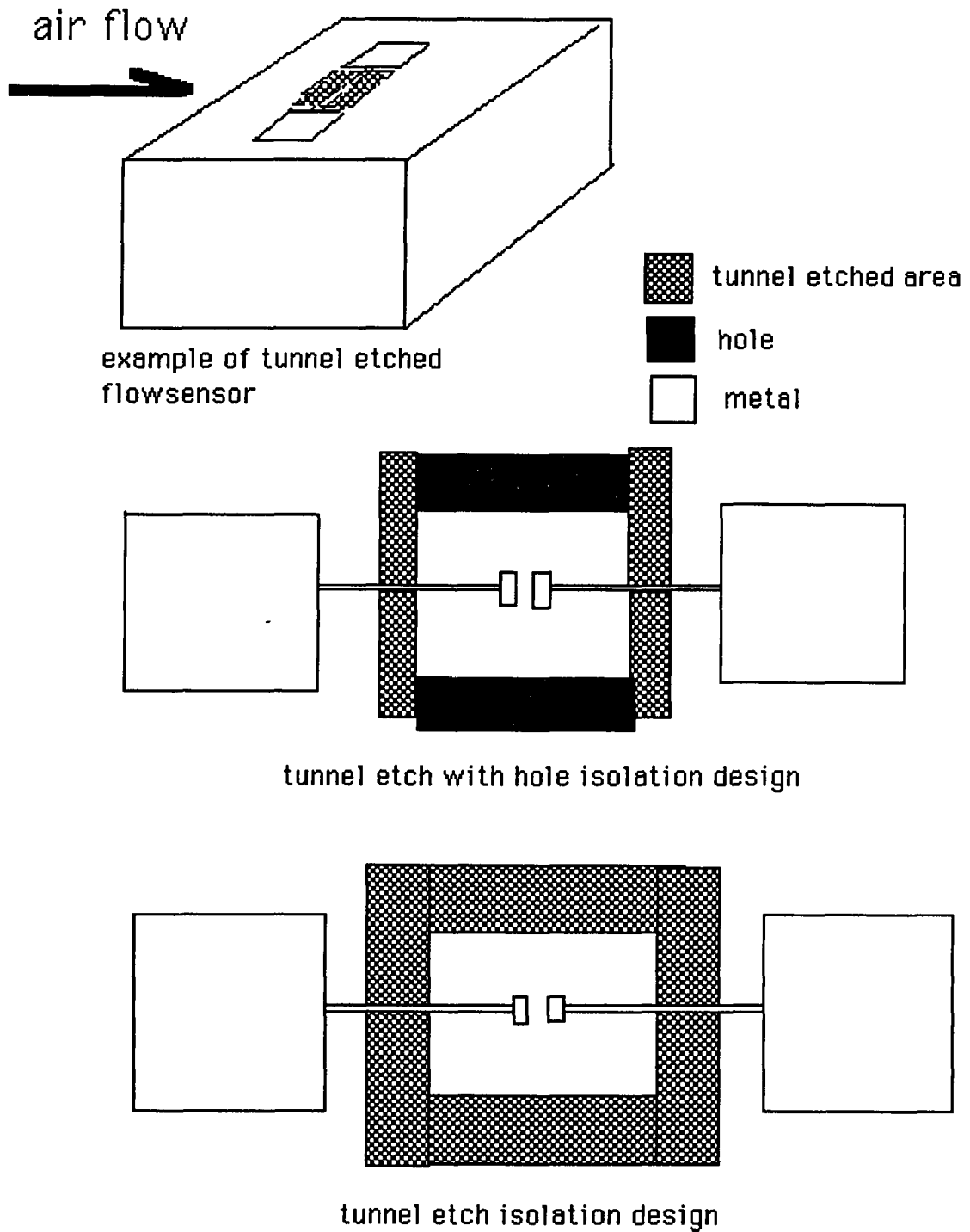


Figure 29 - Thermal Isolation Structures on New Sensor Design

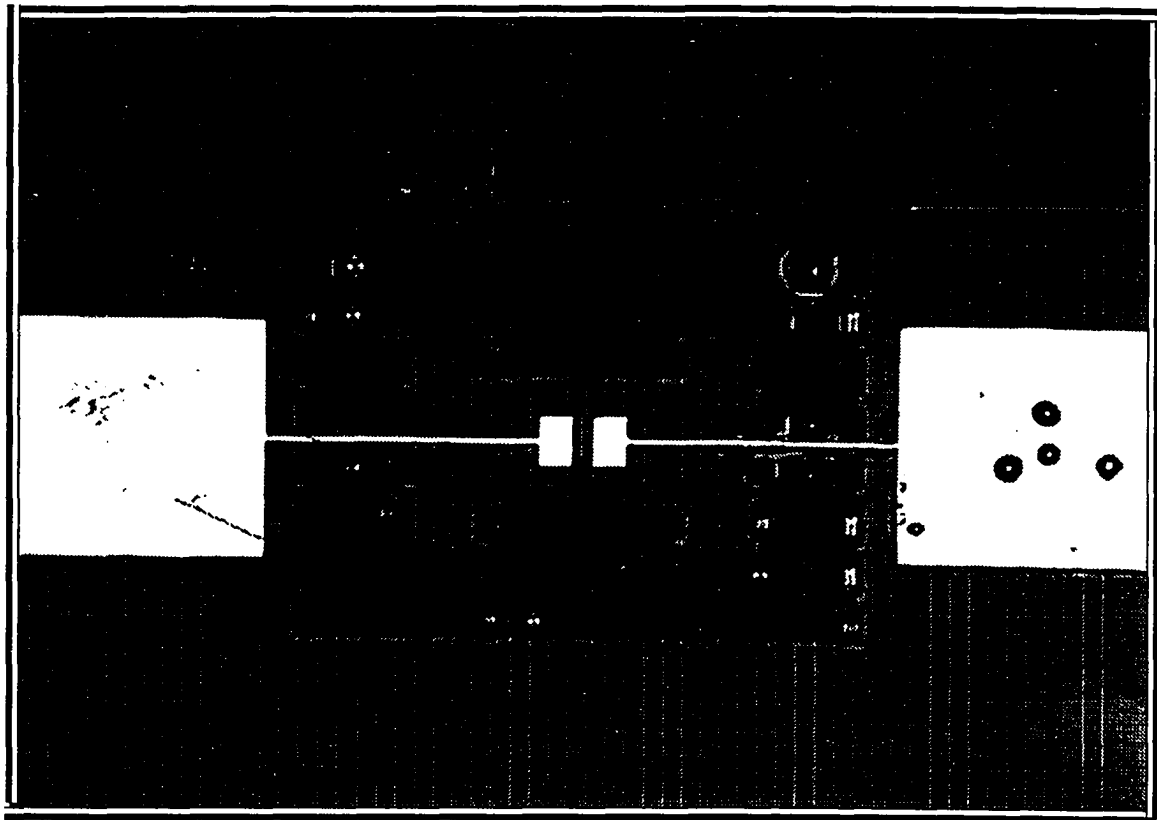
will be combined with the tunnel etch mask. The final hole will not etch through because the back side will be coated with almost a micron of oxide, but can be manually punched thru the oxide during the wire bonding process. Two photographs of different styles of devices are shown in figures 30 and 31. The tunnel etching on both of these has started but is incomplete.

### Manufacturing Considerations

Manufacturability of the new flow sensor was an important issue in the redesign. Several aspects of manufacturing were specifically addressed and incorporated into the new device.

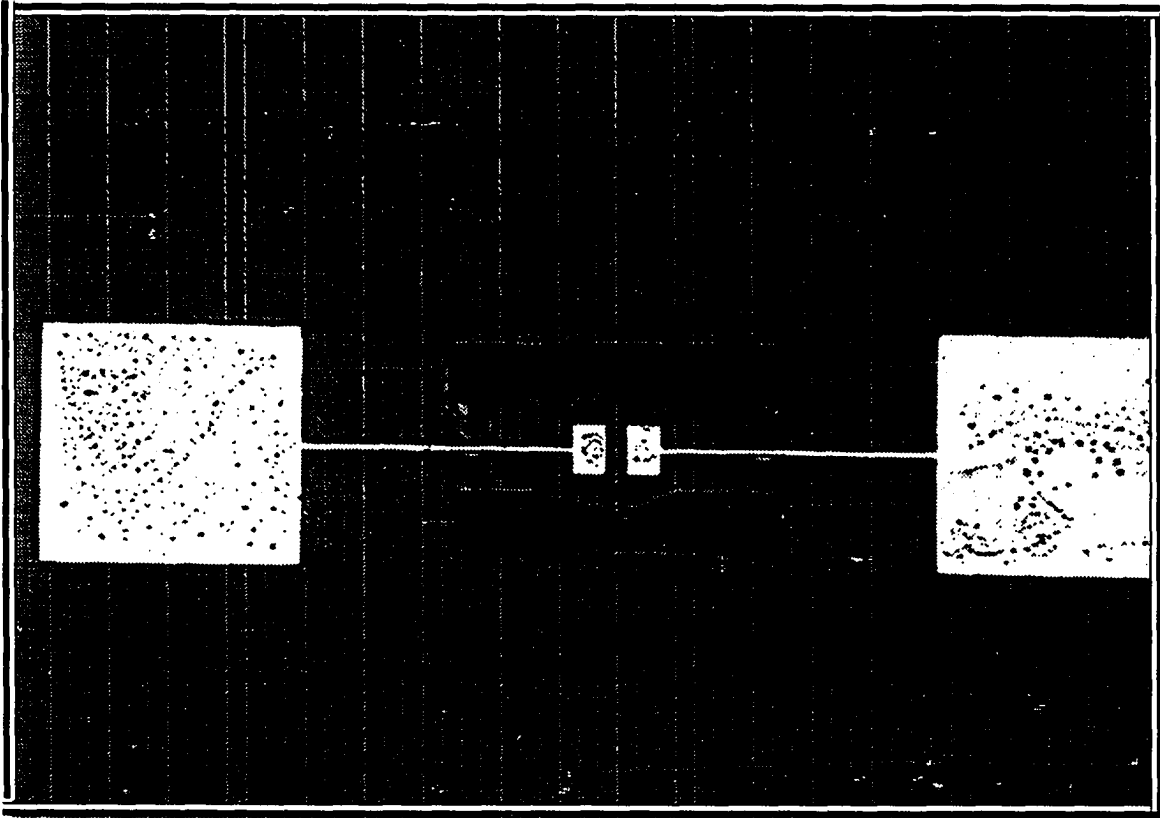
#### Easy Alignment-

Photolithography takes time and skill on the part of the processor to produce a good result. The most difficult alignments are aligning front and back features and aligning very fine detail or tight tolerances. Both of these problems are characteristic of flow sensor version 10.0. When the alignment is not right, the photoresist must be stripped off of the wafer, and the entire lithography process started again. This adds a minimum of 1 1/2 hours to the device processing time. Difficult alignments also take more time on the aligner. This part of the process is a one wafer at a time operation, and added alignment times add up.



**Figure 30 - New Flow Sensor- Tunnel Etching Only Isolation Structure**

**Micro photograph of new design flow sensor showing incomplete tunnel etching isolation structure.**



**Figure 31 - New Flow Sensor - Tunnel Etching and Hole Isolation Structure**

Micro photograph of new design flow sensor showing incomplete tunnel etching isolation structure.



The new design allows for large tolerances on all dimensions, so larger misalignments are still acceptable. The front to back mask is especially tolerant of large movements. The design is also insensitive to misalignments with respect to crystal orientation. To aid in alignment large blank die openings are left in all masks as alignment windows. These windows can be aligned from mask to mask with the unaided eye and speed alignment from over 10 minutes to about 2 minutes.

#### Diaphragm thickness variation-

A timed etch technique is employed to control diaphragm thickness. This is not the best method as etch rates, especially in EDP are constantly changing. Very thin diaphragms take constant monitoring.

The diaphragm problem was countered by having large etch through holes at the end so that diaphragm thickness could vary considerably and still produce good devices. In addition the diaphragm can be left thicker which increases structural integrity for both the finished device and the wafer in process. The second set of devices were processed with a 50 micron diaphragm.

#### Compensation for variations in tunnel etching-

Tunnel etching begins from small holes located all over the surface of the doped region to be tunneled. The holes are 40 microns

apart so that each hole must etch 20 microns before the tunnels connect. Compensation structures are put on the corners of all of the silicon resistor islands as these secondary corners are exposed as the tunnel etching finishes. The location of the etch starting holes were chosen so that the secondary planes would not be exposed until the very end of the tunnel etching. In addition the resistor part of the island is the very center portion, and a fair amount of extra etching can take place before the resistor itself is jeopardized.

#### Number of Masks-

A rough approximation of the difficulty of manufacturing a device is the number of masks required to make it. Every mask represents an additional lithography and the number of masks represent the time required to make the device. The number of masks for both the new sensor and for the old sensor device is four.

#### Time to make devices-

The gold doping in the old flow sensor has been replaced by tunnel etching in the new sensor. The doping required for the tunnel etching is also used to create the doped area for the resistors, so a doping step has been eliminated. In its place the new sensor requires a second oxide to be grown. Unlike the gold doping process, the tunnel etching process is robust, operating successfully under a variety of doping times and temperatures. It is also a uniform process as was seen in the previous chapter. The average time to

produce a wafer of the old design was 1.5 weeks, 13 working days. The time required to create lot 2 of the new design was 6 working days. In addition, all three wafers in lot 2 were successfully processed without loss to breakage.

#### Breakage-

The old flow sensor design was particularly susceptible to breakage, both during processing and during bonding. Several modifications were made to the redesigned device to reduce this problem. The individual devices are sawed apart rather than being etched apart. The delicate sensing element is in the middle of a large structural base. The number of wafers lost to breakage was only 3 out of 20. In addition, the superior strength of each sensor has eliminated the processing step of bonding the wafer to borosilicate glass. This reduced the time and expense of producing the new device.

One last manufacturing technique was employed to increase the strength of the wafers. The technique was first pioneered by John Doty to increase the strength of flow sensor version 10.0 wafers which he was processing. The first oxide etch opens the windows on the back side of the device for an EDP etchant to create the membrane structure. Before this step is done the non-patterned side of the wafer must be painted with photoresist to prevent removal of the oxide on that side. At that time a ring of photoresist is painted

around the edge of the wafer on the patterned side. This ring prevents oxide removal in this area and eventually prevents membrane etching next to the edge of the wafer. An unetched ring all of the way around the wafer greatly enhances its strength. This manufacturing improvement could also be accomplished by a mask modification.

## **CHAPTER 6**

### **THE REDESIGNED SENSOR**

The first sensor successfully produced was of the hole/tunnel etching isolation type. The initial wafers did not work as there was a contact opening which had been mistakenly left off one of the masks. The problem was not discovered until the first wafers were completed and showed an open circuit across the resistor. One wafer was reworked, and the metal lithography repeated. Unfortunately this wafer was broken during the metal lift-off process. This breakage in combination with a poor metalization severely reduced the yield.

#### **Device Testing**

Of the devices which were selected for bonding from this initial wafer only a few had good resistance values, probably due to the rework on the contacts. Out of these a device was selected for testing, and a second device selected as a control. The test device and control device both had the same size surface area on the resistor element, but the control device had no thermal isolation structure (the tunnel etching had not progressed very far). The control device also differed from the test device in that it was sliced thin (it had about 1/4 of the mass of the test device) to expose the underside of the resistor to flow. This was done as part of an

experiment to compare the device with the non-gold doped sensor version 10.0. Another thin sliced device is shown in figure 32. This figure shows how the thin slicing reduced the sensor's mass and allowed cooling from the underside of the sensor.

### Initial Checks

Both the control and the test devices showed a room temperature resistance of between 2000 and 3000 ohms. Both the control device and the test device were initially checked for sensitivity on an oscilloscope. Both devices could be made sensitive to air flow. The control device required 30 volts and 3 mA to produce that sensitivity. This can be compared to a non-gold doped old style (version 10.0) device which requires 20 - 30 volts and 10 mA. The reduced current required for this control device was probably a result of the thin slicing which exposed a large surface for convective heat transfer, while not having as much mass as a full sensor. The test device experienced the same flow sensitivity on the oscilloscope as the control device when operating at around 5 volts and 1.5 mA. The drastic reduction in power, 7.5 milliwatts as compared to 90 milliwatts for the control device was confirmation that the thermal isolation structure was indeed limiting the portion of the device which was responding to the flow.

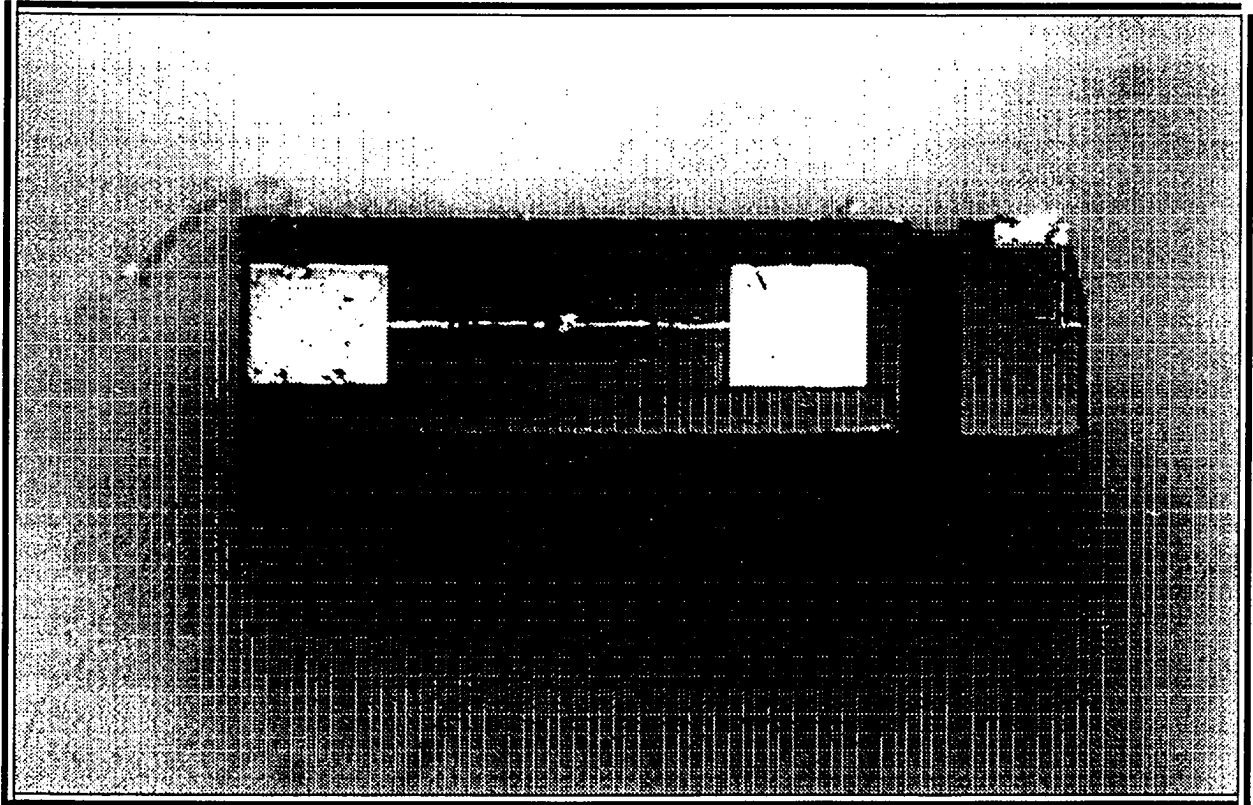


Figure 29 - Thin Slice Flow Sensor

Micro Photograph showing over etched device with the thin slice structure used for the control device.

The test device was then checked for current/voltage characteristics. The device was ohmic on this dynamic sweep for currents below 6 mA. See figure 33.

### Sensitivity Performance Check

The test device was then placed on a weekend flow and current check. The test fixture was a computer controlled mass flow controller, which regulated shop air into the fixture at rates between 0 slpm and 20 slpm. The air is channeled into a baffled expansion chamber and through a static mixer and flow straighteners before it passes the device. See figure 34. The test fixture was actually designed to measure the response to much higher flow rates, but the current mass flow controller is unable to produce those rates. The result of the lower flow rates means that the static mixer is probably unable to give a uniform velocity profile and transients probably exist in the flow.



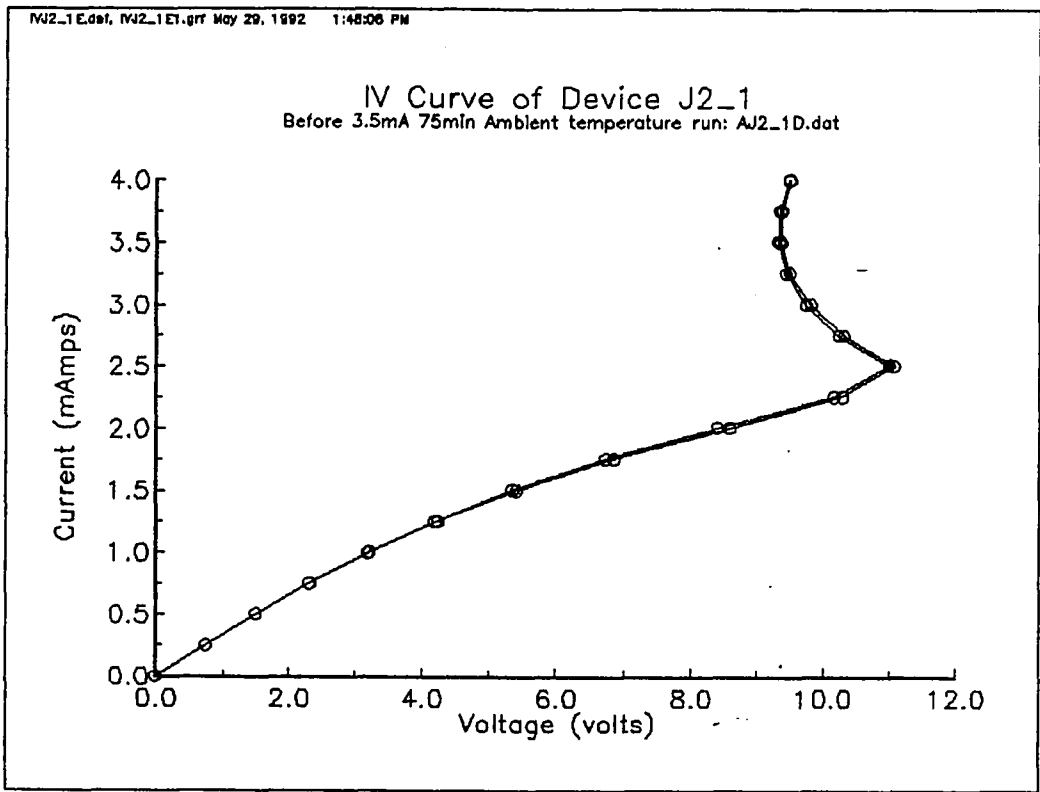


Figure 33 - IV Curve of Device J2 1

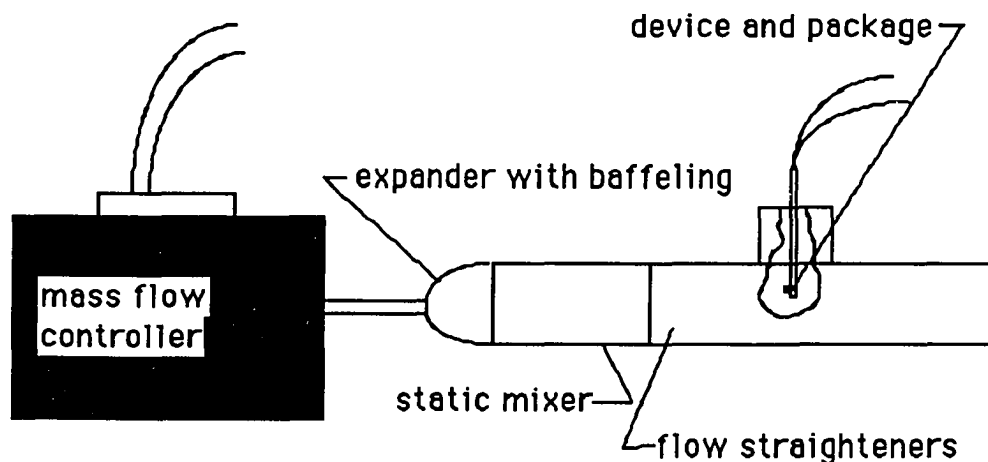


Figure 34 - Test Stand Set-up

The current to the device was controlled by a constant current source and the output of the device was the voltage. The device was run at 5 different current values; 1 mA, 1.5 mA, 2 mA, 2.5 mA and 3 mA. For each current value the flow was changed from 0 slpm to 20 slpm in increments of 4 slpm for a total of 6 different flow rates. Each current level represented 1/2 hour of testing, with data being taken every 8 seconds. After the device was checked at all current levels, the current was taken to zero for four hours and then the test was repeated.

### Test Results

The resulting test took 13,500 separate data points. These

have been graphed in figure 35. The sensitivity of the device for each current range is the voltage change over the different flow rates divided by the difference in average linear velocity. The linear velocity can be found by taking the volumetric flow rate and dividing by the cross sectional area of the pipe. A relative comparison can be made by looking at the slopes of the flow areas for each different current.

The slopes all show decreasing resistance with increasing temperature with the exception of the 3 mA (10.5 volt) area, which shows increasing resistance with increasing temperature. The lower currents occurred when the device was operating in the non-intrinsic region, below 150 °C. It had been originally assumed that operating below the intrinsic region would not yield adequate sensitivity, but this was not the case.

\* Operating the test device at 1 mA and 3 volts gave a sensitivity of around 1 mV/cm/sec. This is roughly equivalent to the sensitivity of version 10.0 of the flow sensor without the gold operating at the 20 - 30 volt, 10 mA, (200 - 300 mW) range.

\* The test device at 1.5 mA and 5 volts has a sensitivity of a little over 4 mV/cm/sec. This current and voltage level is very significant because 5 volts is the standard logic supply voltage. A device which can operate at 5 volts eliminates the need for an additional power supply to run the sensor. 1.5 mA is also very

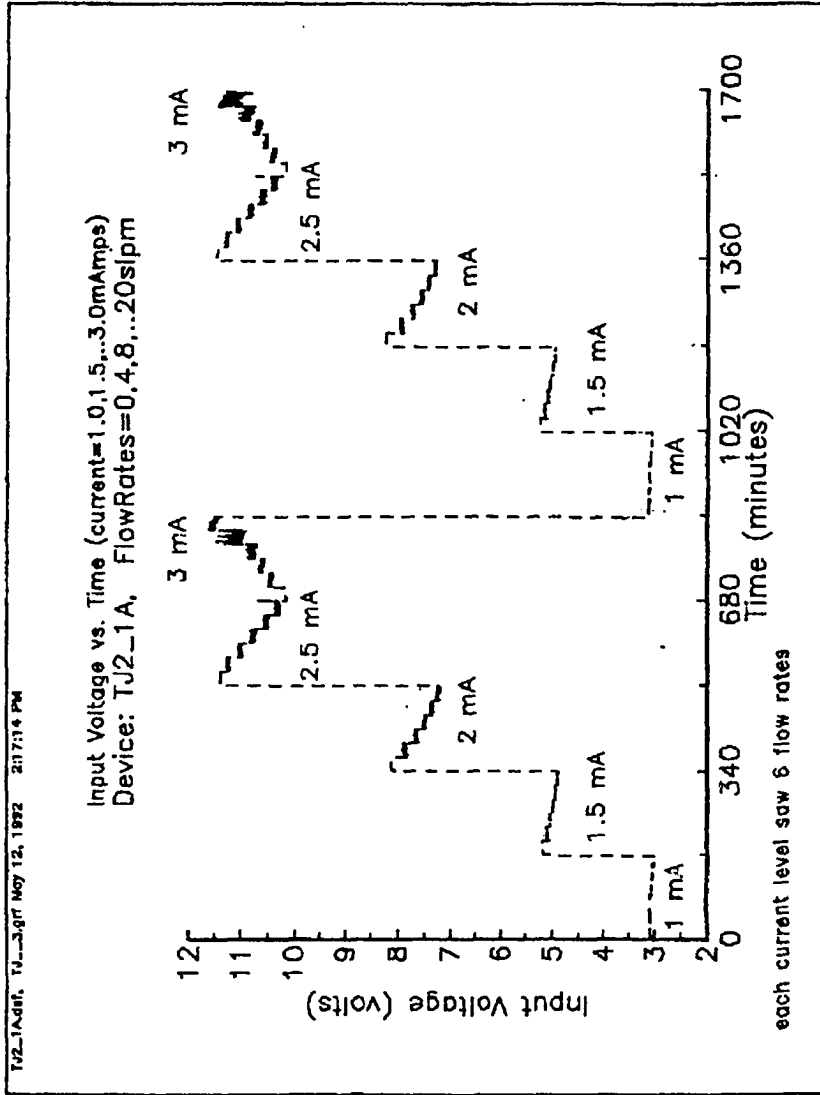


Figure 35 - Input Voltage vs. Time

significant because this current is roughly equivalent to the requirement for a single standard logic gate. This combined power requirement makes the sensor readily applicable to most control logic circuits.

\* The test device at 2 mA and 7.5 volts had a sensitivity of around 15 mV/cm/sec, and at 2.5 mA and 3 mA a sensitivity of about 20 mV/cm/sec was recorded. The 2 mA operating range was the most efficient operating range for the sensor.

**Table 8 - Sensitivity vs Power Requirements**

Current (mA)	Voltage (average)	Power (mW)	Sensitivity (mV/cm/sec)
<b>Redesigned Sensor:</b>			
1	3	3	1
1.5	5	7.5	4
2	7.5	15	15
2.5	10.5	26	20
<b>Non-Gold doped version 10.0:</b>			
10	20 - 30	200 - 300	1

Sensitivity overlay graphs have been generated from the data which show the relative sensitivities for several current levels. For each of these graphs the voltage axis represents 1 volt difference from top to bottom so that the slopes of the responses can be directly compared. See figures 36, 37 and 38.

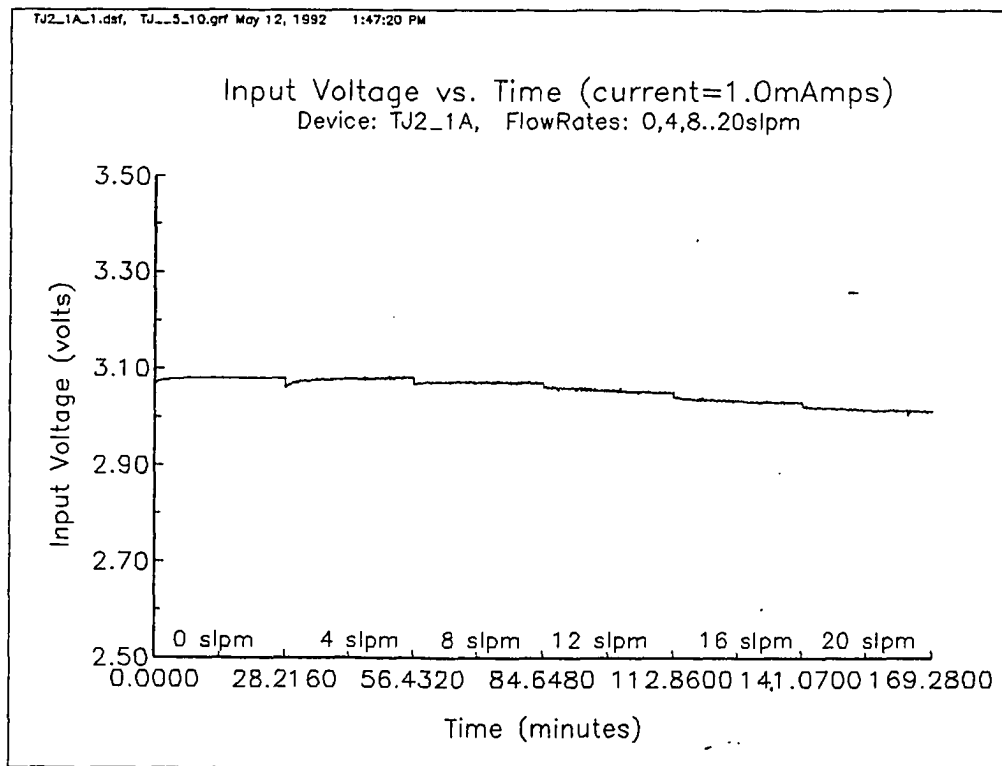


Figure 36 - Input Voltage vs. Time .  
 Current 1 mA

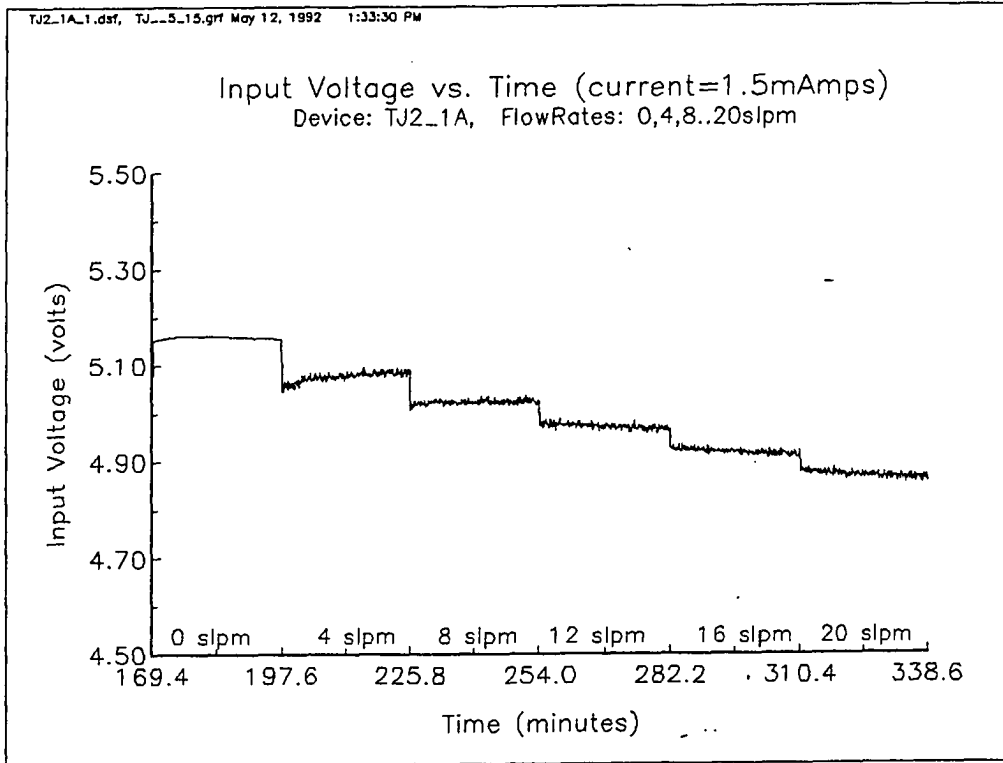


Figure 37 - Input Voltage vs. Time  
 Current 1.5 mA

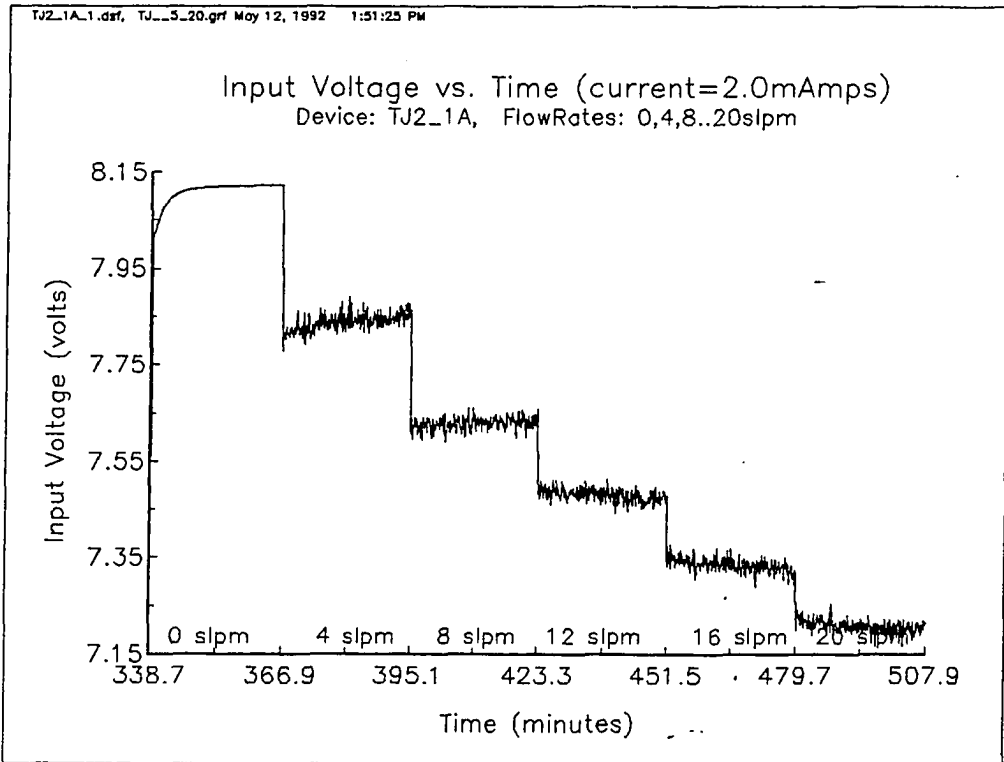


Figure 38 - Input Voltage vs. Time  
 Current 2 mA



The test revealed that an offset was created between the first and second runs of the device, see figures 39 and 40. This offset was a constant voltage offset, rather than a percentage of the output. This is why the offset appears more significant for the 1.5 mA scale than it does for the 2 mA scale. It is currently believed that this offset is the result of contamination between the silicon and the aluminum which occurred sometime during processing. This type of contamination is a common problem and can be cured by a one-time burn in of the device. A one time burn-in does not eliminate contamination, but causes the offset to occur in the manufacturing facility, rather than after the device has been installed by the customer.

The first and second run comparison shows the response of the device to be very repeatable. The slopes of the curves in all cases looked identical. The low flow cases showed an overshoot curve at the initial part of the measurement. When the test data was checked, the output from the mass flow controller was overshooting and not reaching the desired setting until 5 minutes into the 30 minute test.

Another interesting and not yet explained feature of the test was the readout from a thermocouple placed in the flow close to the device. The thermocouple had actually been added to the test set-up for some tests on version 10.0 sensors. When the test on the new

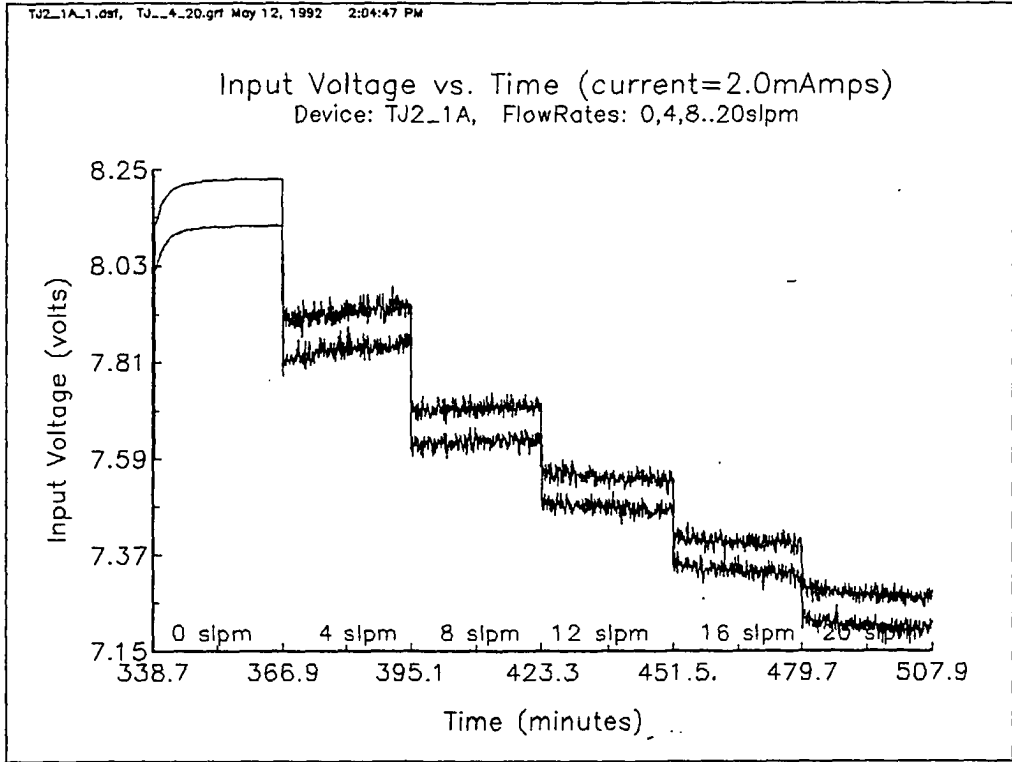


Figure 39 - Input Voltage vs. Time  
Current 2 mA  
Repeatability

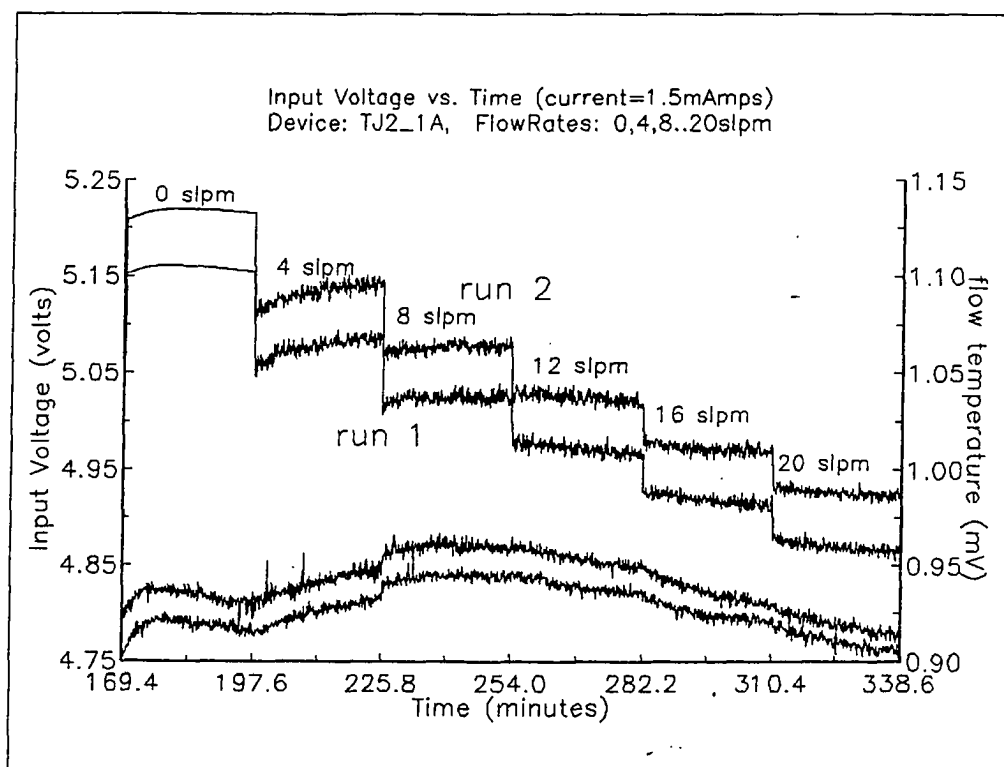


Figure 40 - Input Voltage vs. Time  
Current 1.5 mA  
Repeatability

sensor was initiated, the thermocouple was left in the setup but pulled out away from the device slightly. The output from the thermocouple can be seen on figure 40 on the readout for the 1.5 mA tests. The thermocouple shows a fluctuation in reading which correlates to the fluctuation in the device output. The device, being a single resistor configuration, is not compensated for changes in ambient temperature, and it is possible that the air temperature was fluctuating causing both signals to vary. It is also possible that the thermocouple was in such a position as to be heated by the air blowing past the hot flow sensor, or that some other factor such as internal noise in the equipment affected them both.

#### Ambient Temperature Check

The apparent response of the sensor to changes in ambient temperature were also noted in a second long term sensitivity check performed two weeks later. During the course of that test the burn in seemed to be nearing completion as offsets between runs were slowly being eliminated. Changes in readings at a given flow setting again followed shifts in the thermocouple readout.

An ambient temperature sensitivity check was done on the redesigned sensor at two different current values, 2 mA and 3.5 mA at constant flow. The 2 mA current gave the device good flow sensitivity, yet the device was operating in the non-intrinsic region.

The 3.5 mA range also gave the device good sensitivity, but the device response to temperature was a negative slope to the 2 mA operation. When the resistor was cooled the resistance would increase for operation at 3.5 mA and decrease for 2 mA. It is believed that the device is operating in the intrinsic region at this current level.

To run the experiment, the test pipe was heated with a hot air gun up stream of the sensor. The location of the heating was far enough away from the device that the device end remained cold to the touch. Air passing through the warmed pipe also warmed up. The thermocouple and the sensor were both placed in the flow, with the thermocouple on the opposite side of the sensor mounting package so as not to be effected by any air heating caused by the sensor. The test was run at a constant air flow rate of 8 slpm.

The results of the ambient temperature check are given in figure 41. As expected, the device did respond to changes in ambient temperature, with the non-intrinsic (2mA) operation being much more affected by ambient temperature changes than the intrinsic (3mA) operation. This finding has both positive and negative implications. On the negative side it means that a second resistor for temperature compensation will need to be included in the next redesign. On the positive side there is now no indication of the device having a drift problem, as all shifts in reading have followed ambient temperature readings as given by the thermocouple.

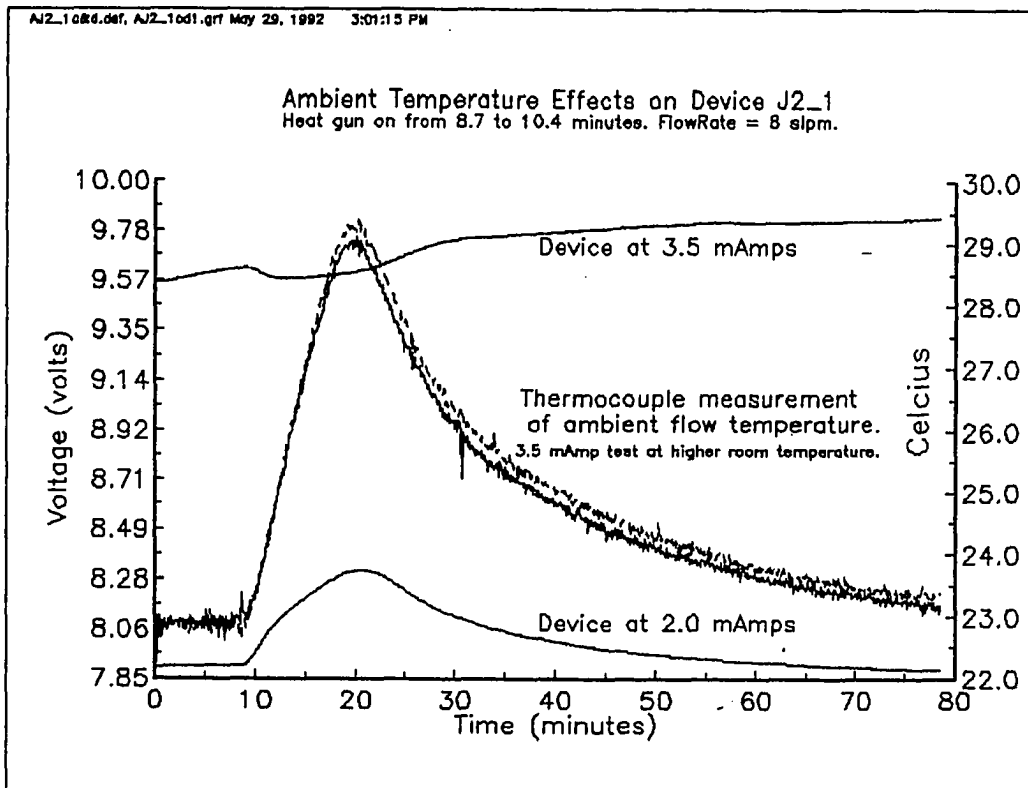


Figure 41 - Ambient Temperature Effects  
On Device J2 1

### Time Response Check

The redesigned device was checked for response to air flow changes at 1.5 mA, 2 mA and 2.5 mA operation. The test was run with a small mass flow controller which blew shop air out over the device. The response of the device was monitored on an oscilloscope, and the time constant was taken to be the time to reach 63% of the final value of a shift.

The time response was measured for both the flow to no flow response and the no flow to flow response. The device responded most rapidly to the no flow to flow situation, with time constants as follows:

**Table 9 - Time Response of Redesigned Device**

---

<u>current</u>	<u>no flow to flow</u>	<u>flow to no flow</u>
1.5 mA	290 ms	1.5 sec
2.0 mA	290 ms	1.5 sec
2.5 mA	260 ms	730 ms

---

It was not possible to test the response time of the device at higher currents as an electrical switching was encountered in this test stand. While it may have been possible to go past this point, the device could have been damaged by a current surge.

## Actual Thermal Isolation

The device was operating at a lower temperature than had been intended, indicating that the thermal isolation structure was not ideal. Without an operating IR microscope it is not possible to determine operating temperature, however knowing that 3 mA appears to have pushed the device into the intrinsic range an educated guess can be made of operating temperature. Since the device should go into the intrinsic region around 150 to 200 °C the device at 1.5 mA is probably operating in the 100°C range. If this is so, the worst case thermal shorting is about 30:1. This represents about 3% of the thermal shorting experienced by the version 10.0 design.

While the isolation structure works well, it is not as good as predicted. The reason for this difference became obvious when the device was examined under a microscope. The diaphragms on which the tunnel etching and holes were made were too thick for either to go to completion. Heat loss due to conduction was still fairly easy through the silicon at the bottom of the diaphragm which was attached to both the body of the device and the hot resistor. The tunnel etching and hole areas did significantly increase the device's resistance to heat lost to conduction as noted above. Another set of wafers is being made with diaphragms varying between 40 and 10 microns thick. These wafers should allow for a 1:1 thermal shorting and even lower power requirements for desired sensitivities.



Operating in the non-intrinsic region opens the way to new applications for the micro-flow sensor. One of the biggest problems for a gas flow sensor is contamination on the heat transfer surface. While some contaminants can be filtered out of the flow, many contaminants will burn onto a hot sensor, eventually causing the sensor to fail. Dr. Francois Padovani, Vice President for Advanced Development, Materials and Controls Group for Texas Instruments reports initial experiments done at Texas Instruments show a burn-on problem even for hot spots only a few tens of microns across. Additionally measurement applications exist for the device in potentially explosive environments, such as natural gas appliances, where a cool sensor adds to the safety of the product. Medical applications may also have more use for a cooler sensor which could be mounted directly to a patient's skin without burning. One suggested application for this device is under the noses of premature infants to monitor their breathing.

### **Conclusions**

Since this first device has shown that acceptable sensitivity can be achieved in the non-intrinsic region, the next redesign on the device will include a shift to that region. This next step will yield a device which will continue to operate below 150°C. Redesigning the

device to allow for thermal isolation on a thicker and more variable diaphragm will also increase the ease of manufacturing the thermal isolation structure. An even more isolated resistor will reduce the power requirements of the device further while enhancing the sensitivity.

Another improvement for the sensor will be the addition of a second resistor either on the same device or as a separate part of the same sensing unit. The second resistor will be able to provide information which in the logic of the device can compensate for ambient temperature changes.

The low power requirements, sensitivity, repeatability and stability of the redesigned sensor are very exciting. While not perfectly thermally isolated, the tunnel etching structure has produced a sensor with performance characteristics which are very marketable. The design is simple and tolerant of manufacturing variations. Most significantly, it proves the value of thermal isolation for this type of device.

## CHAPTER 7

### CONCLUSIONS AND RECOMMENDATIONS

The micro flow sensor and the technology which surrounds its development and implementation is a new and exciting area requiring the expertise of a wide variety of people. The manufacturing issues, operational issues, signal processing issues and safety issues are inherently multidisciplinary, requiring the cooperation of all branches of engineering. This exploration into the manufacturing problems associated with a micro device, developed into a new and novel manufacturing process, a better understanding of the devices operation, and even the creation of a new generation of devices. As with any worthwhile engineering exploration, every new discovery leads to more observations and more questions. Every new manufacturing success causes the designer to try more.

#### Meeting the Objectives

Objective 1- To determine the nature of tunnel etching to an extent that it could be reliably reproduced and used to create structures.

Results - Tunnel etching rates and variations were determined for various phosphorous concentrations, dopant widths, and etch depths. Additionally the relationship between tunnel etching and hydrazine contamination, as well as a build of of phosphorous in the hydrazine,

was explored. Higher etching rates of phosphorous doped oxide in hydrazine were also identified. Structures were designed and manufactured using a novel etch initiation scheme. Design steps to incorporate that scheme into other designs were identified.

Objective 2- To model flow sensor version 10.0 and other potential designs for the purpose of developing a new design which would utilize tunnel etching for a thermal isolation structure.

Results- A heat transfer model was developed which described the thermal shorting of the flow sensor version 10.0, as well as modeled the thermal shorting for potential isolation structures. The model was used to compare 13 different designs for sensitivity and power requirements. The geometry for the new design, the prediction of its sensitivity and power requirements came from this model. The model was also used to predict the sensitivity of flow sensor version 10.0 to changes in natural gas composition and to estimate the actual thermal shorting in the redesigned device.

Objective 3- To design and then manufacture a flow sensor which uses the tunnel etching and then show that the tunnel etching has actually increased the thermal isolation.

Results- A device was designed based on the tunnel etching results and heat transfer model. The design of the device was modified to

make it more robust in manufacture. A device was produced which has a sensitivity of 15 mV/cm/sec at a power of 15 mW. This power requirement is a fraction of the power required for flow sensor version 10.0 or a single resistor device without the isolation structure. The device is repeatable and stable.

### **Tunnel Etching Conclusions**

The information gained from this work will enhance the development of the flow sensor and many other devices which require similar isolation. The process as currently defined requires a wafer to be shallowly doped with phosphorous where ever the tunnel etching is required. The tunnel areas are then covered by a thin layer of oxide, and windows are opened in that oxide to allow etching to begin. The tunnels are etched by placing the prepared wafer in a 50% hydrazine, 50% water solution for the desired length of time to produce the tunnels.

The quantity of phosphorous available to be etched has a great impact of the success of the tunneling process. Higher phosphorous contents cause the tunnels to etch quickly, but also create underetching in non-phosphorous doped etching areas. Too little phosphorous slows the tunneling process until it is undetectable during reasonable etch times. The tunnel depth will increase every time the wafer is placed in the etching solution, although the rate of

etching decreases slightly as the tunnel depth gets great because of the difficulty of getting fresh etchant to the active surface.

Tunnel etching appears to give off to the etching solution some sort of etch enhancer and tunneling occurs all around the etch opening, even in non-doped directions, although at a reduced rate. Windows are best designed to be opened in the center of the tunneling area, rather than at an end. Two windows can expect to connect through a tunnel etch if they are no more than 40 microns apart with a reasonable etching time, generally under two hours depending on the freshness of the etchant. Etch times in excess of 2 hours will produce even longer tunnels, but the quality of the etched wafer begins to suffer due to imperfections in the masking oxide such as pinholes or scratches. The longest tunnel etch produced by the author was over 60 microns.

The tunneling etch rate is such that secondary planes generally keep up with the advancing tunnel surface, so the size of the initial window opening should not be excessively large as that size will be propagated down the tunnel.

Tunnel etching is a controllable and repeatable process, given good surface preparation at the time of phosphorous doping and final etching. Tunnel length variation was less than  $10\mu\text{m}$  for the deepest tunnels etched.

Tunnel etching has been shown to be incorporable into a device for isolation purposes. Other devices requiring similar isolation or oxide bridges for structures can use this method in their designs. This method requires only standard micromachining equipment and materials. Since silicon oxide is also a good electrical insulator, the tunnel etching process should prove just as useful for electrical isolation as for thermal isolation.

Dopant Selective Etching (DSE) has traditionally meant using a dopant to stop the etch process. Dopant Selective Etching must now be expanded to include the idea of doping to enhance the etching process.

### **Modeling and Redesign**

The heat transfer model of the micro flow sensor revealed some interesting problems with trying to create a micro-heat transfer device. The small size of the heated element, and therefore its small surface area make it difficult to get sufficient heat transfer into the surrounding air. Diffusion effects start to play a major role in the heat transfer and traditional boundary layer theory is no longer strongly applicable. The difficulty in getting heat into the surrounding air meant that losses to conduction became extremely significant, and methods to thermally isolate the heated region became increasingly important.

The heat which can be absorbed by the passing gas is also a function of the properties of the gas itself. Changes in gas composition should slightly effect the output reading of the device for the same flow rate.

Finite element modeling remains a valuable tool for structural analysis. While the analysis needed for the flow sensor ended up being thermal in nature, the finite element program has since been used by another micromachining engineer to model a micro pressure sensor, which will read pressure from deflections in a silicon membrane. The IDEAS package is capable of handling both the microscopic dimensions of the devices and the material specifications of single crystal silicon.

While the design of micro sensors can sometimes be an iterative trial and error process, partially because predicting performance on the micron level can be quite complex, heat transfer based devices should start their design with an appropriate model which includes the design parameters needed. Unlike designing in the macro scale where dimensions and structures can easily be modified during and after manufacture, modifications in micro devices are primarily made by making new masks with new designs. This is an expensive and time consuming process. It is in the engineers best interest to have as accurate a model of performance as possible, before the design is ever transferred to a mask.



## **Device Conclusions**

The single resistor flow sensor demonstrated some important ideas arrived at by this work. First it utilized a novel thermal isolation structure which was the result of the heat transfer model and the tunnel etching experiments. The net result was a thermal isolation structure which allows only 3% of the original thermal shorting found in flow sensor version 10.0. Secondly the device demonstrated the importance of thermal isolation to a device of this type. The first redesigned device produced required only 15 mW of power to give 15 mV/cm/sec sensitivity, as compared to a flow sensor version 10.0 without gold which currently requires 500 mW of power to give a sensitivity of 30 mV/cm/sec and does so at a much higher temperature.

## **Recommendations For Further Study**

While the tunnel etching process has been defined and controlled into a repeatable tool there are still some unanswered questions. The chemical reaction which causes the enhanced etch is unknown. Similarly the contaminant which caused the rapid etch/etch stop characteristics is unknown. The fact that a product of that reaction gets into the solution causing enhanced etching elsewhere also needs to be confirmed. The effects of phosphorous in the oxide on both its growth and etching rate are an area of exploration only barely touched by this work.

The microfabrication laboratory at IAMS currently does not have a policy on how frequently many of their chemicals need to be replaced for consistent manufacturing results. Hydrazine is one of these chemicals and shows a noted change in etch rates with freshness. Hydrazine and its etching properties in silicon seem underrepresented in the literature, and more work needs to be done to define how this chemical is working.

On the device end of the project, new devices need to be made with the manufacturing improvements and tested. Characterization of the sensitivity and repeatability will determine whether other modifications are needed to enhance performance, especially toward specific customer applications. Additionally it would be exciting to see the gold stability problem resolved. If it was resolved, then gold could be diffused into this new sensor design allowing for operation at even lower temperatures. It is also possible to redesign the bridge flow sensor using tunnel etching isolation structures to reduce its power requirements.

## Bibliography

1. Anon "Micromachining: A revolution in the making" Mechanical Engineering, Vol. 111, N 3, Mar 1989, pp. 47-48
2. Bryzek, Janusz; Mallon, Joseph R. Jr.; Grace, Roger H. "Silicon's synthesis: Sensors to systems" InTech, Vol. 36, N 1, Jan. 1989, pp. 40-44
3. Buchy, Frank "Silicon Sensors Lead Pressure Transmitter Technology" Chilton's I&CS (Instrument and Control Systems), Vol.60, N 2, Feb. 1987, pp. 37-39
4. Anon "New on th Circuit: Solid-State Pressure Sensors" Mechanical Engineering, Vol. 109, N 5, May 1987, pp. 42-47
5. Igarashi, I "Semiconductor Dynamic Sensors" Sensors and Actuators, Vol. 13, N 1, Jan. 1988, pp. 53-62
6. Delapierre, Gilles "Micro-machining: A survey of the most commonly used processes" Sensors and Actuators, Vol. 17, 1-2 PT1, May 3 1989, pp. 123-138
7. Linden, Y.; Tenerz, L.; Tiren, J.; Hok, B. "Fabrication of Three-Dimensional Structures by means of Doping-Selective Etching (DSE)" Sensors and Actuators, Vol. 16, 1989, pp. 67-82
8. Datta, Madhav; Romankiw, Lubomyr T. "Application of Chemical and Electrochemical Micromachining in the Electronics Industry" Journal of the Electrochemical Society, Vol. 136, N 6, Jun. 1989, pp. 285C-292C
9. Rosen, Jerome "Machining in the Micro Domain" Mechanical Engineering, Vol. 111, N 3, Mar. 1989, pp. 40-46
10. Steckl Microfabrication of Semiconductor Devices, Fall 1991 University of Cincinnati

11. Faust, J. W.; Palik, E. D. "A Study of the Orientation Dependent Etching and the Initial Anodization of Silicon in Aqueous KOH" Journal of the Electrochemical Society, Vol. 130, 1983, pp. 1413-1420
12. Schnakenberg, U. ; Benecke, W. ; Loechel, B. "NH<sub>4</sub>OH-based Etchants for Silicon Micromachining" Sensors and Actuators, A: Physical, Vol. 23, N 1-3, Apr. 1990, pp. 1031-1035
13. Puers, B; Sansen, W. "Compensation Structures for Convex Corner Micromachining in Silicon." Sensors and Actuators, A: Physical, Vol. 23, N 1-3, April 1990, pp.1036-1041
14. Ristic, L.J.; Dhaded, A.C.; Chau, K.; Allegretto, W. "Edges and Corners of Multilayer Dynamic Microstructures." Sensors and Actuators, A: Physical, Vol. 23, n 1-3, April 1990, pp.1042-1047
15. Pons, M. ; Delpech, P.; Schiltz, A.; Inard, A. "Mini-trench Isolation: Trench Etching Oxidation and Refilling Planarization" Microelectronic Engineering, Vol. 5, N 1-4, Dec 1986, Microcircuit Engineering 86, Proceedings of the International Conference on Microlithography, Interlaken, Switzerland, Sept 23-25 1986, pp. 403-404
16. Mehregany, Mehran; Senturia, Stephen D. "Anisotropic etching of Silicon in Hydrazine" Sensors and Actuators, Vol. 13, N 4, Apr. 1988, pp. 375-390
17. Peterson, Kurt; Brown, Joseph "Standard manufacturing processes for advanced silicon sensor families" Technical Digest- IEEE Solid-State Sensor Conference Publ. by IEEE, NY, pp. 31-33
18. Palik, E.D.; Bermudez, V.M.; Glembocki, O. J. "Ellipsometric Study of the Etch-Stop Mechanism in Heavily Doped Silicon" Journal of the Electrochemical Society, Vol. 132, N 1, Jan. 1985, pp. 135-141
19. Palik, E.D.; Bermudez, V.M.; Glembocki, O. J. "Ellipsometric Study of Orientation-Dependent Etching of Silicon in Aqueous KOH" Journal of the Electrochemical Society, Vol. 132, N 4, Apr. 1985, pp. 871-884

20. Raley, N.F.; Sugiyama, Y.; Van Duzer, T "(100) Silicon Etch Rate Dependence in Boron Concentration in EDP water solutions" Journal of the Electrochemical Society, Vol. 131, 1984, pp. 161-171
21. Glembocki, O.J.; Stahlbush, R. E.; Tomkiewicz, M. "Bias-Dependent Etching of Silicon Aqueous KOH" Journal of the Electrochemical Society, Vol. 132, 1985, pp. 145 - 151
22. Lu, Shi-Ji; Zheng, Zheng; Tong, Qin-Yi "New Silicon Micromachining Methods using SOI/SDB Technology" Sensors and Actuators, A: Physical, Vol. 23, N 1-3, Apr. 1990, pp. 961-963
23. Anon "Silicon Micromachining Technology: A Primer" Automotive Engineering (Warrendale, PA), Vol. 94, N 4, Apr. 1986, pp. 61-66
24. Stoev, Ivan Georgiev; Yankov, Rossen Angelov; Jeynes, Chris "Formation of Etch-Stop Structures Utilizing Ion-beam Synthesized Buried Oxide and Nitride Layers in Silicon." Sensors and Actuators, Vol. 19, N 2, Aug. 15 1989, pp. 183-197
25. Ishida, Makoto; Ashiki, Mitsuaki; Sawada, Kazuaki; Yamaguchi, Shinsuke; Nakamura, Tetsuro "Epitaxially Stacked Structures of Si/Al<sub>2</sub>O<sub>3</sub>/Si for Sensor Materials" Sensors and Actuators, A: Physical, Vol. 21, N 1-3, 2 Pt2, 1990, pp. 267-270
26. Ikeda, Kyoichi; Kuwayama, Hideka; Kobayashi, Takashi; Watanabe, Teysuya; Nishikawa, Tadashi; Yoshida, Takashi; Harada, Kinji "Three-dimensional Micromachining of Silicon Pressure Sensor Integrating Resonant Strain Gauge on Diaphragm" Sensors and Actuators, A: Physical, Vol. 23, N 1-3, Apr. 1990, pp. 1007-1010
27. Wang, H. Y.; Ko, Wen H. ; Batzel, D. A. ; Kenny, M. E.; Lando, J. B. "Phthalocyanine Langmuir-Blodgett Film Microsensors for Halogen Gases" Sensors and Actuators, B: Chemical, Vol. B1, N 1-6, 1 Pt1, 1990, pp. 138-141

28. Yamado, K.; Higuchi, K.; Tanigawa, H. "Novel Silicon Accelerometer with a Surrounding Mass Structure" Sensors and Actuators, A: Physical, Vol. 21, n 1-3, 2 Pt2, 1990, pp. 308-311
29. Tiren, J.; Tenerz, L. ; Hok, B. "Batch-fabricated Non-reverse Valve with Cantilever Beam Manufactured by Micromachining of Silicon." Sensors and Actuators, Vol. 18, N 3-4, Jul. 1989, pp. 389-396
30. Van Lintel, H. T. G.; Van De Pol, F. C. M. ; Bouswstra, S. "Piezoelectric Micropump Based on Micromaching of Silicon" Sensors and Actuators, Vol. 15, N 2, Oct. 1988, pp. 153-167
31. Barth, Philip W. "Silicon Fusion Bonding for Fabrication of Sensors, Actuators and Microstructures" Sensors and Actuators, A: Physical, Vol. 23, N 1-3, Apr. 1990, pp. 919-926
32. Jaccodine, R. J. "Use of Modified Free Energy Theorems to Predict Equilibrium Growing and Etching Shapes" Journal of Applied Physics, Vol. 33, 1962, pp. 2643-2647
33. Kittilsland, Gjermund; Stemme, Gorsn; Norden, Bengt "Sub-micron Particle Filter in Silicon" Sensors and Actuators, A: Physical, Vol. 23, n 1-3, Apr. 1990, pp. 904-907
34. Wolffenbuttel, M.R.; Retien, P.P.L. "Design Considerations for a Silicon Capacitive Tactile Cell" Sensors and Actuators, A:Physical, Vol. 24, N 3, Sept. 1990, pp. 187-190
35. Parameswaran, M. ; Ristic, LJ. ; Dhaded, A. C. ; Baltes, H. P. ; Allegretto, W. ; Robinson, A. M. "Fabrication of Microbridges in Standard Complementary Metal Oxide Semiconductor Technology." Canadian Journal of Physics, Vol. 67, N 4, Apr. 1989, pp. 184-189
36. Bouwstra, Siebe; Legtenberg, Rob; Tilmans, Harrie A. C.; Elwenspoek, Miko "Resonating Microbridge Mass Flow Sensor" Sensors and Actuators, A: Physical, Vol. 21, N 1-3, 2 Pt2, 1990, pp. 332-335

37. Johnson, R. G. and Higashi, R. E. "A Highly Sensitive Chip Microtransducer for Airflow and Differential Pressure Sensing Applications" Sensors and Actuators, Vol. 11, 1987, pp. 63-72
38. Tai, Y. C. ; Muller, R. S. "Lightly Doped Polysilicon Bridge as a Flow Meter" Sensors and Actuators, Vol.15, 1988, pp. 63-75
39. Van Oudhenusden, B. W.; Wan Herwaarden, A. W. "High-Sensitivity 2-D Flow Sensor with an Etched Thermal Isolation Structure" Sensors and Actuators, A: Physical, Vol. 22, N 1-3, 3 Pt3, 1990, pp. 425-430
40. Joshi, Shrinivas G. "Use of a Surface-Acoustic-Wave (SAW) Device to Measure Gas Flow" IEEE Transactions on Instrumentation and Measurement, Vol. 38, N 3, Jun. 1989, pp. 824-826
41. Henderson, H. Thurman; Hsieh, Walter "A Miniature Anemometer for Ultrafast Response" Sensors, Dec. 1989, pp. 22 - 26
42. Van Putten, A.F.P. "A Constant Voltage Constant Current Wheatstone Bridge Configuration" Sensors and Actuators, Vol. 13, 1988, pp. 103 - 115
43. Tai, Y. C. ; Muller, R. S. "Thermal Conductivity of Heavily Doped LPCVD Polycrystalline Silicon Films" Journal of Applied Physics, Vol. 63, 1988, pp. 1442-1447
44. Van Oudeuseden , B. W. "The Behavior of a Thermal-gradient Sensor in Laminar and Turbulent Shear Flow" Journal of Physics E: Science and Instruments, Vol. 22, 1989, pp. 490 - 498
45. Ma, S. W.; Gerner, F. M.; Tseui, Y. G. "Composite Expansions on Forced Convection over a Flat Plate with an Unheated Starting Length" To be presented at the national heat transfer conference, San Diego California, August 1992

46. Bolotov, V.V.; Emeksuzyan, V.M.; Spiridonov, V.N. ; Schmalz, K.; Trapp, M. "Radiation-induced Redistribution of Gold in SiO<sub>2</sub> structures" Physica Status Solidi (A) Applied Research, Vol. 133, N 2, Jun. 1989, pp. 315-320
47. Antonova, I.V.; Vasilev, A. V.; Panov, V. I.; Shaimeev, S. S. "Formation of Clusters in Gold Doped Silicon" Physica Status Solidi (A) Applied Research , Vol. 116, N 1, Nov. 1989, pp. K33 - K35
48. Wortman, J. J.; Evans, R. A. "Youngs Modulus, Shear Modulus and Poisson's Ratio in Silicon and Germanium " Journal of Applied Physics, Vol. 36, 1965, pp. 153-156
49. Burton, Gregory N. "Use of multiple internal reflection to enhance transient sensitivity in a gold-doped silicon IRFET" M.S. Thesis University of Cincinnati, December 1981



## APPENDIX A

### HEAT TRANSFER

#### Conduction Model for Existing Flowsensor

The following areas are needed for conduction heat transfer calculations. The dimensions for these areas were taken from the scale drawing of the flow sensor done by the author.

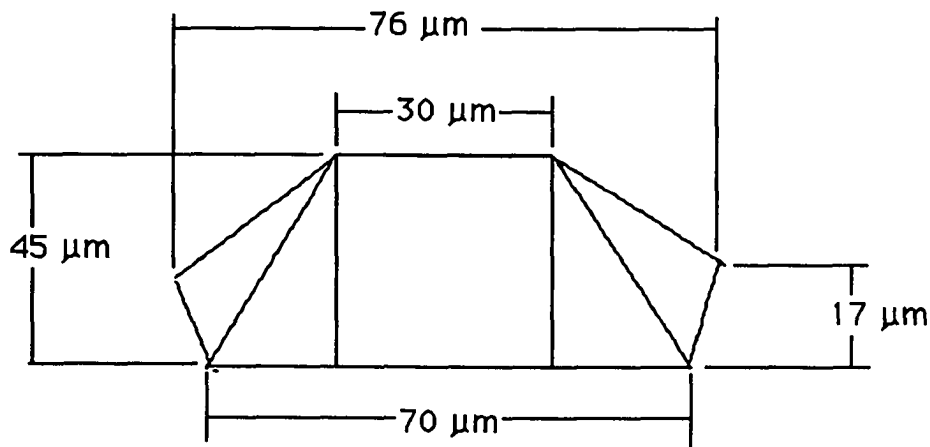


Figure 42 - Cross Sectional View of Bridge Resistor

Cross Sectional Area:

$$A_{CS} = 30 \times 45 + 20 \times 45 + 625 = 1350 + 900 + 625 = 2875 \mu\text{m}^2$$

This represents the surface size through which heat would be conducted away from the hot resistor.

Surface Area:

$$A_s = (152 \times 36.23)^2 + 152 \times 30 = 15573.92 \mu\text{m}^2$$

This represents the surface area through which heat can be lost to convection.

Simplifying assumptions:

- 1) All of the heat is generated at the center of the resistor
- 2) All of the heat generated is either lost through conduction to the feet or by convection to passing air
- 3) The upper and lower limits of the flow will be determined by the design limits for natural gas flowing in a 1" diameter pipe, that is a maximum volumetric flow rate of 200 ft<sup>3</sup>/hr and a minimum volumetric flow rate of 20 ft<sup>3</sup>/hr.
- 4) The flow will be modeled using classical boundary layer theory

Characteristics of the flow:

Velocity Range:

$$20 \text{ ft}^3/\text{hr}$$

$$A_{cs \text{ pipe}} = \pi r^2 = .785 \text{ in}^2 \quad (\text{a1.1})$$

convert to ft<sup>2</sup>

$$.785 \text{ in}^2 \times \left[ \frac{\text{ft}}{12 \text{ in}} \right]^2 = .00545 \text{ ft}^2$$

Average velocity,  $U_{avg}$ , for the flow in the pipe

202

$$20 \frac{\text{ft}^3}{\text{hr}} \left[ \frac{1}{.00545 \text{ ft}^2} \right] = 3667 \frac{\text{ft}}{\text{hr}}$$

$$3667 \frac{\text{ft}}{\text{hr}} \left[ \frac{1 \text{ hr}}{3600 \text{ sec}} \right] = 1.018 \frac{\text{ft}}{\text{sec}}$$

$$1 \text{ ft} = .3048 \text{ m}$$

$$1.018 \frac{\text{ft}}{\text{sec}} \times \frac{.3048 \text{ m}}{1 \text{ ft}} = .310 \frac{\text{m}}{\text{sec}} \quad U_{\text{avg}}$$

$$200 \text{ ft}^3/\text{hr}$$

using the same argument:

$$\frac{200}{.00545} = 36697 = 3.1 \frac{\text{m}}{\text{sec}} \quad U_{\text{avg}}$$

### Reynolds Numbers

Reynolds Numbers calculated for high and low end flow at the flowsensor (local)

$$Re = \frac{U_{\infty} x}{\nu} \quad \text{where } x \text{ is the distance from the leading edge} \quad (\text{a1.2})$$

Assume  $U_{\infty}$  for the flowsensor is equal to  $U_{\text{avg}}$  for the pipe. This assumption is especially valid if a static mixer is used as part of the flowmeter design to give a uniform flow profile.

$$Re_{\text{min}} = \frac{\left[ .310 \frac{\text{m}}{\text{sec}} \right] \left[ 740 \times 10^{-6} \text{ m} \right]}{1.46 \times 10^{-5} \frac{\text{m}^2}{\text{sec}}} = 15.71$$

$$Re_{\max} = \frac{\left[ 3.10 \frac{\text{m}}{\text{sec}} \right] \left[ 740 \times 10^{-6} \right]}{1.46 \times 10^{-5} \frac{\text{m}^2}{\text{sec}}} = 157.1$$

note: VanOudheusden (1989) experimentally tested his flow sensor in laminar and turbulent flow in air. The sensor was 4mm x 3mm x .3mm and the flow next to the sensor was laminar up to a free stream velocity ( $U_{\text{avg}}$ ) of 15 m/sec. The maximum free stream velocity for this situation is  $U_{\text{avg}} = 3.1$  m/sec which is much less. Both the calculations and the experiment support an assumption of locally laminar flow.

#### Calculation of Heat Transfer Coefficient

Pr (air) at room temperature = .7

for laminar, local flow: boundary conditions

$T_w = \text{constant}$  starting at  $X_0 = 590 \mu\text{m}$

$Re < 5 \times 10^5$  and  $.6 < Pr < 50$

$$Nu_x = .332 Re^{\frac{1}{2}} Pr^{\frac{1}{3}} \left[ 1 - \left[ \frac{X_0}{X} \right]^{\frac{3}{4}} \right]^{\frac{1}{3}} \quad (\text{a1.3})$$

High end:

$$Nu_x = .332 (157.1)^{\frac{1}{2}} (.7)^{\frac{1}{3}} \left[ 1 - \left[ \frac{0}{590} \right]^{\frac{3}{4}} \right]^{\frac{1}{3}}$$

$$Nu_x = 3.69$$

Low end:

Similarly

$$Nu_x = .332 (15.7)^{\frac{1}{2}} (.7)^{\frac{1}{3}}$$

$$Nu_x = 1.16$$

### Heat Transfer Coefficients

$$Nu_x = \frac{hL}{K_{air}}$$

(a1.4)

$$K_{air} = .03 \frac{W}{m^{\circ}C} \text{ at room temperature}$$

high end:

$$h_{high} = \frac{3.69 (K_{air})}{L_{resistor}}$$

$$h_{high} = \frac{3.69 \left[ .03 \frac{W}{m^{\circ}C} \right]}{150 \times 10^{-6} m} = 738 \frac{W}{m^2 \text{ } ^{\circ}C}$$

low end:

$$h_{low} = \frac{1.16 \left[ .03 \frac{W}{m^{\circ}C} \right]}{150 \times 10^{-6} m} = 232 \frac{W}{m^2 \text{ } ^{\circ}C}$$

## Thermal Resistance to Heat Transfer by Different Mechanisms

Heat Transfer by Convection:

$$R_{TH} = \frac{1}{h A_s} \quad \text{measured in } \frac{^{\circ}\text{C}}{\text{W}} \quad (\text{a1.5})$$

high end:

$$R_{TH} = \frac{1}{738 \frac{\text{W}}{\text{m}^2 \text{ } ^{\circ}\text{C}} \left[ 15573.92 \times 10^{-12} \text{ m}^2 \right]}$$
$$R_{TH} = 8.7 \times 10^4 \frac{^{\circ}\text{C}}{\text{W}}$$

low end:

$$R_{TH} = \frac{1}{232 \frac{\text{W}}{\text{m}^2 \text{ } ^{\circ}\text{C}} \left[ 15573.92 \times 10^{-12} \text{ m}^2 \right]}$$
$$R_{TH} = 2.77 \times 10^5 \frac{^{\circ}\text{C}}{\text{W}}$$

Heat Transfer by Conduction

$$R_{TH} = \frac{L}{K_{\text{silicon}} A_{cs}} \quad \text{where } L \text{ is the length from the middle of the resistor out to legs} \quad (\text{a1.6})$$

$$R_{TH} = \frac{76 \times 10^{-6} \text{ m}}{125.6 \frac{\text{W}}{\text{m}^{\circ}\text{C}} \left[ 2875 \times 10^{-12} \text{ m}^2 \right]}$$

$$R_{TH} = 210 \frac{\text{ }^{\circ}\text{C}}{\text{W}}$$

This means that the resistance of heat transfer to the air is 100 to 1000 times greater than the resistance of heat transfer to the legs.

## Modeling an Ideal Heat Transfer Flowsensor

### Boundary Layer Background for Flowsensor Calculations

From Newton's law of cooling:

$$q'' = h \left[ T_w - T_{\infty} \right] \quad \text{----- (1)}$$

$$\frac{q}{A_s} = q'' = -k \frac{\partial T}{\partial y} \text{ at the surface} \quad \text{-----(2)}$$

combining (1) and (2)

$$h \left[ T_w - T_{\infty} \right] = -k \frac{\partial T}{\partial y} \quad \text{(a1.8)}$$

where  $T_w$  is the temperature of the wall or surface  
 $T_{\infty}$  is the freestream temperature of the fluid  
 $q''$  is the local heat flux  
 $\delta_t$  is the thermal boundary layer thickness

So all that is needed is the temperature gradient at the wall to define the heat transfer coefficient.

**Boundary Conditions:**

$$T = T_w \quad \text{at } y = 0$$

$$\frac{\partial T}{\partial y} = 0 \quad \text{at } y = \delta_t$$

$$T = T_\infty \quad \text{at } y = \delta_t$$

$$\frac{\partial^2 T}{\partial y^2} = 0 \quad \text{at } y = 0 \quad (\text{no viscous heating})$$

Using these conditions the thermal boundary layer can then be fitted as a cubic polynomial:

$$\frac{\Theta}{\Theta_\infty} = \frac{T - T_w}{T_\infty - T_w} = \frac{3}{2} \frac{y}{\delta_t} - \frac{1}{2} \left[ \frac{y}{\delta_t} \right]^3 \quad (\text{a1.9})$$

and the boundary layer profile

$$\frac{\delta_t}{\delta} = \frac{1}{1.026} \text{Pr}^{-\frac{1}{3}} \left[ 1 - \left[ \frac{X_o}{X} \right]^{\frac{3}{4}} \right]^{\frac{1}{3}} \quad (\text{a1.10})$$

where

$$\text{Pr} = \frac{\nu}{\alpha} \quad (\text{a1.11})$$



The Prandtl number (Pr) has been found to relate the relative thickness of the hydrodynamic and thermal boundary layer. The kinematic viscosity ( $\nu$ ) conveys information about the rate at which momentum may diffuse through a fluid. The thermal diffusivity ( $\alpha$ ) tell the same thing with respect to the diffusion of heat.

$$\text{Pr} = \frac{\nu}{\alpha} = \frac{\frac{\mu}{\rho}}{\frac{k}{\rho C_p}} = \frac{C_p \mu}{k} \quad (\text{a1.12})$$

$$h = \frac{-k \left[ \frac{\partial T}{\partial y} \right]_w}{T_w - T_\infty} \quad (\text{a1.13})$$

$$h_x = .323 k \text{Pr}^{\frac{1}{3}} \left[ \frac{U_\infty}{\nu x} \right]^{\frac{1}{2}} \left[ 1 - \left[ \frac{X_0}{X} \right]^{\frac{3}{4}} \right]^{-\frac{1}{3}} \quad (\text{a1.14})$$

Note: for the following calculations assume the thermal and viscous boundary layer begins at the front of the resistor, then:

$$\frac{X_0}{X} = 1 \quad \text{and,}$$

$$h = .323 k \text{Pr}^{\frac{1}{3}} \left[ \frac{U_\infty}{\nu X} \right]^{\frac{1}{2}} \quad (\text{a1.15})$$

Applying This Information to Parallel and Perpendicular Resistors

Consider the configuration of resistors shown in figure 43, Appendix C, with one resistor perpendicular to the flow, labled (1), and one resistor parallel to the flow, labled (2). The simplifying assumption has been made that the thermal and viscous boundary layer start at the same place, at  $X = X_0$ .

The following are the properties of air at room temperature (300K) used for the calculations:

$$\begin{aligned} \rho &= 1.1774 \text{ Kg/m}^3 \\ C_p &= 1.0057 \text{ KJ/Kg } ^\circ\text{C} \\ \mu &= 1.8462 \times 10^{-5} \text{ Kg/m sec} \\ \nu &= 15.69 \times 10^{-6} \text{ m}^2/\text{sec} \\ k &= .02624 \text{ W/m}^\circ\text{C} \\ \alpha &= .22160 \times 10^4 \text{ m}^2/\text{sec} \\ Pr &= .708 \end{aligned}$$

How does the position of the resistor affect its heat transfer coefficient?

for resistor (1) , perpendicular

low flow,  $U_\infty = .3 \text{ m/sec}$

$$h = .323 \left[ .02624 \frac{\text{W}}{\text{m}^\circ\text{C}} \right] [ .708 ]^{\frac{1}{3}} \left[ \frac{.3 \frac{\text{m}}{\text{sec}}}{15.69 \times 10^{-6} \frac{\text{m}^2}{\text{sec}} (40 \times 10^{-6} \text{ m})} \right]^{\frac{1}{2}}$$

$$h = 165 \frac{\text{W}}{\text{m}^2^\circ\text{C}}$$

High flow,  $U_\infty = 3 \text{ m/sec}$

$$h = .323 \left[ .02624 \frac{\text{W}}{\text{m}^{\circ}\text{C}} \right] [.708]^{\frac{1}{3}} \left[ \frac{3 \frac{\text{m}}{\text{sec}}}{15.69 \times 10^{-6} \frac{\text{m}^2}{\text{sec}} (40 \times 10^{-6} \text{m})} \right]^{\frac{1}{2}}$$

135

$$h = 522 \frac{\text{W}}{\text{m}^2 \text{ } ^{\circ}\text{C}}$$

for resistor (2), parallel

low flow,  $U_{\infty} = .3 \text{ m/sec}$

$$h = .323 \left[ .02624 \frac{\text{W}}{\text{m}^{\circ}\text{C}} \right] [.708]^{\frac{1}{3}} \left[ \frac{.3 \frac{\text{m}}{\text{sec}}}{15.69 \times 10^{-6} \frac{\text{m}^2}{\text{sec}} (150 \times 10^{-6} \text{m})} \right]^{\frac{1}{2}}$$

$$h = 87 \frac{\text{W}}{\text{m}^2 \text{ } ^{\circ}\text{C}}$$

high flow,  $U_{\infty} = 3 \text{ m/sec}$

replacing .3 m/sec with 3 m/sec:

$$h = 269.6 \frac{\text{W}}{\text{m}^2 \text{ } ^{\circ}\text{C}}$$

Relative temperatures of two resistors, one parallel and one perpendicular

The first simplifying assumption for additional heat transfer modeling is that the two resistors are thermally isolated from the surrounding sensor structure. This assumption is based on the principle that tunnel etching will be used to thermally isolate the resistor structure.

Practically speaking, thermal isolation can only be approximated by a tunnel etched structure because there will be a need for both a mechanical and electrical connection to the rest of the sensor and each of these will conduct heat away from the resistor. By using an isolated structure model the calculations more clearly show differences in design strategies, and allow for design modification and improvement.

The current flowsensor uses a wheatstone bridge configuration, with one resistor in parallel with the flow and one resistor perpendicular to it. As was shown in the previous calculations, with the current geometries the heat transfer coefficient of the perpendicular resistor is almost exactly double that of the parallel resistor, regardless of the flow. The higher heat transfer coefficient can be expected to cool the resistor faster, and for an equal power input one would expect that resistor to have a cooler steady state temperature than the parallel one.

To sense this difference in temperature the sensor is modified so that its resistance vs. temperature characteristics vary exponentially. There are two methods to achieve this strong variation. Traditionally the sensor was doped with gold, and more recently experiments have been done to attempt to run the structure at a high enough temperature that the silicon was operating in its intrinsic region.

A balance is created when current is applied to one of the resistors. Current creates heat in the resistor, increasing its temperature. As the temperature increases the amount of energy being lost to convection also increases, as it is a function of the difference between the temperature of the sensor and the temperature of the air. The heat lost to the air decreases the temperature of the resistor. Decreasing the temperature of the resistor increases its resistive value, and increases the heat being disipated in the resistor. For this reason any set of energy in and air flow over the resistor will have a corresponding temperature at which the resistor will be if allowed to reach steady state.

The question then becomes what is the difference in temperature between the parallel and perpendicular resistors over the operating temperature and flow range for the sensor.

## Temperature vs Resistance

Temperature vs resistance data for the gold doped flowsensor was gathered by John Doty using experimental devices doped in the same way that the flowsensor was doped. The data is given in figure 26.

Five points were chosen from this data and plotted, see figure 27, with one axis being a log resistance and one axis being temperature. The function is a weak curve and is approximated by a straight line.

### Points on the graph

#### Point 1

$$R = \frac{1}{1 \times 10^{-3}} = 1000 \Omega \quad T = 1000 \left[ \frac{1}{1.68} \right] - 273 = 322 \text{ } ^\circ\text{C}$$

$$\log R = 3$$

#### Point 2

$$R = \frac{1}{2 \times 10^{-4}} = 5000 \Omega \quad T = 1000 \left[ \frac{1}{2.16} \right] - 273 = 190 \text{ } ^\circ\text{C}$$

$$\log R = 3.7$$

#### Point 3

$$R = \frac{1}{5 \times 10^{-5}} = 20000 \Omega \quad T = 1000 \left[ \frac{1}{2.58} \right] - 273 = 115 \text{ } ^\circ\text{C}$$

$$\log R = 4.3$$

Point 4

$$R = \frac{1}{1 \times 10^{-5}} = 100000 \Omega \quad T = 1000 \left[ \frac{1}{3} \right] - 273 = 60 \text{ } ^\circ\text{C}$$

$$\log R = 5$$

$$y = mx + b \quad b = 5.25 \\ m = -1/130 = - .0077$$

$$\log R = - .0077 T + 5.25 \quad (\text{a1.16})$$

The same information is available about the intrinsic region of silicon. The curve for  $20 \Omega/\mu$  is used because this material begins to operate in the intrinsic region above  $150 \text{ } ^\circ\text{C}$ . The information available does not give resistance, but rather the overall resistivity of the material. The value of resistance for two contacts placed across the material is a function of the resistivity of that material and the distance between contacts, and the surface area through which current can pass. Using the geometry from the gold doped device, the following linear approximation for the resistance verses temperature curve was drawn, see fig 27.

$$y = mx + b \quad b = 3.9 \\ m = - .6900/125 = - .006$$

$$\log R = - .006 T + 3.9 \quad (\text{a1.17})$$

Note the similarity between the curve for gold doped and intrinsic region. The slopes of the two lines are from the change in resistivity vs. temperature characteristics. The intercept is the result of the geometry of the resistor which creates a set resistance for a given resistivity.

#### Temperature Difference between parallel and perpendicular resistors in a wheatstone bridge configuration

For the following calculations it is assumed that the heat transfer coefficient for the perpendicular resistor is assumed to be double

that of the parallel resistor. Since the resistors are arranged in a wheatstone bridge configuration; two parallel resistors opposite two perpendicular resistors, the calculations will be done assuming the current is the same in both a parallel and a perpendicular resistor.

$$i_{\text{perp}} = i_{\text{parallel}} \quad \text{therefore} \quad i_{\text{perp}}^2 = i_{\text{parallel}}^2 \quad \text{-----} \quad (3)$$

Conservation of energy says that at steady state the energy being put into the resistor must be equal to the energy leaving the resistor. Since thermal isolation has been assumed all energy leaving the resistor is in the form of convection. 139

$$i^2 R = h A_s [T - T_{\text{ambient}}]$$

$$i^2 = \frac{h A_s [T - T_{\text{ambient}}]}{R(T)} \quad \text{-----} \quad (4)$$

Combining (3) and (4)

$$\frac{h_1 A_{s1} [T_1 - T_{\text{ambient}}]}{R(T_1)} = \frac{h_2 A_{s2} [T_2 - T_{\text{ambient}}]}{R(T_2)}$$

using the identity that  $h_1 = 2 h_2$  and cancelling surface area because the geometry of both resistors are identical:

$$\frac{2 h_2 [T_1 - T_{\text{ambient}}]}{R(T_1)} = \frac{h_2 [T_2 - T_{\text{ambient}}]}{R(T_2)}$$

regrouping and cancelling  $h_2$

$$\frac{R(T_2)}{R(T_1)} = \frac{T_2 - T_{\text{ambient}}}{2 [T_1 - T_{\text{ambient}}]} \quad \text{-----} \quad (5)$$

Now at this point the functions of resistance and temperature can be inserted. There are two functions, gold doped and non-gold doped . Each will have a different relationship between the temperatures of the resistors. 215

Gold Doped Resistors:

$$\log R = -.0077 T + 5.25$$

$$R(T_1) = 10^{(-.0077 T_1 + 5.25)} \quad \text{-----} \quad (6)$$

$$R(T_2) = 10^{(-.0077 T_2 + 5.25)} \quad \text{-----} \quad (7)$$

Combining equations (5), (6) and (7) and simplifying:

$$10^{(.0077 T_1 - .0077 T_2)} = \frac{T_2 - T_{\text{ambient}}}{2 [T_1 - T_{\text{ambient}}]} \quad (a1.18)$$

Given a value for ambient temperature (30°C) and a value for one of the two temperatures this equation can be solved iteratively for the other resistor temperature. Infrared microscope measurements of a gold doped flow sensor show the operating temperature range to be approximately 280°C to 350°C.

T1 (°C)	T2 (°C)
100	123
150	177
200	230
250	281
300	330
350	380



A plot is made of the difference in temperature between the two resistors versus temperature, see figure 28. The temperature difference can be assumed to be a constant 30 °C when the lower resistor temperature,  $T_1$ , is above 150 °C.

Non Gold Doped Resistors:

$$R(T_1) = 10^{(-.006T_1 + 3.9)} \quad \text{-----} \quad (8)$$

$$R(T_2) = 10^{(-.006T_2 + 3.9)} \quad \text{-----} \quad (9)$$

141

Combining equations (5), (8) and (9) and simplifying:

$$10^{(.006T_1 - .006T_2)} = \frac{T_2 - T_{\text{ambient}}}{2 [T_1 - T_{\text{ambient}}]} \quad (\text{a1.19})$$

Again solving iteratively:

T1 (°C)	T2 (°C)
150	182
200	236
250	288
300	340
350	392

Plotting the difference in temperature between the two resistors vs the cooler resistor gives a slowly increasing function with an approximate slope of 2/50. This increase in temperature difference with increasing temperature actually works against flow sensor sensitivity, however the effect is quite small. See fig 28.

### Checking the performance on several design strategies

In this next section several different device designs will be modeled and checked for sensitivity.

#### Wheatstone Bridge Sensors

Wheatstone bridge sensors have both a parallel and perpendicular resistors, see Appendix C. A constant current is put through the bridge, and a voltage potential is measured across the bridge. The sensitivity of this device is the difference in output voltage signal from the high flow reading to the low flow reading divided by that flow difference. For the following model it is assumed that the two parallel resistors have the same value at any point in time and that the two perpendicular resistors have the same value at all times. This means that for any current input, one half of that current will travel through each half bridge, and one half of the power will be dissipated in each half bridge.

$$\frac{q}{2} = h_{\text{perp}} A_s [T_1 - T_\infty] + h_{\text{parallel}} A_s [T_2 - T_\infty] \quad (\text{a1.20})$$

using the assumption that  $h_{\text{perp}} = 2 h_{\text{parallel}}$  and regrouping:

$$\frac{q}{2} = h A_s \left[ T_1 - T_\infty + \frac{(T_2 - T_\infty)}{2} \right] \quad \text{-----} \quad (10)$$

$$\frac{q}{2} = \left[ \frac{i}{2} \right]^2 [R(T_1) + R(T_2)] \quad \text{-----} \quad (11)$$

Combining (10) and (11) :

$$\left[ \frac{i}{2} \right]^2 [R(T_1) + R(T_2)] = h A_s \left[ T_1 + \frac{T_2}{2} - 1.5 T_\infty \right] \quad (\text{a1.21})$$

Gold doped :  $\log R = -.0077 T + 5.25$

Non Gold doped (above 150 °C) :  $\log R = - .006 T + 3.9$

Original Shapes  $A_s = 6 \times 10^{-9} \text{m}^2$  for 1

We assumed  $R_1 = R_4, R_2 = R_3$  so that half bridges operate the same

$h_{\text{perp}} \text{ -low flow} = 165 \text{ W/m}^\circ\text{C}$

$h_{\text{perp}} \text{ -high flow} = 520 \text{ W/m}^\circ\text{C}$

For gold doped:

$$\left[ \frac{i}{2} \right]^2 \left[ 10^{(-.0077T_1+5.25)} + 10^{(-.0077T_2+5.25)} \right] = h A_s \left[ T_1 + \frac{T_2}{2} - 1.5 T_\infty \right] \text{ ---(12)}$$

from earlier arguments  $\Delta T = 30 \text{ }^\circ\text{C}$  above  $150 \text{ }^\circ\text{C}$  with  $T_2 > T_1$   
 $h$  will vary with flow rate changing the temperature values

For non- gold doped:

$$\left[ \frac{i}{2} \right]^2 \left[ 10^{(-.006T_1+3.9)} + 10^{(-.006T_2+3.9)} \right] = h A_s \left[ T_1 + \frac{T_2}{2} - 1.5 T_\infty \right] \text{ ----(13)}$$

From earlier arguments  $\Delta T$  varies according to

$$T_2 = T_1 (1.04) + 28$$

$h$  will vary with flow rate changing the temperature values

### Gold Doped Present Geometry

Using equation (12) the sensitivity of the flowsensor version 10.0 can be found if it were thermally isolated. Thermal isolation

means that less input current is needed than is currently used to power the device. To solve equation (12) a current is assumed and the relationship between the temperature of the two resistor types is used. The equation is solved iteratively by assuming values of  $T_1$  and  $T_2$ .

Find the sensitivity vs input current:

$$i = 7 \text{ mA}$$

low flow,  $U_\infty = .3 \text{ m/sec}$ ,  $h = 165 \text{ W/m}^\circ\text{C}$

$$T_1 = 490^\circ\text{C} \quad T_2 = 520^\circ\text{C}$$

$$R(T_1) = 30\Omega \quad R(T_2) = 17.6\Omega \quad \Sigma R = 47.6\Omega$$

$$V = iR = .168 \text{ volts}$$

$$V_{\text{out}} = \left[ \frac{30 - 17.6}{47.6} \right] \times .168 = .043$$

high flow,  $U_\infty = 3 \text{ m/sec}$ ,  $h = 520 \text{ W/m}^\circ\text{C}$

$$T_1 = 425^\circ\text{C} \quad T_2 = 455^\circ\text{C}$$

$$R(T_1) = 94.9 \Omega \quad R(T_2) = 17.6 \Omega \quad \Sigma R = 112.5 \Omega$$

$$V = iR = .3939 \text{ volts}$$

$$V_{\text{out}} = \left[ \frac{94.9 - 17.6}{112.5} \right] \times .3939 = .27$$

sensitivity

$$S = \frac{.27 - .043}{2.7} = .084 \frac{\text{V}}{\text{m}} = .84 \frac{\text{mV}}{\text{cm}}$$

$$i = 1.4 \text{ mA}$$

low flow,  $U_{\infty} = .3$  m/sec,  $h = 165$  W/m $^{\circ}$ C

$$T_1 = 330 \text{ }^{\circ}\text{C} \quad T_2 = 360 \text{ }^{\circ}\text{C}$$

$$R(T_1) = 512 \text{ } \Omega \quad R(T_2) = 300 \Omega \quad \Sigma R = 812 \Omega$$

$$V = iR = .568 \text{ volts}$$

$$V_{\text{out}} = \left[ \frac{512 - 300}{812} \right] \times .568 = .148$$

high flow,  $U_{\infty} = 3$  m/sec,  $h = 520$  W/m $^{\circ}$ C

$$T_1 = 270 \text{ }^{\circ}\text{C} \quad T_2 = 300^{\circ}\text{C}$$

$$R(T_1) = 1482.5 \text{ } \Omega \quad R(T_2) = 870.9 \text{ } \Omega \quad \Sigma R = 2353 \text{ } \Omega$$

$$V = iR = 1.647 \text{ volts}$$

$$V_{\text{out}} = \left[ \frac{1482 - 870.9}{2353} \right] \times 1.647 = .428$$

sensitivity

$$S = \frac{.428 - .148}{2.7} = .104 \frac{\text{V}}{\text{m/sec}} = 1.04 \frac{\text{mV}}{\text{cm/sec}}$$

$$i = .6 \text{ mA}$$

low flow,  $U_{\infty} = .3$  m/sec,  $h = 165$  W/m $^{\circ}$ C

$$T_1 = 254 \text{ }^{\circ}\text{C} \quad T_2 = 284 \text{ }^{\circ}\text{C}$$

$$R(T_1) = 1968 \Omega \quad R(T_2) = 1156 \Omega \quad \Sigma R = 3125 \Omega$$

$$V = iR = .9375 \text{ volts}$$

$$V_{\text{out}} = \left[ \frac{1968 - 1156}{3125} \right] \times .9375 = .2436$$

high flow,  $U_{\infty} = 3$  m/sec,  $h = 520$  W/m $^{\circ}$ C

$$T_1 = 200 \text{ }^{\circ}\text{C} \quad T_2 = 230^{\circ}\text{C}$$

$$R(T_1) = 5128 \text{ } \Omega \quad R(T_2) = 3013 \text{ } \Omega \quad \Sigma R = 8141 \text{ } \Omega$$

$$V = iR = 2.4423 \text{ volts}$$

$$V_{\text{out}} = \left[ \frac{5128 - 3013}{8141} \right] \times 2.442 = .635$$

sensitivity

$$S = \frac{.635 - .243}{2.7} = .14 \frac{\text{V}}{\text{m/sec}} = 1.4 \frac{\text{mV}}{\text{cm/sec}}$$

147

**Non-gold doped flowsensor with the same geometry at the same three currents**

$$i = 7 \text{ mA}$$

low flow,  $U_{\infty} = .3$  m/sec,  $h = 165$  W/m $^{\circ}$ C

$$T_1 = 410 \text{ }^{\circ}\text{C} \quad T_2 = 454 \text{ }^{\circ}\text{C}$$

$$R(T_1) = 27.5 \Omega \quad R(T_2) = 14.9 \Omega \quad \Sigma R = 42.4 \Omega$$

$$V = iR = .148 \text{ volts}$$

$$V_{\text{out}} = \left[ \frac{27.5 - 14.9}{42.4} \right] \times .148 = .0439$$

high flow,  $U_{\infty} = 3$  m/sec,  $h = 520$  W/m $^{\circ}$ C

$$T_1 = 337 \text{ }^{\circ}\text{C} \quad T_2 = 378^{\circ}\text{C}$$

$$R(T_1) = 75.5 \text{ } \Omega \quad R(T_2) = 42.8 \text{ } \Omega \quad \Sigma R = 118.3 \text{ } \Omega$$

$$V = iR = .414 \text{ volts}$$

222

high flow,  $U_{\infty} = 3 \text{ m/sec}$ ,  $h = 190 \text{ W/m}^{\circ}\text{C}$

$$T = 296 \text{ }^{\circ}\text{C}$$

$$R(T) = 133 \text{ } \Omega$$

$$V = iR = .4 \text{ volts}$$

sensitivity

$$S = .9 \text{ mV/(cm/sec)}$$

Which is less than  $1.5 \text{ mV/(cm/sec)}$  of the same resistor turned perpendicular to the flow.

The sensitivity of the device can be enhanced by increasing the surface area of the single resistor, while maintaining the overall device size.

If the total surface area of the one resistor is increased 4x, the net surface area will equal the total surface area of the old device. The increase in surface area will be done by making the resistor wider as well as longer, which will also slightly change the heat transfer coefficient .

$$A_s = 2.4 \times 10^{-8} \text{ m}^2$$

$$h_{\text{ low end }} = 108$$

$$h_{\text{ high end }} = 370$$

How does this effect sensitivity?

$$i = .5 \text{ mA}$$

low flow,  $U_{\infty} = .3 \text{ m/sec}$ ,  $h = 165 \text{ W/m}^{\circ}\text{C}$

$$T = 288 \text{ }^{\circ}\text{C}$$

$$V_{\text{out}} = \left[ \frac{75.5 - 42.8}{118.3} \right] \times .414 = .1144$$

sensitivity

$$S = \frac{.1144 - .0439}{2.7} = .026 \frac{\text{V}}{\text{m/sec}} = .26 \frac{\text{mV}}{\text{cm/sec}}$$

$$i = 1.4 \text{ mA}$$

low flow,  $U_{\infty} = .3 \text{ m/sec}$ ,  $h = 165 \text{ W/m}^{\circ}\text{C}$

$$T_1 = 225 \text{ }^{\circ}\text{C} \quad T_2 = 262 \text{ }^{\circ}\text{C}$$

$$R(T_1) = 354.8 \text{ } \Omega \quad R(T_2) = 212 \Omega \quad \Sigma R = 566 \Omega$$

$$V = iR = .400 \text{ volts}$$

148

$$V_{\text{out}} = \left[ \frac{355 - 212}{566} \right] \times .400 = .1009$$

high flow,  $U_{\infty} = 3 \text{ m/sec}$ ,  $h = 520 \text{ W/m}^{\circ}\text{C}$

$$T_1 = 163 \text{ }^{\circ}\text{C} \quad T_2 = 197^{\circ}\text{C}$$

$$R(T_1) = 835 \text{ } \Omega \quad R(T_2) = 519 \text{ } \Omega \quad \Sigma R = 1354 \text{ } \Omega$$

$$V = iR = .9478 \text{ volts}$$

$$V_{\text{out}} = \left[ \frac{835 - 519}{1354} \right] \times .9478 = .2336$$

sensitivity

$$S = \frac{.2336 - .1009}{2.7} = .0491 \frac{\text{V}}{\text{m/sec}} = .491 \frac{\text{mV}}{\text{cm/sec}}$$

$$i = .6 \text{ mA}$$

high flow,  $U_{\infty} = 3 \text{ m/sec}$ ,  $h = 520 \text{ W/m}^{\circ}\text{C}$

224



Temperature will be below 150 °C, and the resistance/temperature relationship is not valid.

**Design Modification: increase the effect of the parallel and perpendicular resistor arrangement**

It is possible to change the geometry of the device, at least in theory, such that the heat transfer coefficient of the perpendicular resistor is 3 times that of the parallel resistor.

$$h = .323 k Pr^{\frac{1}{3}} \left[ \frac{U_{\infty}}{v X} \right]^{\frac{1}{2}} \tag{a1.15}$$

we want  $h_{perp} = 3 h_{parallel}$

$$3 \left[ .323 Pr^{\frac{1}{3}} k \left[ \frac{U_{\infty}}{v x} \right]^{\frac{1}{2}} \right] = .323 Pr^{\frac{1}{3}} k \left[ \frac{U_{\infty}}{v x_1} \right]^{\frac{1}{2}}$$

Cancelling like terms:

$$\frac{3}{x_{new}^{\frac{1}{2}}} = \frac{1}{x_{old}^{\frac{1}{2}}}$$

$$X_{old} = 40 \times 10^{-6} m \text{ therefore } X_{new} = 360 \times 10^{-6} m$$

What does this do to the difference in temperature between the two resistors?

$$\frac{R(T_2)}{R(T_1)} = \frac{(T_2 - T_{\infty})}{3(T_1 - T_{\infty})}$$

Gold doped:

$$10^{(-.0077T_2 + .0077T_1)} = \frac{T_2 - T_{\text{ambient}}}{3(T_1 - T_{\text{ambient}})}$$

Non gold doped:

$$10^{(-.006T_2 + .006T_1)} = \frac{T_2 - T_{\text{ambient}}}{3(T_1 - T_{\text{ambient}})}$$

Solving the gold doped equation iteratively:

T <sub>1</sub> (°C)	T <sub>2</sub> (°C)	ΔT (°C)
150	196	46
200	248	48
250	300	50
300	352	52

$$T_2 = 1.04 T_1 + 40$$

Solving the non-gold doped equation iteratively:

T <sub>1</sub> (°C)	T <sub>2</sub> (°C)	ΔT (°C)
150	203	53
200	258	58
250	312	62
300	363	63

How does this affect sensitivity?

Look at the gold doped design, at the lowest current level (best sensitivity)

$$i = .6 \text{ mA}$$

$$\text{low flow, } U_{\infty} = .3 \text{ m/sec, } h = 165 \text{ W/m}^{\circ}\text{C}$$

$$T_1 = 212 \text{ }^{\circ}\text{C} \quad T_2 = 260 \text{ }^{\circ}\text{C}$$

$$R(T_1) = 4146 \text{ } \Omega \quad R(T_2) = 1770 \text{ } \Omega \quad \Sigma R = 5916 \text{ } \Omega$$

$$V = iR = 1.7747 \text{ volts}$$

$$V_{\text{out}} = \left[ \frac{4146 - 1770}{5916} \right] \times 1.7747 = .712$$

$$\text{high flow, } U_{\infty} = 3 \text{ m/sec, } h = 520 \text{ W/m}^{\circ}\text{C}$$

$$T_1 = 162 \text{ }^{\circ}\text{C} \quad T_2 = 209^{\circ}\text{C}$$

$$R(T_1) = 10060 \text{ } \Omega \quad R(T_2) = 4413 \text{ } \Omega \quad \Sigma R = 14473 \text{ } \Omega$$

$$V = iR = 4.34 \text{ volts}$$

$$V_{\text{out}} = \left[ \frac{10060 - 4413}{14473} \right] \times 4.34 = 1.693$$

sensitivity

$$S = \frac{1.693 - .712}{2.7} = .363 \frac{\text{V}}{\text{m/sec}} = 3.63 \frac{\text{mV}}{\text{cm/sec}}$$

Look at the non-gold doped design at a low current level

$$i = 2 \text{ mA}$$

$$\text{low flow, } U_{\infty} = .3 \text{ m/sec, } h = 165 \text{ W/m}^{\circ}\text{C}$$

$$T_1 = 215 \text{ }^{\circ}\text{C} \quad T_2 = 274 \text{ }^{\circ}\text{C}$$

$$R(T_1) = 407 \Omega \quad R(T_2) = 274\Omega \quad \Sigma R = 681\Omega$$

$$V = iR = .681 \text{ volts}$$

$$V_{\text{out}} = .133$$

high flow,  $U_{\infty} = 3 \text{ m/sec}$ ,  $h = 520 \text{ W/m}^{\circ}\text{C}$

$$T_1 = 160 \text{ }^{\circ}\text{C} \quad T_2 = 214^{\circ}\text{C}$$

$$R(T_1) = 870 \Omega \quad R(T_2) = 413 \Omega \quad \Sigma R = 1283 \Omega$$

$$V = iR = 1.283 \text{ volts}$$

$$V_{\text{out}} = .356$$

sensitivity

$$S = .8 \text{ mV}/(\text{cm}/\text{sec})$$

The resistance vs temperature characteristics which have been used for these calculations was based on the same geometry which was used in the gold doped flow sensor. Adding gold to the silicon not only enhances its temperature response at room temperature, it raises the resistivity of the material. The resistance vs temperature equation can be modified for the non-gold doped sensor by changing the geometry of the sensor. This change will effect only the intercept of the curve, but not the slope.

What would happen to the sensitivity of the device if we increased the resistance at all temperatures?

try:

$$R(T) = 10^{(-.006T + 5.25)}$$

$$i = .6 \text{ mA}$$

low flow,  $U_{\infty} = .3 \text{ m/sec}$ ,  $h = 165 \text{ W/m}^{\circ}\text{C}$

$$T_1 = 225 \text{ }^{\circ}\text{C} \quad T_2 = 312 \text{ }^{\circ}\text{C}$$

$$R(T_1) = 5623 \Omega \quad R(T_2) = 2388\Omega \quad \Sigma R = 8011\Omega$$

228

$$V = iR = 2.4 \text{ volts}$$

$$V_{\text{out}} = .969$$

high flow,  $U_{\infty} = 3 \text{ m/sec}$ ,  $h = 520 \text{ W/m}^{\circ}\text{C}$

$$T1 = 195 \text{ }^{\circ}\text{C} \quad T2 = 252^{\circ}\text{C}$$

$$R(T1) = 1202 \text{ } \Omega \quad R(T2) = 5470 \text{ } \Omega \quad \Sigma R = 17493 \text{ } \Omega$$

$$V = iR = 5.2479 \text{ volts}$$

$$V_{\text{out}} = 1.9659$$

sensitivity

$$S = 3.69 \text{ mV}/(\text{cm}/\text{sec})$$

### Single Resistor Design

The wheatstone bridge configuration is currently used in version 10.0 of the flow sensor. This configuration has the advantage that ambient temperature effects can be removed from the signal and will not bias the flow reading.

A simpler design would be a single resistor. This design has the advantage that the entire input voltage can be the signal, rather than a fraction of it. The design also has the advantage of taking up less space because of requiring fewer lead bonding pads.

The equation for a single resistor is now:

$$i^2 R(T) = h A_s (T - T_{\text{ambient}}) \tag{a1.22}$$

for the non-gold doped enhanced resistance device:

$$R(T) = 10^{(-.006T + 5.25)} \tag{a1.23}$$

If the device consists of one of the wheatstone bridge resistors turned perpendicular to the flow, what will the sensitivity be for a low current?

$$A_s = 6 \times 10^{-9} \text{ m}^2$$

$$h_{\text{low end}} = 165 \text{ W/m}^\circ\text{C}$$

$$h_{\text{high end}} = 550 \text{ W/m}^\circ\text{C}$$

$$i = 1.5 \text{ mA}$$

$$\text{low flow, } U_\infty = .3 \text{ m/sec, } h = 165 \text{ W/m}^\circ\text{C}$$

$$T = 300 \text{ }^\circ\text{C}$$

$$R(T) = 126 \text{ } \Omega$$

$$V = iR = .189 \text{ volts}$$

$$\text{high flow, } U_\infty = 3 \text{ m/sec, } h = 520 \text{ W/m}^\circ\text{C}$$

$$T = 240 \text{ }^\circ\text{C}$$

$$R(T) = 288 \text{ } \Omega$$

$$V = iR = .432 \text{ volts}$$

sensitivity

$$S = .86 \text{ mV}/(\text{cm}/\text{sec})$$

What happens to the sensitivity for the single resistor device if the length and width of the resistor are each increased x2?

$$A_s = 2.4 \times 10^{-8} \text{ m}^2$$

The change in geometry would effect the heat transfer coefficients:

$$h_{\text{low flow}} = .323 (.02624) (.708)^{\frac{1}{3}} \left[ \frac{.3}{15.69 \times 10^{-6} (80 \times 10^{-6})} \right]^{\frac{1}{2}}$$

$$h_{\text{low flow}} = 108 \text{ W/m}^2\text{°C}$$

$$h_{\text{high flow}} = .323 (.02624) (.708)^{\frac{1}{3}} \left[ \frac{3}{15.67 \times 10^{-6} (80 \times 10^{-6})} \right]^{\frac{1}{2}}$$

$$h_{\text{high flow}} = 370 \text{ W/m}^2\text{°C}$$

$$i = 1.5 \text{ mA}$$

$$\text{low flow, } U_{\infty} = .3 \text{ m/sec, } h = 108 \text{ W/m}^2\text{°C}$$

$$T = 185 \text{ °C}$$

$$R(T) = 617 \text{ } \Omega$$

$$V = iR = .924 \text{ volts}$$

$$\text{high flow, } U_{\infty} = 3 \text{ m/sec, } h = 370 \text{ W/m}^2\text{°C}$$

$$T = 250 \text{ °C}$$

$$R(T) = 251 \text{ } \Omega$$

$$V = iR = .376 \text{ volts}$$

sensitivity

$$S = 2 \text{ mV/(cm/sec)}$$

What happens to the sensitivity of the same device if the current is increased?

$$i = 3 \text{ mA}$$

low flow,  $U_{\infty} = .3 \text{ m/sec}$ ,  $h = 108 \text{ W/m}^2\text{°C}$

$$T = 330 \text{ °C}$$

$$R(T) = 83 \text{ } \Omega$$

$$V = iR = .249 \text{ volts}$$

high flow,  $U_{\infty} = 3 \text{ m/sec}$ ,  $h = 370 \text{ W/m}^2\text{°C}$

$$T = 258 \text{ °C}$$

$$R(T) = 225 \text{ } \Omega$$

$$V = iR = .675 \text{ volts}$$

sensitivity

$$S = 1.5 \text{ mV/(cm/sec)}$$

This has the effect of lowering the sensitivity

It would be expected that turning the same device parallel to the flow would also lower the sensitivity.

Turning the device changes the heat transfer coefficients

$$h_{\text{low flow}} = 60 \text{ W/m}^2\text{°C}$$

$$h_{\text{high flow}} = 190 \text{ W/m}^2\text{°C}$$

$$i = 3 \text{ mA}$$

low flow,  $U_{\infty} = .3 \text{ m/sec}$ ,  $h = 60 \text{ W/m}^2\text{°C}$

$$T = 365 \text{ °C}$$

$$R(T) = 51 \text{ } \Omega$$

$$V = iR = .153 \text{ volts}$$

232



high flow,  $U_{\infty} = 3 \text{ m/sec}$ ,  $h = 190 \text{ W/m}^{\circ}\text{C}$

$$T = 296 \text{ }^{\circ}\text{C}$$

$$R(T) = 133 \text{ } \Omega$$

$$V = iR = .4 \text{ volts}$$

sensitivity

$$S = .9 \text{ mV}/(\text{cm}/\text{sec})$$

Which is less than  $1.5 \text{ mV}/(\text{cm}/\text{sec})$  of the same resistor turned perpendicular to the flow.

The sensitivity of the device can be enhanced by increasing the surface area of the single resistor, while maintaining the overall device size.

If the total surface area of the one resistor is increased 4x, the net surface area will equal the total surface area of the old device. The increase in surface area will be done by making the resistor wider as well as longer, which will also slightly change the heat transfer coefficient .

$$A_S = 2.4 \times 10^{-8} \text{ m}^2$$

$$h_{\text{ low end}} = 108$$

$$h_{\text{ high end}} = 370$$

How does this effect sensitivity?

$$i = .5 \text{ mA}$$

low flow,  $U_{\infty} = .3 \text{ m/sec}$ ,  $h = 165 \text{ W/m}^{\circ}\text{C}$

$$T = 288 \text{ }^{\circ}\text{C}$$

$$R(T) = 3326 \, \Omega$$

$$V = iR = 1.66 \text{ volts}$$

high flow,  $U_\infty = 3 \text{ m/sec}$ ,  $h = 520 \text{ W/m}^\circ\text{C}$

$$T = 220 \, ^\circ\text{C}$$

$$R(T) = 8511 \, \Omega$$

$$V = iR = 4.25 \text{ volts}$$

sensitivity

$$S = 9.6 \text{ mV}/(\text{cm}/\text{sec})$$

**Table 10, Part I - Summary of Results**

<u>Design</u>	<u>current</u>	<u>sensitivity</u>
<b>Wheatstone Bridge</b>		
gold doped original geometry	7mA	.84mV/(cm/sec)
gold doped original geometry	1.4mA	1.04mV/(cm/sec)
gold doped original geometry	.6mA	1.4mV/(cm/sec)
non-gold original geometry	7mA	.26mV/(cm/sec)
non-gold original geometry	1.4mA	.491mV/(cm/sec)
gold doped long resistors	.6mA	3.63mV/(cm/sec)
non gold long resistors	2mA	.8mV/(cm/sec)
non gold large resistance long resistors	.6mA	3.69mV/(cm/sec)

**Table 10, Part II - Summary of Results**

<u>Design</u>	<u>current</u>	<u>sensitivity</u>
<b>Single resistor- No Gold</b>		
old surface area perpendicular	1.5mA	.86mV/(cm/sec)
large A <sub>s</sub> perpendicular	1.5mA	2mV/(cm/sec)
large A <sub>s</sub> perpendicular	3mA	1.5mV/(cm/sec)
large A <sub>s</sub> large resistance parallel	3mA	.9mV/(cm/sec)
large A <sub>s</sub> large resistance perpendicular	.5mA	9.6mV/(cm/sec)

The last device described, the single resistor with a large surface area kept perpendicular to the flow, was chosen as the basis for the redesign of the flowsensor version 10.0. While the gold always displayed higher sensitivity in any configuration, manufacturing problems have made gold a less desirable option. If at some later date the manufacture and stability of the gold doped device is established, the single resistor device could be modified and doped with gold for even higher sensitivity.

#### Using Tunnel Etching to Create Thermal Isolation

The calculations above were all made under the assumption of thermal isolation. While perfect thermal isolation is not achievable given the practical limitations on the device, tunnel etching can be used to greatly enhance thermal isolation.

Tunnel etching will remove the silicon between two layers of silicon dioxide, leaving the oxide layer as a mechanical bridge. The isolation is improved by tunnel etching in two ways:

1. The structure available for conduction heat transfer has a greatly reduced cross sectional area, and
2. The oxide has a much lower coefficient of thermal conduction than the silicon.

The heat lost to conduction needs to be on the same order of magnitude as the heat lost to convection. In the present design the heat lost to conduction is 100 to 1000 times greater.

Calculating the heat transfer due to conduction will be solved using a classical thermal resistance model. In this case the heat can leave the resistor either through the silicon dioxide or through the metal leads.

$$k \text{ of SiO}_2 = 1.4 \frac{\text{W}}{\text{m}^\circ\text{C}}$$

$$k \text{ of Aluminum (Al)} = 215 \frac{\text{W}}{\text{m}^\circ\text{C}}$$

for the metal leads:

$$A_{CS} = (1 \times 10^{-6}\text{m}) (5 \times 10^{-6}\text{m}) = 5 \times 10^{-12}\text{m}^2$$

for the oxide membrane:

$$\begin{aligned} A_{CS} &= 2 (.3 \times 10^{-6}\text{m}) ((300 + 300 + 80 + 80) \times 10^{-6}\text{m}) \\ &= 4.56 \times 10^{-10}\text{m}^2 \end{aligned}$$

$$R_{TH} = \frac{L}{k_{\text{SiO}_2} A_{cs}} \quad \text{or} \quad R_{TH} = \frac{L}{k_{\text{Al}} A_{cs}} \quad (\text{a1.24})$$

recall  $R_{TH}$  for convection (worst case)

$$R_{TH} = \frac{1}{h A_s} = \frac{1}{(108)(2.4 \times 10^{-8})} = 3.8 \times 10^5 \frac{^\circ\text{C}}{\text{W}}$$

ideally,  $R_{TH}$  convection  $\ll$   $R_{TH}$  conduction

For each aluminum lead:

$$R_{TH} = \frac{L}{215 \frac{\text{W}}{\text{m}^\circ\text{C}} (5 \times 10^{-12} \text{ m}^2)} = \frac{L}{1.079 \times 10^{-9}}$$

The length of the leads is limited by the resolution on the metal lift-off process. A  $5\mu\text{m}$  width is very thin and the longer the length, the more likely that problems in the lithography will prevent the aluminum from connecting the bonding pad and the contact. The length that was eventually used was  $340\mu\text{m}$ . The net thermal resistance from the Aluminum leads is:

$$R_{TH} = \frac{340 \times 10^{-6}}{2.1 \times 10^{-9}} = 1.7 \times 10^5$$

The tunnel etching can be used alone or in combination with holes etched through the wafer to create isolation structures. Designs featuring both of these isolation strategies have been created by the author for flow sensors. Both structures significantly enhance thermal isolation. For drawings of these devices see figures Appendix C.

For Silicon dioxide:

$$R_{TH} = \frac{L_o}{1.4 \frac{\text{W}}{\text{m}^\circ\text{C}} (4.56 \times 10^{-10} \text{ m}^2)} = \frac{L_o}{6.38 \times 10^{-10}}$$

For oxide with holes along the side of the bridge:

$$R_{TH} = \frac{L_o}{1.4 \frac{W}{m^{\circ}C} (4.8 \times 10^{-11} m^2)} = \frac{L_o}{6.72 \times 10^{-11}}$$

Since one of these thermal resistances will be in parallel with the resistance of the metal leads, they need to be larger than the lead resistance, but not more than one order of magnitude larger. The mechanical considerations are that oxide bridges contain residual stresses from the extra room required for their lattice. When the oxide layer is freed from the underlying silicon it has been known to buckle. Additionally the oxide layers are quite thin, and the longer the layer the weaker the device structure.

For the tunnel etch isolation only design the length which would give a thermal resistance equal to that of the metal leads is:

$$1.7 \times 10^5 = \frac{L_o}{6.38 \times 10^{-10}}$$

$$L_o = 108.4 \mu m$$

The actual design used with tunnel etching as the isolation strategy used a length  $L_o$  of 150  $\mu m$ , which gives a net thermal resistance of  $2.35 \times 10^5 \text{ }^{\circ}C/W$ . The total thermal resistance to conduction heat loss for this device is:

$$\frac{1}{R_{TH}} = \frac{1}{2.35 \times 10^5} + \frac{1}{1.7 \times 10^5}$$

$$R_{TH} = .994 \times 10^5 \frac{^{\circ}C}{W}$$

The other structure used for thermal isolation is a combination of holes and tunnel etching on the resistor end. In this instance the length of the tunnel etch required to produce a thermal resistance equal to that of the aluminum leads is:

$$1.7 \times 10^5 = \frac{L_o}{6.72 \times 10^{-11}}$$

$$L_o = 11.4 \mu\text{m}$$

The length finally decided upon for manufacturing and durability reasons was 30 $\mu\text{m}$ . This gives a thermal resistance of  $4.46 \times 10^5$   $^\circ\text{C}/\text{W}$ . The net thermal resistance to conduction for this device is:

$$\frac{1}{R_{\text{TH}}} = \frac{1}{4.46 \times 10^5} + \frac{1}{1.7 \times 10^5}$$

$$R_{\text{TH}} = 1.2 \times 10^5 \frac{^\circ\text{C}}{\text{W}}$$

The aluminum leads have now become the greatest source of conduction losses, and conduction losses are now in the same order of magnitude as convection losses. Further improvements could be made if the aluminum leads could be made narrower and longer, or if the heat transfer coefficient of the device could be enhanced.



## **APPENDIX B**

### **DATA FROM TUNNEL ETCHING EXPERIMENTS**

The following 76 pages contain the data taken during the tunnel etching experiments as recorded as depth of tunnel etching. For every data point there is a column and one with the same heading followed by a '. The second column is the actual measurement converted into microns. The conversion is a function of the optical piece which the readings were taken through. Since all of these readings were taken under the same magnification to enhance uniformity, all dimensions are multiplied by 2.4.

The columns represent the different doping widths of the phosphorous, 5, 15, 45 and 135 microns. They are marked 5, 15, 50 and 150 as that was the label which was mistakenly used when the data was recorded.

950°C 10Ω/sq cm 0.5 Hour Etch

	5μ do	5μ do'	5μ undo	5μ undo'	15μ do	15μ do'	15μ undo	15μ undo'	50μ do
1	1.0	2.4	.5	1.2	1.0	2.4	.2	0.5	1.0
2	1.0	2.4	.2	0.5	1.0	2.4	.2	0.5	1.0
3	1.0	2.4	.2	0.5	1.0	2.4	.2	0.5	1.0
4	1.0	2.4	.2	0.5	1.0	2.4	.2	0.5	1.0
5	1.0	2.4	.2	0.5	1.0	2.4	0	0.0	1.0
6	1.0	2.4	.2	0.5	1.0	2.4	.2	0.5	1.0
7	1.0	2.4	.2	0.5	1.0	2.4	.2	0.5	1.0
8	1.0	2.4	.2	0.5	1.0	2.4	.2	0.5	1.0
9	1.0	2.4	.2	0.5	1.0	2.4	.2	0.5	1.0
10	1.0	2.4	.2	0.5	1.0	2.4	.2	0.5	1.0
11	.2	0.5	.2	0.5	.7	1.7	.2	0.5	1.0
12	.5	1.2	.2	0.5	1.0	2.4	.2	0.5	1.0
13	.5	1.2	.2	0.5	.7	1.7	.2	0.5	1.0
14	1.0	2.4	.2	0.5	1.0	2.4	.2	0.5	1.5
15	1.0	2.4	0	0.0	1.0	2.4	.2	0.5	1.0
16	1.0	2.4	0	0.0	1.0	2.4	0	0.0	1.0
17	.7	1.7	.2	0.5	1.0	2.4	.2	0.5	1.0
18	1.0	2.4	.2	0.5	1.0	2.4	.2	0.5	1.0
19	1.0	2.4	.2	0.5	1.0	2.4	0	0.0	1.0
20	1.0	2.4	.2	0.5	1.0	2.4	0	0.0	1.0
21	1.0	2.4	.2	0.5	1.0	2.4	.2	0.5	1.0
22	1.0	2.4	.2	0.5	1.0	2.4	.2	0.5	1.0
23	1.0	2.4	.2	0.5	1.0	2.4	0	0.0	1.0
24	1.0	2.4	.2	0.5	1.0	2.4	.2	0.5	1.0
25	1.0	2.4	.2	0.5	.7	1.7	0	0.0	1.0

950°C 10Ω/sq cm 0.5 Hour Etch						
	50μ do'	50μ undo	50μ undo'	150μ do	150μ do'	150μ undo
1	2.4	.2	0.5	1.0	2.4	.2
2	2.4	.5	1.2	1.0	2.4	.2
3	2.4	.2	0.5	1.0	2.4	.5
4	2.4	.2	0.5	1.0	2.4	.2
5	2.4	0	0.0	1.0	2.4	0
6	2.4	.2	0.5	1.0	2.4	.2
7	2.4	.2	0.5	1.0	2.4	.2
8	2.4	.2	0.5	1.0	2.4	.2
9	2.4	.2	0.5	1.0	2.4	.2
10	2.4	.2	0.5	1.0	2.4	.5
11	2.4	.2	0.5	1.0	2.4	.2
12	2.4	.2	0.5	1.0	2.4	.2
13	2.4	.2	0.5	1.0	2.4	.2
14	3.6	.2	0.5	1.2	2.9	.2
15	2.4	.2	0.5	1.0	2.4	.2
16	2.4	.2	0.5	1.0	2.4	.2
17	2.4	.2	0.5	1.0	2.4	.2
18	2.4	.2	0.5	1.0	2.4	.2
19	2.4	.2	0.5	1.0	2.4	.2
20	2.4	.2	0.5	1.0	2.4	.5
21	2.4	.2	0.5	1.0	2.4	.2
22	2.4	.2	0.5	1.0	2.4	.2
23	2.4	.2	0.5	1.0	2.4	.2
24	2.4	.2	0.5	1.5	3.6	.2
25	2.4	.5	1.2	1.0	2.4	.2

950°C 10Ω/sq cm 1.5 Hour Eich

	5μ do	5μ do'	5μ undo	5μ undo'	15μ do	15μ do'	15μ undo	15μ undo'	50μ do
1	2.0	4.8	1.0	2.4	3.0	7.2	1.0	2.4	3.0
2	2.5	6.0	1.0	2.4	3.0	7.2	1.0	2.4	3.5
3	3.0	7.2	1.5	3.6	3.5	8.4	1.0	2.4	3.5
4	3.0	7.2	1.0	2.4	4.0	9.6	1.5	3.6	4.0
5	3.0	7.2	1.0	2.4	3.0	7.2	1.0	2.4	4.0
6	3.5	8.4	1.0	2.4	4.0	9.6	1.0	2.4	4.0
7	4.0	9.6	1.0	2.4	4.0	9.6	1.0	2.4	4.0
8	3.5	8.4	1.0	2.4	4.0	9.6	1.0	2.4	4.5
9	4.0	9.6	1.0	2.4	4.0	9.6	1.0	2.4	4.0
10	3.0	7.2	1.0	2.4	4.0	9.6	1.0	2.4	4.0
11	2.5	6.0	1.0	2.4	3.0	7.2	1.0	2.4	3.0
12	3.0	7.2	1.0	2.4	3.0	7.2	1.5	3.6	3.0
13	2.0	4.8	1.0	2.4	3.0	7.2	1.0	2.4	4.0
14	3.0	7.2	1.0	2.4	3.5	8.4	1.0	2.4	4.0
15	3.0	7.2	1.0	2.4	4.0	9.6	1.0	2.4	4.0
16	3.0	7.2	1.0	2.4	3.0	7.2	1.0	2.4	4.0
17	3.0	7.2	1.0	2.4	4.0	9.6	1.0	2.4	4.0
18	3.5	8.4	1.0	2.4	4.0	9.6	1.0	2.4	4.0
19	4.0	9.6	1.0	2.4	4.0	9.6	1.0	2.4	4.0
20	3.0	7.2	1.0	2.4	4.0	9.6	1.0	2.4	4.0
21	3.5	8.4	1.0	2.4	4.0	9.6	1.0	2.4	5.0
22	3.5	8.4	1.0	2.4	4.0	9.6	1.0	2.4	4.5
23	3.0	7.2	1.0	2.4	4.0	9.6	1.0	2.4	4.0
24	4.0	9.6	1.0	2.4	4.5	10.8	1.0	2.4	5.0
25	3.0	7.2	1.0	2.4	4.0	9.6	1.0	2.4	4.5

950°C 10Ω/sq cm 1.5 Hour Etch						
	50μ do'	50μ undo	50μ undo'	150μ do	150μ do'	150μ undo'
1	7.2	1.5	3.6	3.0	7.2	4.8
2	8.4	1.5	3.6	3.5	8.4	3.6
3	8.4	1.5	3.6	4.0	9.6	4.8
4	9.6	2.0	4.8	4.0	9.6	3.6
5	9.6	1.0	2.4	4.0	9.6	3.6
6	9.6	1.0	2.4	4.5	10.8	2.4
7	9.6	1.0	2.4	4.0	9.6	2.4
8	10.8	1.0	2.4	4.5	10.8	2.4
9	9.6	1.0	2.4	4.0	9.6	3.6
10	9.6	1.5	3.6	4.0	9.6	3.6
11	7.2	1.0	2.4	3.5	8.4	2.4
12	7.2	1.0	2.4	4.0	9.6	3.6
13	9.6	1.0	2.4	4.0	9.6	2.4
14	9.6	1.0	2.4	4.5	10.8	2.4
15	9.6	1.0	2.4	4.0	9.6	2.4
16	9.6	1.0	2.4	4.0	9.6	2.4
17	9.6	1.0	2.4	4.0	9.6	2.4
18	9.6	1.0	2.4	4.0	9.6	2.4
19	9.6	1.0	2.4	4.0	9.6	3.6
20	9.6	1.0	2.4	4.0	9.6	2.4
21	12.0	1.0	2.4	5.0	12.0	2.4
22	10.8	1.0	2.4	5.0	12.0	2.4
23	9.6	1.0	2.4	5.0	12.0	2.4
24	12.0	1.0	2.4	5.0	12.0	2.4
25	10.8	1.0	2.4	5.0	12.0	2.4

950°C 10Ω/sq cm 2.5 Hour Etch

	5μ do	5μ do'	5μ undo	5μ undo'	15μ do	15μ do'	15μ undo	15μ undo'	50μ do
1	7.0	16.8	2.0	4.8	8.0	19.2	1.0	2.4	9.0
2	6.0	14.4	1.5	3.6	7.0	16.8	2.0	4.8	8.5
3	7.0	16.8	1.5	3.6	7.0	16.8	1.5	3.6	8.0
4	8.0	19.2	1.5	3.6	8.0	19.2	1.5	3.6	9.0
5	6.5	15.6	2.0	4.8	7.0	16.8	2.0	4.8	8.0
6	6.0	14.4	1.5	3.6	7.5	18.0	1.5	3.6	8.0
7	6.5	15.6	1.5	3.6	7.0	16.8	2.0	4.8	8.0
8	6.0	14.4	1.5	3.6	7.0	16.8	1.5	3.6	7.5
9	5.5	13.2	1.5	3.6	6.5	15.6	1.5	3.6	7.0
10	5.5	13.2	1.5	3.6	6.0	14.4	2.0	4.8	7.0
11	5.0	12.0	1.5	3.6	5.5	13.2	2.0	4.8	6.0
12	5.0	12.0	1.5	3.6	6.0	14.4	2.0	4.8	6.5
13	5.5	13.2	1.5	3.6	6.0	14.4	1.5	3.6	7.0
14	6.5	15.6	1.5	3.6	6.5	15.6	1.5	3.6	8.0
15	7.0	16.8	1.5	3.6	7.0	16.8	2.0	4.8	8.0
16	5.5	13.2	3.0	7.2	6.0	14.4	2.5	6.0	6.0
17	6.0	14.4	1.5	3.6	6.0	14.4	1.5	3.6	6.5
18	5.0	12.0	1.5	3.6	6.0	14.4	2.0	4.8	7.0
19	6.0	14.4	1.5	3.6	7.0	16.8	1.5	3.6	6.5
20	6.0	14.4	1.5	3.6	6.5	15.6	2.0	4.8	7.0
21	7.0	16.8	1.5	3.6	8.0	19.2	2.0	4.8	7.0
22	7.0	16.8	1.5	3.6	8.0	19.2	2.0	4.8	9.0
23	7.0	16.8	1.5	3.6	7.5	18.0	2.0	4.8	8.0
24	5.5	13.2	1.5	3.6	6.0	14.4	1.5	3.6	8.5
25	6.0	14.4	1.5	3.6	7.0	16.8	1.5	3.6	8.0
26									

1

950°C 10Ω/sq cm 2.5 Hour Etch							
	50μ do'	50μ undo	50μ undo'	150μ do	150μ do'	150μ undo	150m undo'
1	21.6	2.0	4.8	9.0	21.6	2.0	4.8
2	20.4	1.5	3.6	9.0	21.6	2.0	4.8
3	19.2	2.0	4.8	8.5	20.4	2.0	4.8
4	21.6	1.5	3.6	9.0	21.6	2.0	4.8
5	19.2	2.0	4.8	9.0	21.6	2.0	4.8
6	19.2	2.0	4.8	7.0	16.8	2.0	4.8
7	19.2	2.0	4.8	8.5	20.4	2.0	4.8
8	18.0	2.0	4.8	8.0	19.2	2.5	6.0
9	16.8	2.0	4.8	8.0	19.2	2.0	4.8
10	16.8	2.0	4.8	7.0	16.8	2.5	6.0
11	14.4	2.0	4.8	6.5	15.6	2.0	4.8
12	15.6	2.0	4.8	7.0	16.8	2.5	6.0
13	16.8	1.5	3.6	8.0	19.2	2.0	4.8
14	19.2	2.0	4.8	8.0	19.2	2.0	4.8
15	19.2	2.0	4.8	8.0	19.2	2.0	4.8
16	14.4	2.5	6.0	6.5	15.6	2.0	4.8
17	15.6	2.0	4.8	7.0	16.8	2.0	4.8
18	16.8	2.0	4.8	7.0	16.8	2.0	4.8
19	15.6	2.0	4.8	7.0	16.8	2.5	6.0
20	16.8	2.0	4.8	7.5	18.0	2.5	6.0
21	16.8	2.0	4.8	8.5	20.4	2.0	4.8
22	21.6	2.0	4.8	9.0	21.6	2.0	4.8
23	19.2	2.0	4.8	9.0	21.6	2.5	6.0
24	20.4	2.0	4.8	9.0	21.6	2.5	6.0
25	19.2	2.0	4.8	8.0	19.2	2.0	4.8
26							





950°C 10Ω/sq cm 3.5 Hour Etch

150μm undo'

1	9.6
2	8.4
3	8.4
4	7.2
5	12.0
6	10.8
7	9.6
8	7.2
9	8.4
10	9.6
11	
12	
13	
14	
15	
16	
17	
18	
19	
20	
21	
22	
23	
24	
25	
26	

950°C 20Ω/sq cm 1 Hour Etch

	5μ do	5μ do'	5μ undo	5μ undo'	15μ do	15μ do'	15μ undo	15μ undo'	50μ do
1	3.0	7.20	1.5	3.60	3.0	7.20	1.0	2.40	3.0
2	3.0	7.20	.5	1.20	3.0	7.20	.7	1.68	3.0
3	3.0	7.20	.5	1.20	3.0	7.20	1.0	2.40	3.0
4	3.0	7.20	.5	1.20	3.0	7.20	1.0	2.40	3.0
5	3.0	7.20	1.0	2.40	3.0	7.20	1.0	2.40	3.0
6	3.0	7.20	1.0	2.40	3.0	7.20	1.0	2.40	3.0
7	3.0	7.20	1.0	2.40	2.5	6.00	1.0	2.40	3.0
8	2.5	6.00	1.0	2.40	2.5	6.00	1.0	2.40	2.5
9	3.0	7.20	1.0	2.40	3.0	7.20	1.0	2.40	2.5
10	2.5	6.00	1.0	2.40	2.5	6.00	1.0	2.40	2.0
11	3.0	7.20	1.0	2.40	3.0	7.20	1.0	2.40	3.0
12	3.0	7.20	1.0	2.40	2.5	6.00	1.0	2.40	3.0
13	3.0	7.20	1.0	2.40	3.5	8.40	1.0	2.40	4.0
14	2.0	4.80	1.0	2.40	3.0	7.20	1.0	2.40	3.0
15	3.5	8.40	1.0	2.40	3.5	8.40	1.0	2.40	3.0
16	1.5	3.60	1.0	2.40	2.5	6.00	1.0	2.40	2.5
17	3.0	7.20	1.0	2.40	3.0	7.20	1.0	2.40	2.5
18	3.0	7.20	1.0	2.40	3.0	7.20	1.0	2.40	3.0
19	3.0	7.20	1.0	2.40	3.0	7.20	1.0	2.40	4.0
20	4.0	9.60	1.0	2.40	3.5	8.40	1.0	2.40	3.5
21	4.0	9.60	1.0	2.40	3.5	8.40	1.0	2.40	3.0
22	4.0	9.60	1.0	2.40	4.0	9.60	1.0	2.40	3.5
23	4.0	9.60	1.0	2.40	4.0	9.60	1.0	2.40	4.0
24	4.0	9.60	1.0	2.40	3.5	8.40	1.0	2.40	4.0
25	3.5	8.40	1.0	2.40	4.0	3.60	1.0	2.40	4.0

950°C 20Ω/sq cm 1 Hour Etch						
	50μ do'	50μ undo	50μ undo'	150μ do	150μ do'	150μ undo'
1	7.20	.7	1.68	4.0	9.60	1.20
2	7.20	.7	1.68	3.0	7.20	2.40
3	7.20	.7	1.68	2.5	6.00	0.72
4	7.20	1.0	2.40	3.0	7.20	1.20
5	7.20	.5	1.20	3.5	8.40	2.40
6	7.20	1.0	2.40	2.5	6.00	2.40
7	7.20	1.0	2.40	3.0	7.20	2.40
8	6.00	1.0	2.40	2.5	6.00	2.40
9	6.00	1.0	2.40	2.5	6.00	2.40
10	4.80	1.0	2.40	2.5	6.00	2.40
11	7.20	1.0	2.40	2.5	6.00	2.40
12	7.20	1.0	2.40	3.0	7.20	2.40
13	9.60	1.0	2.40	2.5	6.00	2.40
14	7.20	1.0	2.40	3.0	7.20	2.40
15	7.20	1.0	2.40	3.0	7.20	2.40
16	6.00	1.0	2.40	3.0	7.20	2.40
17	6.00	1.0	2.40	3.0	7.20	2.40
18	7.20	1.0	2.40	2.5	6.00	2.40
19	9.60	1.0	2.40	3.0	7.20	2.40
20	8.40	1.0	2.40	3.0	7.20	2.40
21	7.20	1.0	2.40	4.0	9.60	2.40
22	8.40	1.0	2.40	4.0	9.60	2.40
23	9.60	1.0	2.40	4.0	9.60	2.40
24	9.60	1.0	2.40	4.5	10.80	2.40
25	9.60	1.0	2.40	4.0	9.60	2.40

950°C 20Ω/sq cm 2 Hour Etch

	5μ do	5μ do'	5μ undo	5μ undo'	15μ do	15μ do'	15μ undo	15μ undo'	50μ do
1	7.0	16.80	3.0	7.20	8.0	19.20	3.0	7.20	8.5
2	7.0	16.80	2.0	4.80	7.0	16.80	3.0	7.20	8.0
3	7.0	16.80	3.0	7.20	8.0	19.20	3.5	8.40	8.0
4	9.0	21.60	3.0	7.20	7.0	16.80	3.0	7.20	9.0
5	8.0	19.20	3.0	7.20	8.0	19.20	3.0	7.20	9.0
6	8.0	19.20	3.0	7.20	8.0	19.20	3.0	7.20	8.0
7	8.0	19.20	3.0	7.20	8.5	20.40	3.0	7.20	8.5
8	8.0	19.20	3.0	7.20	8.0	19.20	3.0	7.20	8.0
9	7.0	16.80	3.0	7.20	7.5	18.00	2.5	6.00	7.0
10	7.5	18.00	2.5	6.00	7.0	16.80	2.5	6.00	6.0
11	8.0	19.20	3.0	7.20	8.0	19.20	3.5	8.40	8.0
12	8.5	20.40	2.5	6.00	8.5	20.40	3.0	7.20	8.5
13	8.5	20.40	3.0	7.20	8.0	19.20	3.0	7.20	9.0
14	8.5	20.40	3.0	7.20	8.5	20.40	3.0	7.20	9.0
15	8.5	20.40	3.0	7.20	8.0	19.20	3.0	7.20	9.0
16	8.0	19.20	3.0	7.20	8.0	19.20	3.0	7.20	8.5
17	8.5	20.40	3.0	7.20	8.0	19.20	3.0	7.20	8.0
18	8.0	19.20	3.0	7.20	9.0	21.60	3.0	7.20	8.5
19	9.0	21.60	3.0	7.20	8.5	20.40	3.0	7.20	9.0
20	8.0	19.20	3.0	7.20	8.0	19.20	3.0	7.20	9.0
21	8.0	19.20	3.0	7.20	8.0	19.20	3.0	7.20	9.0
22	8.5	20.40	3.0	7.20	9.0	21.60	3.0	7.20	9.0
23	8.0	19.20	3.0	7.20	8.5	20.40	3.0	7.20	9.0
24	9.0	21.60	3.0	7.20	9.0	21.60	3.0	7.20	9.0
25	8.5	20.40	3.0	7.20	8.5	20.40	3.0	7.20	9.0

950°C 20Ω/sq cm 2 Hour Etch

	50μ do'	50μ undo'	50μ do'	50μ undo'	150μ do'	150μ undo'	150μ do'	150μ undo'
1	20.4	3.0	7.2	7.2	8.5	20.40	3.0	7.20
2	19.2	3.0	7.2	7.2	9.0	21.60	3.0	7.20
3	19.2	3.5	8.4	7.2	8.5	20.40	3.0	7.20
4	21.6	3.0	7.2	7.2	9.0	21.60	3.0	7.20
5	21.6	3.0	7.2	7.2	9.0	21.60	3.0	7.20
6	19.2	3.0	7.2	7.2	9.0	21.60	3.0	7.20
7	20.4	3.0	7.2	7.2	9.0	21.60	3.0	7.20
8	19.2	3.0	7.2	7.2	9.0	21.60	3.0	7.20
9	16.8	2.5	6.0	6.0	8.0	19.20	3.0	7.20
10	14.4	2.5	6.0	6.0	6.5	15.60	2.0	4.80
11	19.2	3.5	8.4	7.2	8.5	20.40	3.5	8.40
12	20.4	3.0	7.2	7.2	9.0	21.60	3.0	7.20
13	21.6	3.0	7.2	7.2	9.0	21.60	3.0	7.20
14	21.6	3.0	7.2	7.2	9.0	21.60	3.0	7.20
15	21.6	3.0	7.2	7.2	9.0	21.60	3.5	8.40
16	20.4	3.0	7.2	7.2	9.0	21.60	3.0	7.20
17	19.2	3.0	7.2	7.2	8.5	20.40	3.0	7.20
18	20.4	3.0	7.2	7.2	9.0	21.60	3.0	7.20
19	21.6	3.0	7.2	7.2	9.0	21.60	3.5	8.40
20	21.6	3.0	7.2	7.2	9.0	21.60	3.0	7.20
21	21.6	3.0	7.2	7.2	9.0	21.60	3.0	7.20
22	21.6	3.0	7.2	7.2	9.5	22.80	3.5	8.40
23	21.6	3.0	7.2	7.2	9.0	21.60	3.0	7.20
24	21.6	3.0	7.2	7.2	9.0	21.60	3.0	7.20
25	21.6	3.0	7.2	7.2	10.0	24.00	3.0	7.20
26								
27								

950°C 20Ω/sq cm 3.5 Hour Etch

	5μ do	5μ do'	5μ undo	5μ undo'	15μ do	15μ do'	15μ undo	15μ undo'	50μ do
1	14.0	33.60	6.0	14.40	14.0	33.60	6.0	14.40	14.0
2	14.0	33.60	6.0	14.40	14.0	33.60	6.0	14.40	15.0
3	15.0	36.00	7.0	16.80	14.0	33.60	6.0	14.40	14.0
4	13.0	31.20	5.0	12.00	13.0	31.20	5.0	12.00	14.0
5	13.0	31.20	5.0	12.00	13.0	31.20	5.0	12.00	13.0
6	16.0	38.40	7.5	18.00	15.0	36.00	8.0	19.20	17.0
7	15.5	37.20	8.0	19.20	16.0	38.40	7.0	16.80	16.0
8	15.0	36.00	6.0	14.40	15.0	36.00	8.0	19.20	16.0
9	15.0	36.00	7.0	16.80	15.0	36.00	8.0	19.20	15.0
10	13.5	32.40	7.0	16.80	14.0	33.60	6.0	14.40	14.0
11	13.0	31.20	5.0	12.00	14.0	33.60	6.0	14.40	12.0
12	14.0	33.60	5.0	12.00	13.0	31.20	5.0	12.00	13.0
13	13.0	31.20	5.5	13.20	14.0	33.60	6.0	14.40	13.0
14	14.0	33.60	7.0	16.80	14.0	33.60	7.5	18.00	15.0
15	15.0	36.00	6.0	14.40	15.0	36.00	7.0	16.80	15.0
16	14.0	33.60	6.0	14.40	15.0	36.00	6.0	14.40	15.0
17	14.0	33.60	5.0	12.00	15.0	36.00	5.0	12.00	15.0
18	15.5	37.20	7.0	16.80	15.0	36.00	6.0	14.40	16.0
19	15.0	36.00	7.0	16.80	15.0	36.00	5.0	12.00	16.0
20	15.0	36.00	6.5	15.60	14.5	34.80	6.0	14.40	16.0
21	15.0	36.00	6.0	14.40	15.5	37.20	8.0	19.20	17.0
22	16.0	38.40	8.0	19.20	16.0	38.40	8.0	19.20	16.0
23	15.0	36.00	7.0	16.80	16.0	38.40	8.0	19.20	16.0
24	16.0	38.40	7.0	16.80	16.0	38.40	7.0	16.80	16.0
25	15.0	36.00	7.0	16.80	16.0	38.40	8.0	19.20	16.0
26									

950°C 20Ω/sq cm 3.5 Hour Etch									
	50μ do'	50μ undo	50μ undo'	150μ do	150μ do'	150μ undo	150μ undo'	Column 17	Column 18
1	33.60	6.0	14.40	15.0	36.00	6.0	14.40		
2	36.00	6.5	15.60	14.0	33.60	6.5	15.60		
3	33.60	6.0	14.40	14.0	33.60	6.5	15.60		
4	33.60	6.0	14.40	14.0	33.60	6.0	14.40		
5	31.20	5.0	12.00	13.0	31.20	5.0	12.00		
6	40.80	8.5	20.40	18.0	43.20	7.5	18.00		
7	38.40	7.0	16.80	17.0	40.80	7.0	16.80		
8	38.40	8.0	19.20	16.0	38.40	8.0	19.20		
9	36.00	8.0	19.20	15.0	36.00	8.0	19.20		
10	33.60	6.0	14.40	14.5	34.80	6.0	14.40		
11	28.80	6.0	14.40	14.0	33.60	5.0	12.00		
12	31.20	5.0	12.00	13.5	32.40	5.5	13.20		
13	31.20	5.0	12.00	14.0	33.60	5.5	13.20		
14	36.00	8.0	19.20	15.5	37.20	6.0	14.40		
15	36.00	7.0	16.80	17.0	40.80	8.0	19.20		
16	36.00	6.0	14.40	16.0	38.40	7.0	16.80		
17	36.00	7.0	16.80	16.0	38.40	5.0	12.00		
18	38.40	6.5	15.60	17.0	40.80	8.0	19.20		
19	38.40	6.0	14.40	17.0	40.80	7.0	16.80		
20	38.40	7.0	16.80	18.0	43.20	7.0	16.80		
21	40.80	8.0	19.20	16.0	38.40	6.5	15.60		
22	38.40	8.0	19.20	16.0	38.40	8.0	19.20		
23	38.40	8.0	19.20	16.0	38.40	7.0	16.80		
24	38.40	8.0	19.20	17.0	40.80	8.0	19.20		
25	38.40	8.0	19.20	17.0	40.80	8.0	19.20		
26									

975°C 10Ω/sq cm 0.5 Hour Etch

	5μ do	5μ do'	5μ undo	5μ undo'	15μ do	15μ do'	15μ undo	15μ undo'	50μ do
1	1.0	2.4	.2	0.5	1.0	2.4	.2	0.5	1.0
2	1.0	2.4	.2	0.5	1.0	2.4	.2	0.5	1.0
3	1.0	2.4	.2	0.5	1.0	2.4	.2	0.5	1.0
4	1.0	2.4	.2	0.5	1.0	2.4	.2	0.5	.7
5	1.0	2.4	.2	0.5	1.0	2.4	0	0.0	1.0
6	1.0	2.4	.2	0.5	1.0	2.4	.2	0.5	1.0
7	.5	1.2	0	0.0	1.0	2.4	.2	0.5	1.0
8	1.0	2.4	.2	0.5	1.0	2.4	.2	0.5	1.0
9	.5	1.2	0	0.0	1.0	2.4	.2	0.5	1.0
10	.2	0.5	.2	0.5	1.0	2.4	.2	0.5	1.0
11	1.0	2.4	.5	1.2	1.0	2.4	.2	0.5	1.0
12	1.0	2.4	.2	0.5	1.0	2.4	.2	0.5	1.0
13	1.0	2.4	.2	0.5	1.0	2.4	.2	0.5	1.0
14	1.0	2.4	0	0.0	1.0	2.4	0	0.0	1.0
15	1.0	2.4	0	0.0	1.0	2.4	0	0.0	1.0
16	1.0	2.4	.2	0.5	1.0	2.4	0	0.0	1.0
17	1.0	2.4	0	0.0	1.0	2.4	.2	0.5	1.0
18	1.0	2.4	.5	1.2	1.0	2.4	.2	0.5	1.0
19	1.0	2.4	.2	0.5	1.0	2.4	.2	0.5	1.0
20	1.0	2.4	.2	0.5	1.0	2.4	.2	0.5	.2
21	1.0	2.4	.2	0.5	1.0	2.4	.2	0.5	1.0
22	1.0	2.4	.2	0.5	1.0	2.4	.2	0.5	1.0
23	1.0	2.4	0	0.0	1.0	2.4	0	0.0	1.0
24	1.0	2.4	0	0.0	1.0	2.4	0	0.0	1.0
25	1.0	2.4	0	0.0	1.0	2.4	0	0.0	1.0



975°C 10Ω/sq cm 0.5 Hour Etch

	50μ do'	50μ undo	50μ undo'	150μ do	150μ do'	150μ undo	150μ undo'
1	2.4	.2	0.5	1.0	2.4	.2	0.5
2	2.4	.2	0.5	1.0	2.4	.2	0.5
3	2.4	.2	0.5	1.0	2.4	.2	0.5
4	1.7	.2	0.5	1.0	2.4	.2	0.5
5	2.4	.2	0.5	1.0	2.4	.5	1.2
6	2.4	.2	0.5	1.0	2.4	0	0.0
7	2.4	.5	1.2	.7	1.7	0	0.0
8	2.4	.2	0.5	1.0	2.4	.2	0.5
9	2.4	.2	0.5	1.0	2.4	0	0.0
10	2.4	.2	0.5	.7	1.7	.2	0.5
11	2.4	.2	0.5	1.0	2.4	.5	1.2
12	2.4	.2	0.5	1.0	2.4	.2	0.5
13	2.4	0	0.0	1.0	2.4	0	0.0
14	2.4	.2	0.5	1.0	2.4	.2	0.5
15	2.4	0	0.0	1.0	2.4	.2	0.5
16	2.4	.2	0.5	1.0	2.4	.2	0.5
17	2.4	.2	0.5	1.5	3.6	.5	1.2
18	2.4	.2	0.5	1.0	2.4	.2	0.5
19	2.4	.2	0.5	1.0	2.4	.2	0.5
20	0.5	0	0.0	.5	1.2	0	0.0
21	2.4	.2	0.5	1.0	2.4	.2	0.5
22	2.4	.2	0.5	1.0	2.4	.2	0.5
23	2.4	.2	0.5	1.0	2.4	.2	0.5
24	2.4	0	0.0	1.0	2.4	0	0.0
25	2.4	0	0.0	1.0	2.4	0	0.0

975°C 10Ω/sq cm 1.5 Hour Etch

	5μ do	5μ do'	5μ undo	5μ undo'	15μ do	15μ do'	15μ undo	15μ undo'	50μ do
1	3.0	7.2	1.0	2.4	4.0	9.6	1.0	2.4	5.0
2	4.0	9.6	1.0	2.4	4.0	9.6	1.0	2.4	5.0
3	3.5	8.4	1.0	2.4	4.0	9.6	1.0	2.4	5.0
4	4.0	9.6	1.0	2.4	4.0	9.6	1.0	2.4	5.0
5	4.0	9.6	1.0	2.4	4.5	10.8	1.0	2.4	5.0
6	4.0	9.6	1.0	2.4	4.0	9.6	1.0	2.4	5.0
7	2.0	4.8	.5	1.2	4.5	10.8	1.0	2.4	5.0
8	1.5	3.6	.5	1.2	4.0	9.6	1.0	2.4	4.0
9	1.0	2.4	0	0.0	4.0	9.6	1.0	2.4	5.0
10	3.0	7.2	1.0	2.4	4.0	9.6	1.0	2.4	4.0
11	3.0	7.2	1.0	2.4	4.0	9.6	1.0	2.4	4.0
12	3.0	7.2	1.0	2.4	3.0	7.2	1.0	2.4	3.0
13	2.5	6.0	1.0	2.4	3.0	7.2	1.0	2.4	3.0
14	2.0	4.8	1.0	2.4	2.5	6.0	1.0	2.4	2.5
15	4.0	9.6	1.0	2.4	4.0	9.6	1.0	2.4	4.0
16	4.0	9.6	1.0	2.4	5.0	12.0	1.0	2.4	5.0
17	5.0	12.0	1.0	2.4	5.0	12.0	1.0	2.4	5.0
18	4.0	9.6	1.0	2.4	5.0	12.0	1.0	2.4	5.0
19	4.5	10.8	1.0	2.4	5.0	12.0	1.0	2.4	5.0
20	4.0	9.6	1.0	2.4	4.5	10.8	1.0	2.4	5.0
21	4.0	9.6	1.0	2.4	5.0	12.0	1.0	2.4	5.5
22	4.0	9.6	1.0	2.4	4.5	10.8	1.0	2.4	5.0
23	4.0	9.6	1.0	2.4	5.0	12.0	1.0	2.4	5.0
24	4.0	9.6	1.0	2.4	5.0	12.0	1.0	2.4	5.0
25	4.0	9.6	1.0	2.4	5.0	12.0	1.0	2.4	6.0

975°C 10Ω/sq cm 1.5 Hour Etch

	50μ do'	50μ undo	50μ undo'	150μ do	150μ do'	150μ undo	150μ undo'
1	12.0	1.0	2.4	5.0	12.0	1.0	2.4
2	12.0	1.0	2.4	5.0	12.0	1.0	2.4
3	12.0	1.0	2.4	5.0	12.0	1.0	2.4
4	12.0	1.0	2.4	5.0	12.0	1.5	3.6
5	12.0	1.0	2.4	5.0	12.0	1.5	3.6
6	12.0	1.0	2.4	5.0	12.0	1.0	2.4
7	12.0	1.0	2.4	5.0	12.0	1.0	2.4
8	9.6	1.0	2.4	3.0	7.2	1.0	2.4
9	12.0	1.5	3.6	5.0	12.0	1.5	3.6
10	9.6	1.0	2.4	4.0	9.6	1.5	3.6
11	9.6	1.0	2.4	4.0	9.6	1.0	2.4
12	7.2	1.0	2.4	3.5	8.4	1.0	2.4
13	7.2	1.5	3.6	3.0	7.2	1.5	3.6
14	6.0	1.0	2.4	3.0	7.2	1.0	2.4
15	9.6	1.0	2.4	6.0	14.4	1.0	2.4
16	12.0	1.0	2.4	5.0	12.0	1.0	2.4
17	12.0	1.0	2.4	5.0	12.0	1.0	2.4
18	12.0	1.2	2.9	6.0	14.4	1.0	2.4
19	12.0	2.0	4.8	6.0	14.4	1.0	2.4
20	12.0	1.5	3.6	5.0	12.0	1.0	2.4
21	13.2	1.0	2.4	5.0	12.0	1.0	2.4
22	12.0	1.0	2.4	5.0	12.0	1.0	2.4
23	12.0	1.0	2.4	5.0	12.0	1.5	3.6
24	12.0	1.0	2.4	5.0	12.0	1.0	2.4
25	14.4	1.0	2.4	5.5	13.2	1.0	2.4

975°C 10Ω/sq cm 3.5 Hour Etch

	5μ do	5μ do'	15μ do	15μ do'	50μ do	50μ do'	150μ do	150μ do'	150μ do'	150μ do'
1	11.0	26.4	12.0	28.8	13.0	31.2	13.5	32.4	32.4	4.0
2	11.0	26.4	12.0	28.8	13.0	31.2	13.0	31.2	31.2	4.0
3	11.5	27.6	12.0	28.8	13.0	31.2	13.5	32.4	32.4	4.0
4	12.0	28.8	12.0	28.8	13.0	31.2	13.5	32.4	32.4	4.0
5	11.5	27.6	12.0	28.8	13.0	31.2	13.5	32.4	32.4	5.0
6	12.5	30.0	12.0	28.8	13.0	31.2	15.0	36.0	36.0	4.0
7	12.0	28.8	14.0	33.6	14.0	33.6	13.5	32.4	32.4	
8	11.0	26.4	12.0	28.8	12.0	28.8	13.0	31.2	31.2	
9	11.0	26.4	10.0	24.0	13.0	31.2	13.5	32.4	32.4	
10	11.0	26.4	12.0	28.8	11.0	26.4	13.0	31.2	31.2	
11	11.0	26.4	13.0	31.2	13.0	31.2	14.0	33.6	33.6	
12	13.0	31.2	13.0	31.2	14.0	33.6	14.0	33.6	33.6	
13	13.0	31.2	14.0	33.6	14.0	33.6	14.0	33.6	33.6	
14	13.0	31.2	14.0	33.6	15.0	36.0	15.0	36.0	36.0	
15	16.0	38.4	14.0	33.6	15.0	36.0	15.0	36.0	36.0	
16	14.0	33.6	14.0	33.6	15.0	36.0	15.0	36.0	36.0	
17	13.0	31.2	13.0	31.2	15.0	36.0	15.0	36.0	36.0	
18	13.5	32.4	14.0	33.6	15.0	36.0	15.0	36.0	36.0	
19	13.0	31.2	14.0	33.6	14.5	34.8	15.5	37.2	37.2	
20	13.0	31.2	14.0	33.6	14.5	34.8	15.0	36.0	36.0	
21	13.0	31.2	15.0	36.0	15.5	37.2	15.5	37.2	37.2	
22	13.0	31.2	14.0	33.6	15.0	36.0	15.5	37.2	37.2	
23	14.0	33.6	14.0	33.6	15.0	36.0	15.5	37.2	37.2	
24	13.5	32.4	14.0	33.6	15.0	36.0	15.5	37.2	37.2	
25	13.0	31.2	14.0	33.6	15.0	36.0	15.0	36.0	36.0	
26										

975°C 10Ω/sq cm 3.5 Hour Etch

150μm undo'

9.6  
9.6  
9.6  
9.6  
12.0  
9.6

1 2 3 4 5 6 7 8 9 10 11 12 13 14 15 16 17 18 19 20 21 22 23 24 25 26

975°C 20Ω/sq cm 1.5 Hour Etch

	5μ	5μ dop'	5μ undop'	15μ do	15μ do'	15μ undop'	15μ do	15μ do'	15μ undop'	50μ do
1	3.5	8.40	2.40	5.5	13.20	1.5	1.5	3.60	3.60	5.2
2	5.0	12.00	2.40	3.2	7.68	1.0	1.0	2.40	2.40	6.0
3	6.0	14.40	3.60	5.0	12.00	1.5	1.5	3.60	3.60	6.0
4	6.0	14.40	3.60	4.5	10.80	1.5	1.5	3.60	3.60	5.5
5	6.0	14.40	3.60	7.0	16.80	1.5	1.5	3.60	3.60	6.0
6	6.0	14.40	3.60	6.0	14.40	1.5	1.5	3.60	3.60	7.0
7	5.5	13.20	3.60	6.5	15.60	2.0	2.0	4.80	4.80	6.0
8	6.0	14.40	3.60	6.0	14.40	2.0	2.0	4.80	4.80	6.5
9	6.5	15.60	4.80	6.5	15.60	2.0	2.0	4.80	4.80	7.0
10	6.5	15.60	4.80	6.0	14.40	2.0	2.0	4.80	4.80	7.0
11	6.5	15.60	4.80	6.5	15.60	2.0	2.0	4.80	4.80	7.0
12	6.5	15.60	4.80	6.5	15.60	2.0	2.0	4.80	4.80	7.0
13	7.0	16.80	4.80	7.0	16.80	2.0	2.0	4.80	4.80	6.5
14	7.0	16.80	6.00	7.0	16.80	2.0	2.0	4.80	4.80	7.0
15	7.0	16.80	7.20	7.0	16.80	2.0	2.0	4.80	4.80	7.0
16	7.5	18.00	4.80	8.0	19.20	2.0	2.0	4.80	4.80	7.5
17	7.5	18.00	4.80	8.0	19.20	2.0	2.0	4.80	4.80	7.5
18	7.0	16.80	4.80	7.0	16.80	2.0	2.0	4.80	4.80	8.5
19	7.0	16.80	4.80	7.0	16.80	2.0	2.0	4.80	4.80	7.0
20	7.0	16.80	7.20	6.5	15.60	2.0	2.0	4.80	4.80	7.0
21	7.0	16.80	4.80	6.5	15.60	2.0	2.0	4.80	4.80	6.5
22	6.0	14.40	4.80	5.5	13.20	2.0	2.0	4.80	4.80	6.0
23	5.5	13.20	4.80	5.5	13.20	2.0	2.0	4.80	4.80	5.5
24	6.5	15.60	4.80	6.5	15.60	2.0	2.0	4.80	4.80	6.0
25	6.5	15.60	4.80	6.5	15.60	2.0	2.0	4.80	4.80	7.0
26	7.0	16.80	4.80	7.0	16.80	2.0	2.0	4.80	4.80	6.5
27	7.0	16.80	4.80	7.0	16.80	2.0	2.0	4.80	4.80	7.0
28	7.5	18.00	4.80	7.5	18.00	2.0	2.0	4.80	4.80	6.5
29	6.0	14.40	7.20	6.0	14.40	3.0	2.5	6.00	6.00	6.0
30	7.0	16.80	4.80	6.0	14.40	2.0	2.0	4.80	4.80	7.0
31	7.0	16.80	3.60	7.0	16.80	1.5	1.5	3.60	3.60	6.0
32	6.5	15.60	3.60	5.5	13.20	1.5	1.5	3.60	3.60	7.0
33	6.5	15.60	3.60	6.0	14.40	1.5	1.5	3.60	3.60	6.0
34	6.0	14.40	3.60	6.0	14.40	1.5	1.5	3.60	3.60	6.0
35	7.0	16.80	3.60	6.5	15.60	1.5	1.5	3.60	3.60	6.0
36	6.5	15.60	3.60	7.0	16.80	1.5	2.0	4.80	4.80	6.5
37	7.0	16.80	4.80	7.0	16.80	2.0	2.0	4.80	4.80	6.5
38	6.5	15.60	4.80	8.5	20.40	2.0	2.0	4.80	4.80	8.0
39	6.5	15.60	4.80	6.5	15.60	2.0	2.0	4.80	4.80	8.0
40	7.0	16.80	7.20	7.0	16.80	3.0	2.0	4.80	4.80	7.5
41	7.0	16.80	4.80	7.0	16.80	2.0	2.0	4.80	4.80	7.0
42	8.0	19.20	4.80	8.0	19.20	2.0	2.5	6.00	6.00	7.0

975°C 20Ω/sq cm 1.5 Hour Etch

	5μ dop	5μ dop'	5μ undo	5μ undop'	15μ do	15μ do'	15μ undo	15μ undop'	50μ do
43	7.0	16.80	2.0	4.80	9.0	21.60	3.0	7.20	8.5
44	7.0	16.80	3.0	7.20	8.0	19.20	2.5	6.00	7.0
45	7.0	16.80	2.0	4.80	7.0	16.80	2.5	6.00	7.5
46	7.0	16.80	2.0	4.80	7.0	16.80	2.0	4.80	8.0
47	6.5	15.60	2.0	4.80	7.0	16.80	2.5	6.00	6.5
48	7.0	16.80	2.5	6.00	8.0	19.20	2.5	6.00	8.0
49	6.0	14.40	2.0	4.80	6.0	14.40	2.0	4.80	7.0
50	7.0	16.80	2.0	4.80	7.0	16.80	2.0	4.80	7.0
51									
52									
53									
54									
55									
56									
57									
58									
59									
60									
61									
62									
63									
64									
65									
66									
67									
68									
69									
70									
71									
72									
73									
74									
75									
76									
77									
78									
79									
80									
81									
82									
83									
84									

975°C 20Ω/sq cm 1.5 Hour Etch

	50μ do'	50μ undo	50μ undo'	150μ do	150μ do'	150μ undo	150μ undo'	μ	Pg7A do'
1	12.48	2.0	4.80	6.5	15.60	2.0	4.80	5	8.40
2	14.40	1.5	3.60	6.0	14.40	2.0	4.80	5	12.00
3	14.40	1.5	3.60	6.5	15.60	2.0	4.80	5	14.40
4	13.20	2.0	4.80	7.0	16.80	2.0	4.80	5	14.40
5	14.40	1.5	3.60	7.5	18.00	2.0	4.80	5	14.40
6	16.80	1.5	3.60	7.0	16.80	2.0	4.80	5	14.40
7	14.40	1.5	3.60	8.0	19.20	2.0	4.80	5	13.20
8	15.60	2.0	4.80	8.0	19.20	2.0	4.80	5	14.40
9	16.80	2.0	4.80	8.5	20.40	2.0	4.80	5	15.60
10	16.80	2.0	4.80	7.0	16.80	2.0	4.80	5	15.60
11	16.80	2.0	4.80	7.0	16.80	2.0	4.80	5	15.60
12	15.60	2.0	4.80	7.0	16.80	1.5	3.60	5	15.60
13	16.80	2.0	4.80	7.5	18.00	2.5	6.00	5	16.80
14	16.80	2.0	4.80	8.0	19.20	2.0	4.80	5	16.80
15	18.00	2.0	4.80	8.0	19.20	2.0	4.80	5	16.80
16	18.00	2.0	4.80	8.5	20.40	2.0	4.80	5	18.00
17	20.40	3.0	7.20	8.0	19.20	3.0	7.20	5	18.00
18	16.80	2.0	4.80	8.0	19.20	2.5	6.00	5	16.80
19	16.80	2.0	4.80	7.5	18.00	2.0	4.80	5	16.80
20	16.80	2.5	6.00	7.0	16.80	3.0	7.20	5	16.80
21	15.60	2.0	4.80	7.0	16.80	2.0	4.80	5	16.80
22	14.40	2.0	4.80	7.0	16.80	2.0	4.80	5	14.40
23	13.20	2.0	4.80	6.0	14.40	2.0	4.80	5	13.20
24	14.40	2.0	4.80	6.0	14.40	1.5	3.60	5	15.60
25	16.80	2.0	4.80	7.0	16.80	2.0	4.80	5	15.60
26	15.60	2.0	4.80	7.0	16.80	2.0	4.80	5	15.60
27	16.80	2.0	4.80	8.0	19.20	2.5	6.00	5	16.80
28	15.60	2.0	4.80	7.5	18.00	2.0	4.80	5	18.00
29	14.40	2.0	4.80	7.5	18.00	2.0	4.80	5	14.40
30	16.80	2.0	4.80	7.0	16.80	2.0	4.80	5	16.80
31	14.40	1.5	3.60	8.5	20.40	1.5	3.60	5	16.80
32	16.80	2.0	4.80	7.0	16.80	2.0	4.80	5	15.60
33	14.40	1.5	3.60	7.0	16.80	2.0	4.80	5	15.60
34	14.40	1.5	3.60	7.0	16.80	2.0	4.80	5	14.40
35	15.60	2.0	4.80	7.0	16.80	2.0	4.80	5	16.80
36	15.60	2.0	4.80	7.5	18.00	2.0	4.80	5	15.60
37	15.60	2.0	4.80	7.0	16.80	2.0	4.80	5	16.80
38	19.20	4.0	9.60	7.0	16.80	2.0	4.80	5	15.60
39	19.20	1.5	3.60	7.0	16.80	2.0	4.80	5	15.60
40	18.00	2.0	4.80	7.0	16.80	2.0	4.80	5	16.80
41	16.80	2.0	4.80	8.0	19.20	2.5	6.00	5	16.80
42	16.80	3.0	7.20	7.5	18.00	3.0	7.20	5	19.20



975°C 20Ω/sq cm 1.5 Hour Etch

	50μ do'	50μ undo	50μ undo'	150μ do	150μ do'	150μ undo	150μ undo'	μ	Pg7A do'
43	20.40	2.5	6.00	8.0	19.20	2.5	6.00	5	16.80
44	16.80	2.0	4.80	8.0	19.20	2.0	4.80	5	16.80
45	18.00	2.5	6.00	7.0	16.80	2.0	4.80	5	16.80
46	19.20	3.0	7.20	7.5	18.00	3.0	7.20	5	16.80
47	15.60	2.0	4.80	7.0	16.80	2.0	4.80	5	15.60
48	19.20	2.5	6.00	8.0	19.20	3.0	7.20	5	16.80
49	16.80	3.0	7.20	8.0	19.20	3.0	7.20	5	14.40
50	16.80	1.5	3.60	8.0	19.20	2.0	4.80	5	16.80
51								15	13.20
52								15	7.68
53								15	12.00
54								15	10.80
55								15	16.80
56								15	14.40
57								15	15.60
58								15	14.40
59								15	15.60
60								15	14.40
61								15	15.60
62								15	15.60
63								15	16.80
64								15	16.80
65								15	16.80
66								15	16.80
67								15	19.20
68								15	19.20
69								15	16.80
70								15	16.80
71								15	15.60
72								15	15.60
73								15	13.20
74								15	13.20
75								15	15.60
76								15	15.60
77								15	16.80
78								15	16.80
79								15	18.00
80								15	14.40
81								15	14.40
82								15	16.80
83								15	13.20
84								15	14.40
								15	14.40

975°C 20Ω/sq cm 2.5 Hour Etch

	5μ do	5μ do'	5μ undd	5μ undd'	15μ do	15μ do'	15 undd	15 undd'	50μ do
1	11.5	27.60	4.0	9.60	12.0	28.80	5.0	12.00	13.0
2	11.5	27.60	5.0	12.00	12.0	28.80	5.0	12.00	13.0
3	11.5	27.60	5.0	12.00	12.0	28.80	5.0	12.00	12.0
4	11.0	26.40	4.0	9.60	11.0	26.40	4.0	9.60	12.0
5	11.0	26.40	4.0	9.60	12.5	30.00	5.0	12.00	11.0
6	11.0	26.40	4.0	9.60	10.0	24.00	3.0	7.20	11.5
7	11.5	27.60	4.0	9.60	10.0	24.00	4.0	9.60	11.0
8	11.0	26.40	5.0	12.00	11.0	26.40	4.0	9.60	12.0
9	12.0	28.80	4.0	9.60	11.0	26.40	4.5	10.80	11.0
10	8.0	19.20	3.0	7.20	9.0	21.60	3.0	7.20	9.0
11	8.5	20.40	2.5	6.00	10.0	24.00	3.0	7.20	11.0
12	12.0	28.80	5.0	12.00	12.0	28.80	5.0	12.00	12.0
13	11.0	26.40	4.0	9.60	11.0	26.40	4.0	9.60	11.5
14	13.0	31.20	4.5	10.80	13.0	31.20	5.0	12.00	12.0
15	12.0	28.80	4.0	9.60	12.0	28.80	4.5	10.80	9.0
16	12.0	28.80	6.0	14.40	12.0	28.80	5.5	13.20	13.0
17	12.5	30.00	5.0	12.00	13.0	31.20	4.0	9.60	12.0
18	12.5	30.00	5.0	12.00	12.5	30.00	5.0	12.00	13.0
19	13.0	31.20	6.5	15.60	12.5	30.00	5.5	13.20	13.0
20	13.0	31.20	5.0	12.00	13.0	31.20	6.0	14.40	13.0
21	10.0	24.00	4.5	10.80	11.0	26.40	4.0	9.60	10.0
22	7.0	16.80	1.5	3.60	7.0	16.80	2.0	4.80	9.0
23	9.0	21.60	2.5	6.00	11.0	26.40	4.0	9.60	9.0
24	10.0	24.00	4.0	9.60	11.0	26.40	4.0	9.60	11.5
25	11.5	27.60	4.5	10.80	11.5	27.60	4.5	10.80	11.5
26	10.0	24.00	3.5	8.40	11.5	27.60	4.5	10.80	14.0
27	5.0	12.00	1.0	2.40	9.0	21.60	3.0	7.20	11.5
28	10.0	24.00	3.5	8.40	11.5	27.60	4.0	9.60	10.5
29	7.0	16.80	2.0	4.80	9.0	21.60	3.0	7.20	12.0
30	11.0	26.40	3.5	8.40	8.5	20.40	2.5	6.00	9.0
31	10.0	24.00	3.0	7.20	10.0	24.00	4.0	9.60	11.0
32	12.5	30.00	5.0	12.00	12.0	28.80	5.0	12.00	7.0
33	12.0	28.80	5.0	12.00	12.5	30.00	6.0	14.40	12.0
34	13.0	31.20	5.0	12.00	13.0	31.20	6.0	14.40	12.0
35	12.0	28.80	5.0	12.00	12.5	30.00	5.0	12.00	12.0
36	13.0	31.20	5.0	12.00	12.5	30.00	5.0	12.00	12.5
37	11.5	27.60	4.0	9.60	12.0	28.80	4.0	9.60	13.0
38	12.0	28.80	5.0	12.00	12.0	28.80	5.0	12.00	13.0
39	11.5	27.60	4.0	9.60	13.0	31.20	5.5	13.20	13.5
40	13.0	31.20	5.5	13.20	13.0	31.20	6.0	14.40	13.0
41	13.0	31.20	6.0	14.40	13.5	32.40	6.0	14.40	14.0
42	14.0	33.60	6.0	14.40	13.0	31.20	6.0	14.40	14.0

975°C 20Ω/sq cm 2.5 Hour Etch

	5μ do	5μ do'	5μ undo	5μ undo'	15μ do	15μ do'	15 undo	15 undo'	50μ do
43	13.0	31.20	6.0	14.40	13.0	31.20	6.0	14.40	14.0
44	12.5	30.00	5.0	12.00	12.0	28.80	6.0	14.40	13.0
45	12.0	28.80	7.0	16.80	6.0	14.40	2.0	4.80	13.0
46	12.0	28.80	5.0	12.00	12.0	28.80	6.0	14.40	12.5
47	12.0	28.80	6.0	14.40	14.0	33.60	5.0	12.00	14.0
48	13.0	31.20	6.0	14.40	13.0	31.20	6.0	14.40	13.0
49	13.0	31.20	6.0	14.40	14.0	33.60	6.0	14.40	14.5
50	13.0	31.20	5.0	12.00	13.0	31.20	6.0	14.40	13.0
51									

975°C 20Ω/sq cm 2.5 Hour Etch

	50μ do'	50μ undo	50μ undo'	150μ do	150μ do'	150μ undo	150μ undo'
1	31.20	5.0	12.00	13.0	31.20	0.0	0.00
2	31.20	5.0	12.00	9.0	21.60	4.0	9.60
3	28.80	6.0	14.40	12.0	28.80	6.0	14.40
4	28.80	5.0	12.00	12.0	28.80	5.0	12.00
5	26.40	4.0	9.60	14.5	34.80	5.0	12.00
6	27.60	5.0	12.00	13.0	31.20	5.0	12.00
7	26.40	4.0	9.60	12.0	28.80	5.0	12.00
8	28.80	4.5	10.80	11.5	27.60	4.0	9.60
9	26.40	4.5	10.80	12.0	28.80	5.0	12.00
10	21.60	3.0	7.20	11.0	26.40	4.0	9.60
11	26.40	4.0	9.60	12.0	28.80	5.0	12.00
12	28.80	4.0	9.60	13.5	32.40	5.0	12.00
13	27.60	4.0	9.60	12.0	28.80	4.5	10.80
14	28.80	5.0	12.00	13.0	31.20	5.0	12.00
15	21.60	3.0	7.20	11.0	26.40	4.0	9.60
16	31.28	4.0	9.60	14.0	33.60	5.0	12.00
17	28.80	4.0	9.60	13.0	31.20	5.0	12.00
18	31.20	5.0	12.00	12.5	30.00	5.0	12.00
19	31.20	5.0	12.00	14.0	33.60	5.0	12.00
20	31.20	5.0	12.00	14.0	33.60	6.0	14.40
21	24.00	5.0	12.00	12.0	28.80	6.0	14.40
22	21.60	2.5	6.00	9.0	21.60	2.0	4.80
23	21.60	3.0	7.20	12.0	28.80	4.0	9.60
24	27.60	4.0	9.60	12.0	28.80	5.0	12.00
25	27.60	4.5	10.80	12.0	28.80	4.0	9.60
26	33.60	4.5	10.80	15.0	36.00	4.0	9.60
27	27.60	4.0	9.60	12.0	28.80	4.5	10.80
28	25.20	3.0	7.20	11.5	27.60	4.0	9.60
29	28.80	3.5	8.40	8.0	19.20	2.0	4.80
30	21.60	3.0	7.20	8.0	19.20	3.0	7.20
31	26.40	4.0	9.60	11.5	27.60	5.0	12.00
32	16.80	3.0	7.20	14.0	33.60	5.0	12.00
33	28.80	5.0	12.00	13.5	32.40	4.0	9.60
34	28.80	5.0	12.00	15.0	36.00	5.5	13.20
35	28.80	5.0	12.00	14.0	33.60	6.0	14.40
36	30.00	5.0	12.00	13.5	32.40	6.0	14.40
37	31.20	5.0	12.00	12.5	30.00	5.0	12.00
38	31.20	6.0	14.40	13.5	32.40	6.0	14.40
39	32.40	5.0	12.00	13.0	31.20	5.0	12.00
40	31.20	6.0	14.40	14.0	33.60	6.0	14.40
41	33.60	6.5	15.60	14.5	34.80	5.5	13.20
42	33.60	5.5	13.20	15.0	36.00	6.0	14.40

975°C 20Ω/sq cm 2.5 Hour Etch

	50μ do'	50μ undo	50μ undo'	150μ do	150μ do'	150μ undo	150μ undo'
43	33.60	4.0	9.60	15.0	36.00	6.0	14.40
44	31.20	6.0	14.40	14.0	33.60	6.5	15.60
45	31.20	6.0	14.40	14.0	33.60	6.0	14.40
46	30.00	6.0	14.40	14.0	33.60	6.0	14.40
47	33.60	6.0	14.40	15.5	37.20	8.0	19.20
48	31.20	6.5	15.60	14.0	33.60	6.0	14.40
49	34.80	6.0	14.40	14.0	33.60	6.5	15.60
50	31.20	5.5	13.20	14.0	33.60	5.0	12.00
51							

975°C 20Ω/sq cm 3.5 Hour Etch

	5μ do	5μ do'	5μ do'	5μ do'	5μ do'	15μ do	15μ do'	15μ do'	15μ do'	15μ do'	15μ do'	50μ do
1	16.0	38.40	8.0	19.20	12.0	28.80	5.0	12.00	15.0	12.00	15.0	15.0
2	16.0	38.40	8.0	19.20	16.0	38.40	8.0	19.20	16.0	19.20	16.0	16.0
3	15.0	36.00	6.0	14.40	15.0	36.00	6.5	15.60	16.0	15.60	16.0	16.0
4	16.0	38.40	6.0	14.40	16.0	38.40	7.0	16.80	18.0	16.80	18.0	18.0
5	16.0	38.40	6.5	15.60	16.5	39.60	6.0	14.40	18.0	14.40	18.0	18.0
6	16.0	38.40	7.5	18.00	16.0	38.40	6.0	14.40	18.0	14.40	18.0	18.0
7	16.0	38.40	7.0	16.80	16.0	38.40	7.0	16.80	17.0	16.80	17.0	17.0
8	15.0	36.00	5.0	12.00	16.0	38.40	6.0	14.40	17.0	14.40	17.0	17.0
9	15.0	36.00	6.5	15.60	16.0	38.40	9.0	21.60	16.0	21.60	16.0	16.0
10	15.0	36.00	7.0	16.80	16.5	39.60	7.0	16.80	17.0	16.80	17.0	17.0
11	17.0	40.80	9.0	21.60	17.5	42.00	8.0	19.20	17.5	19.20	17.5	17.5
12	17.0	40.80	9.0	21.60	16.0	38.40	8.0	19.20	17.0	19.20	17.0	17.0
13	17.0	40.80	7.0	16.80	18.0	43.20	8.0	19.20	17.0	19.20	17.0	17.0
14	16.0	38.40	7.0	16.80	17.0	40.80	8.0	19.20	17.0	19.20	17.0	17.0
15	15.0	36.00	7.0	16.80	15.0	36.00	7.0	16.80	16.0	16.80	16.0	16.0
16	17.0	40.80	9.0	21.60	17.0	40.80	7.0	16.80	18.0	21.60	18.0	18.0
17	16.0	38.40	7.0	16.80	17.0	40.80	7.0	16.80	17.0	16.80	17.0	17.0
18	18.0	43.20	8.0	19.20	16.0	38.40	7.0	16.80	18.0	16.80	18.0	18.0
19	17.0	40.80	8.0	19.20	17.0	40.80	8.0	19.20	17.0	19.20	17.0	17.0
20	16.0	38.40	9.0	21.60	17.0	40.80	9.0	21.60	17.0	21.60	17.0	17.0
21	14.0	33.60	5.0	12.00	14.0	33.60	5.0	12.00	14.0	12.00	14.0	14.0
22	14.0	33.60	5.0	12.00	12.0	28.80	5.0	12.00	13.0	12.00	13.0	13.0
23	10.0	24.00	3.5	8.40	10.0	24.00	4.0	9.60	11.0	9.60	11.0	11.0
24	11.0	26.40	4.0	9.60	14.0	33.60	5.0	12.00	16.0	12.00	16.0	16.0
25	15.0	36.00	5.0	12.00	16.0	38.40	5.0	12.00	16.0	12.00	16.0	16.0
26	14.0	33.60	6.0	14.40	16.0	38.40	6.0	14.40	14.0	14.40	14.0	14.0
27	11.0	26.40	4.0	9.60	13.0	31.20	5.0	12.00	14.0	12.00	14.0	14.0
28	15.0	36.00	5.0	12.00	17.0	40.80	5.0	12.00	12.0	12.00	12.0	12.0
29	14.0	33.60	5.0	12.00	13.0	31.20	5.0	12.00	14.0	12.00	14.0	14.0
30	15.0	36.00	5.0	12.00	15.0	36.00	5.0	12.00	15.0	12.00	15.0	15.0
31	15.0	36.00	6.0	14.40	16.0	38.40	7.0	16.80	16.0	16.80	16.0	16.0
32	16.0	38.40	7.0	16.80	16.0	38.40	7.0	16.80	16.5	16.80	16.5	16.5
33	16.0	38.40	7.0	16.80	16.0	38.40	7.0	16.80	17.0	16.80	17.0	17.0
34	16.0	38.40	7.0	16.80	15.0	36.00	6.0	14.40	16.0	14.40	16.0	16.0
35	15.0	36.00	7.0	16.80	16.0	38.40	7.0	16.80	16.0	16.80	16.0	16.0
36	17.0	40.80	9.0	21.60	17.0	40.80	9.0	21.60	17.0	21.60	17.0	17.0
37	16.0	38.40	8.0	19.20	17.0	40.80	8.0	19.20	17.0	19.20	17.0	17.0
38	17.0	40.80	9.0	21.60	16.0	38.40	8.0	19.20	17.0	19.20	17.0	17.0
39	17.0	40.80	9.0	21.60	16.5	39.60	8.0	19.20	17.0	19.20	17.0	17.0
40	18.0	43.20	9.0	21.60	17.0	40.80	9.0	21.60	17.0	21.60	17.0	17.0
41	18.0	43.20	9.0	21.60	17.5	42.00	8.5	20.40	19.0	20.40	19.0	19.0
42	17.0	40.80	10.0	24.00	19.0	45.60	10.0	24.00	18.0	24.00	18.0	18.0

975°C 20Ω/sq cm 3.5 Hour Etch

	5μ do	5μ do'	5μ undo	5μ undo'	15μ do	15μ do'	15μ undo	15μ undo'	50μ do
43	17.0	40.80	10.0	24.00	18.0	43.20	10.0	24.00	19.0
44	18.0	43.20	10.0	24.00	18.0	43.20	10.0	24.00	19.0
45	16.0	38.40	10.0	24.00	17.0	40.80	10.0	24.00	18.0
46	17.0	40.80	11.0	26.40	18.0	43.20	10.0	24.00	18.0
47	18.0	43.20	10.0	24.00	19.0	45.60	11.0	26.40	18.0
48	17.0	40.80	10.0	24.00	18.0	43.20	10.0	24.00	18.0
49	16.0	38.40	8.0	19.20	17.0	40.80	10.0	24.00	17.5
50	17.0	40.80	9.0	21.60	18.0	43.20	8.5	20.40	18.5
51									

975°C 20Ω/sq cm 3.5 Hour Etch

	50μ do'	50μ und0	50μ und0'	150μ do	150μ do'	150μ und0	150μ und0'
1	36.00	7.0	16.80	17.0	40.80	9.0	21.60
2	38.40	8.0	19.20	16.0	38.40	7.5	18.00
3	38.40	7.5	18.00	17.5	42.00	7.0	16.80
4	43.20	8.0	19.20	18.5	44.40	7.0	16.80
5	43.20	8.0	19.20	18.0	43.20	7.0	16.80
6	43.20	8.0	19.20	20.0	48.00	7.5	18.00
7	40.80	7.0	16.80	18.0	43.20	8.0	19.20
8	40.80	9.0	21.60	18.0	43.20	8.0	19.20
9	38.40	9.0	21.60	18.0	43.20	9.0	21.60
10	40.80	8.0	19.20	17.0	40.80	7.0	16.80
11	42.00	10.0	24.00	19.0	45.60	9.0	21.60
12	40.80	7.5	18.00	17.5	42.00	9.0	21.60
13	40.80	8.0	19.20	18.0	43.20	7.0	16.80
14	40.80	9.0	21.60	18.0	43.20	9.0	21.60
15	38.40	7.0	16.80	17.0	40.80	8.0	19.20
16	43.20	10.0	24.00	19.0	45.60	9.0	21.60
17	40.80	8.0	19.20	18.0	43.20	8.0	19.20
18	43.20	9.5	22.80	18.0	43.20	8.0	19.20
19	40.80	8.5	20.40	18.0	43.20	9.0	21.60
20	40.80	10.0	24.00	18.0	43.20	9.0	21.60
21	33.60	5.0	12.00	12.0	28.80	5.0	12.00
22	31.20	5.0	12.00	12.0	28.80	6.0	14.40
23	26.40	4.0	9.60	10.0	24.00	4.0	9.60
24	38.40	6.0	14.40	16.0	38.40	6.0	14.40
25	38.40	8.0	19.20	16.0	38.40	7.0	16.80
26	33.60	5.0	12.00	17.0	40.80	7.0	16.80
27	40.80	5.0	12.00	13.0	31.20	4.0	9.60
28	28.80	5.0	12.00	12.0	28.80	5.0	12.00
29	33.60	5.0	12.00	14.0	33.60	5.0	12.00
30	36.00	6.0	14.40	15.0	36.00	4.0	9.60
31	38.40	8.0	19.20	17.0	40.80	6.0	14.40
32	39.60	8.0	19.20	18.0	43.20	8.0	19.20
33	40.80	7.0	16.80	17.0	40.80	7.0	16.80
34	38.40	7.0	16.80	16.0	38.40	7.0	16.80
35	40.80	8.0	19.20	18.0	43.20	8.0	19.20
36	45.60	9.0	21.60	19.0	45.60	9.0	21.60
37	40.80	10.0	24.00	18.0	43.20	10.0	24.00
38	40.80	9.0	21.60	18.0	43.20	8.0	19.20
39	43.20	10.0	24.00	19.0	45.60	9.0	21.60
40	40.80	9.0	21.60	17.0	40.80	9.0	21.60
41	45.60	10.0	24.00	20.0	48.00	9.0	21.60
42	43.20	8.0	19.20	19.0	45.60	9.0	21.60



975°C 20Ω/sq cm 3.5 Hour Etch

	50μ do'	50μ undo	50μ undo'	150μ do	150μ do'	150μ undo	150μ undo'
43	45.60	12.0	28.80	20.0	48.00	12.0	28.80
44	45.60	11.0	26.40	20.0	48.00	11.0	26.40
45	43.20	10.0	24.00	18.0	43.20	10.0	24.00
46	43.20	10.0	24.00	18.0	43.20	10.0	24.00
47	43.20	11.0	26.40	19.0	45.60	12.0	28.80
48	43.20	11.0	26.40	19.0	45.60	10.0	24.00
49	42.00	10.0	24.00	18.0	43.20	10.0	24.00
50	44.40	10.0	24.00	19.0	45.60	10.0	24.00
51							

1000°C 10Ω/sq cm 0.5 Hour Etch

	5μ do	5μ do'	5μ undo	5μ undo'	15μ do	15μ do'	15μ undo	15μ undo'	50μ do
1	1.0	2.4	.5	1.2	1.5	3.6	.5	1.2	1.5
2	1.5	3.6	.5	1.2	1.5	3.6	.5	1.2	1.5
3	2.0	4.8	.5	1.2	2.0	4.8	.5	1.2	2.0
4	1.5	3.6	.5	1.2	2.0	4.8	.5	1.2	2.0
5	2.0	4.8	.5	1.2	2.0	4.8	.5	1.2	2.0
6	2.0	4.8	0	0.0	2.0	4.8	0	0.0	2.0
7	2.0	4.8	0	0.0	2.0	4.8	0	0.0	2.5
8	2.0	4.8	0	0.0	2.0	4.8	0	0.0	2.0
9	2.0	4.8	0	0.0	2.0	4.8	.2	0.5	2.0
10	2.0	4.8	.5	1.2	2.0	4.8	.5	1.2	2.0
11	1.5	3.6	.5	1.2	1.5	3.6	.5	1.2	1.5
12	1.5	3.6	.5	1.2	1.5	3.6	.5	1.2	2.0
13	2.0	4.8	.5	1.2	2.0	4.8	.5	1.2	2.0
14	2.0	4.8	.2	0.5	2.0	4.8	.2	0.5	2.0
15	1.5	3.6	0	0.0	2.0	4.8	0	0.0	2.0
16	3.0	7.2	0	0.0	3.0	7.2	0	0.0	3.0
17	3.0	7.2	.2	0.5	2.5	6.0	.2	0.5	3.0
18	3.0	7.2	.2	0.5	3.0	7.2	.2	0.5	3.0
19	3.0	7.2	0	0.0	3.0	7.2	.2	0.5	3.0
20	3.0	7.2	.2	0.5	3.0	7.2	0	0.0	3.0
21	2.0	4.8	0	0.0	2.5	6.0	0	0.0	2.5
22	2.0	4.8	0	0.0	2.5	6.0	0	0.0	2.5
23	2.0	4.8	0	0.0	2.5	6.0	0	0.0	2.5
24	2.5	6.0	0	0.0	2.5	6.0	0	0.0	2.5
25	2.5	6.0	0	0.0	2.5	6.0	.2	0.5	2.0

1000°C 10Ω/sq cm 0.5 Hour Etch									
	50μ do'	50μ undo	50μ undo'	150μ do	150μ do'	150μ undo	150μ undo'		
1	3.6	.5	1.2	2.0	4.8	.5	1.2		1.2
2	3.6	.5	1.2	2.0	4.8	.5	1.2		1.2
3	4.8	.5	1.2	2.0	4.8	.5	1.2		1.2
4	4.8	.5	1.2	2.0	4.8	.7	1.7		1.7
5	4.8	.5	1.2	2.0	4.8	.5	1.2		1.2
6	4.8	0	0.0	2.5	6.0	0	0.0		0.0
7	6.0	0	0.0	2.5	6.0	0	0.0		0.0
8	4.8	0	0.0	2.0	4.8	0	0.0		0.0
9	4.8	0	0.0	2.0	4.8	0	0.0		0.0
10	4.8	.5	1.2	2.0	4.8	.5	1.2		1.2
11	3.6	.5	1.2	2.0	4.8	.5	1.2		1.2
12	4.8	.2	0.5	2.0	4.8	.2	0.5		0.5
13	4.8	.2	0.5	2.0	4.8	.2	0.5		0.5
14	4.8	0	0.0	2.0	4.8	0	0.0		0.0
15	4.8	0	0.0	2.5	6.0	0	0.0		0.0
16	7.2	.2	0.5	3.0	7.2	0	0.0		0.0
17	7.2	.2	0.5	3.0	7.2	0	0.0		0.0
18	7.2	0	0.0	3.0	7.2	.2	0.5		0.5
19	7.2	.2	0.5	3.0	7.2	.2	0.5		0.5
20	7.2	0	0.0	3.0	7.2	.2	0.5		0.5
21	6.0	0	0.0	2.0	4.8	.2	0.5		0.5
22	6.0	.2	0.5	3.0	7.2	.2	0.5		0.5
23	6.0	.2	0.5	3.0	7.2	.2	0.5		0.5
24	6.0	0	0.0	3.0	7.2	.2	0.5		0.5
25	4.8	0	0.0	2.5	6.0	0	0.0		0.0

1000°C 10Ω/sq cm 1.5 Hour Etch

	5μ do	5μ do'	5μ undo	5μ undo'	15μ do	15μ do'	15μ undo	15μ undo'	50μ do
1	4.0	9.6	1.0	2.4	6.0	14.4	1.5	3.6	7.0
2	5.5	13.2	1.0	2.4	6.0	14.4	1.0	2.4	6.0
3	6.0	14.4	1.5	3.6	7.0	16.8	1.5	3.6	7.0
4	6.0	14.4	1.5	3.6	7.0	16.8	1.5	3.6	7.5
5	7.0	16.8	1.5	3.6	7.0	16.8	1.2	2.9	8.0
6	9.5	22.8	1.5	3.6	10.0	24.0	1.5	3.6	10.0
7	9.0	21.6	1.5	3.6	9.0	21.6	1.5	3.6	10.0
8	9.0	21.6	1.5	3.6	9.0	21.6	1.5	3.6	9.0
9	8.0	19.2	1.5	3.6	9.0	21.6	1.5	3.6	9.0
10	8.0	19.2	1.0	2.4	8.0	19.2	1.2	2.9	9.0
11	6.0	14.4	1.0	2.4	6.5	15.6	1.0	2.4	7.0
12	8.0	19.2	1.0	2.4	7.5	18.0	1.0	2.4	8.0
13	8.0	19.2	1.0	2.4	8.0	19.2	1.0	2.4	9.0
14	9.0	21.6	1.0	2.4	8.0	19.2	1.0	2.4	9.0
15	9.0	21.6	1.0	2.4	9.0	21.6	1.5	3.6	10.0
16	10.0	24.0	1.0	2.4	9.5	22.8	1.0	2.4	9.5
17	9.0	21.6	2.0	4.8	9.0	21.6	1.0	2.4	10.0
18	10.0	24.0	1.0	2.4	10.0	24.0	1.0	2.4	11.0
19	10.0	24.0	1.5	3.6	10.0	24.0	1.5	3.6	11.0
20	11.0	26.4	2.0	4.8	11.0	26.4	1.5	3.6	11.0
21	9.0	21.6	1.5	3.6	10.0	24.0	1.0	2.4	10.0
22	10.0	24.0	1.5	3.6	10.0	24.0	2.0	4.8	10.0
23	10.0	24.0	1.0	2.4	10.0	24.0	1.0	2.4	10.0
24	10.0	24.0	2.0	4.8	10.0	24.0	1.5	3.6	10.0
25	10.0	24.0	1.5	3.6	10.0	24.0	1.0	2.4	10.0

1000°C 10Ω/sq cm 1.5 Hour Etch						
	50μ do'	50μ undo	50μ undo'	150μ do	150μ do'	150μ undo'
1	16.8	1.0	2.4	7.0	16.8	2.4
2	14.4	1.0	2.4	8.0	19.2	4.8
3	16.8	1.5	3.6	8.0	19.2	3.6
4	18.0	1.5	3.6	8.0	19.2	4.8
5	19.2	1.5	3.6	8.0	19.2	3.6
6	24.0	1.5	3.6	10.0	24.0	3.6
7	24.0	1.5	3.6	10.0	24.0	3.6
8	21.6	1.0	2.4	10.0	24.0	3.6
9	21.6	2.0	4.8	10.0	24.0	3.6
10	21.6	1.2	2.9	9.0	21.6	4.8
11	16.8	1.2	2.9	7.5	18.0	3.6
12	19.2	1.0	2.4	9.0	21.6	2.4
13	21.6	1.0	2.4	9.0	21.6	2.4
14	21.6	1.5	3.6	9.0	21.6	3.6
15	24.0	1.5	3.6	10.0	24.0	4.8
16	22.8	1.0	2.4	11.0	26.4	3.6
17	24.0	1.0	2.4	11.0	26.4	2.4
18	26.4	1.0	2.4	11.0	26.4	3.6
19	26.4	1.5	3.6	11.0	26.4	2.9
20	26.4	2.0	4.8	11.0	26.4	4.8
21	24.0	1.5	3.6	10.0	24.0	2.4
22	24.0	2.0	4.8	10.0	24.0	4.8
23	24.0	1.5	3.6	10.0	24.0	2.4
24	24.0	1.5	3.6	10.0	24.0	3.6
25	24.0	1.0	2.4	11.0	26.4	3.6

1000°C 10Ω/sq cm 2.5 Hour Etch

	5μ do	5μ do'	5μ undo	5μ undo'	15μ do	15μ do'	15μ undo	15μ undo'	50μ do
1	14.0	33.6	3.0	7.2	15.0	36.0	2.5	6.0	15.0
2	14.0	33.6	2.5	6.0	15.5	37.2	3.0	7.2	16.0
3	16.0	38.4	2.0	4.8	16.0	38.4	2.5	6.0	16.0
4	15.0	36.0	2.5	6.0	15.0	36.0	2.0	4.8	15.0
5	15.0	36.0	2.0	4.8	15.0	36.0	2.0	4.8	15.0
6	16.0	38.4	2.0	4.8	16.0	38.4	2.0	4.8	16.0
7	14.0	33.6	2.0	4.8	14.0	33.6	2.5	6.0	14.0
8	11.5	27.6	2.0	4.8	12.0	28.8	2.0	4.8	12.0
9	11.0	26.4	2.0	4.8	11.0	26.4	2.0	4.8	14.0
10	10.0	24.0	2.0	4.8	11.0	26.4	2.0	4.8	11.0
11	13.5	32.4	2.0	4.8	14.0	33.6	2.0	4.8	14.0
12	13.0	31.2	2.0	4.8	16.0	38.4	2.0	4.8	14.0
13	13.0	31.2	3.0	7.2	14.0	33.6	2.0	4.8	14.0
14	17.0	40.8	2.0	4.8	16.0	38.4	2.0	4.8	17.0
15	17.0	40.8	2.5	6.0	17.0	40.8	2.5	6.0	18.0
16	18.0	43.2	2.0	4.8	19.0	45.6	2.5	6.0	17.0
17	18.0	43.2	2.5	6.0	19.0	45.6	3.0	7.2	19.0
18	18.0	43.2	2.5	6.0	18.5	44.4	2.0	4.8	19.0
19	18.0	43.2	2.5	6.0	18.5	44.4	2.5	6.0	18.5
20	18.5	44.4	2.5	6.0	19.0	45.6	2.5	6.0	19.0
21	18.0	43.2	2.5	6.0	18.5	44.4	2.5	6.0	19.0
22	18.0	43.2	2.5	6.0	18.0	43.2	2.5	6.0	19.0
23	18.0	43.2	2.0	4.8	18.0	43.2	2.5	6.0	19.0
24	19.0	45.6	2.5	6.0	19.0	45.6	3.0	7.2	19.0
25	18.5	44.4	2.5	6.0	19.0	45.6	3.0	7.2	18.5

1000°C 10Ω/sq cm 2.5 Hour Etch

	50μ do'	50μ undo	50μ undo'	150μ do	150μ do'	150μ undo	150μ undo'
1	36.0	3.0	7.2	16.0	38.4	4.0	9.6
2	38.4	3.0	7.2	16.0	38.4	4.0	9.6
3	38.4	3.0	7.2	18.0	43.2	4.0	9.6
4	36.0	2.0	4.8	16.0	38.4	3.0	7.2
5	36.0	2.5	6.0	16.0	38.4	3.5	8.4
6	38.4	2.5	6.0	16.0	38.4	3.5	8.4
7	33.6	2.5	6.0	14.0	33.6	3.5	8.4
8	28.8	2.0	4.8	13.0	31.2	3.0	7.2
9	33.6	3.0	7.2	12.0	28.8	3.0	7.2
10	26.4	2.5	6.0	11.0	26.4	3.0	7.2
11	33.6	2.0	4.8	15.0	36.0	2.5	6.0
12	33.6	2.5	6.0	17.0	40.8	4.0	9.6
13	33.6	2.0	4.8	14.0	33.6	4.0	9.6
14	40.8	2.0	4.8	17.0	40.8	3.0	7.2
15	43.2	2.5	6.0	18.0	43.2	2.5	6.0
16	40.8	3.0	7.2	19.0	45.6	2.5	6.0
17	45.6	3.0	7.2	19.0	45.6	2.5	6.0
18	45.6	2.5	6.0	19.0	45.6	2.5	6.0
19	44.4	2.5	6.0	19.0	45.6	3.0	7.2
20	45.6	2.5	6.0	19.5	46.8	3.0	7.2
21	45.6	3.0	7.2	19.0	45.6	2.5	6.0
22	45.6	2.5	6.0	19.0	45.6	2.5	6.0
23	45.6	2.5	6.0	19.5	46.8	2.5	6.0
24	45.6	3.0	7.2	19.0	45.6	3.0	7.2
25	44.4	3.0	7.2	19.0	45.6	3.0	7.2

1000°C 10Ω/sq cm 3.5 Hour Etch

	5μ do	5μ do'	5μ undo	5μ undo'	15μ do	15μ do'	15μ undo	15μ undo'	50μ do
1	20.0	48.0			21.0	50.4			21.5
2	20.0	48.0			21.5	51.6			22.0
3	22.0	52.8			22.0	52.8			25.0
4	21.5	51.6			21.5	51.6			23.0
5	22.0	52.8			22.0	52.8			22.5
6	27.0	64.8			26.0	62.4			26.0
7	25.5	61.2			25.0	60.0			25.0
8	25.0	60.0			24.0	57.6			24.0
9	23.0	55.2			23.0	55.2			22.0
10	21.0	50.4			20.0	48.0			20.0
11	21.0	50.4			21.0	50.4			22.0
12	23.0	55.2			23.0	55.2			23.0
13	24.0	57.6			24.0	57.6			24.0
14	24.0	57.6	3.5	8.4	25.0	60.0	4.0	9.6	26.0
15	26.0	62.4	4.0	9.6	26.0	62.4	4.0	9.6	26.0
16	26.0	62.4	4.0	9.6	26.5	63.6	4.0	9.6	26.5
17	26.0	62.4	5.5	13.2	26.5	63.6	5.0	12.0	26.5
18	26.5	63.6	4.0	9.6	27.0	64.8	4.0	9.6	27.0
19	26.0	62.4	4.0	9.6	26.0	62.4	4.0	9.6	26.5
20	26.0	62.4	4.0	9.6	27.0	64.8	4.0	9.6	27.0
21	26.0	62.4	4.0	9.6	27.0	64.8	4.0	9.6	27.0
22	26.0	62.4	4.0	9.6	26.5	63.6	4.0	9.6	27.0
23	26.5	63.6	4.0	9.6	27.0	64.8	4.0	9.6	27.0
24	27.0	64.8	4.0	9.6	27.0	64.8	4.0	9.6	27.5
25	27.0	64.8	4.0	9.6	27.5	66.0	4.0	9.6	27.0
26									



1000°C 10Ω/sq cm 3.5 Hour Etch

	50μ do'	50μ undo	50μ undo'	150μ do	150μ do'	150μ undo	150μ undo'
1	51.6			22.0	52.8		
2	52.8			23.0	55.2		
3	60.0			26.0	62.4		
4	55.2			23.0	55.2		
5	54.0			23.0	55.2		
6	62.4			27.0	64.8		
7	60.0			26.0	62.4		
8	57.6			24.0	57.6		
9	52.8			23.0	55.2		
10	48.0			20.0	48.0		
11	52.8			23.0	55.2		
12	55.2			24.0	57.6		
13	57.6			25.0	60.0		
14	62.4	4.0	9.6	27.0	64.8	4.0	9.6
15	62.4	3.5	8.4	26.0	62.4	5.0	12.0
16	63.6	5.0	12.0	27.0	64.8	4.0	9.6
17	63.6	4.0	9.6	27.0	64.8	4.0	9.6
18	64.8	4.0	9.6	27.5	66.0	4.0	9.6
19	63.6	4.0	9.6	27.0	64.8	4.0	9.6
20	64.8	4.0	9.6	28.0	67.2	4.0	9.6
21	64.8	4.0	9.6	27.0	64.8	5.0	12.0
22	64.8	4.0	9.6	27.5	66.0	4.0	9.6
23	64.8	4.0	9.6	27.0	64.8	4.0	9.6
24	66.0	4.0	9.6	27.0	64.8	4.0	9.6
25	64.8	5.0	12.0	28.0	67.2	4.0	9.6
26							

1000°C 20Ω/sq cm 0.5 Hour Etch

	5μ do	5μ do'	5μ undo	5μ undo'	15μ do	15μ do'	15μ undo	15μ undo'	50μ do
1	2.0	4.80	.5	1.20	2.0	4.80	.5	1.20	2.0
2	2.0	4.80	.7	1.68	2.0	4.80	1.0	2.40	2.0
3	2.0	4.80	1.0	2.40	2.0	4.80	1.0	2.40	2.0
4	2.0	4.80	1.0	2.40	2.0	4.80	1.0	2.40	2.0
5	2.0	4.80	1.0	2.40	2.0	4.80	1.0	2.40	2.0
6	1.5	3.60	1.0	2.40	1.5	3.60	1.0	2.40	2.0
7	2.0	4.80	1.0	2.40	2.0	4.80	.7	1.68	2.0
8	1.5	3.60	1.0	2.40	2.0	4.80	1.5	3.60	1.0
9	2.0	4.80	1.0	2.40	4.0	9.60	1.0	2.40	3.0
10	2.0	4.80	1.0	2.40	2.0	4.80	1.0	2.40	2.0
11	2.0	4.80	1.5	3.60	2.0	4.80	1.2	2.88	2.0
12	2.0	4.80	1.2	2.88	2.0	4.80	1.2	2.88	2.0
13	2.0	4.80	1.0	2.40	2.0	4.80	1.0	2.40	1.5
14	2.0	4.80	1.5	3.60	2.0	4.80	1.5	3.60	2.0
15	2.0	4.80	1.5	3.60	2.0	4.80	1.0	2.40	2.0
16	2.0	4.80	1.2	2.88	2.0	4.80	1.5	3.60	2.0
17	2.0	4.80	1.0	2.40	2.0	4.80	1.2	2.88	2.0
18	2.0	4.80	1.2	2.88	2.0	4.80	1.5	3.60	2.0
19	2.0	4.80	1.2	2.88	2.0	4.80	1.2	2.88	2.0
20	2.0	4.80	1.2	2.88	2.0	4.80	1.0	2.40	2.0
21	1.5	3.60	.2	0.48	1.5	3.60	0	0.00	1.5
22	1.0	2.40	0	0.00	1.0	2.40	0	0.00	1.5
23	1.0	2.40	0	0.00	2.0	4.80	.2	0.48	1.5
24	2.0	4.80	.2	0.48	2.0	4.80	.5	1.20	2.0
25	2.0	4.80	.2	0.48	2.0	4.80	1.0	2.40	2.0

1000°C 20Ω/sq cm 0.5 Hour Etch

	50μ do'	50μ undo	50μ undo'	150μ do	150μ do'	150μ undo	150μ undo'
1	4.80	.5	1.20	2.0	4.80	.5	1.20
2	4.80	.7	1.68	2.0	4.80	.7	1.68
3	4.80	1.0	2.40	2.0	4.80	1.0	2.40
4	4.80	1.0	2.40	2.0	4.80	1.0	2.40
5	4.80	1.0	2.40	2.0	4.80	1.0	2.40
6	4.80	1.0	2.40	2.0	4.80	1.0	2.40
7	4.80	.7	1.68	1.5	3.60	1.0	2.40
8	2.40	.2	0.48	2.0	4.80	1.0	2.40
9	7.20	1.0	2.40	2.0	4.80	.5	1.20
10	4.80	1.0	2.40	2.0	4.80	1.0	2.40
11	4.80	1.5	3.60	2.0	4.80	1.5	3.60
12	4.80	1.0	2.40	2.0	4.80	1.2	2.88
13	3.60	1.2	2.88	1.5	3.60	1.2	2.88
14	4.80	1.5	3.60	2.0	4.80	1.5	3.60
15	4.80	1.0	2.40	2.0	4.80	1.0	2.40
16	4.80	1.5	3.60	2.0	4.80	1.5	3.60
17	4.80	1.0	2.40	1.5	3.60	1.0	2.40
18	4.80	1.2	2.88	2.0	4.80	1.2	2.88
19	4.80	1.0	2.40	2.0	4.80	1.2	2.88
20	4.80	1.0	2.40	1.5	3.60	1.0	2.40
21	3.60	.5	1.20	2.0	4.80	1.5	3.60
22	3.60	0	0.00	1.5	3.60	0	0.00
23	3.60	.2	0.48	1.5	3.60	.2	0.48
24	4.80	0	0.00	2.0	4.80	0	0.00
25	4.80	.7	1.68	2.0	4.80	.5	1.20

1000°C 20Ω/sq cm 1.5 Hour Etch

	5μ do	5μ do'	5μ undo	5μ undo'	15μ do	15μ do'	15μ undo	15μ undo'	50μ do
1	7.0	16.80	4.0	9.60	7.0	16.80	4.0	9.60	7.0
2	7.0	16.80	4.0	9.60	7.0	16.80	4.0	9.60	7.0
3	7.0	16.80	4.5	10.80	7.0	16.80	5.0	12.00	7.0
4	7.0	16.80	5.0	12.00	7.0	16.80	5.0	12.00	7.0
5	7.0	16.80	5.0	12.00	7.0	16.80	5.0	12.00	7.0
6	7.0	16.80	5.5	13.20	7.0	16.80	5.0	12.00	7.5
7	7.5	18.00	6.0	14.40	7.0	16.80	6.0	14.40	8.0
8	7.0	16.80	5.0	12.00	7.0	16.80	5.0	12.00	7.0
9	7.0	16.80	6.0	14.40	7.0	16.80	5.5	13.20	6.0
10	7.0	16.80	5.0	12.00	7.0	16.80	5.0	12.00	7.0
11	7.0	16.80	5.0	12.00	7.0	16.80	6.0	14.40	7.0
12	7.0	16.80	6.0	14.40	7.0	16.80	6.0	14.40	7.0
13	7.0	16.80	6.0	14.40	7.0	16.80	6.0	14.40	8.0
14	7.0	16.80	6.0	14.40	7.0	16.80	6.0	14.40	7.0
15	8.0	19.20	6.0	14.40	7.0	16.80	6.0	14.40	7.5
16	7.0	16.80	5.0	12.00	7.0	16.80	4.0	9.60	7.0
17	7.0	16.80	4.5	10.80	7.0	16.80	5.0	12.00	7.0
18	7.0	16.80	5.0	12.00	7.0	16.80	5.0	12.00	7.0
19	8.0	19.20	5.0	12.00	7.5	18.00	5.0	12.00	7.0
20	7.5	18.00	5.0	12.00	7.0	16.80	5.0	12.00	8.0
21	8.0	19.20	7.0	16.80	8.0	19.20	7.0	16.80	8.0
22	7.5	18.00	5.5	13.20	7.5	18.00	6.5	15.60	8.0
23	7.0	16.80	5.0	12.00	8.0	19.20	6.0	14.40	8.0
24	7.0	16.80	5.0	12.00	7.0	16.80	5.0	12.00	8.0
25	8.0	19.20	6.0	14.40	8.0	19.20	6.0	14.40	8.5

1000°C 20Ω/sq cm 1.5 Hour Etch

	50μ do'	50μ undo	50μ undo'	150μ do	150μ do'	150μ undo	150μ undo'
1	16.80	4.0	9.60	7.0	16.80	4.0	9.60
2	16.80	4.0	9.60	7.0	16.80	4.5	10.80
3	16.80	4.5	10.80	7.0	16.80	4.5	10.80
4	16.80	5.0	12.00	7.0	16.80	5.0	12.00
5	16.80	5.0	12.00	7.0	16.80	5.0	12.00
6	18.00	5.5	13.20	7.0	16.80	6.0	14.40
7	19.20	6.0	14.40	8.0	19.20	6.0	14.40
8	16.80	5.0	12.00	6.5	15.60	5.0	12.00
9	14.40	4.0	9.60	7.0	16.80	5.0	12.00
10	16.80	5.0	12.00	7.0	16.80	6.0	14.40
11	16.80	5.0	12.00	6.5	15.60	5.0	12.00
12	16.80	6.0	14.40	7.0	16.80	6.0	14.40
13	19.20	6.0	14.40	7.0	16.80	6.0	14.40
14	16.80	6.0	14.40	7.0	16.80	6.0	14.40
15	18.00	7.0	16.80	7.0	16.80	6.5	15.60
16	16.80	4.5	10.80	9.5	22.80	4.0	9.60
17	16.80	4.5	10.80	7.0	16.80	5.0	12.00
18	16.80	5.0	12.00	7.0	16.80	5.0	12.00
19	16.80	5.0	12.00	7.5	18.00	5.0	12.00
20	19.20	5.0	12.00	7.5	18.00	5.0	12.00
21	19.20	7.0	16.80	8.0	19.20	7.0	16.80
22	19.20	6.0	14.40	8.0	19.20	6.0	14.40
23	19.20	5.0	12.00	7.0	16.80	5.0	12.00
24	19.20	6.0	14.40	7.0	16.80	4.0	9.60
25	20.40	6.5	15.60	8.0	19.20	7.0	16.80

1000°C 20Ω/sq cm 2.5 Hour Etch

	5μ do	5μ do'	5μ undo	5μ undo'	15μ do	15μ do'	15μ undo	15μ undo'	50μ do
1	14.0	33.60	7.0	16.80	14.0	33.60	7.5	18.00	14.5
2	14.0	33.60	9.0	21.60	14.0	33.60	9.0	21.60	14.0
3	14.0	33.60	8.0	19.20	14.0	33.60	8.0	19.20	14.0
4	14.0	33.60	9.5	22.80	14.0	33.60	11.0	26.40	14.0
5	15.0	36.00	10.0	24.00	14.0	33.60	10.0	24.00	14.0
6	15.0	36.00	15.0	36.00	16.0	38.40	15.0	36.00	16.0
7	15.0	36.00	14.0	33.60	15.0	36.00	13.0	31.20	15.0
8	15.0	36.00	14.0	33.60	15.0	36.00	14.0	33.60	16.0
9	15.0	36.00	14.0	33.60	15.0	36.00	13.0	31.20	15.0
10	15.0	36.00	15.0	36.00	16.0	38.40	15.0	36.00	16.0
11	15.0	36.00	12.0	28.80	14.5	34.80	12.0	28.80	15.0
12	15.0	36.00	13.0	31.20	15.0	36.00	12.0	28.80	15.0
13	15.0	36.00	13.0	31.20	15.0	36.00	13.5	32.40	15.0
14	15.0	36.00	13.0	31.20	15.0	36.00	13.0	31.20	15.0
15	15.0	36.00	14.0	33.60	15.0	36.00	13.0	31.20	15.0
16	14.0	33.60	9.0	21.60	14.0	33.60	9.0	21.60	14.0
17	14.0	33.60	14.0	33.60	14.0	33.60	14.0	33.60	15.0
18	15.0	36.00	12.0	28.80	15.0	36.00	11.0	26.40	15.0
19	15.0	36.00	12.0	28.80	15.0	36.00	11.0	26.40	15.0
20	14.0	33.60	12.0	28.80	15.0	36.00	11.0	26.40	15.0
21	16.0	38.40	16.0	38.40	16.0	38.40	15.0	36.00	17.0
22	15.0	36.00	14.0	33.60	15.0	36.00	14.0	33.60	15.0
23	15.0	36.00	15.0	36.00	15.0	36.00	13.0	31.20	15.0
24	15.0	36.00	13.0	31.20	15.0	36.00	14.0	33.60	15.0
25	16.0	38.40	16.0	38.40	16.0	38.40	15.0	36.00	17.0

1000°C 20Ω/sq cm 2.5 Hour Etch

	50μ do'	50μ und0	50μ und0'	150μ do	150μ do'	150μ und0	150μ und0'
1	34.80	8.0	19.20	14.0	33.60	8.0	19.20
2	33.60	8.0	19.20	14.0	33.60	8.0	19.20
3	33.60	9.0	21.60	14.0	33.60	9.0	21.60
4	33.60	10.0	24.00	15.0	36.00	10.0	24.00
5	33.60	10.0	24.00	14.0	33.60	10.0	24.00
6	38.40	14.0	33.60	15.0	36.00	13.0	31.20
7	36.00	13.0	31.20	15.0	36.00	13.0	31.20
8	38.40	14.0	33.60	16.0	38.40	13.0	31.20
9	36.00	14.0	33.60	15.0	36.00	14.0	33.60
10	38.40	15.0	36.00	16.0	38.40	14.0	33.60
11	36.00	13.0	31.20	15.0	36.00	12.0	28.80
12	36.00	13.0	31.20	15.5	37.20	13.5	32.40
13	36.00	13.0	31.20	15.0	36.00	12.0	28.80
14	36.00	15.0	36.00	15.0	36.00	13.0	31.20
15	36.00	13.0	31.20	15.0	36.00	13.0	31.20
16	33.60	11.0	26.40	14.0	33.60	10.0	24.00
17	36.00	14.0	33.60	15.0	36.00	11.5	27.60
18	36.00	11.5	27.60	15.0	36.00	11.5	27.60
19	36.00	11.5	27.60	15.0	36.00	12.0	28.80
20	36.00	12.0	28.80	15.0	36.00	12.0	28.80
21	40.80	15.0	36.00	17.0	40.80	15.0	36.00
22	36.00	13.0	31.20	16.0	38.40	12.0	28.80
23	36.00	13.0	31.20	16.0	38.40	12.0	28.80
24	36.00	13.0	31.20	15.0	36.00	12.0	28.80
25	40.80	13.0	31.20	18.0	43.20	12.0	28.80

1000°C 20Ω/sq cm 3.5 Hour Etch

	5μ do	5μ do'	5μ undo	5μ undo'	15μ do	15μ do'	15μ undo	15μ undo'	50μ do
1	19.0	45.60	9.0	21.60	19.0	45.60	9.0	21.60	19.0
2	19.0	45.60	10.0	24.00	19.0	45.60	11.0	26.40	21.0
3	19.0	45.60	12.0	28.80	19.0	45.60	11.5	27.60	19.0
4	19.0	45.60	11.0	26.40	19.0	45.60	10.0	24.00	20.0
5	19.0	45.60	13.0	31.20	20.0	48.00	15.0	36.00	19.0
6	21.0	50.40	21.0	50.40	22.0	52.80	20.0	48.00	22.0
7	21.0	50.40	20.0	48.00	21.0	50.40	20.0	48.00	21.0
8	21.0	50.40	20.0	48.00	22.0	52.80	20.0	48.00	22.0
9	21.0	50.40	20.0	48.00	20.0	48.00	20.0	48.00	21.0
10	20.0	48.00	21.0	50.40	21.0	50.40	20.0	48.00	21.0
11	20.0	48.00	19.0	45.60	22.0	52.80	19.0	45.60	23.0
12	20.0	48.00	20.0	48.00	20.0	48.00	20.0	48.00	21.0
13	21.0	50.40	20.0	48.00	21.0	50.40	20.0	48.00	21.0
14	20.5	49.20	20.0	48.00	22.0	52.80	20.0	48.00	22.0
15	21.0	50.40	20.0	48.00	21.5	51.60	20.0	48.00	22.0
16	21.0	50.40	19.0	45.60	21.0	50.40	19.0	45.60	22.0
17	20.0	48.00	20.0	48.00	21.0	50.40	21.0	50.40	21.0
18	20.0	48.00	19.0	45.60	21.0	50.40	19.0	45.60	22.0
19	21.0	50.40	17.0	40.80	22.0	52.80	16.0	38.40	22.0
20	21.0	50.40	15.0	36.00	21.0	50.40	15.0	36.00	21.0
21	21.0	50.40	21.0	50.40	22.0	52.80	21.0	50.40	22.0
22	22.0	52.80	20.0	48.00	22.0	52.80	20.0	48.00	22.0
23	18.0	43.20	19.0	45.60	19.0	45.60	19.0	45.60	20.0
24	19.5	46.80	20.0	48.00	19.0	45.60	20.0	48.00	20.0
25	21.0	50.40	19.0	45.60	22.0	52.80	19.0	45.60	22.0



1000°C 20Ω/sq cm 3.5 Hour Etch

	50μ do'	50μ undo	50μ undo'	150μ do	150μ do'	150μ undo	150μ undo'
1	45.60	10.0	24.00	19.0	45.60	10.0	24.00
2	50.40	10.5	25.20	20.0	48.00	10.0	24.00
3	45.60	11.0	26.40	20.0	48.00	10.0	24.00
4	48.00	12.0	28.80	19.5	46.80	11.5	27.60
5	45.60	15.0	36.00	20.0	48.00	15.5	37.20
6	52.80	20.0	48.00	23.0	55.20	19.0	45.60
7	50.40	19.0	45.60	21.0	50.40	19.0	45.60
8	52.80	20.0	48.00	22.0	52.80	19.0	45.60
9	50.40	19.0	45.60	21.0	50.40	18.0	43.20
10	50.40	20.0	48.00	22.0	52.80	19.0	45.60
11	55.20	18.0	43.20	23.0	55.20	17.0	40.80
12	50.40	19.0	45.60	22.0	52.80	19.0	45.60
13	50.40	20.0	48.00	21.5	51.60	19.5	46.80
14	52.80	20.0	48.00	22.0	52.80	18.0	43.20
15	52.80	20.0	48.00	22.0	52.80	19.0	45.60
16	52.80	19.0	45.60	22.0	52.80	19.0	45.60
17	50.40	21.0	50.40	21.0	50.40	20.0	48.00
18	52.80	20.0	48.00	22.0	52.80	19.0	45.60
19	52.80	17.0	40.80	22.0	52.80	16.0	38.40
20	50.40	14.0	33.60	21.0	50.40	14.5	34.80
21	52.80	20.0	48.00	22.0	52.80	19.0	45.60
22	52.80	19.0	45.60	22.5	54.00	18.0	43.20
23	48.00	18.0	43.20	21.0	50.40	17.0	40.80
24	48.00	20.0	48.00	21.0	50.40	20.0	48.00
25	52.80	20.0	48.00	22.0	52.80	19.0	45.60
26							

Heavy Oxide 2 Hour Etch

	5μ do	5μ do'	15μ do	15μ do'	50μ do	50μ do'	150μ do	150μ do'
1	0	0.0	0	0.0	0	0.0	0	0.0
2	0	0.0	0	0.0	0	0.0	0	0.0
3	0	0.0	0	0.0	0	0.0	0	0.0
4	.5	1.2	.7	1.7	.5	1.2	.5	1.2
5	.5	1.2	.7	1.7	.7	1.7	.3	0.7
6	.5	1.2	.5	1.2	.5	1.2	.3	0.7
7	.7	1.7	.5	1.2	.3	0.7	.3	0.7
8	.7	1.7	.3	0.7	.5	1.2	.4	1.0
9	.3	0.7	.3	0.7	.3	0.7	.3	0.7
10	0	0.0	.3	0.7	.4	1.0	.2	0.5
11	.7	1.7	.5	1.2	.4	1.0	.5	1.2
12	.5	1.2	.3	0.7	.7	1.7	.5	1.2
13	.5	1.2	.7	1.7	.5	1.2	.3	0.7
14	.3	0.7	.3	0.7	.3	0.7	.3	0.7
15	.3	0.7	.3	0.7	.2	0.5	.2	0.5
16	.5	1.2	.5	1.2	.5	1.2	.3	0.7
17	.3	0.7	.3	0.7	.5	1.2	.3	0.7
18	.5	1.2	.7	1.7	.3	0.7	.3	0.7
19	.5	1.2	.3	0.7	.3	0.7	.3	0.7
20	.5	1.2	.5	1.2	.5	1.2	.5	1.2
21	0	0.0	0	0.0	0	0.0	0	0.0
22	.3	0.7	.3	0.7	.5	1.2	.7	1.7
23	.5	1.2	.5	1.2	.5	1.2	.5	1.2
24	.5	1.2	.5	1.2	.3	0.7	.3	0.7
25	.3	0.7	.5	1.2	.5	1.2	.3	0.7
26	.7	1.7	.5	1.2	.3	0.7	.2	0.5
27	.3	0.7	.5	1.2	.5	1.2	.3	0.7
28	.3	0.7	.5	1.2	.5	1.2	.5	1.2
29	.3	0.7	.5	1.2	.5	1.2	.5	1.2
30	.5	1.2	.5	1.2	.5	1.2	.5	1.2
31	.6	1.4	.5	1.2	.3	0.7	.3	0.7
32	.5	1.2	.3	0.7	.5	1.2	0	0.0
33	.5	1.2	.3	0.7	.3	0.7	.2	0.5
34	.3	0.7	.5	1.2	.5	1.2	.5	1.2
35	.7	1.7	.7	1.7	.5	1.2	.5	1.2
36	.3	0.7	.5	1.2	.5	1.2	.5	1.2
37	.5	1.2	.7	1.7	.7	1.7	.3	0.7
38	.7	1.7	.5	1.2	.3	0.7	.5	1.2
39	.3	0.7	.3	0.7	.3	0.7	.5	1.2
40	.3	0.7	.3	0.7	.3	0.7	.3	0.7
41	.7	1.7	0	0.0	0	0.0	1.0	2.4
42	0	0.0	0	0.0	0	0.0	0	0.0

Heavy Oxide 2 Hour Etch

	5μ do	5μ do'	15μ do	15μ do'	50μ do	50μ do'	150μ do	150μ do'
43	0	0.0	0	0.0	0	0.0	.2	0.5
44	.2	0.5	.2	0.5	.2	0.5	.2	0.5
45	.5	1.2	.7	1.7	1.0	2.4	.7	1.7
46	.2	0.5	.2	0.5	.2	0.5	.2	0.5
47	0	0.0	1.5	3.6	0	0.0	0	0.0
48	.2	0.5	.2	0.5	0	0.0	0	0.0
49	.8	1.9	.2	0.5	.2	0.5	.2	0.5
50	.5	1.2	.5	1.2	.5	1.2	.5	1.2

Heavy Oxide 3.5 Hour Etch

	5μ do	5μ do'	15μ do	15μ do'	50μ do	50μ do'	150μ do	150μ do'
1	1.0	2.4	1.2	2.9	.7	1.7	.2	0.5
2	.7	1.7	.7	1.7	1.0	2.4	1.0	2.4
3	.7	1.7	1.0	2.4	.7	1.7	.2	0.5
4	1.0	2.4	1.2	2.9	1.0	2.4	1.0	2.4
5	1.0	2.4	.7	1.7	1.0	2.4	1.0	2.4
6	1.0	2.4	1.2	2.9	1.0	2.4	1.0	2.4
7	1.0	2.4	1.0	2.4	1.0	2.4	1.0	2.4
8	.5	1.2	1.0	2.4	.5	1.2	0	0.0
9	.7	1.7	.7	1.7	1.0	2.4	1.0	2.4
10	1.0	2.4	.7	1.7	.7	1.7	0	0.0
11	1.0	2.4	1.2	2.9	1.2	2.9	1.2	2.9
12	.7	1.7	1.0	2.4	1.0	2.4	1.0	2.4
13	1.0	2.4	1.0	2.4	.5	1.2	.2	0.5
14	1.0	2.4	1.0	2.4	1.0	2.4	1.0	2.4
15	1.0	2.4	.7	1.7	.2	0.5	.7	1.7
16	.5	1.2	.2	0.5	.5	1.2	.5	1.2
17	1.0	2.4	.7	1.7	1.0	2.4	1.2	2.9
18	1.0	2.4	1.2	2.9	1.2	2.9	.7	1.7
19	1.0	2.4	1.0	2.4	1.0	2.4	1.2	2.9
20	1.0	2.4	1.0	2.4	.7	1.7	1.0	2.4
21	1.0	2.4	1.0	2.4	1.2	2.9	1.0	2.4
22	1.0	2.4	1.2	2.9	.7	1.7	1.2	2.9
23	1.0	2.4	1.2	2.9	1.0	2.4	1.2	2.9
24	1.2	2.9	1.0	2.4	1.2	2.9	1.5	3.6
25	1.0	2.4	1.5	3.6	1.2	2.9	1.0	2.4
26	1.2	2.9	1.2	2.9	1.0	2.4	1.2	2.9
27	2.0	4.8	2.0	4.8	1.5	3.6	1.0	2.4
28	1.0	2.4	1.0	2.4	1.2	2.9	1.2	2.9
29	.1	0.2	.5	1.2	.7	1.7	.7	1.7
30	1.0	2.4	.7	1.7	.7	1.7	.2	0.5
31	1.0	2.4	1.2	2.9	1.2	2.9	1.0	2.4
32	.7	1.7	1.0	2.4	1.0	2.4	1.2	2.9
33	1.0	2.4	1.0	2.4	1.0	2.4	1.2	2.9
34	3.0	7.2	3.0	7.2	1.5	3.6	1.0	2.4
35	1.0	2.4	1.0	2.4	1.2	2.9	1.0	2.4
36	.7	1.7	1.0	2.4	1.2	2.9	1.0	2.4
37	.7	1.7	1.0	2.4	2.0	4.8	2.0	4.8
38	.7	1.7	1.0	2.4	1.0	2.4	1.2	2.9
39	.7	1.7	1.0	2.4	1.0	2.4	1.0	2.4
40	1.2	2.9	1.2	2.9	1.0	2.4	1.2	2.9
41	1.2	2.9	.2	0.5	.2	0.5	1.2	2.9
42	0	0.0	1.2	2.9	1.2	2.9	1.0	2.4

Heavy Oxide 3.5 Hour EICH

	5μ do	5μ do'	15μ do	15μ do'	50μ do	50μ do'	150μ do	150μ do'
43	1.2	2.9	1.5	3.6	1.2	2.9	1.5	3.6
44	1.2	2.9	1.0	2.4	.5	1.2	1.0	2.4
45	1.0	2.4	0	0.0	1.0	2.4	1.0	2.4
46	1.0	2.4	1.0	2.4	1.0	2.4	2.0	4.8
47	2.0	4.8	1.0	2.4	0	0.0	2.0	4.8
48	0	0.0	1.0	2.4	0	0.0	1.0	2.4
49	0	0.0	0	0.0	.5	1.2	0	0.0
50	0	0.0	.5	1.2	1.2	2.9	.5	1.2
51								

Heavy Oxide 4.5 Hour Etch

	5μ do	5μ do'	5μ undo	5μ undo'	15μ do	15μ do'	15μ undo	15μ undo'	50μ do
1	1.0	2.4	1.0	2.4	.2	0.5	0	0.0	.7
2	1.5	3.6	1.0	2.4	1.0	2.4	.2	0.5	.5
3	1.5	3.6	1.0	2.4	1.5	3.6	1.0	2.4	1.5
4	1.0	2.4	1.0	2.4	1.5	3.6	0	0.0	1.2
5	2.0	4.8	1.0	2.4	1.7	4.1	0	0.0	1.5
6	1.0	2.4	1.0	2.4	1.0	2.4	0	0.0	1.0
7	1.0	2.4	1.0	2.4	1.0	2.4	0	0.0	.7
8	1.0	2.4	1.0	2.4	1.0	2.4	0	0.0	1.0
9	1.0	2.4	1.0	2.4	1.0	2.4	0	0.0	1.0
10	1.0	2.4	1.0	2.4	1.0	2.4	0	0.0	1.5
11	2.0	4.8	1.0	2.4	2.0	4.8	1.0	2.4	2.0
12	2.0	4.8	1.0	2.4	2.0	4.8	1.5	3.6	2.0
13	2.0	4.8	.5	1.2	2.0	4.8	1.0	2.4	2.0
14	1.5	3.6	0	0.0	2.0	4.8	.5	1.2	2.0
15	1.0	2.4	.5	1.2	1.0	2.4	1.0	2.4	2.0
16	1.0	2.4	1.0	2.4	1.0	2.4	.5	1.2	1.5
17	2.0	4.8	1.0	2.4	1.5	3.6	1.0	2.4	2.5
18	2.0	4.8	.5	1.2	2.0	4.8	.5	1.2	2.0
19	2.0	4.8	0	0.0	1.5	3.6	.7	1.7	2.0
20	2.0	4.8	.5	1.2	1.0	2.4	.7	1.7	1.5
21	2.5	6.0	1.0	2.4	2.0	4.8	1.0	2.4	2.0
22	2.0	4.8	1.0	2.4	2.0	4.8	1.0	2.4	1.5
23	2.0	4.8	1.0	2.4	2.5	6.0	1.0	2.4	2.5
24	2.0	4.8	1.0	2.4	2.0	4.8	.7	1.7	2.0
25	2.0	4.8	.7	1.7	2.0	4.8	.7	1.7	2.0
26	1.0	2.4	.5	1.2	0	0.0	0	0.0	1.0
27	2.0	4.8	1.5	3.6	.7	1.7	1.0	2.4	1.5
28	2.0	4.8	1.0	2.4	2.0	4.8	1.0	2.4	2.0
29	2.0	4.8	.5	1.2	2.0	4.8	1.0	2.4	2.0
30	1.2	2.9	.7	1.7	2.0	4.8	1.0	2.4	2.0
31	1.0	2.4	1.0	2.4	1.5	3.6	.7	1.7	1.5
32	1.5	3.6	.5	1.2	2.0	4.8	.5	1.2	2.0
33	1.0	2.4	.7	1.7	1.5	3.6	1.0	2.4	2.0
34	1.5	3.6	1.0	2.4	2.0	4.8	1.0	2.4	2.0
35	2.0	4.8	.5	1.2	2.0	4.8	.5	1.2	1.5
36	2.0	4.8	1.0	2.4	2.0	4.8	.7	1.7	1.5
37	2.0	4.8	.7	1.7	2.0	4.8	1.0	2.4	2.0
38	2.0	4.8	0	0.0	2.0	4.8	1.0	2.4	2.0
39	2.0	4.8	.5	1.2	2.0	4.8	.7	1.7	2.0
40	1.5	3.6	.7	1.7	1.5	3.6	.5	1.2	1.5
41	2.0	4.8	1.0	2.4	2.0	4.8	1.0	2.4	2.0
42	2.0	4.8	.7	1.7	1.5	3.6	1.0	2.4	1.5

Heavy Oxide 4.5 Hour Etch

	5μ do	5μ do'	5μ undo	5μ undo'	15μ do	15μ do'	15μ undo	15μ undo'	50μ do
43	.2	0.5	0	0.0	1.5	3.6	0	0.0	1.7
44	1.0	2.4	0	0.0	2.0	4.8	.5	1.2	1.0
45	1.5	3.6	1.0	2.4	1.5	3.6	.5	1.2	2.0
46	0	0.0	0	0.0	0	0.0	0	0.0	2.0
47	0	0.0	0	0.0	.2	0.5	0	0.0	1.5
48	1.5	3.6	0	0.0	1.5	3.6	.5	1.2	1.5
49	.5	1.2	0	0.0	2.0	4.8	1.5	3.6	2.0
50	.7	1.7	0	0.0	.7	1.7	0	0.0	1.5

Heavy Oxide 4.5 Hour Etch

	50μ do'	50μ undo	50μ undo'	150μ do	150μ do'	150μ undo	150μ undo'
1	1.7	.2	0.5	1.0	2.4	.2	0.5
2	1.2	0	0.0	.5	1.2	.2	0.5
3	3.6	0	0.0	1.5	3.6	0	0.0
4	2.9	0	0.0	1.0	2.4	0	0.0
5	3.6	0	0.0	1.0	2.4	1.0	2.4
6	2.4	0	0.0	1.0	2.4	0	0.0
7	1.7	0	0.0	1.0	2.4	0	0.0
8	2.4	0	0.0	1.0	2.4	0	0.0
9	2.4	0	0.0	1.0	2.4	0	0.0
10	3.6	1.5	3.6	1.0	2.4	0	0.0
11	4.8	1.0	2.4	2.0	4.8	1.0	2.4
12	4.8	1.0	2.4	2.0	4.8	1.0	2.4
13	4.8	.5	1.2	2.0	4.8	.7	1.7
14	4.8	0	0.0	2.0	4.8	1.0	2.4
15	4.8	1.0	2.4	2.0	4.8	1.0	2.4
16	3.6	1.0	2.4	2.0	4.8	1.2	2.9
17	6.0	1.0	2.4	1.2	2.9	1.0	2.4
18	4.8	1.0	2.4	2.0	4.8	.7	1.7
19	4.8	.5	1.2	2.0	4.8	1.0	2.4
20	3.6	1.0	2.4	2.0	4.8	.7	1.7
21	4.8	1.0	2.4	1.5	3.6	1.0	2.4
22	3.6	1.0	2.4	2.0	4.8	1.0	2.4
23	6.0	1.0	2.4	2.0	4.8	1.0	2.4
24	4.8	1.0	2.4	2.0	4.8	1.0	2.4
25	4.8	1.0	2.4	2.0	4.8	1.2	2.9
26	2.4	1.0	2.4	2.0	4.8	1.0	2.4
27	3.6	.7	1.7	1.5	3.6	1.0	2.4
28	4.8	1.0	2.4	2.0	4.8	1.0	2.4
29	4.8	1.0	2.4	2.0	4.8	.7	1.7
30	4.8	1.0	2.4	2.0	4.8	1.0	2.4
31	3.6	0	0.0	2.0	4.8	1.0	2.4
32	4.8	.5	1.2	2.0	4.8	1.0	2.4
33	4.8	1.0	2.4	2.0	4.8	1.0	2.4
34	4.8	0	0.0	2.0	4.8	1.0	2.4
35	3.6	1.0	2.4	1.5	3.6	.7	1.7
36	3.6	.7	1.7	2.0	4.8	0	0.0
37	4.8	.7	1.7	2.0	4.8	.5	1.2
38	4.8	.7	1.7	2.0	4.8	.5	1.2
39	4.8	1.0	2.4	2.0	4.8	.5	1.2
40	3.6	.5	1.2	1.5	3.6	1.0	2.4
41	4.8	1.0	2.4	2.0	4.8	1.0	2.4
42	3.6	0	0.0	2.0	4.8	1.0	2.4



Heavy Oxide 4.5 Hour Etch

	50μ do'	50μ undo	50μ undo'	150μ do	150μ do'	150μ undo	150μ undo'
43	4.1	.7	1.7	.7	1.7	0	0.0
44	2.4	0	0.0	2.0	4.8	0	0.0
45	4.8	.5	1.2	2.5	6.0	.7	1.7
46	4.8	1.5	3.6	2.0	4.8	.7	1.7
47	3.6	1.5	3.6	2.0	4.8	2.0	4.8
48	3.6	1.0	2.4	1.5	3.6	0	0.0
49	4.8	1.0	2.4	2.0	4.8	0	0.0
50	3.6	0	0.0	2.0	4.8	.7	1.7

Heavy Oxide 5.5 Hour Eich

	5μ do	5μ do'	5μ undo	5μ undo'	15μ do	15μ do'	15μ undo	15μ undo'	50μ do
1	2.0	4.8	1.0	2.4	1.0	2.4	0	0.0	.5
2	1.0	2.4	1.0	2.4	0	0.0	0	0.0	1.0
3	1.0	2.4	.5	1.2	2.0	4.8	1.0	2.4	1.0
4	1.5	3.6	1.0	2.4	1.0	2.4	0	0.0	1.5
5	1.5	3.6	1.0	2.4	2.0	4.8	.7	1.7	1.0
6	2.0	4.8	1.0	2.4	2.0	4.8	.7	1.7	1.5
7	2.0	4.8	1.0	2.4	2.0	4.8	1.0	2.4	2.0
8	1.2	2.9	0	0.0	1.5	3.6	1.0	2.4	1.1
9	2.0	4.8	1.0	2.4	2.0	4.8	1.0	2.4	2.0
10	2.0	4.8	2.5	6.0	.5	1.2	0	0.0	1.5
11	1.5	3.6	1.0	2.4	2.0	4.8	1.0	2.4	2.0
12	1.5	3.6	1.0	2.4	1.5	3.6	.7	1.7	2.0
13	2.5	6.0	.5	1.2	2.5	6.0	1.0	2.4	2.5
14	2.0	4.8	.7	1.7	2.0	4.8	.7	1.7	2.0
15	2.0	4.8	.7	1.7	2.0	4.8	1.0	2.4	2.5
16	2.0	4.8	1.0	2.4	2.0	4.8	1.0	2.4	2.0
17	2.0	4.8	.7	1.7	2.0	4.8	.5	1.2	2.0
18	2.0	4.8	0	0.0	2.0	4.8	.5	1.2	2.0
19	1.5	3.6	1.0	2.4	1.5	3.6	1.0	2.4	2.0
20	2.0	4.8	1.0	2.4	2.0	4.8	1.0	2.4	1.5
21	2.0	4.8	1.0	2.4	2.0	4.8	1.0	2.4	2.0
22	2.0	4.8	1.0	2.4	2.0	4.8	1.0	2.4	1.0
23	1.5	3.6	1.0	2.4	2.0	4.8	2.0	4.8	2.0
24	2.0	4.8	1.0	2.4	2.5	6.0	1.0	2.4	3.0
25	2.0	4.8	1.0	2.4	3.0	7.2	2.0	4.8	3.0
26	2.5	6.0	1.0	2.4	3.0	7.2	1.5	3.6	2.5
27	2.5	6.0	1.0	2.4	2.0	4.8	1.0	2.4	2.0
28	3.0	7.2	1.0	2.4	2.5	6.0	1.0	2.4	2.5
29	2.0	4.8	1.0	2.4	1.5	3.6	1.0	2.4	2.0
30	0	0.0	0	0.0	1.5	3.6	1.0	2.4	1.5
31	2.0	4.8	1.0	2.4	2.0	4.8	1.0	2.4	2.0
32	2.0	4.8	1.0	2.4	2.0	4.8	1.0	2.4	2.0
33	2.0	4.8	.7	1.7	2.5	6.0	.7	1.7	2.5
34	2.0	4.8	.7	1.7	2.0	4.8	1.0	2.4	2.0
35	2.0	4.8	.7	1.7	2.0	4.8	1.0	2.4	2.0
36	2.0	4.8	1.0	2.4	2.5	6.0	1.0	2.4	2.5
37	2.5	6.0	1.0	2.4	2.5	6.0	1.5	3.6	2.0
38	2.0	4.8	.7	1.7	2.0	4.8	2.0	4.8	2.5
39	2.0	4.8	1.5	3.6	2.0	4.8	1.5	3.6	2.5
40	2.5	6.0	1.0	2.4	3.0	7.2	1.0	2.4	3.0
41	1.0	2.4	0	0.0	.7	1.7	0	0.0	1.5
42	0	0.0	0	0.0	2.0	4.8	1.0	2.4	2.5

Heavy Oxide 5.5 Hour Etch

	5μ do	5μ do'	5μ undo	5μ undo'	15μ do	15μ do'	15μ undo	15μ undo'	50μ do
43	2.0	4.8	.5	1.2	2.0	4.8	1.0	2.4	2.5
44	0	0.0	0	0.0	0	0.0	0	0.0	2.0
45	0	0.0	0	0.0	0	0.0	0	0.0	2.0
46	2.5	6.0	1.0	2.4	2.0	4.8	1.5	3.6	2.5
47	.5	1.2	.5	1.2	2.0	4.8	1.0	2.4	2.5
48	2.0	4.8	1.0	2.4	0	0.0	0	0.0	2.0
49	2.0	4.8	1.5	3.6	2.0	4.8	1.0	2.4	3.0
50	0	0.0	0	0.0	2.0	4.8	1.5	3.6	2.0

Heavy Oxide 5.5 Hour Etch

	50μ do'	50μ undo	50μ undo'	150μ do	150μ do'	150μ undo	150μ undo'
1	1.2	0	0.0	.5	1.2	0	0.0
2	2.4	0	0.0	.5	1.2	0	0.0
3	2.4	.5	1.2	1.0	2.4	.7	1.7
4	3.6	1.0	2.4	1.0	2.4	.5	1.2
5	2.4	1.0	2.4	1.0	2.4	1.0	2.4
6	3.6	1.0	2.4	2.0	4.8	2.0	4.8
7	4.8	1.0	2.4	1.0	2.4	.7	1.7
8	2.6	1.0	2.4	1.2	2.9	1.0	2.4
9	4.8	.7	1.7	1.0	2.4	1.0	2.4
10	3.6	1.5	3.6	0	0.0	0	0.0
11	4.8	1.0	2.4	2.0	4.8	1.0	2.4
12	4.8	1.0	2.4	2.0	4.8	1.0	2.4
13	6.0	1.0	2.4	2.5	6.0	1.0	2.4
14	4.8	1.0	2.4	2.5	6.0	1.0	2.4
15	6.0	1.0	2.4	2.0	4.8	.7	1.7
16	4.8	1.0	2.4	2.5	6.0	.7	1.7
17	4.8	1.0	2.4	2.0	4.8	.5	1.2
18	4.8	.5	1.2	2.0	4.8	1.0	2.4
19	4.8	1.0	2.4	2.0	4.8	1.0	2.4
20	3.6	1.0	2.4	2.0	4.8	1.0	2.4
21	4.8	1.0	2.4	2.0	4.8	1.0	2.4
22	2.4	1.0	2.4	2.0	4.8	1.0	2.4
23	4.8	2.0	4.8	2.0	4.8	1.0	2.4
24	7.2	1.0	2.4	2.5	6.0	1.0	2.4
25	7.2	1.0	2.4	2.5	6.0	1.0	2.4
26	6.0	1.0	2.4	3.0	7.2	1.0	2.4
27	4.8	1.0	2.4	2.5	6.0	1.0	2.4
28	6.0	1.0	2.4	2.0	4.8	1.0	2.4
29	4.8	1.0	2.4	2.0	4.8	1.0	2.4
30	3.6	1.0	2.4	1.5	3.6	.7	1.7
31	4.8	1.0	2.4	3.0	7.2	1.0	2.4
32	4.8	1.0	2.4	2.5	6.0	1.0	2.4
33	6.0	1.0	2.4	3.0	7.2	1.0	2.4
34	4.8	1.0	2.4	2.5	6.0	1.0	2.4
35	6.0	1.5	3.6	2.0	4.8	1.0	2.4
36	6.0	1.0	2.4	2.0	4.8	2.0	4.8
37	4.8	1.5	3.6	3.0	7.2	1.5	3.6
38	6.0	.7	1.7	2.5	6.0	1.5	3.6
39	6.0	1.5	3.6	2.0	4.8	1.0	2.4
40	7.2	1.0	2.4	3.0	7.2	1.0	2.4
41	3.6	0	0.0	2.5	6.0	1.5	3.6
42	6.0	1.5	3.6	2.5	6.0	0	0.0

	Heavy Oxide 5.5 Hour Etch					
	50μ do'	50μ undo	50μ undo'	150μ do	150μ do'	150μ undo
43	6.0	1.5	3.6	2.0	4.8	0
44	4.8	1.5	3.6	2.5	6.0	2.5
45	4.8	2.0	4.8	2.5	6.0	1.0
46	6.0	1.0	2.4	2.5	6.0	1.5
47	6.0	1.0	2.4	2.0	4.8	1.0
48	4.8	1.0	2.4	2.5	6.0	1.0
49	7.2	1.5	3.6	3.0	7.2	2.0
50	4.8	1.0	2.4	2.0	4.8	1.0

150μ undo'

0.0  
6.0  
2.4  
3.6  
2.4  
2.4  
4.8  
2.4

Old Hydrazine 1.5 Hour Etch

	5μ do	5μ do'	5μ undo	5μ undo'	15μ do	15μ do'	15μ undo	15μ undo'	50μ do
1	1.5	3.60	1.5	3.60	1.5	3.60	1.5	3.60	1.7
2	1.0	2.40	1.0	2.40	1.2	2.88	1.0	2.40	1.5
3	1.5	3.60	1.5	3.60	1.0	2.40	1.0	2.40	1.0
4	1.5	3.60	1.5	3.60	1.5	3.60	1.5	3.60	1.5
5	1.5	3.60	1.5	3.60	1.5	3.60	1.5	3.60	1.5
6	1.5	3.60	1.5	3.60	2.0	4.80	2.0	4.80	1.5
7	2.0	4.80	2.0	4.80	2.0	4.80	2.0	4.80	2.0
8	1.5	3.60	1.5	3.60	2.0	4.80	2.0	4.80	1.5
9	1.5	3.60	1.5	3.60	1.5	3.60	1.5	3.60	1.5
10	1.0	2.40	1.0	2.40	1.0	2.40	1.5	3.60	1.5
11	1.0	2.40	1.0	2.40	1.5	3.60	1.5	3.60	1.5
12	.5	1.20	1.0	2.40	2.0	4.80	1.5	3.60	1.5
13	1.0	2.40	1.0	2.40	1.0	2.40	1.0	2.40	1.5
14	1.0	2.40	1.0	2.40	1.5	3.60	1.5	3.60	1.5
15	1.0	2.40	1.0	2.40	1.0	2.40	1.5	3.60	1.5
16	1.0	2.40	1.0	2.40	1.0	2.40	1.0	2.40	1.0
17	1.0	2.40	1.0	2.40	1.0	2.40	1.0	2.40	2.0
18	1.0	2.40	1.0	2.40	1.0	2.40	1.0	2.40	1.5
19	1.0	2.40	1.0	2.40	1.0	2.40	1.0	2.40	1.5
20	1.0	2.40	1.0	2.40	1.0	2.40	1.0	2.40	1.0
21	1.0	2.40	1.0	2.40	1.0	2.40	1.5	3.60	1.0
22	1.0	2.40	1.0	2.40	1.5	3.60	1.5	3.60	1.0
23	1.0	2.40	1.0	2.40	1.5	3.60	1.5	3.60	1.0
24	1.0	2.40	1.5	3.60	1.5	3.60	1.5	3.60	1.5
25	1.0	2.40	1.5	3.60	1.5	3.60	2.0	4.80	1.5

Old Hydrazine 1.5 Hour Eich

	50μ do'	50μ undo	50μ undo'	150μ do	150μ do'	150μundo	150μ undo'
1	4.08	1.7	4.08	1.0	2.40	1.0	2.40
2	3.60	1.5	3.60	1.5	3.60	2.0	4.80
3	2.40	1.0	2.40	1.5	3.60	1.5	3.60
4	3.60	1.0	2.40	2.0	4.80	2.0	4.80
5	3.60	1.5	3.60	1.5	3.60	1.5	3.60
6	3.60	2.0	4.80	1.5	3.60	1.5	3.60
7	4.80	2.0	4.80	1.5	3.60	1.5	3.60
8	3.60	1.5	3.60	1.5	3.60	1.5	3.60
9	3.60	2.0	4.80	2.0	4.80	2.0	4.80
10	3.60	1.5	3.60	2.0	4.80	1.5	3.60
11	3.60	1.5	3.60	2.0	4.80	2.0	4.80
12	3.60	1.0	2.40	2.0	4.80	2.0	4.80
13	3.60	1.0	2.40	2.0	4.80	2.0	4.80
14	3.60	1.5	3.60	1.5	3.60	1.5	3.60
15	3.60	1.5	3.60	1.5	3.60	1.5	3.60
16	2.40	1.0	2.40	1.0	2.40	1.0	2.40
17	4.80	2.0	4.80	2.0	4.80	2.0	4.80
18	3.60	1.5	3.60	1.0	2.40	1.5	3.60
19	3.60	2.0	4.80	1.0	2.40	1.0	2.40
20	2.40	1.0	2.40	1.0	2.40	1.5	3.60
21	2.40	1.0	2.40	1.0	2.40	1.0	2.40
22	2.40	1.0	2.40	1.5	3.60	1.0	2.40
23	2.40	1.5	3.60	2.0	4.80	2.5	6.00
24	3.60	1.5	3.60	1.0	2.40	1.5	3.60
25	3.60	2.0	4.80	1.5	3.60	1.0	2.40

Old Hydrazine 2.5 Hour Etch

	5μ do	5μ do'	5μ undo	5μ undo'	15μ do	15μ do'	15μ undo	15μ undo'	50μ do
1	2.0	4.80	2.0	4.80	3.0	7.20	2.5	6.00	3.0
2	2.0	4.80	2.0	4.80	2.0	4.80	2.5	6.00	3.0
3	2.5	6.00	2.5	6.00	3.0	7.20	2.5	6.00	3.0
4	2.5	6.00	2.0	4.80	2.5	6.00	2.5	6.00	2.0
5	2.5	6.00	2.5	6.00	2.5	6.00	2.5	6.00	3.0
6	4.0	9.60	3.5	8.40	3.5	8.40	4.0	9.60	5.0
7	3.0	7.20	3.0	7.20	3.0	7.20	3.0	7.20	3.0
8	3.0	7.20	3.0	7.20	3.0	7.20	3.0	7.20	3.0
9	3.0	7.20	3.0	7.20	3.0	7.20	3.0	7.20	3.0
10	2.5	6.00	2.5	6.00	3.0	7.20	3.0	7.20	2.5
11	1.0	2.40	1.5	3.60	2.0	4.80	2.0	4.80	2.5
12	2.0	4.80	2.0	4.80	2.0	4.80	2.5	6.00	2.0
13	2.0	4.80	2.0	4.80	2.5	6.00	2.5	6.00	3.0
14	2.5	6.00	2.5	6.00	2.5	6.00	2.5	6.00	3.0
15	3.0	7.20	2.5	6.00	3.0	7.20	3.0	7.20	3.0
16	2.0	4.80	2.0	4.80	2.0	4.80	3.0	7.20	2.0
17	3.0	7.20	3.0	7.20	2.0	4.80	2.0	4.80	3.0
18	2.0	4.80	2.0	4.80	2.5	6.00	3.0	7.20	5.0
19	3.0	7.20	3.0	7.20	3.0	7.20	3.0	7.20	3.0
20	2.0	4.80	2.0	4.80	3.0	7.20	3.0	7.20	3.0
21	3.0	7.20	3.0	7.20	3.0	7.20	3.0	7.20	3.0
22	3.0	7.20	3.0	7.20	2.5	6.00	2.5	6.00	3.0
23	3.0	7.20	3.0	7.20	3.0	7.20	3.0	7.20	3.0
24	3.0	7.20	3.0	7.20	3.0	7.20	3.0	7.20	4.0
25	3.0	7.20	3.0	7.20	3.0	7.20	4.0	9.60	4.0



Old Hydrazine 2.5 Hour Etch							
	50µ do'	50µ undo	50µ undo'	150µ do	150µ do'	150µ undo	150µ undo'
1	7.20	3.0	7.20	3.5	8.40	3.5	8.40
2	7.20	3.0	7.20	3.0	7.20	3.0	7.20
3	7.20	2.5	6.00	3.0	7.20	3.0	7.20
4	4.80	2.5	6.00	3.0	7.20	3.0	7.20
5	7.20	3.0	7.20	3.0	7.20	3.5	8.40
6	12.00	5.0	12.00	3.5	8.40	4.0	9.60
7	7.20	3.0	7.20	3.0	7.20	3.0	7.20
8	7.20	3.0	7.20	3.5	8.40	3.5	8.40
9	7.20	3.0	7.20	3.0	7.20	3.0	7.20
10	6.00	3.0	7.20	3.0	7.20	3.0	7.20
11	6.00	2.5	6.00	2.0	4.80	2.0	4.80
12	4.80	2.5	6.00	3.0	7.20	3.0	7.20
13	7.20	3.0	7.20	3.0	7.20	3.0	7.20
14	7.20	3.0	7.20	3.0	7.20	3.0	7.20
15	7.20	3.0	7.20	2.0	4.80	3.0	7.20
16	4.80	2.0	4.80	3.0	7.20	2.5	6.00
17	7.20	3.0	7.20	3.0	7.20	3.0	7.20
18	12.00	5.0	12.00	3.0	7.20	3.0	7.20
19	7.20	3.0	7.20	2.0	4.80	2.0	4.80
20	7.20	3.0	7.20	3.0	7.20	3.0	7.20
21	7.20	3.0	7.20	3.5	8.40	3.0	7.20
22	7.20	3.0	7.20	4.0	9.60	3.5	8.40
23	7.20	3.0	7.20	3.0	7.20	3.0	7.20
24	9.60	4.0	9.60	3.0	7.20	3.0	7.20
25	9.60	3.0	7.20	4.0	9.60	3.0	7.20

Old Hydrazine 3.5 Hour Etch

	5μ do	5μ do'	5μ undo	5μ undo'	15μ do	15μ do'	15μ undo	15μ undo'	50μ do
1	4.0	9.60	4.0	9.60	5.0	12.00	5.0	12.00	5.0
2	5.0	12.00	5.0	12.00	6.0	14.40	5.0	12.00	6.0
3	7.0	16.80	6.0	14.40	6.0	14.40	6.0	14.40	9.0
4	6.0	14.40	6.0	14.40	6.0	14.40	6.0	14.40	5.0
5	5.0	12.00	4.0	9.60	8.0	19.20	5.0	12.00	5.0
6	5.0	12.00	5.0	12.00	5.0	12.00	5.0	12.00	5.0
7	5.0	12.00	5.0	12.00	5.0	12.00	5.0	12.00	5.0
8	4.0	9.60	5.0	12.00	4.0	9.60	5.0	12.00	6.0
9	4.5	10.80	5.0	12.00	4.0	9.60	5.0	12.00	5.0
10	4.0	9.60	4.0	9.60	3.0	7.20	3.0	7.20	5.0
11	3.5	8.40	3.0	7.20	4.0	9.60	4.0	9.60	5.0
12	4.0	9.60	4.0	9.60	4.0	9.60	5.0	12.00	5.0
13	4.0	9.60	4.0	9.60	4.0	9.60	5.0	12.00	5.0
14	4.0	9.60	4.0	9.60	3.0	7.20	3.0	7.20	5.0
15	5.0	12.00	4.0	9.60	3.5	8.40	4.0	9.60	5.0
16	4.0	9.60	4.0	9.60	5.0	12.00	5.0	12.00	6.0
17	4.0	9.60	5.0	12.00	4.0	9.60	6.0	14.40	5.5
18	4.0	9.60	5.0	12.00	4.0	9.60	5.0	12.00	6.0
19	4.0	9.60	5.0	12.00	4.0	9.60	5.0	12.00	4.0
20	4.0	9.60	4.0	9.60	4.0	9.60	4.0	9.60	5.0
21	5.0	12.00	5.0	12.00	5.0	12.00	5.5	13.20	6.0
22	6.0	14.40	6.0	14.40	6.0	14.40	7.0	16.80	7.0
23	6.0	14.40	6.0	14.40	6.0	14.40	7.0	16.80	6.0
24	6.0	14.40	5.0	12.00	6.0	14.40	7.0	16.80	6.0
25	5.0	12.00	5.0	12.00	6.0	14.40	6.0	14.40	6.0

Old Hydrazine 3.5 Hour Etch

	50μ do'	50μ undo	50μ undo'	150μ do	150μ do'	150μ undo	150μ undo'
1	12.00	5.0	12.00	5.0	12.00	6.0	14.40
2	14.40	7.0	16.80	7.0	16.80	6.0	14.40
3	21.60	6.0	14.40	8.0	19.20	7.0	16.80
4	12.00	7.0	16.80	5.0	12.00	5.0	12.00
5	12.00	5.0	12.00	6.0	14.40	5.0	12.00
6	12.00	6.0	14.40	5.0	12.00	5.5	13.20
7	12.00	5.0	12.00	6.0	14.40	6.0	14.40
8	14.40	6.0	14.40	5.0	12.00	4.0	9.60
9	12.00	6.0	14.40	5.0	12.00	4.5	10.80
10	12.00	4.0	9.60	5.0	12.00	5.0	12.00
11	12.00	5.0	12.00	5.0	12.00	5.0	12.00
12	12.00	5.0	12.00	5.0	12.00	5.0	12.00
13	12.00	5.0	12.00	5.0	12.00	4.5	10.80
14	12.00	5.0	12.00	5.0	12.00	5.0	12.00
15	12.00	5.0	12.00	9.0	21.60	10.0	24.00
16	14.40	6.5	15.60	4.0	9.60	4.0	9.60
17	13.20	5.0	12.00	7.0	16.80	6.0	14.40
18	14.40	6.0	14.40	10.0	24.00	10.0	24.00
19	9.60	4.0	9.60	7.0	16.80	7.0	16.80
20	12.00	5.0	12.00	5.0	12.00	6.0	14.40
21	14.40	5.0	12.00	7.0	16.80	6.0	14.40
22	16.80	6.0	14.40	8.0	19.20	7.0	16.80
23	14.40	6.0	14.40	6.0	14.40	7.0	16.80
24	14.40	7.0	16.80	7.0	16.80	7.0	16.80
25	14.40	7.0	16.80	11.00	26.40	11.0	26.40

New Hydrazine 1.5 Hour Etch

	5μ do	5μ do'	5μ undo	5μ undo'	15μ do	15μ do'	15μ undo	15μ undo'	50μ do
1	1.0	2.4	1.0	2.4	1.0	2.4	1.0	2.4	1.0
2	1.0	2.4	1.0	2.4	1.0	2.4	1.0	2.4	1.0
3	1.0	2.4	1.2	2.9	1.0	2.4	1.0	2.4	1.0
4	1.0	2.4	1.0	2.4	1.0	2.4	1.2	2.9	1.0
5	1.0	2.4	1.0	2.4	1.0	2.4	1.0	2.4	1.0
6	1.0	2.4	1.0	2.4	1.0	2.4	1.2	2.9	1.0
7	1.0	2.4	1.5	3.6	1.0	2.4	1.0	2.4	1.0
8	1.2	2.9	1.0	2.4	1.0	2.4	1.0	2.4	1.0
9	1.0	2.4	1.5	3.6	1.2	2.9	1.0	2.4	1.5
10	1.0	2.4	1.5	3.6	1.2	2.9	1.2	2.9	1.0
11	1.0	2.4	1.0	2.4	1.0	2.4	1.0	2.4	1.0
12	1.0	2.4	1.0	2.4	1.0	2.4	1.2	2.9	1.0
13	1.0	2.4	1.0	2.4	1.0	2.4	1.0	2.4	1.0
14	1.0	2.4	1.0	2.4	1.0	2.4	1.0	2.4	1.0
15	1.0	2.4	1.0	2.4	1.2	2.9	1.2	2.9	1.0
16	1.0	2.4	1.0	2.4	1.0	2.4	.7	1.7	.5
17	.7	1.7	.7	1.7	.5	1.2	.5	1.2	.7
18	0	0.0	0	0.0	0	0.0	0	0.0	0
19	0	0.0	0	0.0	0	0.0	0	0.0	0
20	.2	0.5	.2	0.5	.2	0.5	.2	0.5	.2
21	1.0	2.4	1.0	2.4	1.2	2.9	1.2	2.9	1.2
22	1.0	2.4	1.0	2.4	1.0	2.4	1.0	2.4	1.0
23	1.0	2.4	1.0	2.4	1.0	2.4	1.0	2.4	1.2
24	1.0	2.4	1.2	2.9	1.0	2.4	1.0	2.4	1.2
25	1.0	2.4	1.0	2.4	1.0	2.4	1.0	2.4	1.0
26									

New Hydrazine 1.5 Hour Etch

	50μ do'	50μ undo	50μ undo'	150μ do	150μ do'	150μ undo	150μ undo'
1	2.4	1.0	2.4	1.0	2.4	1.0	2.4
2	2.4	1.0	2.4	1.0	2.4	1.0	2.4
3	2.4	1.2	2.9	1.0	2.4	1.2	2.9
4	2.4	1.2	2.9	1.0	2.4	1.0	2.4
5	2.4	1.2	2.9	1.0	2.4	1.0	2.4
6	2.4	1.0	2.4	1.0	2.4	1.0	2.4
7	2.4	1.2	2.9	1.0	2.4	1.0	2.4
8	2.4	1.2	2.9	1.0	2.4	1.0	2.4
9	3.6	1.5	3.6	1.5	3.6	1.5	3.6
10	2.4	1.2	2.9	1.0	2.4	1.0	2.4
11	2.4	1.0	2.4	1.0	2.4	1.0	2.4
12	2.4	1.0	2.4	1.0	2.4	1.0	2.4
13	2.4	1.0	2.4	1.0	2.4	1.0	2.4
14	2.4	1.2	2.9	1.0	2.4	1.0	2.4
15	2.4	1.0	2.4	1.0	2.4	1.0	2.4
16	1.2	.5	1.2	.7	1.7	.7	1.7
17	1.7	.5	1.2	.5	1.2	.5	1.2
18	0.0	0	0.0	0	0.0	0	0.0
19	0.0	0	0.0	0	0.0	0	0.0
20	0.5	.2	0.5	.1	0.2	.1	0.2
21	2.9	1.0	2.4	1.0	2.4	1.0	2.4
22	2.4	1.0	2.4	1.0	2.4	1.0	2.4
23	2.9	1.0	2.4	1.0	2.4	1.0	2.4
24	2.9	1.0	2.4	1.0	2.4	1.0	2.4
25	2.4	1.0	2.4	1.0	2.4	1.0	2.4
26							

New Hydrazine 2.5 Hour Etch

	5μ do	5μ do'	5μ undo	5μ undo'	15μ do	15μ do'	15μ undo	15μ undo'	50μ do
1	2.0	4.8	2.0	4.8	2.0	4.8	2.0	4.8	2.5
2	2.0	4.8	2.0	4.8	2.0	4.8	2.5	6.0	2.0
3	2.0	4.8	2.0	4.8	2.0	4.8	2.0	4.8	2.0
4	2.0	4.8	2.5	6.0	2.0	4.8	2.0	4.8	2.0
5	2.0	4.8	2.0	4.8	2.0	4.8	2.5	6.0	2.0
6	2.0	4.8	2.0	4.8	2.5	6.0	2.0	4.8	2.5
7	2.0	4.8	2.0	4.8	2.0	4.8	2.5	6.0	2.0
8	3.0	7.2	3.0	7.2	2.0	4.8	2.0	4.8	2.5
9	2.0	4.8	2.0	4.8	2.5	6.0	2.5	6.0	2.0
10	2.0	4.8	2.0	4.8	2.0	4.8	2.0	4.8	2.0
11	2.5	6.0	2.0	4.8	2.0	4.8	2.0	4.8	2.0
12	2.0	4.8	2.0	4.8	2.5	6.0	2.5	6.0	2.5
13	2.0	4.8	2.0	4.8	2.0	4.8	2.0	4.8	3.0
14	2.0	4.8	2.5	6.0	2.5	6.0	2.0	4.8	2.0
15	2.0	4.8	2.0	4.8	2.5	6.0	2.5	6.0	2.0
16	2.0	4.8	2.0	4.8	2.0	4.8	2.0	4.8	2.0
17	2.0	4.8	2.0	4.8	1.5	3.6	2.0	4.8	2.0
18	1.0	2.4	1.0	2.4	1.0	2.4	0	0.0	1.5
19	1.0	2.4	1.0	2.4	1.0	2.4	1.5	3.6	1.0
20	1.0	2.4	1.0	2.4	1.0	2.4	1.0	2.4	1.0
21	2.0	4.8	2.0	4.8	2.0	4.8	2.0	4.8	2.0
22	2.0	4.8	2.5	6.0	2.0	4.8	2.0	4.8	2.0
23	2.0	4.8	2.0	4.8	2.0	4.8	2.0	4.8	2.0
24	2.0	4.8	2.5	6.0	2.0	4.8	2.5	6.0	2.0
25	2.0	4.8	2.0	4.8	2.0	4.8	2.0	4.8	2.5
26	2.0	4.8	2.0	4.8	2.0	4.8	2.0	4.8	2.5

I

New Hydrazine 2.5 Hour Etch

	50μ do'	50μ undo	50μ undo'	150μ do	150μ do'	150μ undo	150μ undo'
1	6.0	2.5	6.0	2.5	6.0	2.5	6.0
2	4.8	2.0	4.8	2.0	4.8	2.0	4.8
3	4.8	2.0	4.8	2.5	6.0	2.0	4.8
4	4.8	2.0	4.8	2.0	4.8	2.0	4.8
5	4.8	2.0	4.8	2.0	4.8	2.0	4.8
6	6.0	2.0	4.8	2.0	4.8	2.5	6.0
7	4.8	2.0	4.8	2.5	6.0	2.0	4.8
8	6.0	2.0	4.8	2.0	4.8	2.0	4.8
9	4.8	2.5	6.0	2.5	6.0	2.5	6.0
10	4.8	2.0	4.8	2.0	4.8	2.0	4.8
11	4.8	2.0	4.8	2.0	4.8	2.0	4.8
12	6.0	2.5	6.0	2.5	6.0	2.5	6.0
13	7.2	2.5	6.0	2.0	4.8	2.0	4.8
14	4.8	2.0	4.8	2.0	4.8	2.0	4.8
15	4.8	2.0	4.8	2.0	4.8	2.0	4.8
16	4.8	2.0	4.8	1.5	3.6	1.5	3.6
17	4.8	2.0	4.8	1.5	3.6	1.5	3.6
18	3.6	1.0	2.4	1.5	3.6	1.5	3.6
19	2.4	1.0	2.4	1.0	2.4	1.0	2.4
20	2.4	1.0	2.4	1.0	2.4	1.0	2.4
21	4.8	2.0	4.8	2.5	6.0	2.0	4.8
22	4.8	2.0	4.8	2.0	4.8	2.0	4.8
23	4.8	2.0	4.8	2.0	4.8	2.0	4.8
24	4.8	2.0	4.8	2.0	4.8	2.0	4.8
25	6.0	2.5	6.0	2.5	6.0	2.5	6.0
26							

New Hydrazine 3.5 Hour Etch

	5μ do	5μ do'	5μ undo	5μ undo'	15μ do	15μ do'	15μ undo	15μ undo'	50μ do
1	4.0	9.6	4.0	9.6	4.0	9.6	4.0	9.6	4.0
2	4.0	9.6	4.0	9.6	4.0	9.6	4.0	9.6	4.0
3	4.0	9.6	4.0	9.6	4.0	9.6	4.0	9.6	4.0
4	4.0	9.6	4.0	9.6	4.0	9.6	4.0	9.6	4.0
5	4.0	9.6	4.0	9.6	4.0	9.6	4.0	9.6	4.0
6	4.0	9.6	4.0	9.6	4.0	9.6	4.0	9.6	4.0
7	4.0	9.6	4.0	9.6	4.0	9.6	4.0	9.6	4.0
8	4.0	9.6	4.0	9.6	4.0	9.6	4.0	9.6	4.0
9	4.0	9.6	4.0	9.6	4.0	9.6	4.0	9.6	4.0
10	3.5	8.4	4.0	9.6	4.0	9.6	4.0	9.6	4.0
11	4.0	9.6	4.0	9.6	3.5	8.4	3.5	8.4	3.5
12	3.5	8.4	3.5	8.4	4.0	9.6	4.0	9.6	3.5
13	4.0	9.6	4.0	9.6	3.5	8.4	4.0	9.6	4.0
14	3.5	8.4	4.0	9.6	3.5	8.4	4.0	9.6	4.0
15	3.5	8.4	4.0	9.6	4.0	9.6	4.0	9.6	4.0
16	3.5	8.4	4.0	9.6	3.5	8.4	4.0	9.6	3.0
17	3.5	8.4	4.0	9.6	4.0	9.6	4.0	9.6	4.0
18	3.5	8.4	3.5	8.4	3.0	7.2	3.0	7.2	3.5
19	3.5	8.4	3.0	7.2	3.0	7.2	3.5	8.4	3.0
20	3.0	7.2	3.0	7.2	3.0	7.2	3.0	7.2	3.0
21	4.0	9.6	4.0	9.6	4.0	9.6	4.0	9.6	4.0
22	4.0	9.6	4.0	9.6	3.5	8.4	4.0	9.6	4.0
23	4.0	9.6	4.0	9.6	4.0	9.6	4.0	9.6	4.0
24	3.0	7.2	4.0	9.6	3.0	7.2	2.5	6.0	4.0
25	4.0	9.6	4.0	9.6	4.0	9.6	3.5	8.4	4.0



New Hydrazine 3.5 Hour Etch

	50μ do'	50μ undo	50μ undo'	150μ do	150μ do'	150μ undo	150μ undo'
1	9.6	4.0	9.6	4.0	9.6	4.0	9.6
2	9.6	4.0	9.6	4.0	9.6	4.0	9.6
3	9.6	4.0	9.6	4.0	9.6	4.0	9.6
4	9.6	4.0	9.6	4.0	9.6	4.0	9.6
5	9.6	4.0	9.6	3.5	8.4	4.0	9.6
6	9.6	4.0	9.6	4.0	9.6	4.5	10.8
7	9.6	4.0	9.6	4.0	9.6	4.0	9.6
8	9.6	4.0	9.6	3.5	8.4	4.0	9.6
9	9.6	4.5	10.8	4.0	9.6	4.0	9.6
10	9.6	4.0	9.6	4.0	9.6	3.5	8.4
11	8.4	4.0	9.6	4.0	9.6	4.0	9.6
12	8.4	4.0	9.6	4.0	9.6	4.0	9.6
13	9.6	3.5	8.4	4.0	9.6	4.0	9.6
14	9.6	3.5	8.4	4.0	9.6	4.0	9.6
15	9.6	4.0	9.6	4.0	9.6	4.0	9.6
16	7.2	3.5	8.4	3.0	7.2	3.5	8.4
17	9.6	4.0	9.6	4.0	9.6	3.0	7.2
18	8.4	3.5	8.4	3.0	7.2	4.0	9.6
19	7.2	3.0	7.2	3.0	7.2	3.0	7.2
20	7.2	3.0	7.2	3.0	7.2	3.0	7.2
21	9.6	4.0	9.6	4.0	9.6	4.0	9.6
22	9.6	4.0	9.6	4.0	9.6	3.5	8.4
23	9.6	4.0	9.6	4.0	9.6	3.5	8.4
24	9.6	3.0	7.2	3.0	7.2	3.0	7.2
25	9.6	4.0	9.6	4.0	9.6	4.0	9.6

## APPENDIX C

### IR SCOPE READINGS AND CALCULATIONS

Measurements were taken of a gold doped flow sensor under no-flow conditions using an infrared microscope. These measurements were taken on the radiance scale, as the temperature of the device was exceeding 165°C.

To properly operate the IR scope on the radiance scale, the device is set for radiance with emissivity set a 1. The radiometric scale is linear proportional to the irradiance at the entrance aperture. The scale is calibrated in units of effective radiance :

$$\text{milliwatts-steradian}^{-1}\text{-cm}^{-2}$$

The electrical dectector output is given by:

$$E = R K [ N_{\text{total}} - N_o ]$$

where:

E = dectector output (volts)

R = dectector responsivity (volts/watt)

K = optical constant (steradians/cm<sup>2</sup>)

N<sub>total</sub> = radiation collected from the target

N = ambient background

The reading given by the scope the full amount of radiation it receives from the device. If the device had an emissivity of 1, and

the background temperature radiance is known, this reading could be related to temperature through a look-up graph provided with the scope. Since the emissivity of the device is not one a more complex calculation is needed.

The first problem is to determine the effective blackbody background radiation caused by the room temperature. These numbers can be looked up on a graph provided with the instrument once the room temperature (in °C) is known. On the day the IR measurements were taken the temperature of the room was 25°C and the effective blackbody background radiation was:

$$N_o = 3.5 \times 10^{-3} \frac{W}{cm^2 \text{ ster}}$$

To obtain target temperatures from the radiance scale the target emissivity must be known. The value of the radiance ( $N_{tot} - N_o$ ) read on the radiance scale should first be divided by the target emissivity,

$$N_{BBT} = \left[ \frac{N_{total} - N_o}{\epsilon_t} \right] + N_o$$

where  $N_{BBT}$  = radiation emitted by a black body at the target temperature.

The emissivity of chrome and silicon differ dramatically.

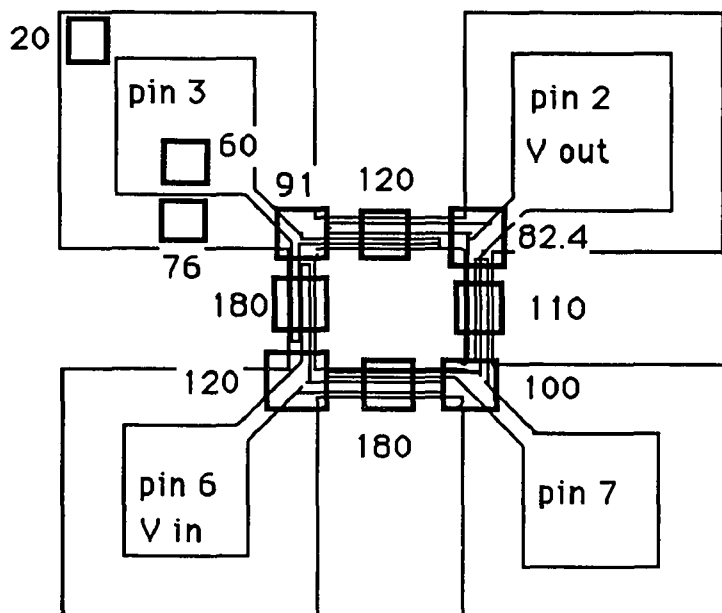
Chromium  $\epsilon = .08 - .28$

unglazed silica brick  $\epsilon = .8 - .85$

Once this calculation was done the value of NBBT could be looked up on radiance graphs provided by the microscope manufacturer to find actual sensor temperature.

The first difficulty encountered was that it was difficult to determine what value of emissivity should be used to calculate the temperature of various spots on the sensor. Since comparable geometric areas will have equal proportions of chromium and silicon dioxide radiating at the microscope, comparable area readings can be used to determine if one part of the geometry is warmer than another. This type of comparison is possible only on comparable geometries, since other places on the sensor will have different proportions of silicon dioxide and chromium and the reading will be correspondingly different for the same actual device temperature.

Infrared Microscope Readings for  
Gold doped, no flow, version 10.0



Estimates were made of approximate emissivity values based on the proportion of chromium and silicon dioxide in the viewing window. As these calculations show, slight variations in emissivity values lead to big differences in temperatures found. For example in the center of the bridge we have about 75% chromium and 25% oxide (round viewing window 36 $\mu$ m in diameter). If those percentages are used with the emissivities to give an overall emissivity the result is:

$$(0.75)(0.1) + (0.25)(0.8) = .275$$

$$\frac{.120}{.275} + .0035 = .6035 \text{ which yields a temperature of } 290 \text{ }^\circ\text{C}$$

but if somewhat higher and lower emissivity values are used:

$$N_{\text{BBT}} = \frac{.120}{.5} + .0035 = .2435 \text{ which yields a temperature of } 240^{\circ}\text{C}$$

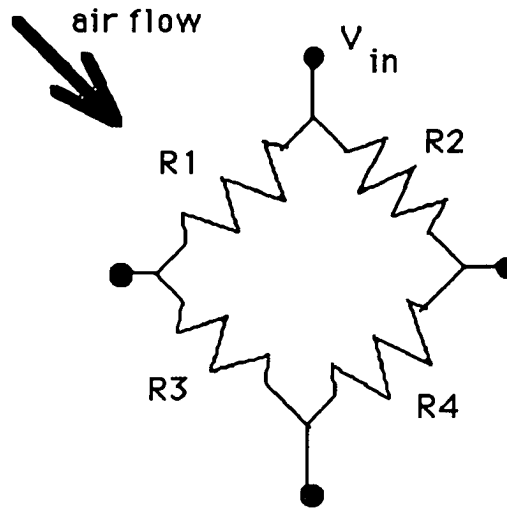
$$N_{\text{BBT}} = \frac{.120}{.1} + .0035 = 1.20 \text{ which yields a temperature of } 370^{\circ}\text{C}$$

These represent the high and low extremes which are possible as readings for the cool bridge resistors. The same type of calculations show the temperature of the warm resistors to be  $310^{\circ}\text{C}$  when an emissivity of .275 is used. When .2 is used for an emissivity rather than .275 the temperature reading is  $350^{\circ}\text{C}$

One temperature reading can be made with a fair amount of confidence, and that is a reading taken over only the chromium pad. In this case the emissivity is the emissivity of the chromium only and the temperature read calculates as  $280^{\circ}\text{C}$

From this information and the additional information provided by John Doty that positive photoresist chars when painted onto the surface of an active device and photoresist does not burn at temperatures under  $300^{\circ}\text{C}$ ; the conclusion is made that the bridge resistors are sitting just over  $300^{\circ}\text{C}$ , probably  $310^{\circ}\text{C}$  to  $320^{\circ}\text{C}$  while the large feet are at about  $280^{\circ}\text{C}$ .

## THE WHEATSTONE BRIDGE AND HOW IT WORKS



Let  $R_1 = R_2 = R_3 = R_4 = R$

then  $V_o = 0$

Let  $R_1 = R_4 = R(T_1)$

$R_2 = R_3 = R(T_2)$

Then

$$V_{out} = V_{in} \left[ \frac{R_4}{R_3 + R_4} - \frac{R_2}{R_1 + R_2} \right]$$

$$V_{out} = V_{in} \left[ \frac{R_1 R_4 - R_2 R_3}{(R_1 + R_2)(R_3 + R_4)} \right]$$

Substituting in the resistance identities and combining:

$$V_{\text{out}} = V_{\text{in}} \left[ \frac{(R(T_1) - R(T_2))(R(T_1) + R(T_2))}{(R(T_1) + R(T_2))^2} \right]$$

$$V_{\text{out}} = V_{\text{in}} \left[ \frac{R(T_1) - R(T_2)}{R(T_1) + R(T_2)} \right]$$

### ENGINEERING DRAWINGS

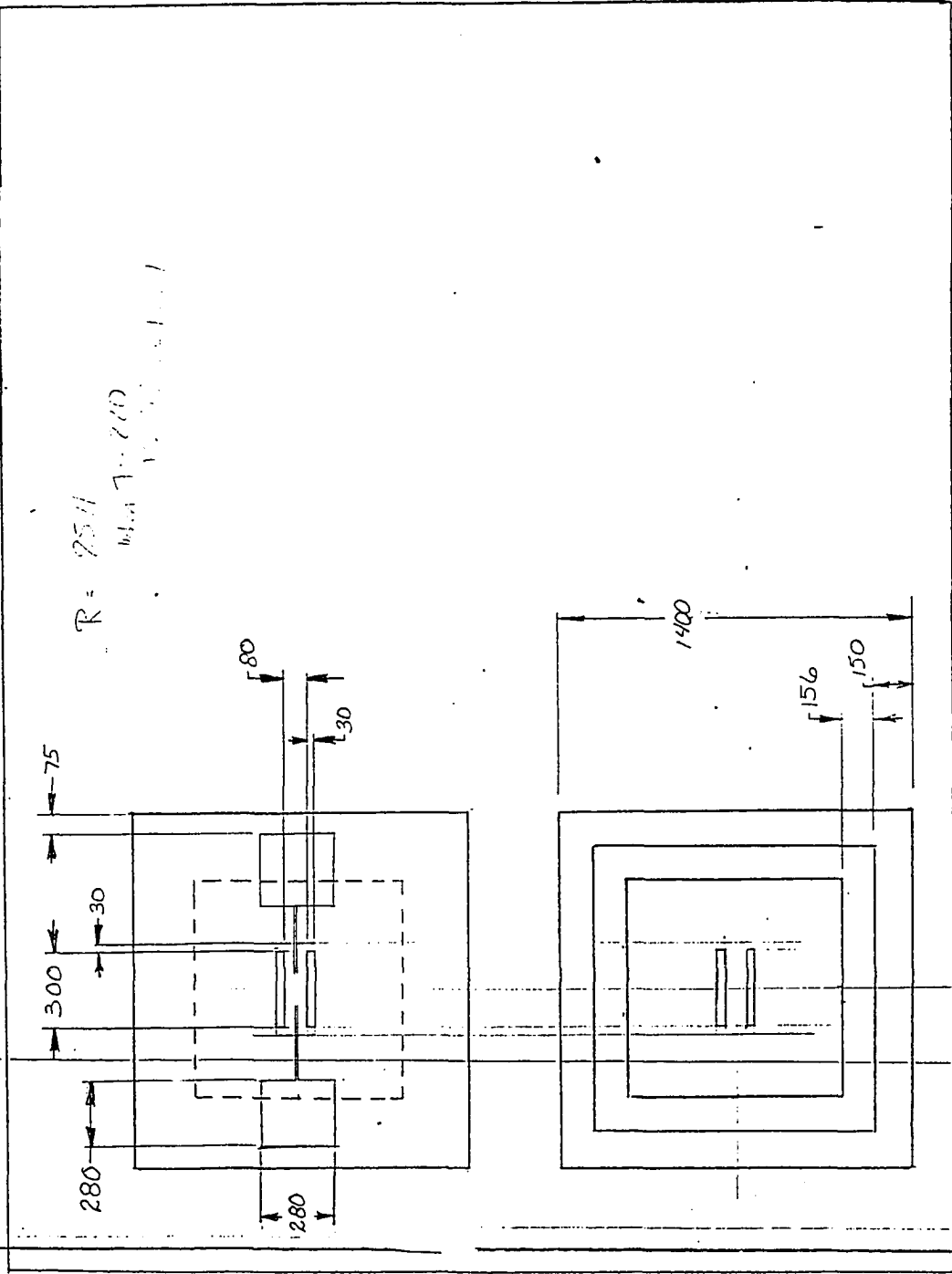
The following are the engineering drawings used to produce the new version of the flow sensor.



OVER VIEW DRAWING VERSION I 2/6 18.5.54

R = 254

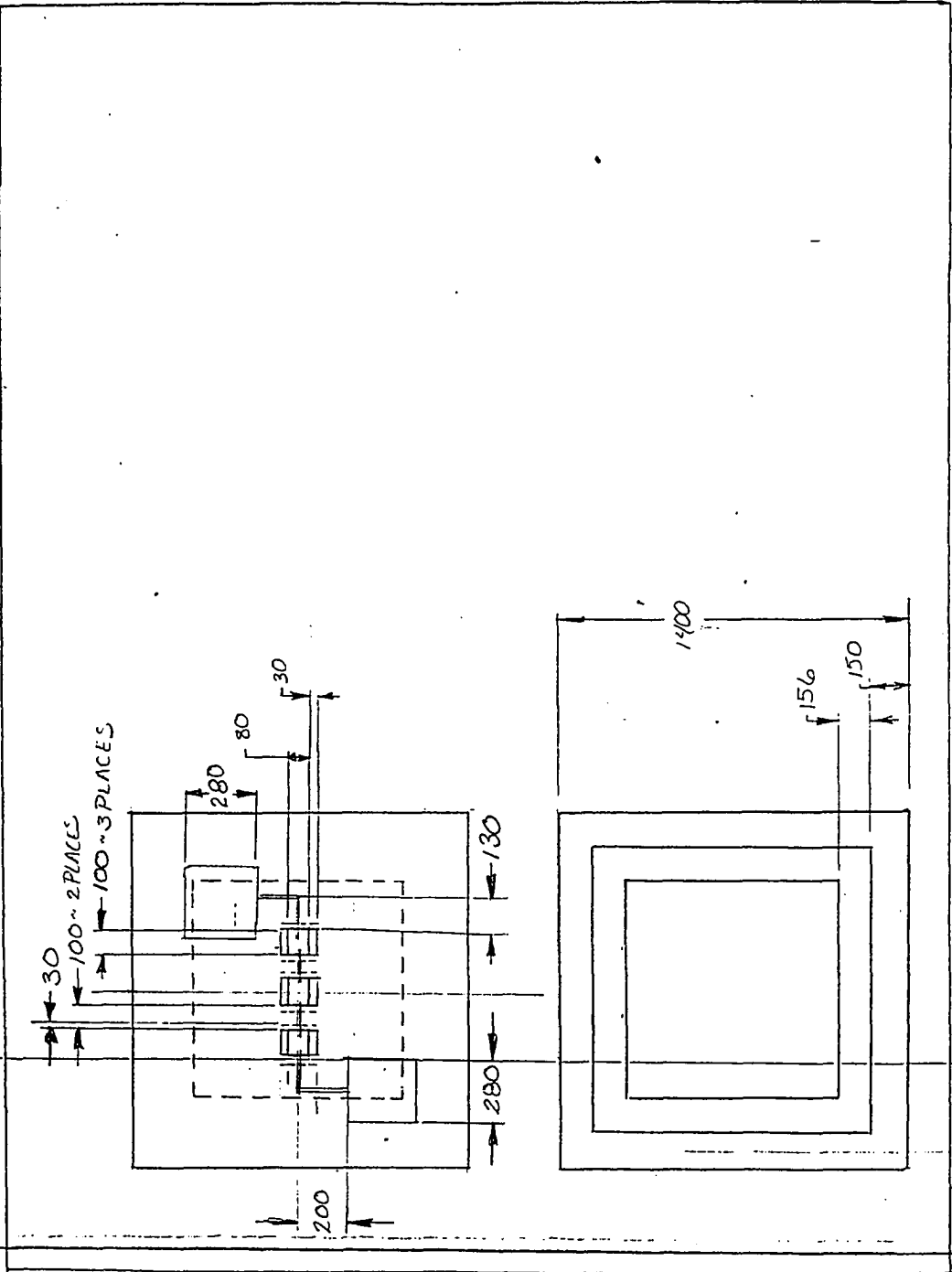
WATER TOWER



WATER TOWER

OVERVIEW DRAWING V. 1 2

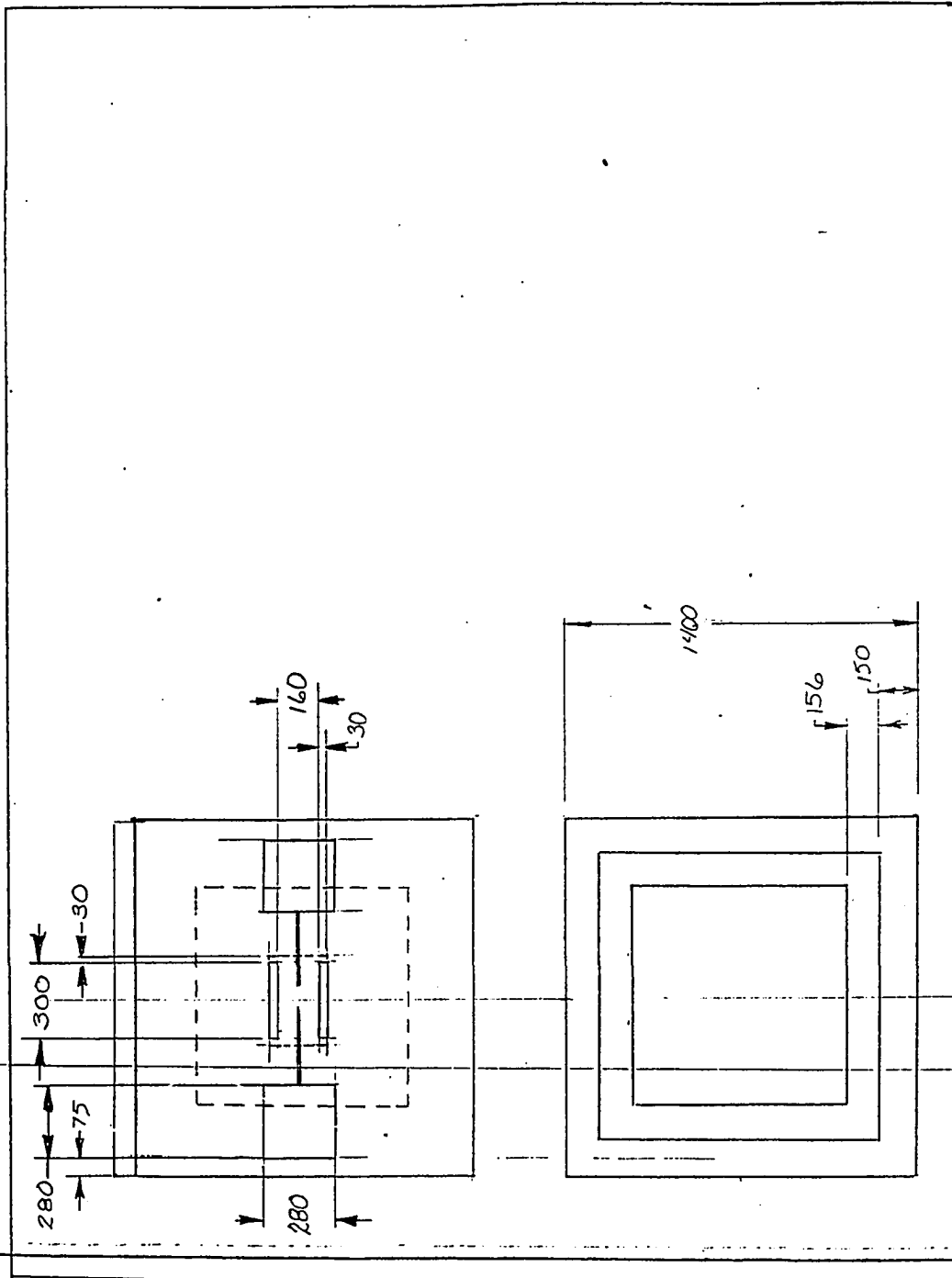
1/11/54



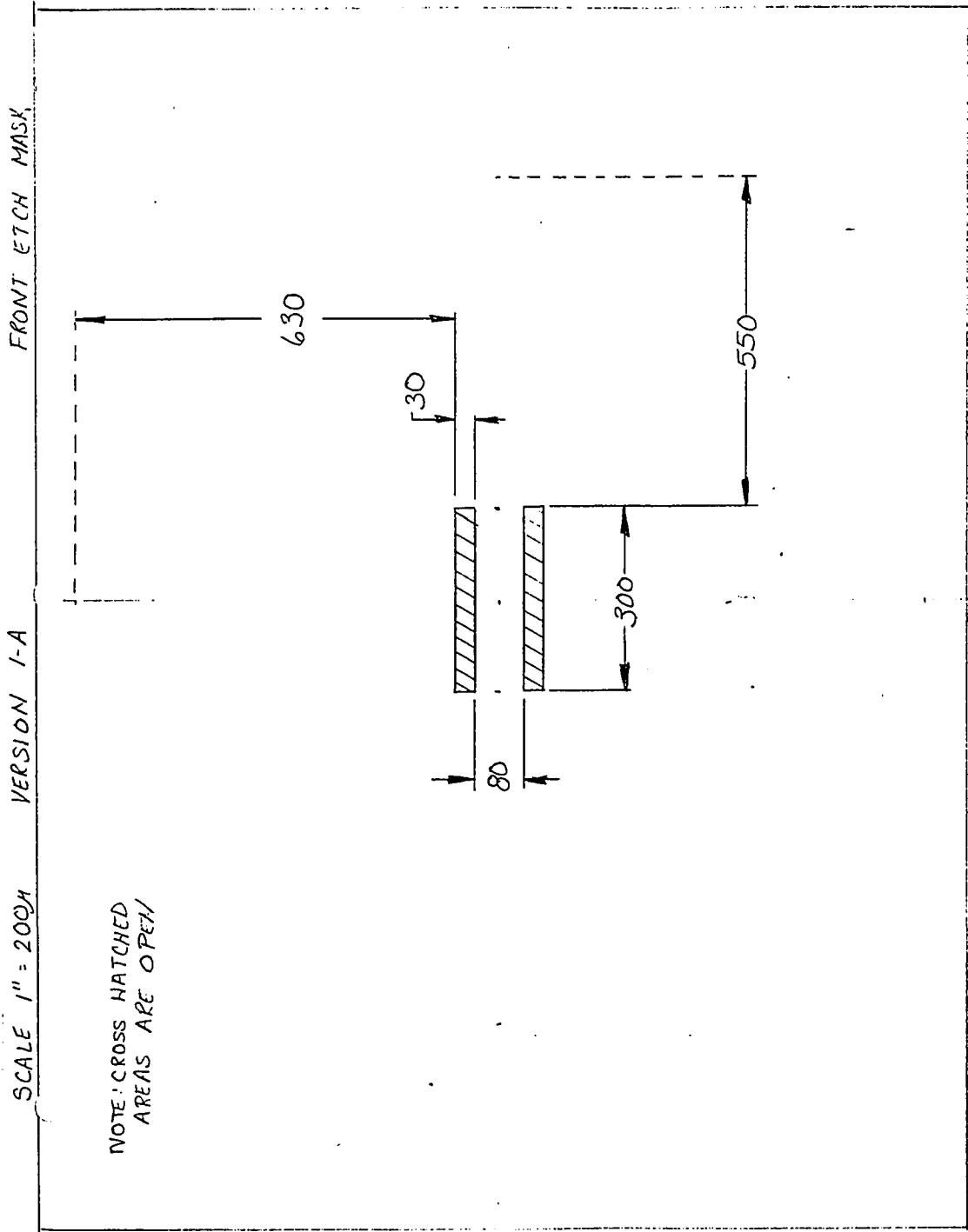
S.G. MILITARY 29-77

OVERVIEW DRAWING VERSION 3

11/15/21



T. J. WILSON 2-7-21



J.G. WHITNEY 2-11-92

FRONT CATCH MASK

VERSION 2-A

SCALE 1" = 200M

NOTE: CROSS HATCHED  
REGIONS ARE OPEN

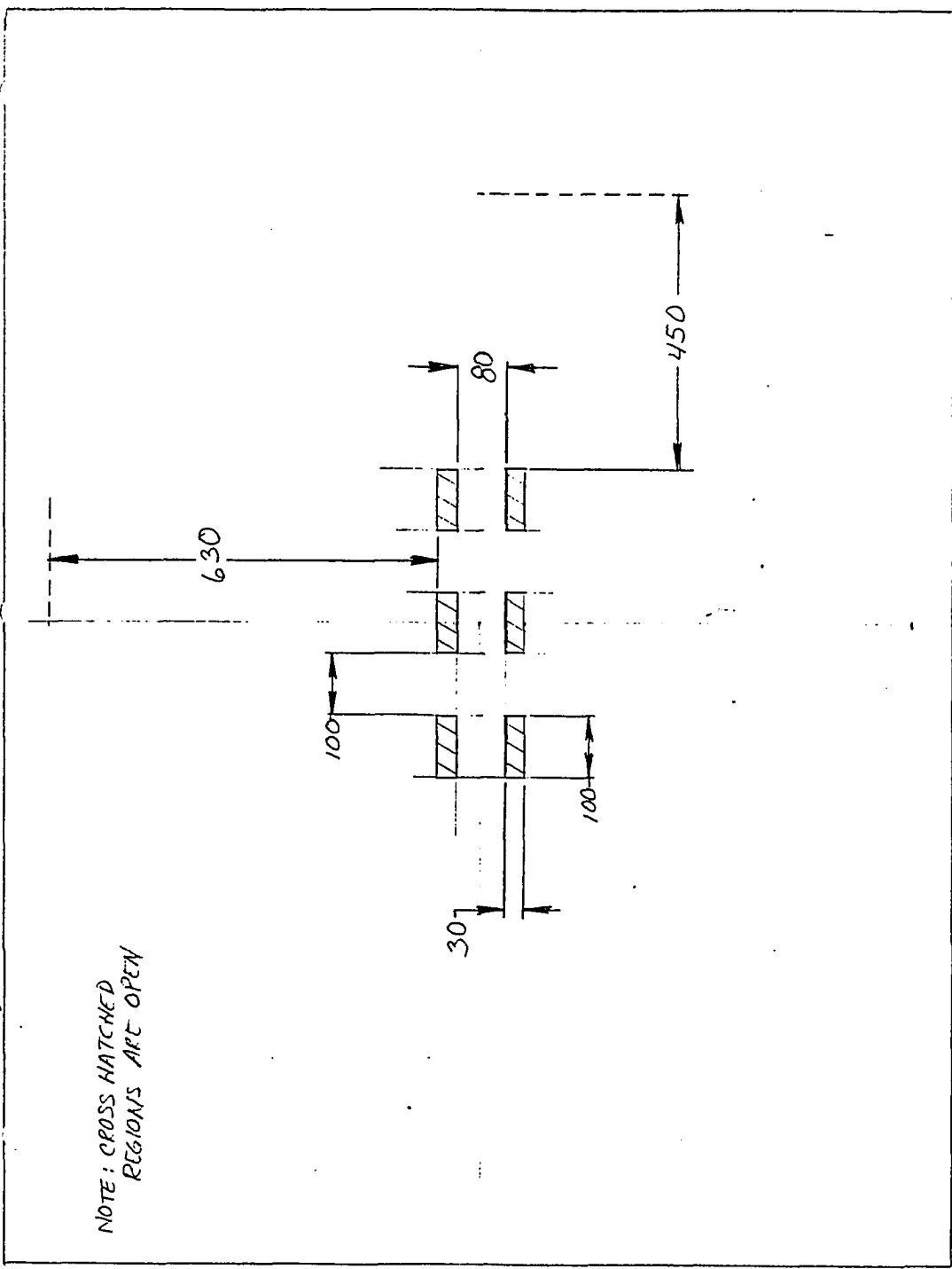


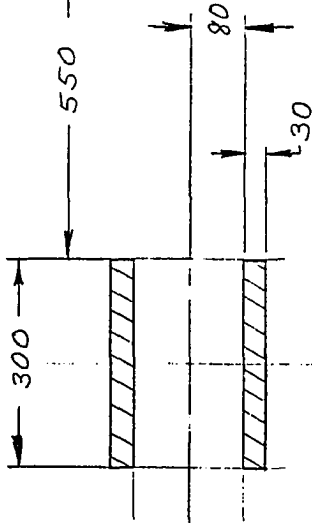
FIG. WHITNEY 3-11-92

FRONT ETCH MASK

VERSION 3-A

SCALE 1" = 200H

NOTE: CROSS HATCHED  
AREA IS OPEN

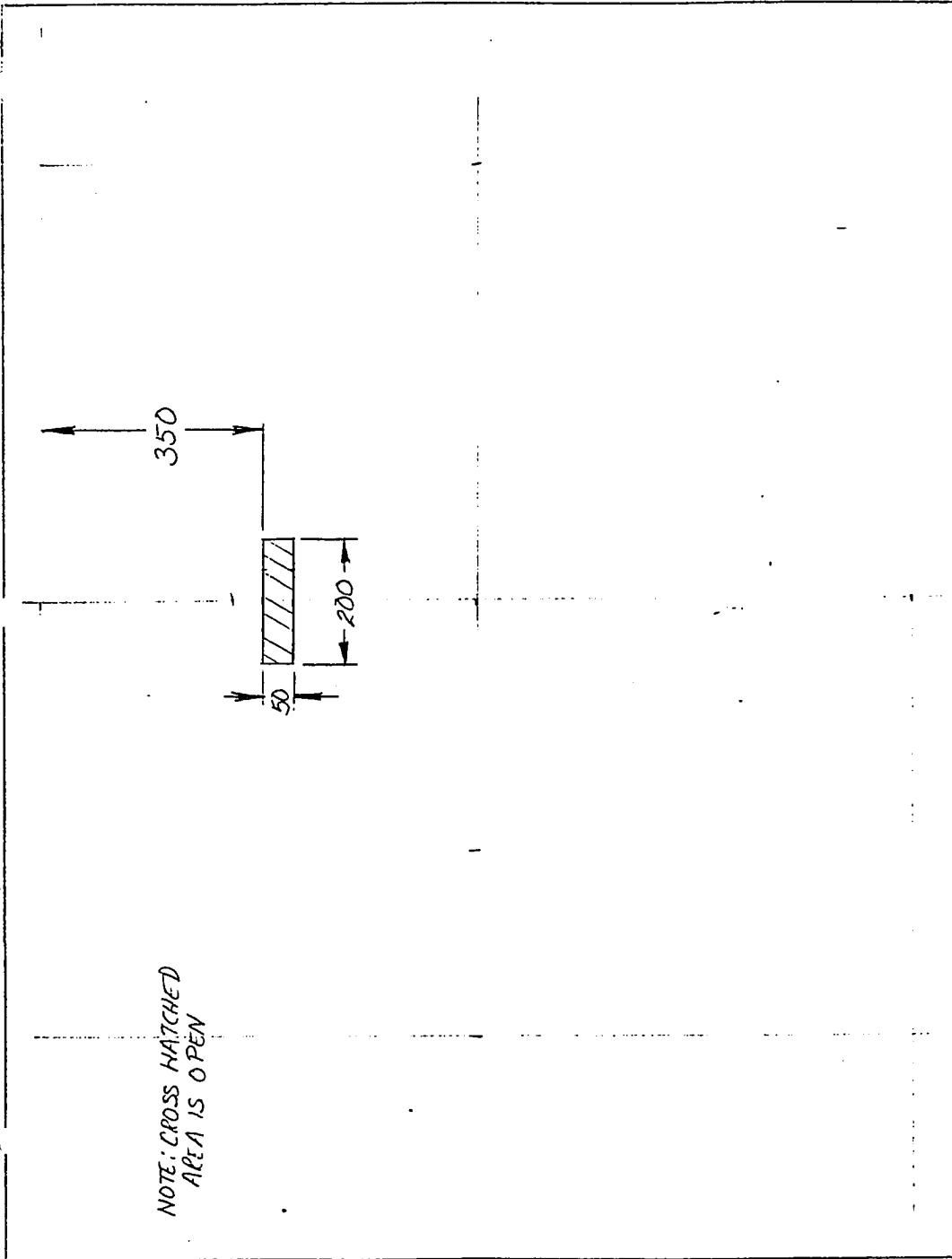


J. G. WHITNEY 3-10-92

FRONT ETCH MASK

VERSION 3-B, 2-B, 1-B

SCALE 1" = 200 $\mu$

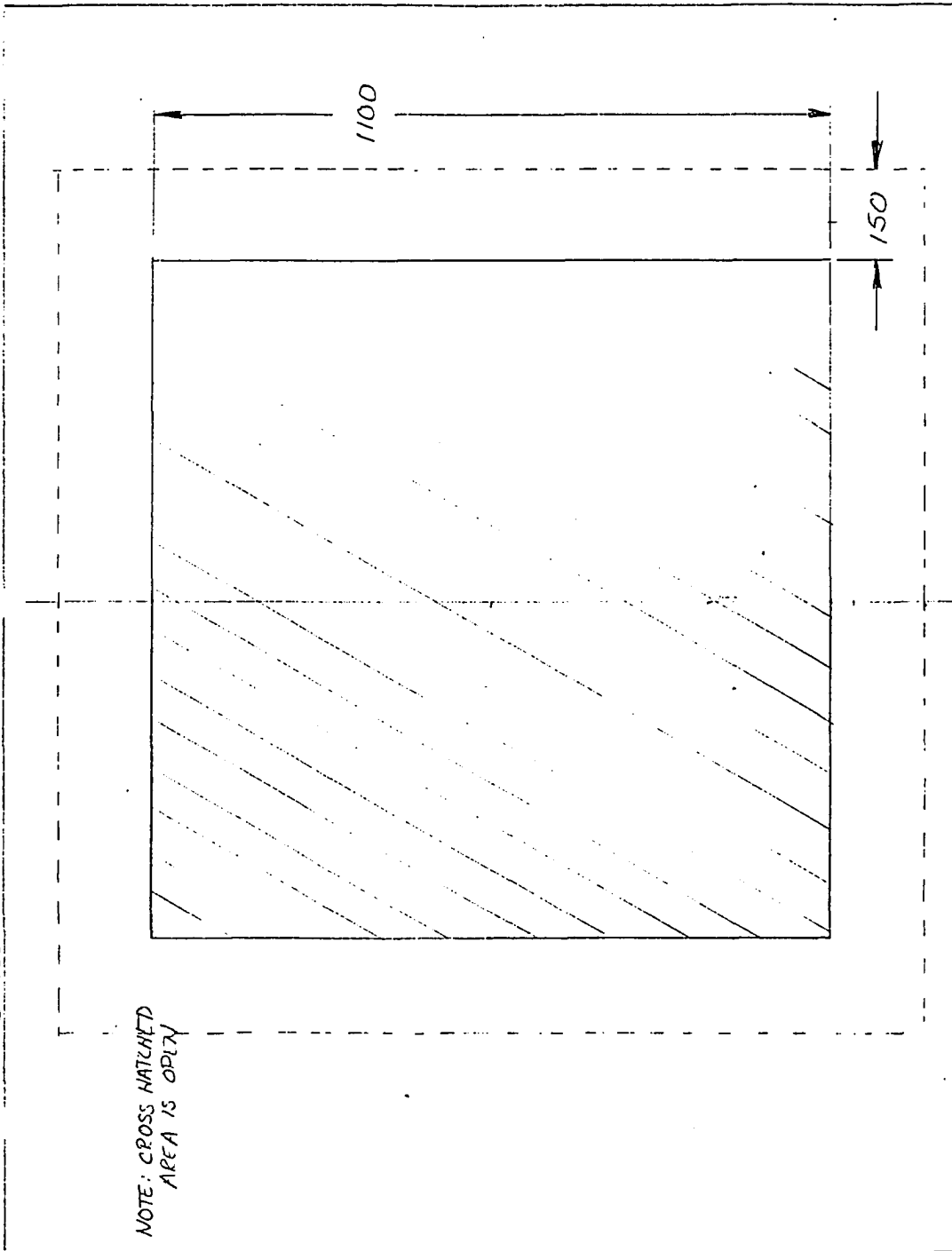


J.G. WHITNEY 8-10-97

VERSION 1A-B, 2A-B, 3A-B

BACKSIDE MASK

SCALE 1" = 200µ



NOTE: CROSS HATCHED  
AREA IS OPEN

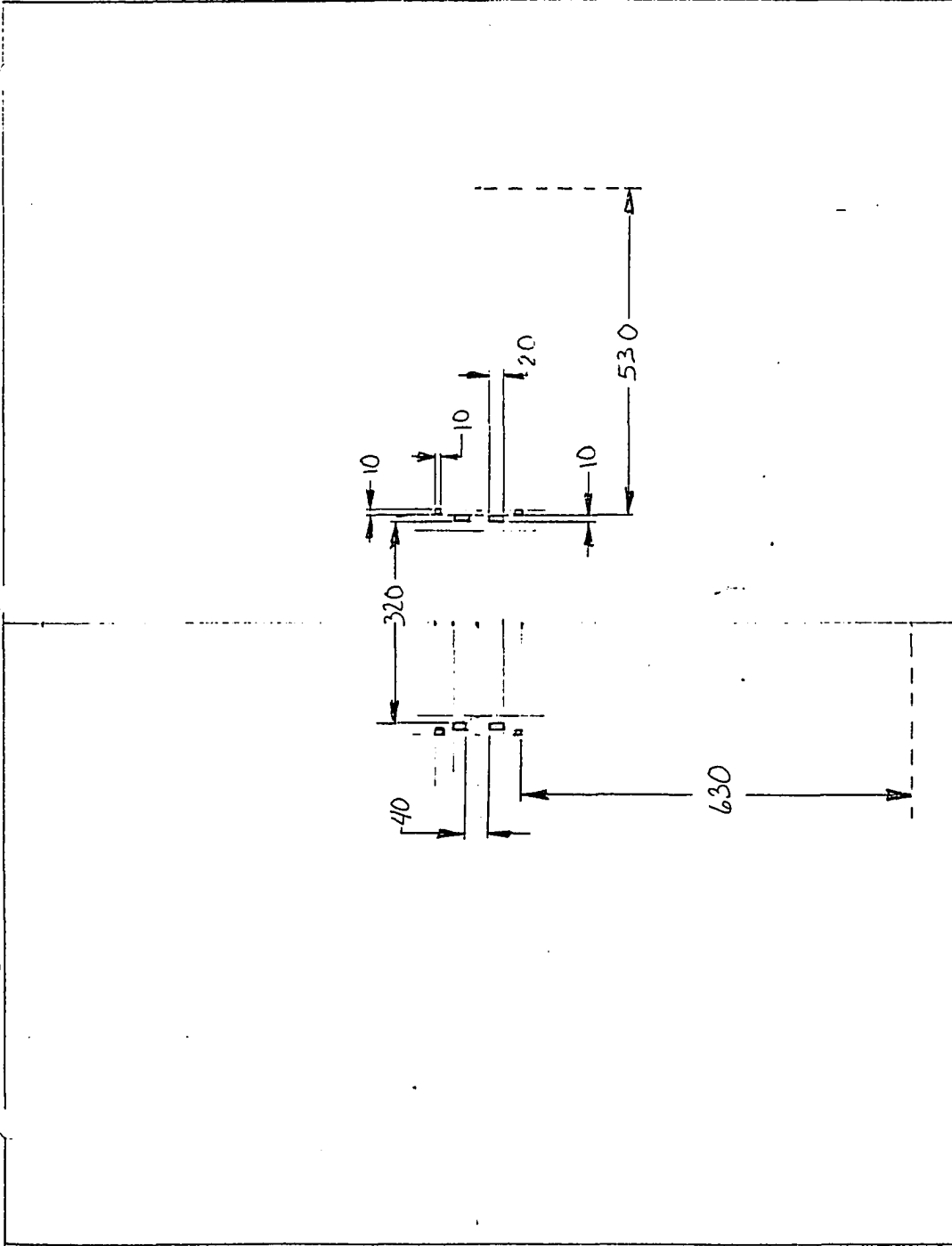
D.G. WHITNEY 3-10-92



SCALE 1" = 200μ

VERSION 1-A

TUNNEL ETCH MASK

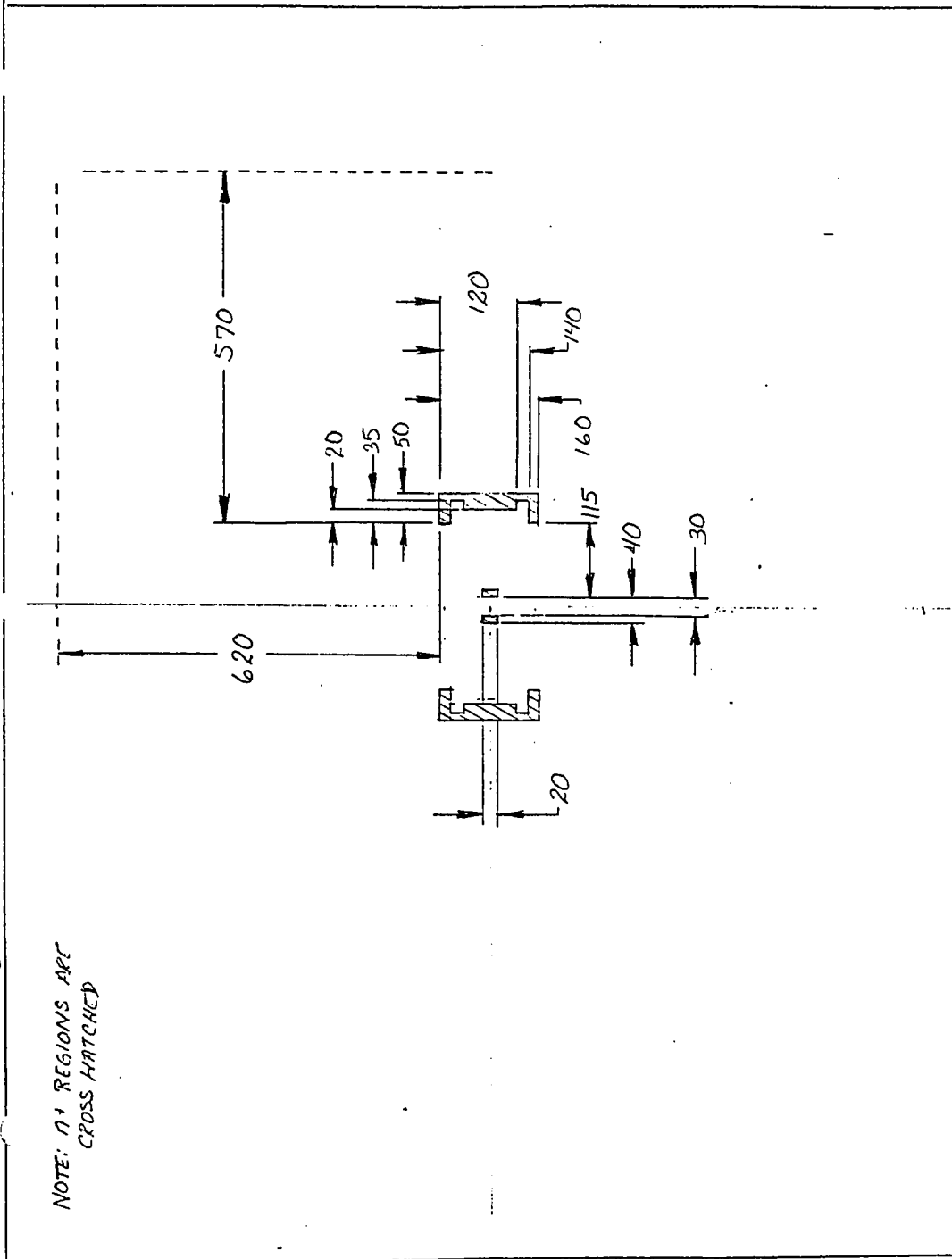


J.G. WHITNEY 3-11-92

SCALE 1" = 200μ

VERSION 1A

n+ DOPING MASK



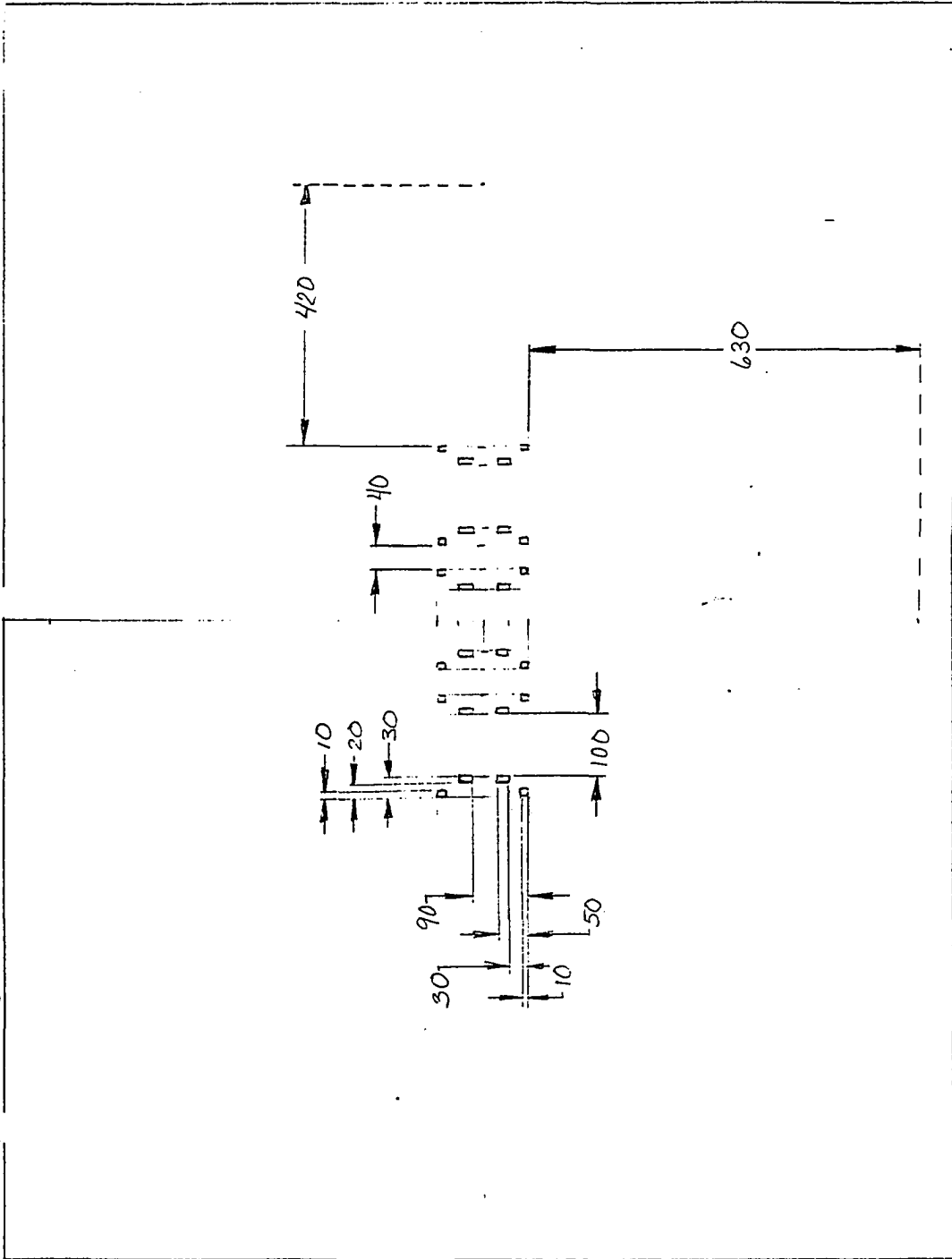
NOTE: n+ REGIONS ARE  
CROSS HATCHED

J.G. WINNERY 8. 92

TUNNEL ETCH MASK

VERSION 2-A

SCALE 1" = 200μ

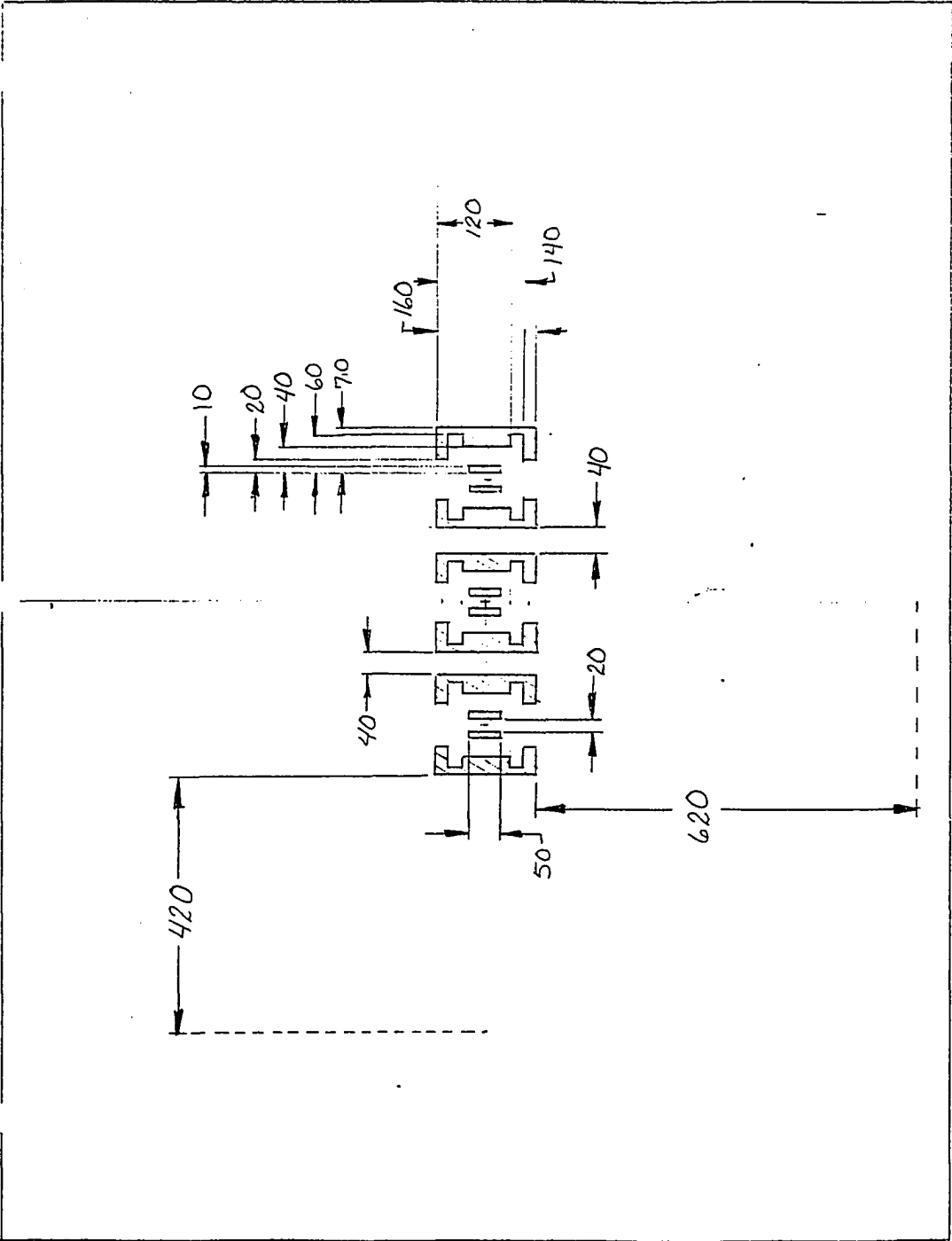


J.G. WHITNEY 3-11-92

SCALE 1" = 200μ

VERSION 2-A

N+ DOPING MASK

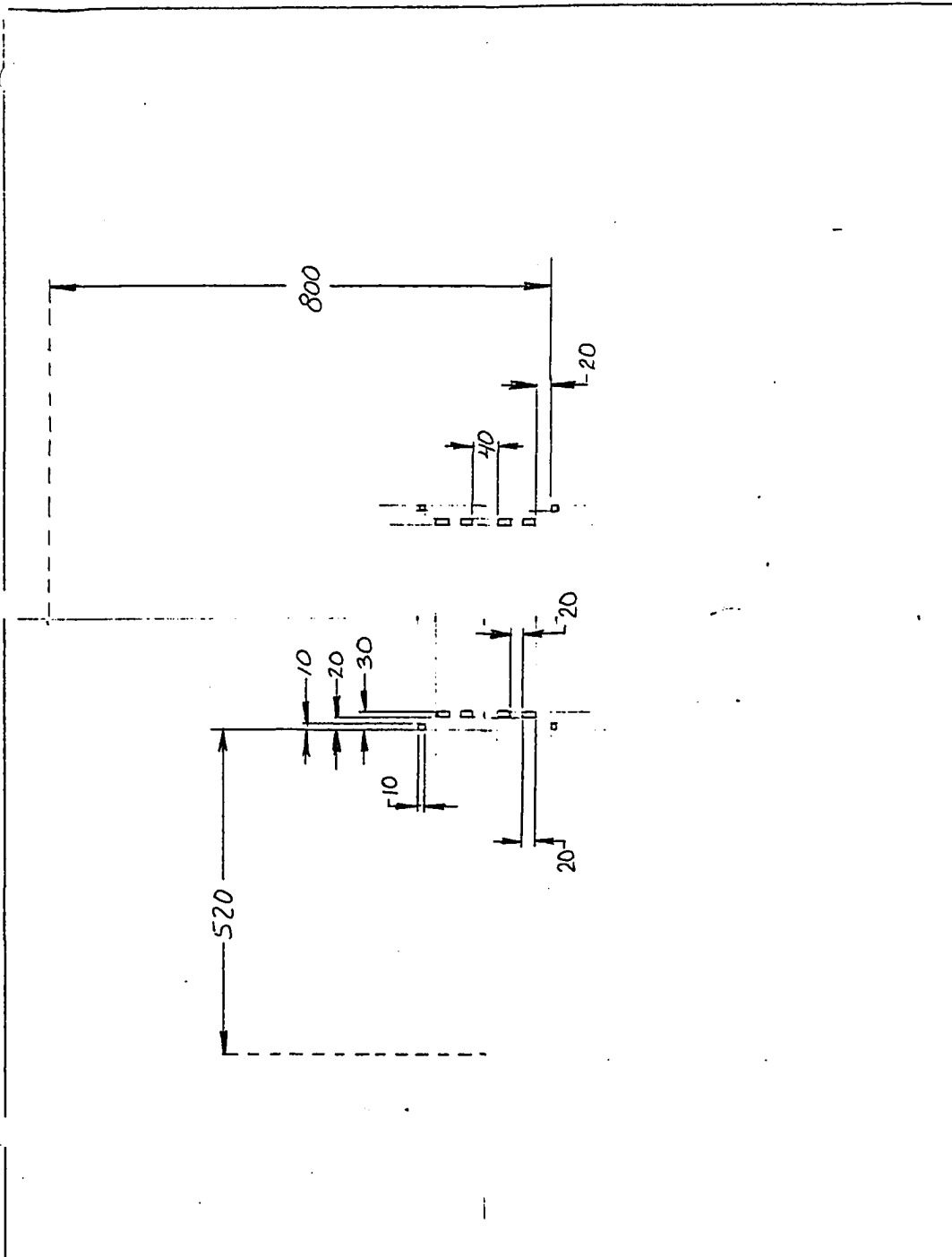


J. G. WHITNEY 3-11-72

VERSION 3-A TUNNEL ETCH MASK

VERSION 3-A

SCALE 1" = 200μ

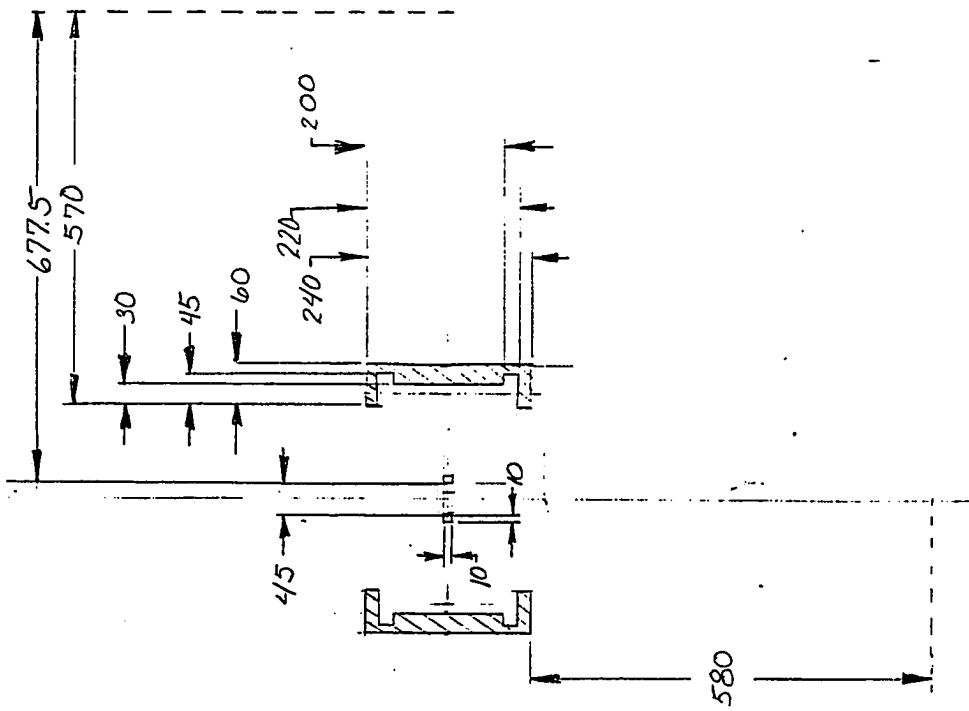


J.G. WHITNEY 3-11-92

VERSION 3-A n+ DOPING MASK

SCALE 1" = 200μ

NOTE: n+ REGIONS ARE CROSS-HATCHED

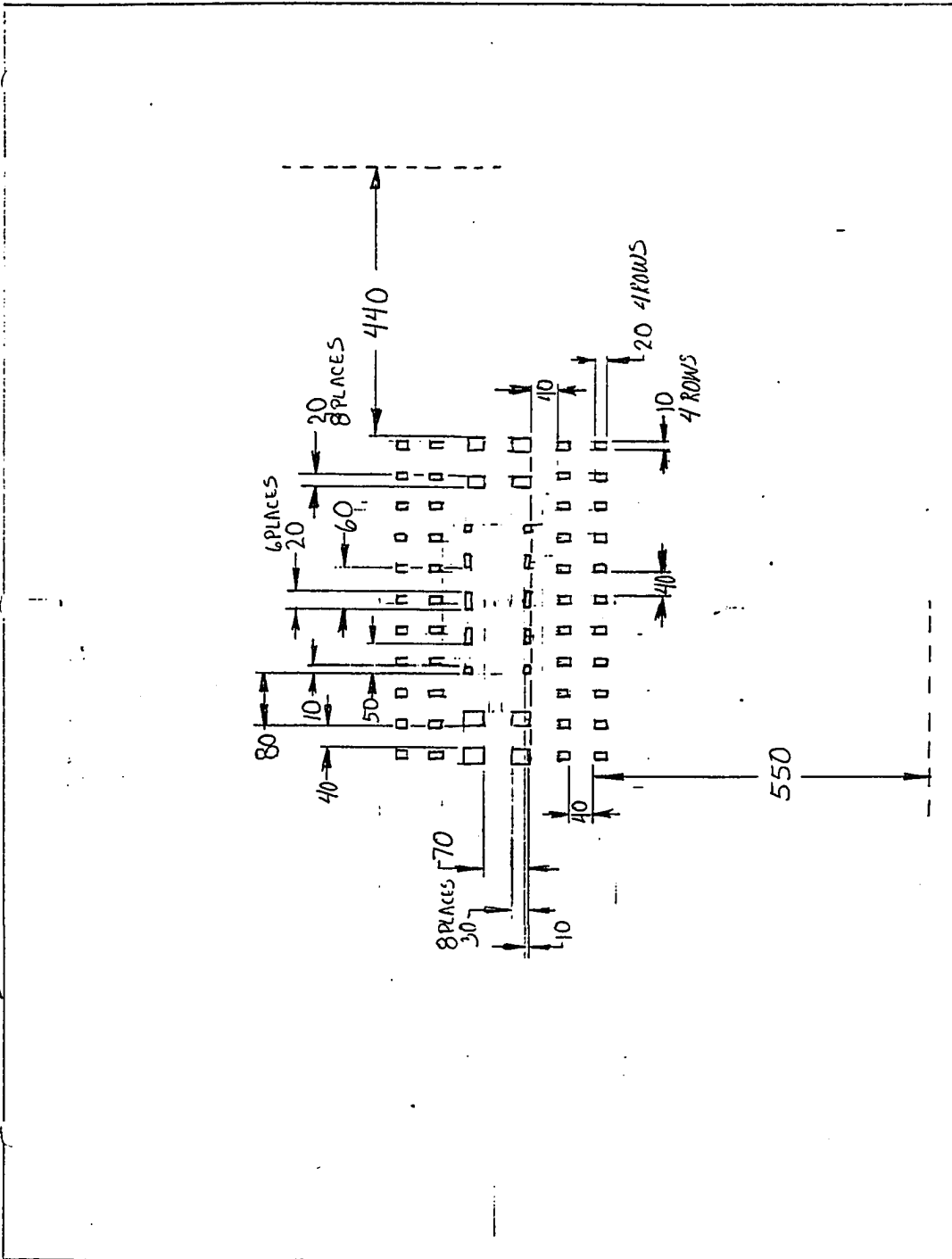


J. G. WHITNEY 3-10-92

TUNNEZ ETCH MASKS

VERSION 1-B

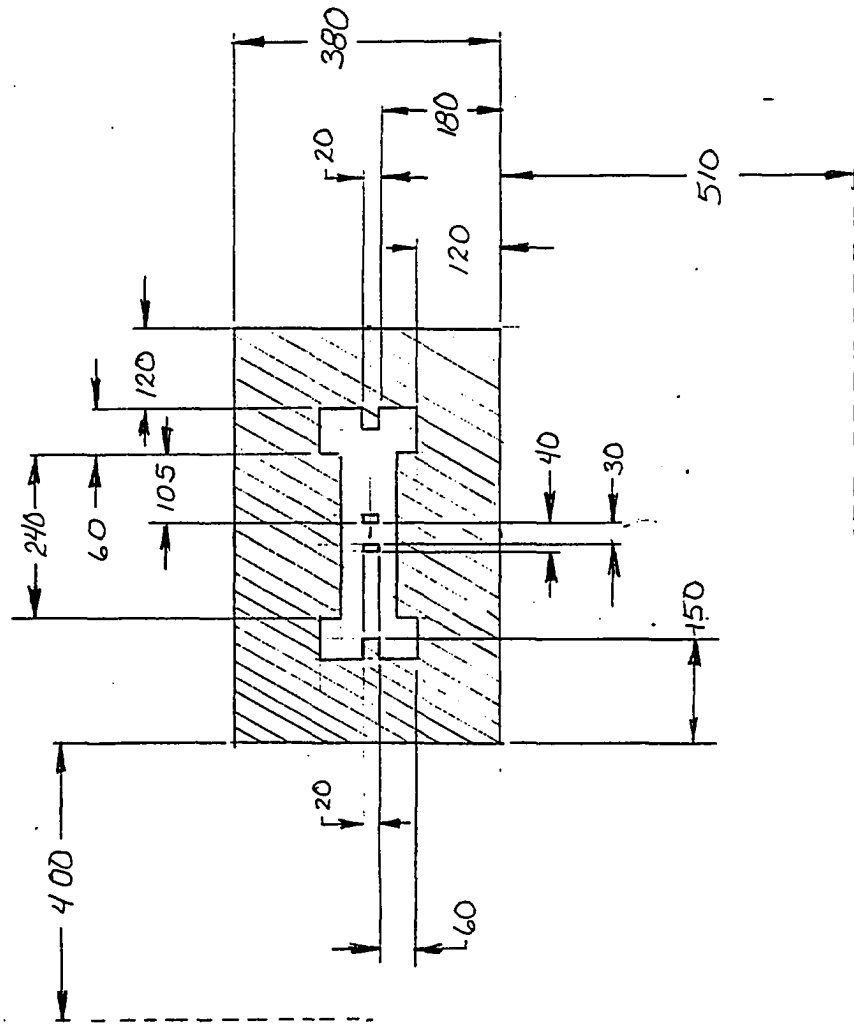
SCALE 1" = 200μ



J.G. WHITNEY 3-11-92

SCALE 1" = 200μm      VERSION 1-B      n<sup>+</sup> DOPING MASK

NOTE: n<sup>+</sup> REGIONS  
ARE CROSS HATCHED



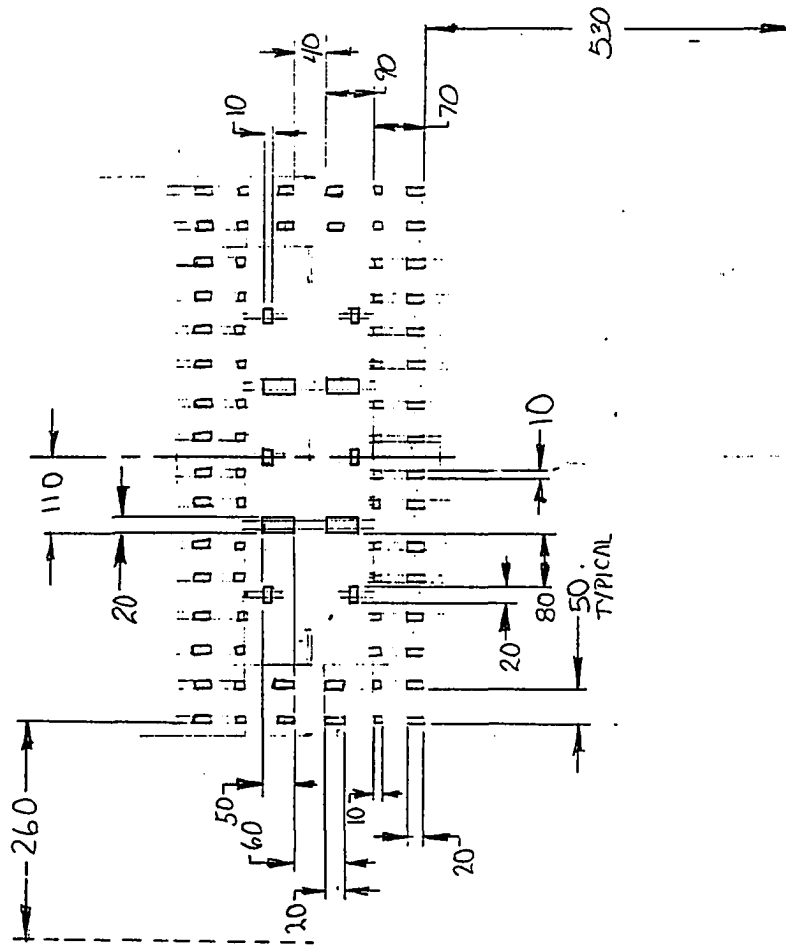
J.G. WHITNEY 3-11-92



TUNNEL ETCH MASK

VERSION 2-B

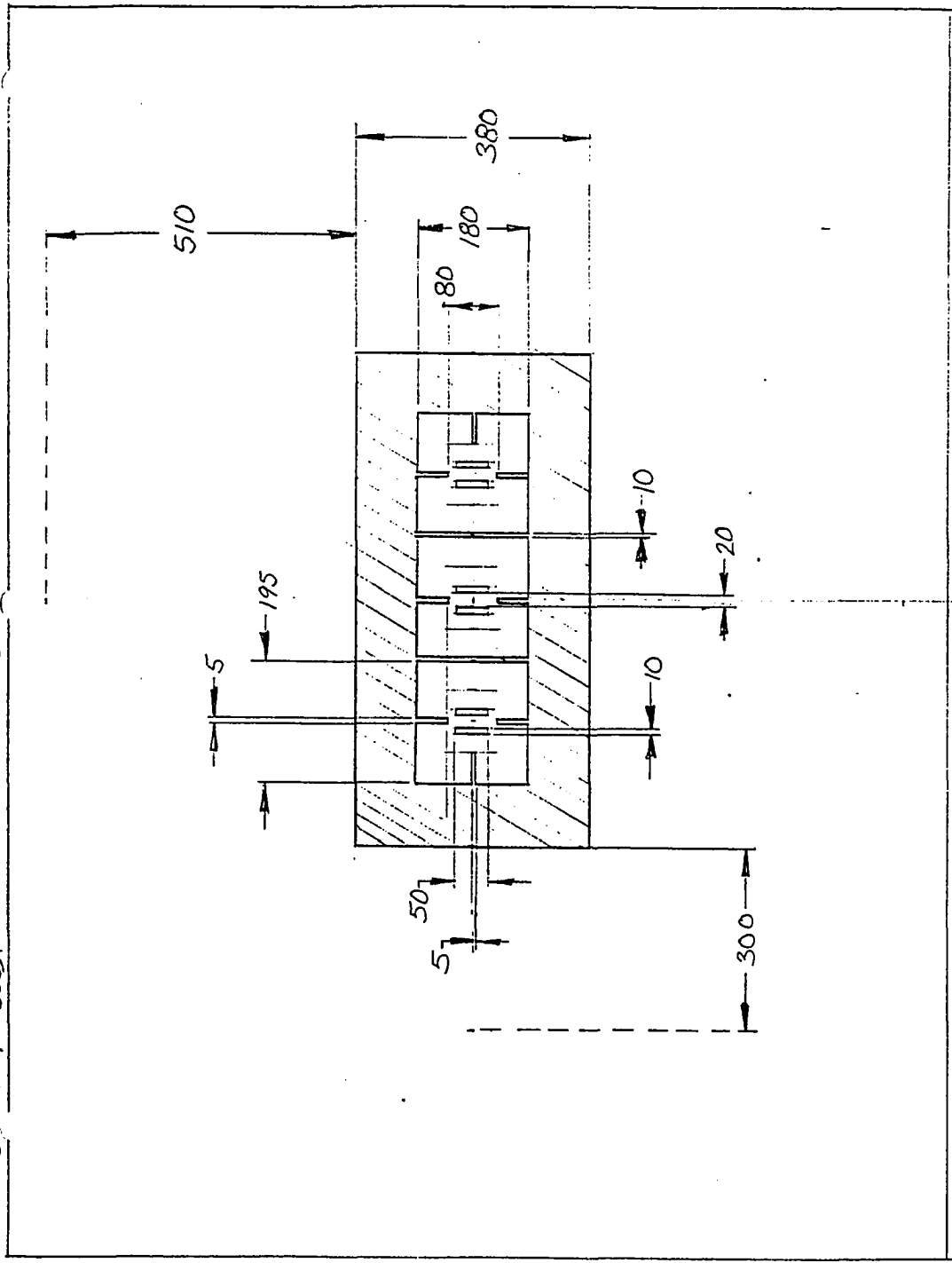
SCALE 1" = 200μ



T.G. WHITNEY 3-11-92

VERSION 2-B N<sup>+</sup> DOPING MASK

SCALE 1" = 200μ



J. WHITNEY 3-11-92

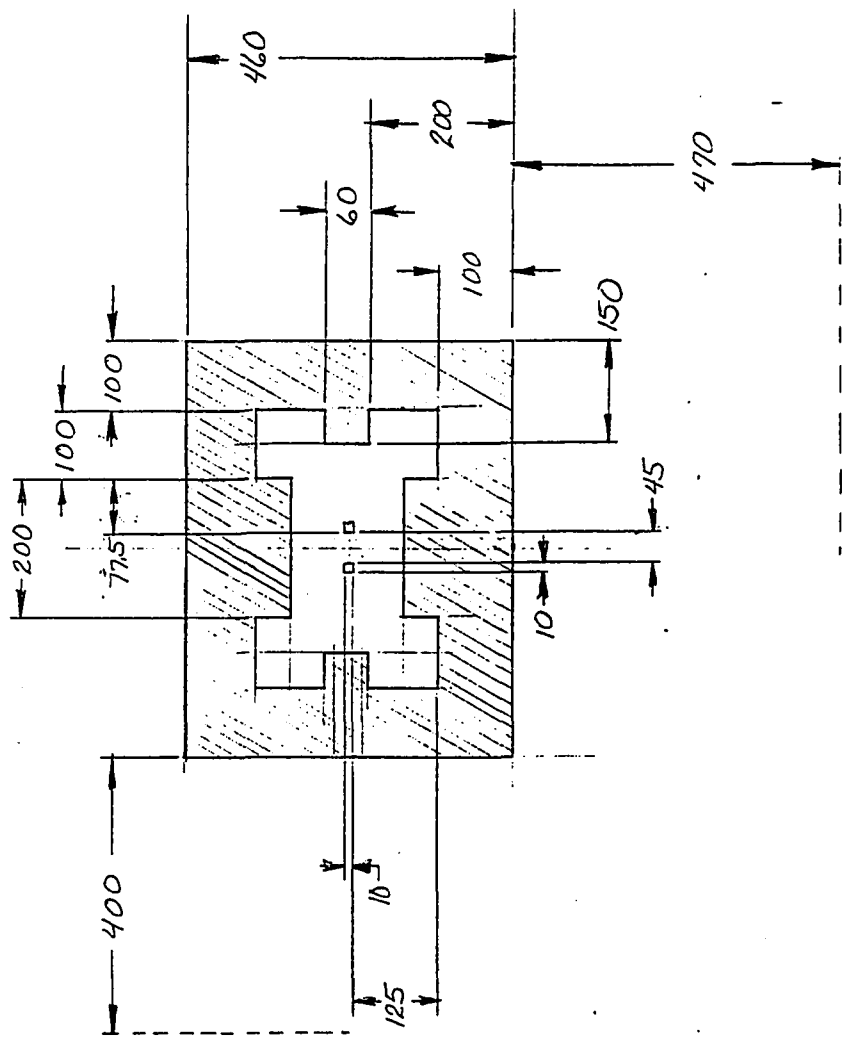


SCALE 1" = 200M

VERSION 3-B

N<sup>+</sup> DOPING MASK

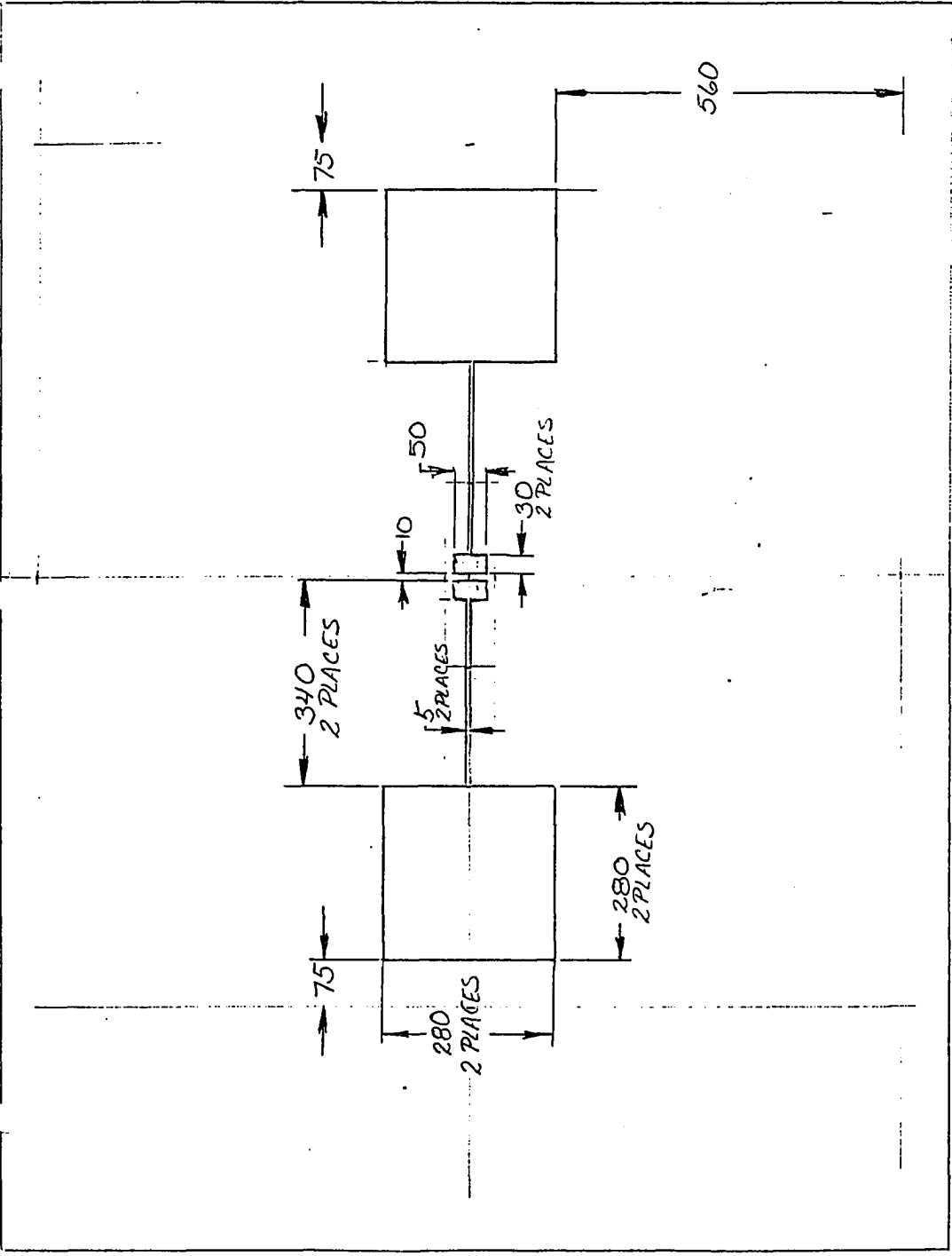
NOTE: N<sup>+</sup> REGIONS  
ARE CROSS-HATCHED



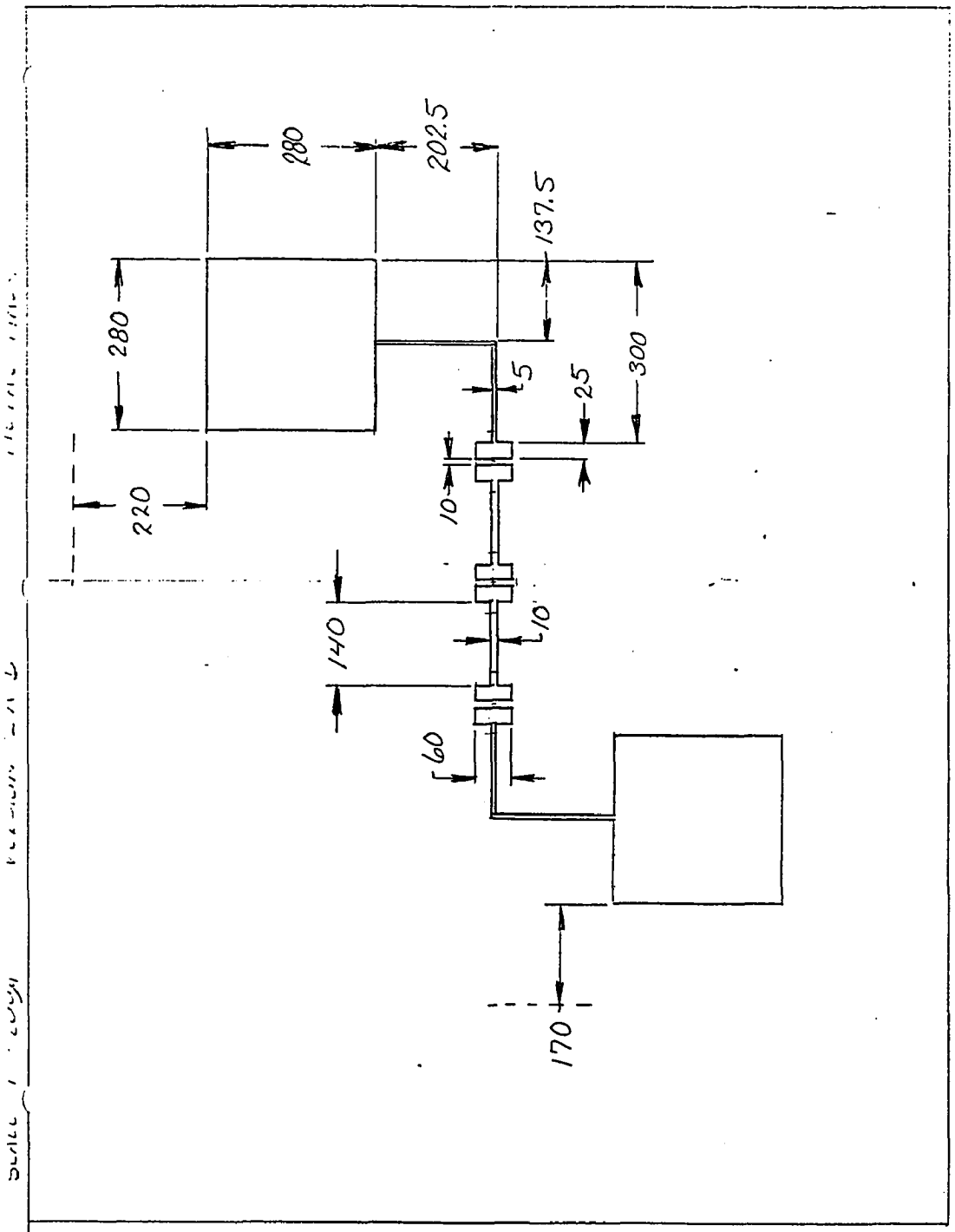
J. G. WHITNEY 3-10-92

VERSION 1A-B METAL LIFT-OFF MASK

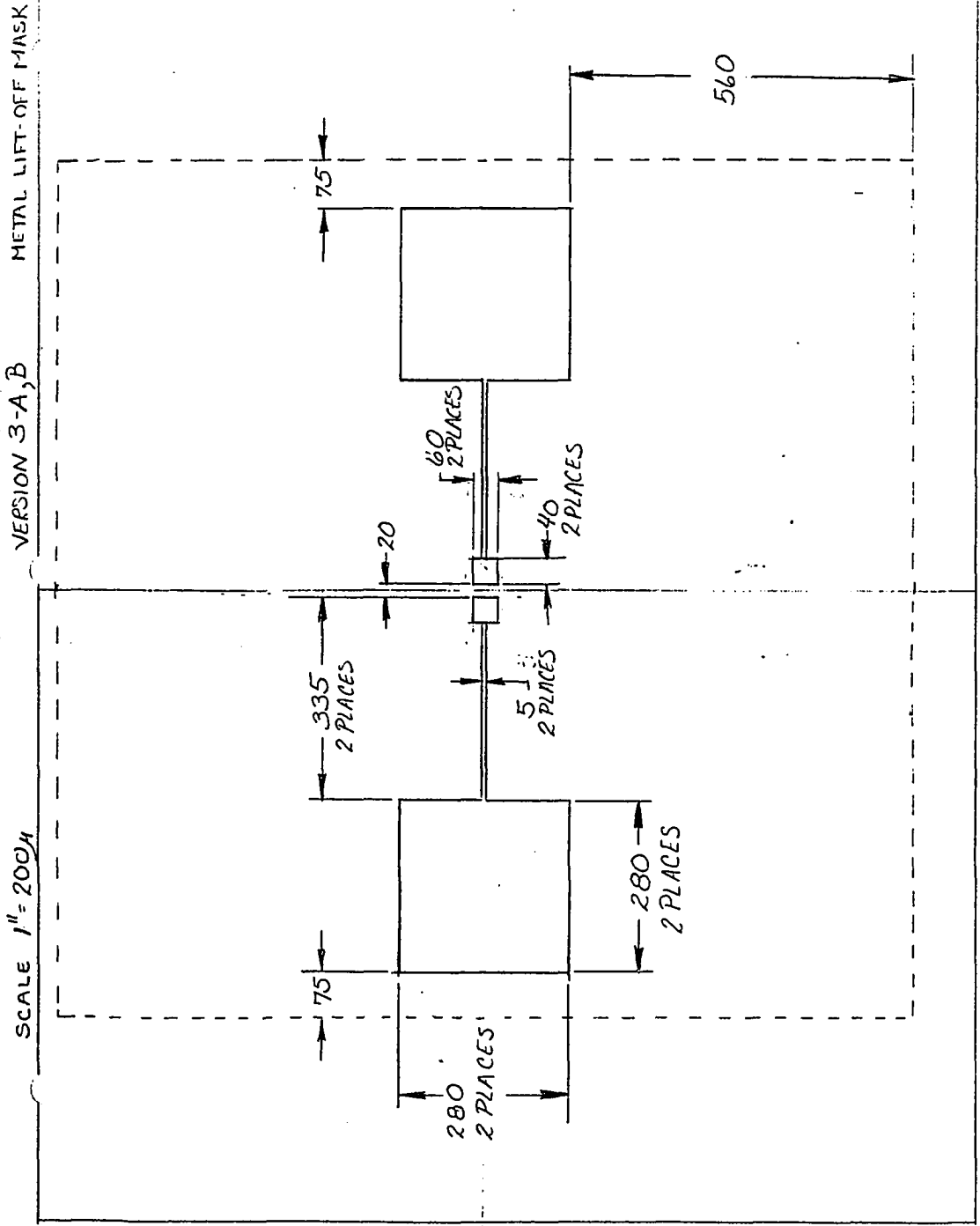
SCALE 1"=200A



J.G. WHITNEY 3-10-92



J.G. WHITNEY 3-11-92



J.G. WHITNEY 3-10-92